EFFECTS OF PHYSICAL AND CHEMICAL PROCESSES IN STORMS ON REACTOR ACCIDENT CONSEQUENCES

PETER ALISTER STOTT

Air Pollution Group

Nuclear Power Section

Department of Mechanical Engineering

Imperial College of Science, Technology and Medicine

A thesis submitted for

The Degree of Doctor of Philosophy

of the University of London

and

The Diploma of Imperial College

October 1988

Abstract

A computer model has been developed to examine the manner in which precipitation can concentrate deposition of radioactivity released to the atmosphere from a nuclear power station accident. It simulates transport of radionuclides through storm systems with different dynamical characteristics. In one spatial dimension, time evolving convective showers are simulated and in two dimensions, orographic, rearward sloping cold frontal and convective systems are modelled. Cloud microphysics is parametrised for warm clouds.

The scavenging of gaseous iodine is incorporated in one-dimensional simulations. The chemistry of its absorption by cloud water and subsequent aqueous phase oxidation are included. Studies are made of the variation of its efficiencies of rainout to the ground and export to higher layers of the atmosphere with absorption and oxidation rates.

Aerosols are incorporated in both one-dimensional and two-dimensional simulations. Results are used to illustrate the variable efficiency of removal in rainfall of different types. Hypothetical accidents, postulated for risk assessment purposes, are used to illustrate how the simple methods used hitherto in safety studies may be inadequate. The model is also used to show how, following Chernobyl, localised hot spots of contamination could have resulted from the dynamical and microphysical processes in precipitation systems. They included areas of orographically enhanced deposition in Cumbria, concentrations of ^{137}Cs in frontal precipitation in Sweden that varied markedly over small distances and problems in Russia where convective storms up to 100km from Chernobyl may have led to sufficiently high levels of contamination to justify evacuation.

For my mother and father

Acknowledgements

First and foremost, I would like to thank my supervisor, Dr. Helen ApSimon, for her guidance and assistance throughout the course of this work which was supported by the Nuclear Installations Inspectorate of the Health and Safety Executive. I am also very grateful to Professor A. J. H. Goddard for his help in administrative matters and for his continued interest in the progress of my work.

My thanks go to my colleagues in the Nuclear Power Section and the Air Pollution Group for many helpful discussions. I am particularly grateful to Keith Simms for his useful comments, especially in the early stages of my studies. That I have retained my sanity during the last three years owes a lot to NUPIX, the brainchild of Rob Cannell, and to my regular NUPIX correspondents who sent such scintillating messages.

Sincere thanks to my friends for their encouragement. It came from many sources and was invaluable. The long haul of writing up was given a tremendous boost by a wonderful break in the Canadian Rocky Mountains. Warm, grateful thanks to Catherine Malcolm for her invitation to myself, David Perry and Alison Ferrier to come over the ocean and to Catherine and Murray for being such marvellous hosts.

Finally, I thank my parents, without whose support and encouragement this thesis would not have been possible.

Contents

Title 1
Abstract 2
Acknowledgements 4
Contents 5
Tables 8
Figures 12

Chapter 1 Introduction 17
1.1 Motivation 17
1.2 Consequence assessment and wet deposition 19
1.3 Structure of thesis 28

Chapter 2 Nuclear Accident Consequence Analysis 29
2.1 Introduction 29
2.2 Modelling theory 30
2.2.1 Accidental releases 30
2.2.2 Dispersion 32
2.2.3 Deposition 41
2.2.3.1 Dry deposition 41
2.2.3.2 Wet deposition 42
2.2.4 Emergency reference levels and dose commitments 44
2.3 Results and discussion 46
2.3.1 Serious PWR accidents 46
2.3.2 PWR design basis and Magnox single channel melt and depressurisation accidents 50
2.3.3 Chernobyl 53
2.4 Summary and conclusions 58

Chapter 3 1D Model 60
3.1 Introduction 60
3.2 Model description 61
3.2.1 General form 61
3.2.2 1D form 67
3.3 Cloud model 69
3.3.1 Parametrisation of microphysical processes 71
3.3.2 Cloud model results and sensitivity studies 75
3.4 Cloud model incorporating particulate pollution 88
3.4.1 Parametrisation of microphysical processes 88

3.4.2 Pollutant material budget 99
3.4.3 Model results and sensitivity studies 102
3.5 Summary and conclusions 107

Chapter 4 Chemistry 113
4.1 Introduction 113
4.2 Gaseous scavenging assuming equilibrium 114
4.2.1 Basic theory 114
4.2.2 Comparison of numerical calculation with analytic calculation in the limiting case of a very low updraught velocity 119
4.2.3 More general modelling studies 126
4.3 Gaseous scavenging incorporating absorption and desorption 132
4.3.1 Theory 132
4.3.2 Results and discussion 142
4.4 Summary and conclusions 147

Chapter 5 2D Model 149
5.1 Introduction 149
5.2 Model description 150
5.3 Orographic precipitation 153
5.3.1 Description of orographic precipitation 153
5.3.2 Calculation of possible enhancement 155
5.3.3 Descripition of modelling 158
5.3.4 Results and discussion 161
5.4 Cold frontal precipitation 170
5.4.1 Description of cold frontal precipitation 170
5.4.2 Description of modelling 171
5.4.3 Results and discussion 175
5.5 Convective precipitation 181
5.5.1 Description of convective precipitation 181
5.5.2 Estimation of possible concentration factors 183
5.5.3 Description of modelling 189
5.5.4 Results and conclusions 191
5.6 Summary and conclusions 195

Chapter 6 Application of cloud modelling studies to accident consequence analysis. 199
6.1 Introduction 199
6.2 Orographic precipitation 202

6.2.1 Discussion : observation and modelling 202
6.2.2 Results 203
6.2.2.1 Serious PWR accidents 203
6.2.2.2 Magnox and PWR design basis accidents 210
6.2.2.3 Chernobyl 213
6.3 Frontal precipitation 216
6.3.1 Discussion : observation and modelling 216
6.3.2 Results 223
6.3.2.1 Serious PWR accidents 223
6.3.2.2 Magnox and PWR design basis accidents 227
6.3.2.3 Chernobyl 227
6.4 Convective precipitation 232
6.4.1 Discussion : observation and modelling 232
6.4.2 Results 232
6.4.2.1 Serious PWR accidents 232
6.4.2.2 Magnox and PWR design basis accidents 236
6.4.2.3 Chernobyl 236
6.5 Summary and conclusions 241

Chapter 7 Summary and Recommendations for Future Work 245

Appendix A Numerical considerations 249
A.1 1D form 249
A.1.1 Characteristic equations 249
A.1.2 Stability 251
A.2 2D form 253

Appendix B Calculation of reference level deposition rates 256
B.1 5mSv emergency reference level due to ingestion of milk for UK1 256
B.2 5mSv emergency reference level due to inhalation of ground gamma radiation for Magnox single channel melt and depressurisation accident 257

References 258

Tables

2.1 Inventory of radionuclides for PWR (from Clarke, 1979) 31

2.2 Release categories and their characteristic parameters (from Clarke, 1979) 31

2.3 Source term for a PWR design basis accident (from Taylor, 1986) 33

2.4 Source term for a Magnox single channel melt and depressurisation accident (from Taylor, 1986) 34

2.5 Typical values of wind speed and depth of mixing layer (from Clarke, 1979) 37

2.6 Coefficients given by Hosker(1974) to derive the vertical standard deviation of the plume for various stability categories (from Clarke, 1979) 39

2.7 Coefficients in expression for standard deviation of lateral dispersion 39

2.8 Emergency reference levels and counter-measures as recommended by the International Commission for Radiological Protection 45

2.9 Patterns of contamination for serious PWR accidents, ERL of 5mSv whole body dose equivalent due to ingestion of milk, no rain 47

2.10 Patterns of contamination for serious PWR accidents, ERL of 500mSv whole body dose equivalent due to inhalation of ground gamma radiation, no rain 47

2.11 Patterns of contamination for serious PWR accidents, ERL of 5mSv whole body dose equivalent due to ingestion of milk, 0.5 mm/hr rain from source 47

2.12 Patterns of contamination for design basis accidents, ERL of 5mSv whole body dose due to ingestion of milk, no rain 51

2.13 Patterns of contamination for design basis accidents, ERL of 5mSv whole body dose due to inhalation of ground gamma radiation, no rain 51

2.14 Patterns of contamination for design basis accidents, ERL of 5mSv whole body dose due to ingestion of milk, 0.5mm/hr rain from source 51

2.15 Patterns of contamination for design basis accidents, ERL of 5mSv whole body dose due to ground inhalation of ground radiation, 0.5 mm/hr rain from source 52

2.16 Patterns of contamination for design basis accidents, ERL of 5mSv whole body dose due to ingestion of milk, 25 mm/hr rain 52

2.17 Patterns of contamination for design basis accidents, ERL of 5mSv whole body dose due to inhalation of ground gamma radiation, 25 mm/hr rain 52
2.18 Predicted total Cs deposition in Sweden(kBq/m^2) 55
3.1 Cloud model parameters for standard run 76
3.2 Variation of ground level steady state precipitation quantities with raindrop distribution 88
3.3 Collection efficiencies based on Beard and Grovers'(1974) interpolation scheme averaged across raindrop spectrum 98
3.4 Parameter values for standard cloud run including hygroscopic particulates 103
4.1 Comparison of analytic and numerical calculations of cloud removal efficiencies of SO_2 124
4.2 Variation of efficiencies of rainout and export with pH and oxidation rate, T = 4000s, instantaneous equilibrium 130
4.3 Variation of efficiencies of rainout and export with pH and oxidation rate, T = 2000s, instantaneous equilibrium 130
4.4 Percentage of material gaseous or particulate in form 131
4.5 Variation of efficiencies of rainout and export with pH and oxidation rate, T = 4000s, gaseous absorption/desorption 143
4.6 Variation of efficiencies of rainout and export with pH and oxidation rate, T = 2000s, gaseous absorption/desorption 143
5.1 Parameter values for standard orographic run 162
5.2 Orographic sensitivity studies: variation of model parameters 165
5.3 Peak values of equivalent and effective washout coefficients, deposition and precipitation rates 167
5.4 Efficiencies of rainout and export for orographic runs 170
5.5 Model parameters for cold frontal runs 177
5.6 Model parameters for convective storm runs 192
6.1 Depletion of Gaussian plume 206
6.2 Characteristics of six sharp surface cold fronts(from Browning, 1983) 222
6.3 UK1 - distances out to which 5mSv milk ERL exceeded(100 % iodine in particulate form) - cold frontal precipitation 224
6.4 UK1 - distances out to which 5mSv milk ERL exceeded(25 % iodine in particulate form) - cold frontal precipitation 224
6.5 UK1 - distances out to which 500mSv ground gamma ERL is exceeded - cold frontal precipitation 224
6.6 UK8 - distances out to which 5mSv milk ERL exceeded(100 % iodine in particulate form) - cold frontal precipitation 225

6.7 UK8 - distances out to which 5mSv milk ERL exceeded(25 % iodine in particulate form) - cold frontal precipitation 225
6.8 UK8 - distances out to which 500mSv ground gamma ERL is exceeded - cold frontal precipitation 225
6.9 Magnox - distances out to which 5mSv milk ERL exceeded (100 % iodine in particulate form) - cold frontal precipitation 228
6.10 Magnox - distances out to which 5mSv milk ERL exceeded (25 % iodine in particulate form) - cold frontal precipitation 228
6.11 PWR design basis - distances out to which 5mSv milk ERL exceeded (100 % iodine in particulate form) - cold frontal precipitation 228
6.12 PWR design basis - distances out to which 5mSv milk ERL exceeded (25 % iodine in particulate form) - cold frontal precipitation 229
6.13 Magnox - distances out to which 5mSv ground gamma ERL exceeded - cold frontal precipitation 229
6.14 PWR design basis - distances out to which 5mSv ground gamma ERL exceeded - cold frontal precipitation 229
6.15 Predicted ^{137}Cs concentration in cold frontal precipitation in Eastern Sweden 230
6.16 UK1 - distances out to which 5mSv milk ERL exceeded(100 % iodine in particulate form) - convective precipitation 234
6.17 UK1 - distances out to which 5mSv milk ERL exceeded(25 % iodine in particulate form) - convective precipitation 234
6.18 UK1 - distances out to which 500mSv ground gamma ERL is exceeded - convective precipitation 234
6.19 UK8 - distances out to which 5mSv milk ERL exceeded(100 % iodine in particulate form) - convective precipitation 235
6.20 UK8 - distances out to which 5mSv milk ERL exceeded(25 % iodine in particulate form) - convective precipitation 235
6.21 UK8 - distances out to which 500mSv ground gamma ERL is exceeded - convective precipitation 235
6.22 Magnox - distances out to which 5mSv milk ERL exceeded (100 % iodine in particulate form) - convective precipitation 237
6.23 Magnox - distances out to which 5mSv milk ERL exceeded (25 % iodine in particulate form) - convective precipitation 237
6.24 PWR design basis - distances out to which 5mSv milk ERL exceeded (100 % iodine in particulate form) - convective precipitation 237
6.25 PWR design basis - distances out to which 5mSv milk ERL 238

exceeded (25 % iodine in particulate form) - convective precipitation

6.26 Magnox - distances out to which 5mSv ground gamma ERL exceeded - convective precipitation 238

6.27 PWR design basis - distances out to which 5mSv ground gamma ERL exceeded - convective precipitation 238

6.28 Predicted deposition and ground gamma dose beneath convective storm at 100km from Chernobyl 239

Figures

1.1 The frequency distributions of the incidence of various health effects from degraded core accidents for one year's operation of the reactor(from Kelly and Clarke, 1982) 20

1.2 Airflow in convective storms(from Browning and Ludlam, 1962) 25

1.3 Schematic portrayal of airflow at a classical ana cold front showing the warm conveyor belt undergoing rearward sloping ascent(from Browning,1985) 26

1.4 Schematic portrayal of airflow in a mid-latitude cyclone in which the warm conveyor belt is undergoing forward sloping ascent(from Browning, 1985) 26

2.1 Distances out to which 5mSv ingestion of milk ERL is exceeded for UK1 accident 49

2.2 Distances out to which 500mSv inhalation of ground gamma ERL is exceeded for UK1 accident 49

2.3 Recorded values of precipitation(mm) over Sweden for the period April 28 06 UTC to April 30 06 UTC(from Persson et al, 1987) 55

2.4 Estimated deposition of $^{137}Cs(kBqm^{-2})$ over Sweden(from Persson et al,1987) 55

2.5 Comparison of modelled deposition from Chernobyl with 500mSv inhalation of ground gamma ERL, 2mm/hr precipitation rate from 10 to 30 km 57

3.1 Microphysical processes for water substance 72

3.2 Cloud water development, $G = 2.16.10^{-3}(1 - 10^{-4} z)$ 77

3.3 Rain water development, $G = 2.16.10^{-3}(1 - 10^{-4} z)$ 77

3.4 Cloud water development, $G = 3.10^{-3}(1 - 10^{-4} z)$ 78

3.5 Rain water development, $G = 3.10^{-3}(1 - 10^{-4} z)$ 78

3.6 Development of precipitation rates at ground 79

3.7 Cloud water development, $N_c = 50\ cc^{-1}$ 82

3.8 Rain water development, $N_c = 50\ cc^{-1}$ 82

3.9 Cloud water development, $N_c = 5000\ cc^{-1}$ 83

3.10 Rain water development, $N_c = 5000\ cc^{-1}$ 83

3.11 Cloud water development, $a = 0.1\ g/m^3$ 84

3.12 Rain water development, $a = 0.1\ g/m^3$ 84

3.13 Cloud water development, $a = 1.0\ g/m^3$ 85

3.14 Rain water development, $a = 1.0\ g/m^3$ 85

3.15 Cloud water development, $N_0 = 5.10^6\ m^{-4}$ 86

3.16 Rain water development, $N_0 = 5.10^6$ m^{-4} 86
3.17 Cloud water development, $N_0 = 5.10^7$ m^{-4} 87
3.18 Rain water development, $N_0 = 5.10^7$ m^{-4} 87
3.19 Microphysical processes for particulate pollution 89
3.20 Comparison of collection efficiency, E_A, determined from interpolation scheme with values from Mason(1971) (from Beard and Grover, 1974) 95
3.21 Comparison of collection efficiency, E_A, determined from interpolation scheme with experiment involving particles with $\rho_A = 1 g/cm^3$(from Beard and Grover, 1974) 95
3.22 Collection efficiencies for particles of density of carbon ($\rho_A = 2250$ kg/m^3) 96
3.23 Collection efficiencies for particles of density of caesium hydroxide ($\rho_A = 3675 kg/m^3$) 96
3.24 Collection efficiencies for particles of density of caesium iodide ($\rho_A = 4510 kg/m^3$) 97
3.25 Variation of $I(R) = R^{5/2} e^{-2\lambda R}$ with raindrop radius, R 97
3.26 Development of particulate material in air - standard run 103
3.27 Development of particulate material in cloud water - standard run 104
3.28 Development of particulate material in rain water - standard run 104
3.29 Rainout and export efficiencies for hygroscopic particles and standard run parameters, k = 0 106
3.30 Rainout and export efficiencies for hydrophobic particles and standard run parameters, k = 0 106
3.31 Rainout and export efficiencies for hygroscopic particles and standard run parameters, $k = 10^{-4}$ 108
3.32 Rainout and export efficiencies for hydrophobic particles and standard run parameters, $k = 10^{-4}$ 108
3.33 Rainout and export efficiencies for hygroscopic particles, $E_A = 0.2$, $k = 10^{-4}$ 109
3.34 Rainout and export efficiencies for hydrophobic particles, $E_A = 0.2$, $k = 10^{-4}$ 109
3.35 Rainout and export efficiencies for hygroscopic particles, T = 2000s, $k = 10^{-4}$ 110
3.36 Rainout and export efficiencies for hydrophobic particles, T = 2000s, $k = 10^{-4}$ 110
4.1 Henry's Law coefficient, H', for molecular iodine at 25°C (from Eggleton, 1967) 118

4.2 Variation of Henry's Law coefficient, H', with iodine concentration(from Gittus et al, 1982) 118
4.3 Comparison of numerically and analytically calculated cloud and rain water quantities at steady state for an updraught of height, 10 km and maximum velocity, 0.5 m/s 125
4.4 Microphysical processes for gaseous and particulate pollutants assuming instantaneous equilibrium for gases 127
4.5 Microphysical processes for gaseous and particulate pollutants including absorption and desorption of gases to and from raindrops 140
4.6 Rainout and export efficiencies for gaseous material, pH = 5, $k_t = 2.10^{-3}$ 145
4.7 Rainout and export efficiencies for gaseous material, pH = 5, $k_t = 0$ 145
4.8 Variation of rainout efficiencies with pH 146
5.1 Field of streamlines for two dimensional updraught circulation 152
5.2 Field of streamlines for two dimensional orographic circulation - standard run 160
5.3 Effective washout coefficient for standard orographic run(no 1) 164
5.4 Steady state deposition and precipitation rates for orographic run number 1 164
5.5 Steady state deposition and precipitation rates for orographic run number 2 167
5.6 Steady state deposition and precipitation rates for orographic run number 3 168
5.7 Steady state deposition and precipitation rates for orographic run number 4 168
5.8 Steady state deposition and precipitation rates for orographic run number 5 169
5.9 Steady state deposition and precipitation rates for orographic run number 6 169
5.10 Transverse circulation at the surface cold front at 1124 on 6th February, 1969(from Browning and Harold, 1970) 172
5.11 Field of streamlines for two dimensional cold frontal circulation 1 176
5.12 Field of streamlines for two dimensional cold frontal circulation 2 176
5.13 Steady state precipitation rate for cold frontal circulation 1 178
5.14 Steady state precipitation rate for cold frontal circulation 2 178

5.15 Effective washout coefficients for cold frontal circulation 1 180
5.16 Effective washout coefficients for cold frontal circulation 2 180
5.17 Schematic vertical cross sections through a single-cell storm at various stages of its life cycle(from Atkinson, 1981) 182
5.18 Schematic plan position indicator sections and vertical cross-sections for a multi-cell storm at various stages of its life cycle (from Atkinson, 1981) 182
5.19 Three-dimensional air-flow in a severe storm that travels to the right of the winds in the middle troposphere(from Atkinson, 1981) 184
5.20 Two-dimensional schematic model of convective storm circulation (from Atkinson, 1981) 184
5.21 Schematic model of a severe multi-cell hail storm showing a vertical section along the storm's direction of travel through a sequence of evolving cells(from Atkinson, 1981) 185
5.22 Field of streamlines for two-dimensional convective shower circulation 185
5.23 Steady state precipitation rate for first convective storm 193
5.24 Steady state deposition rate for first convective storm 193
5.25 Effective washout coefficients for first convective storm 194
5.26 Precipitation rate for second convective storm 196
5.27 Effective washout coefficients for second convective storm 196
6.1 Schematic diagram of stages in analysis of consequences from accidental releases using storm models for wet deposition 201
6.2 Downwind distances at which the 5mSv ingestion of milk ERL is exceeded for UK1 release and deposition in orographic precipitation 207
6.3 Downwind distances at which the 5mSv ingestion of milk ERL is exceeded for UK8 release and deposition in orographic precipitation 207
6.4 Downwind distances at which the 500mSv inhalation of ground gamma ERL is exceeded for UK1 release and deposition in orographic precipitation 208
6.5 Downwind distances at which the 500mSv inhalation of ground gamma ERL is exceeded for UK8 release and deposition in orographic precipitation 208
6.6 Specimen trajectories originating from Chernobyl(from ApSimon et al, 1987) 209
6.7 Downwind distances at which the 5mSv ingestion of milk ERL is exceeded for the Magnox single channel melt and 211

depressurisation accident and deposition in orographic precipitation
6.8 Downwind distances at which the 5mSv ingestion of milk ERL is exceeded for the PWR design basis accident and deposition in orographic precipitation 211
6.9 Downwind distances at which the 5mSv inhalation of ground gamma ERL is exceeded for the Magnox single channel melt and depressurisation accident and deposition in orographic precipitation 212
6.10 Downwind distances at which the 5mSv inhalation of ground gamma ERL is exceeded for the PWR design basis accident and deposition in orographic precipitation 212
6.11 Sequence of surface analyses at 6h intervals showing frontal positions and isobars(4 mb spacing) between 18 GMT 2 May and 00 GMT 4 May(from Monk and Jonas, 1986) 214
6.12 Rainfall accumulations (mm) during the passage of the Chernobyl cloud(from Monk and Jonas, 1986) 215
6.13 Predicted deposition from Chernobyl in orographic precipitation 217
6.14 Schematic portrayal of inflow in a mid-latitude cyclone in which the warm conveyor belt is undergoing forward sloping ascent(from Browning, 1985) 219
6.15 Schematic portrayal of the same situation as figure(6.14) with the warm conveyor belt undergoing forward sloping ascent but drawing attention to the split front characteristic and the overall precipitation distribution(from Browning, 1985) 219
6.16 Schematic portrayal of calculation of deposition at the ground beneath moving system 220
6.17 Concentration of ^{137}Cs in precipitation(kBq/l) during the period April 28-30, 1986(from Persson et al, 1987) 231

1 Introduction

1.1 Motivation

The environmental safety of nuclear power is a matter for great public interest and scrutiny. In particular, much concern is directed towards the consequences of an accidental release of radioactivity to the atmosphere. The implications of such an event may become more serious if the radionuclides released are deposited upon the ground in precipitation. In the past, accident consequence analyses have employed a considerably simplified treatment of wet deposition. Including the effects of the physical and chemical processes in storms may lead to greatly enhanced concentrations of pollutants in precipitation and correspondingly higher levels of contamination. This thesis aims to describe these processes in a computer model and to use it to consider the implications for accident consequence assessment.

Nuclear fission is not the only means of electricity generation to make an environmental impact. For instance, emissions of sulphur dioxide from coal fired power stations are blamed by environmental pressure groups for 'acid rain'. Another problem, which is potentially more serious on a World-wide scale, results from emissions of carbon dioxide. These are contributing to the global atmospheric warming known as the 'greenhouse effect'. Nuclear power is unusual however, in that popular concern is directed as much towards the possible consequences of an accidental release as towards the effects of routine operation. This is hardly surprising perhaps, in view of the fact that there have been two major accidents in the last decade. The excursion at Three Mile Island in 1979 involved no discharge to the atmosphere. It came perilously close however and it raised public awareness to the awful possibility of a large release of radioactivity in a densely populated area. The accident at Chernobyl in 1986

did result in a substantial release. But for the efficient actions of the Russian authorities in speedily evacuating the local population, the consequences could have been worse. As it was, 29 people, mainly reactor operators and firemen who doused the initial explosion and fire, were killed immediately or soon afterwards. The predicted collective dose commitment to the people of Europe outside the USSR over the next fifty years has been calculated to be $1.6.10^5$ man Sv (ApSimon and Wilson, 1987a). Dividing by the affected population of 530 million ammounts to an average dose commitment per individual of 0.35 mSv. This is small compared to the maximum permissible lifetime dose of 70 mSv and health effects in Western Europe due to the Chernobyl accident are unlikely to be detectable against the natural background. Nevertheless, the release made an impact on a large area and there were significant consequences over 2000 kilometres away in Britain.

Away from the vicinity of Chernobyl, the most serious effects were associated with precipitation. Two problems attracted particular attention. Sheep, grazing on upland pastures in Northern England and Wales, ate grass contaminated by rain containing radionuclides that were carried across Britain on the weekend of 3rd and 4th of May, 1986. As a result, farmers were prevented from selling their lambs for slaughter. These controls persisted for many months and some are still in operation. Across the North Sea in Lappland, reindeer were also affected when polluted rain fell on their grazing supply of grass and lichen. The Lapps' livelihood, dependent on the sale of part of their herd for meat, was put in jeopardy. Fortunately the threat was averted when the Norwegian government agreed to pay compensation for reindeer carcasses declared unfit for human consumption. Although there are other factors to be taken into consideration, such as the slowness with which radionuclides leach through upland soils, in both cases the influence of precipitation was

crucial. The interaction between precipitation and radionuclides forms an important link in the causal chain between an accidental release and its eventual effects. It is worthy of careful consideration.

1.2 Consequence assessment and wet deposition

An accidental release of radionuclides from a nuclear power station to the atmosphere could be the result of many possible sets of circumstances. There are correspondingly many possible release patterns. In fault tree analysis, every sequence of events that can be foreseen to lead to an accidental discharge is determined and is assigned a probability of occurrence per year of reactor operation. To assess the environmental impacts of such releases, the number of hypothetical accidents can be reduced to a more manageable number by grouping together similar release patterns. These are called reference accidents. In probabilistic risk analysis (PRA), a measure of the overall risk from a reactor's operation is determined by summing the resultant effects of all the reference accidents weighted by their probability of occurrence. An example of the result of such a calculation for degraded core PWR accidents is given in figure(1.1).

Probabilistic risk analysis is an important tool for use in determining whether a reactor satisfies required safety criteria. However, it is also useful to examine particular accidents individually. For instance, modelling of the Chernobyl release was used immediately following the accident to determine the passage of the material as it spread across Europe (ApSimon et al,1987). For hypothetical accidents it may be instructive to consider 'worst case scenarios'. If a release is scavenged by heavy rain, high pollutant concentrations may be deposited on a small area. This would be particularly serious if the rainstorm were above a town or city. Although this is extremely unlikely, since the consequences could be grave, it might still be significant in PRA.

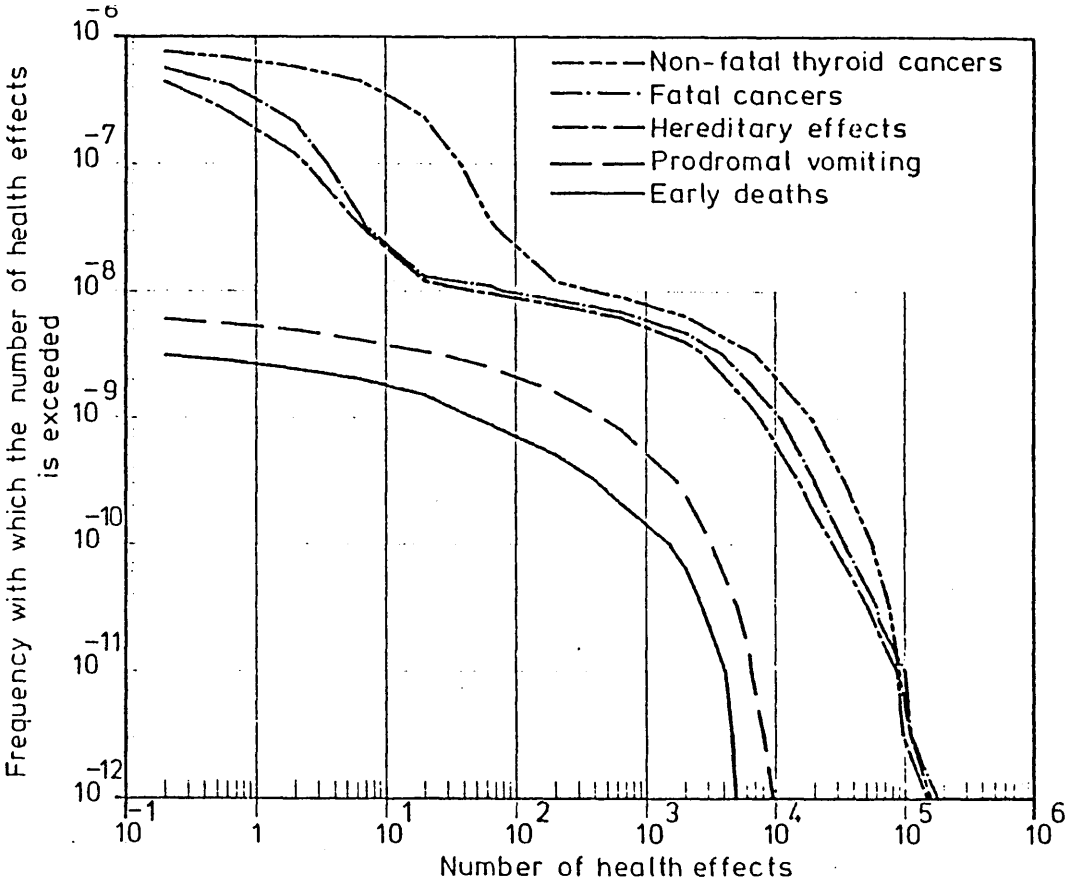


Figure 1.1 The frequency distributions of the incidence of various health effects from degraded core accidents for one year's operation of the reactor (from Kelly and Clarke, 1982)

Emergency procedures would be improved if it could be predicted where the worst effects are likely to be felt. Of particular concern would be those areas subject to precipitation. Estimates of deposition would allow expected dose rates to be calculated and appropriate counter-measures to be taken. Guidelines for dose rates at which to take action, such as evacuation or sheltering, have been provided by the International Commission for Radiological Protection (ICRP). It would also be helpful to predict less serious effects. Following the Chernobyl accident, an earlier knowledge of the deposition in precipitation over upland areas in Britain might have helped to anticipate the problems with sheep described in section 1.1.

One potentially useful tool is provided by the RAINPATCH model (Simms, 1988). This calculates spatial distributions of precipitation and pollutant material from which it derives the pattern of wet deposition. Dispersion of pollutants is modelled by a puff-based formulation and the distribution of precipitation is derived from radar data. RAINPATCH was highly successful at modelling the pattern of Chernobyl ^{137}Cs deposition over Britain; model results agreed well with levels of ^{137}Cs measured on grass by the Institute for Terrestrial Ecology (ApSimon et al, 1988). However RAINPATCH does not model the dynamic, microphysical and chemical processes that are involved in wet deposition. As discussed below, such processes may significantly enhance deposition, especially beneath particular precipitation systems. One example of such a system produced the orographic rain containing Chernobyl ^{137}Cs that affected British upland sheep.

Wet deposition of radionuclides is described in RAINPATCH and in many other consequence assessment models by the 'washout model'. This describes deposition in precipitation by assuming that a certain fraction, Λ, of total pollutant material is instantaneously deposited on the ground each

second. Λ is known as the washout coefficient and is expressed mathematically as

$$\Lambda = \frac{D_r}{\int X_a (x, y, z)\, dz}. \qquad (1.1)$$

D_r is the deposition rate and

$$\int X_a (x, y, z)\, dz$$

is the total integrated pollution in air above point (x, y, z=0) on the ground. The washout model treats wet deposition as though initially clean rain drops fall into polluted air from above, scavenging pollutants as they fall to ground. Often however, pollutants are taken up by water drops within a rain cloud before being rained out. Although the washout model provides a good description of deposition close to the source of a low level release, in other circumstances it might not. The following examples illustrate when it would fail to describe deposition well. In frontal systems, warm air is carried upwards in a gently sloping conveyor belt which transports boundary layer air many thousands of kilometres from its starting point. As it rises higher, instabilities may break out aloft leading to precipitation. Alternatively the conveyor belt may meet the cold frontal surface and rise sharply, causing a line of precipitation behind the surface cold front. In both cases, polluted precipitation may be falling through a boundary layer of clean air. Precipitation is often enhanced on high ground by the seeder-feeder mechanism, in which rain from high level stratus clouds falls through hill top cloud. If the hill cloud already contains polluted drops, these will be scavenged by rain more effectively than the pollutant particles themselves. A convective storm draws in a large volume of boundary layer air to feed its strong updraught and deposits large quantities of precipitation on a small area. Pollutants drawn into the storm

will be concentrated within its core and may produce high levels of deposition. The washout model is inadequate in all these cases. To calculate wet deposition more accurately, a model must attempt to describe both the dynamics of storm systems and the microphysics and chemistry of water and pollutant interactions.

The most important microphyical processes which lead to precipitation formation can be described briefly as follows. Cloud is formed when air rises to above its saturation level and water vapour condenses to allow cloud droplets to form on small hygroscopic particles. These are known as cloud condensation nuclei. It would take much longer than is observed for drops to grow by condensation alone to sufficient size that they can fall to ground without totally evaporating. Instead, there are two theories which allow precipitation formation on sufficiently small timescales. If part of the cloud is below 0^{o} C, ice crystals can form and grow at the expense of supercooled water droplets, because the saturation vapour pressure with respect to ice is less than that with respect to supercooled water at the same temperature. These ice crytals soon become large enough to fall through the cloud collecting cloud droplets. As they reach higher temperatures lower down they may melt to fall to ground as rain. Alternatively, they may fall as sleet or snow. In warm cloud, where temperatures are greater than 0^{o} C, collisions between droplets lead to the formation of rain. There is a spectrum of droplet sizes within the cloud with the larger ones having a downward motion relative to the smaller ones. As they fall they sweep out cloud drops to produce precipitation sized drops at ground level.

The dynamic motions that lead to air rising to above its saturation level have three basic causes. Convective situations arise on sunny days when air near the ground becomes warmer and hence more buoyant than surrounding air. Formation of cloud releases latent heat of condensation,

adding to the buoyancy of air and driving an updraught. Once rain has begun to fall, the storm cell may be short-lived if rain falls directly into the updraught. This is because rain evaporates in subsaturated air, cooling takes place and the supply of warm air is cut off. If there is wind shear however, rain may fall into different air and produce a downdraught through evaporative cooling. In this case heavy sustained rainfall may result. A typical windfield of a convective storm in which updraught and downdraught twist around and sustain each other is shown in figure(1.2).

Frontal situations, which provide a high proportion of rainfall in Britain, arise from large scale horizontal convergence of air. Fronts are familiar from their depiction on weather maps on which a front marks the boundary of a warm wedge of air intruding into colder Northerly latititudes. Precipitation development is principally controlled by a broad 'conveyor belt' of air, a few hundreds of kilometres wide and several kilometres deep, which flows roughly parallel to and ahead of the cold front. The conveyor belt also has a small flow perpendicular to the front; it is termed rearward sloping ascent if the flow is towards and forward sloping if it is away from the front. In the case of rearward sloping ascent the warm air is lifted abruptly at up to several metres per second where it meets the surface cold front. This results in a narrow band of precipitation. The air rises two to three kilometres during this ascent and subsequently ascends much more gradually at a few tens of centimetres per second, producing a broader belt of lighter rain. This is illustrated schematically in figure(1.3). In the case of forward sloping ascent the conveyor belt rises over the surface warm front and turns anticyclonically ahead of it. The warm, moist air in the conveyor belt is overrun by a flow of drier and colder air which leads to the generation of potential instability. The convective elements which result produce a cellular structure of precipitation. This is illustrated schematically in figure(1.4).

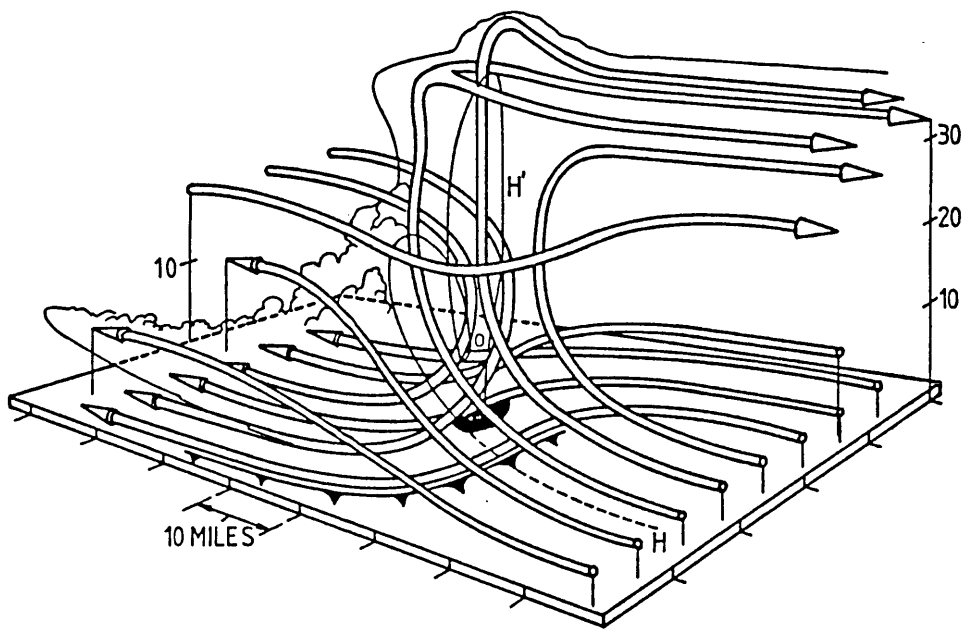


Figure 1.2 Airflow in convective storms (from Browning and Ludlam, 1962)

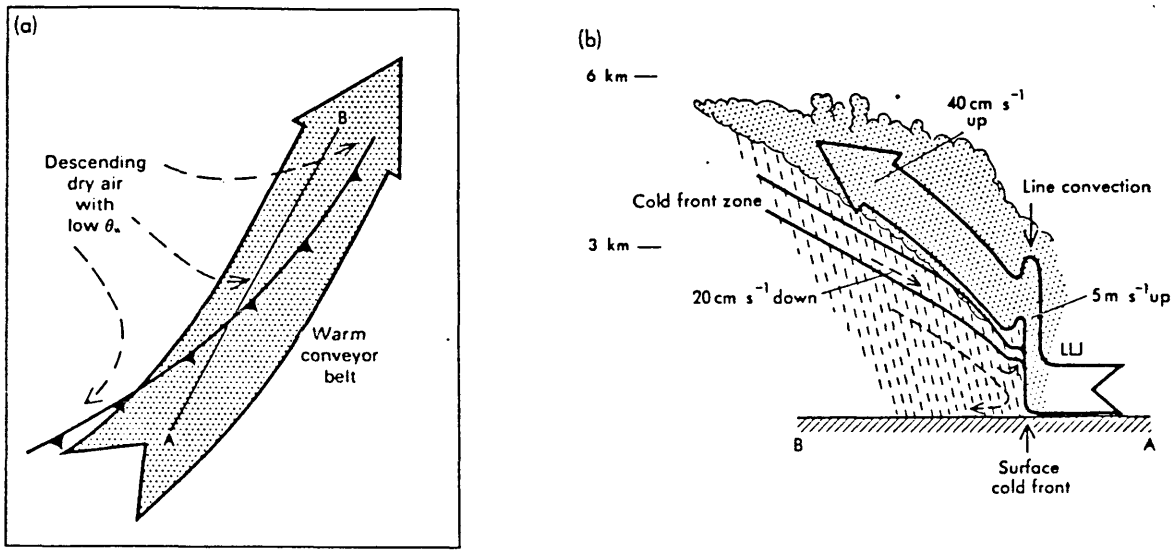


Figure 1.3 Schematic portrayal of airflow at a classical ana cold front showing the warm conveyor belt (bold arrow) undergoing rearward sloping ascent above the cold frontal zone with the cold air (dashed lines) descending beneath it: (a) plan view, (b) vertical section along AB in (a). (from Browning, 1985)

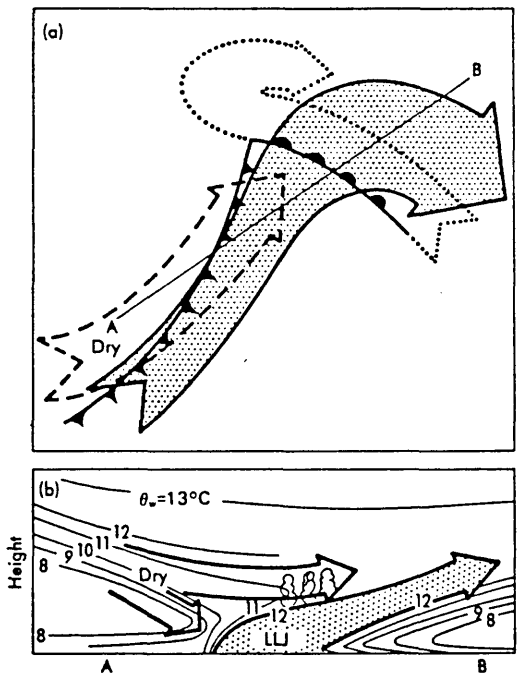


Figure 1.4 Schematic portrayal of airflow in a mid-latitude cyclone in which the warm conveyor belt (bold arrow with stippled shading) is undergoing forward sloping ascent ahead of a kata cold front before rising above a flow of cold air ahead of the warm front (dotted arrow). Dry, cold middle-tropospheric air (dashed arrow) is shown overrunning the cold front and generating potential instability in the upper portion of the warm conveyor belt : (a) plan view, (b) vertical section along AB in (a). (from Browning, 1985)

Finally, orographic cloud comes about as a result of air being forced to rise when it meets a mountain barrier. There is usually insufficient time for cloud droplets in air flowing over the hill to coalesce to form precipitation. Instead, raindrops from high level stratus cloud can sweep out hill cloud droplets to produce enhanced levels of precipitation at the ground. This is known as the seeder-feeder mechanism.

Before pollutant material can be deposited in precipitation it must become involved in the dynamic and microphysical processes described above. Some proportion of a release from a nuclear power station is likely to be in gaseous form, with the rest being particulate. Noble gases such as xenon and krypton do not undergo microphysical interactions and so do not suffer wet deposition. Reactive gases such as iodine can be absorbed into and desorbed from cloud drops depending on their relative concentrations in air and in cloud water. Once in solution they may undergo chemical reactions to other species, allowing the absorption of more gas from air until the solution in the cloud drop has reached saturation. Particulates are classified either as hygroscopic or hydrophobic, the essential difference being that the hygroscopic particles may act as cloud condensation nuclei whereas hydrophobic particles cannot. Both types of particle can be collected by falling raindrops, rather in the manner that cloud droplets are swept out. For all types of pollutants, their transport through the atmosphere will be affected by the large scale dynamic motions present in storm systems. It is the cumulative effect of all these processes which leads ultimately to wet deposition and which is described in the washout model by a single rate coefficient, Λ.

1.3 Structure of thesis

The aim of this thesis is to analyse the effects on reactor accident consequences of the physical and chemical processes operating in storms. These effects are analysed within the framework of consequence analysis that is established in Chapter 2. The severity of accidents are characterized using emergency reference levels by calculating areas where they are exceeded and within which appropriate action is necessary. The specification of accidental releases and the modelling of the dispersion and deposition of released material and resulting dose commitments are discussed. Wet deposition is simulated by the washout model. This is replaced in Chapter 6 by the storm models developed in the intervening chapters, so that the importance of modelling cloud processes for consequence assessment can be investigated. The formulation of the basic cloud model is developed in Chapter 3 from conservation principles and is applied in one spatial dimension to scavenging of particulate materials. Scavenging of gaseous materials is considered in Chapter 4. This involves studying the chemistry of uptake of gases by drops and subsequent aqueous phase reactions. The model is extended to two dimensions in Chapter 5 where it is applied to the three types of precipitation system; orographic, frontal and convective. The limitations of the cloud modelling described in this thesis and recommendations for further improvements are discussed in the concluding chapter.

2 Nuclear Accident Consequence Analysis

2.1 Introduction

Following a nuclear power station accident, wet deposition is likely to be associated with many of the most severe consequences felt away from the immediate vicinity of the release. The total dose commitment to the affected population is often calculated, but the patchy nature of precipitation may cause some areas to receive much higher doses than the average for the country or region. These areas can be identified as those for which specified levels of dose are exceeded. Levels at which it is recommended that action to protect the population should be taken, known as emergency reference levels, have been set by the International Commission for Radiological Protection (I.C.R.P.). In this chapter, these are used to investigate the possible consequences resulting from a range of nuclear accident types.

In section 2.2, the techniques which are used to analyse the consequences of nuclear accidents are described. The analysis involves several stages. Firstly, release scenarios are specified. Secondly, the dispersion of released material and its removal to ground by deposition are simulated. Finally the uptake of radionuclides by people, either directly or via the foodchain, is modelled in order to calculate the doses received by the affected population. Results are discussed in section 2.3 for hypothetical degraded core and design basis accidents and for the accident at Chernobyl.

Of the many varieties of nuclear power plant operating around the World, the most common are pressurised water reactors (PWRs). They are of particular relevance to nuclear power safety in Britain. Following a public enquiry, Britain's first commercial PWR is being built at Sizewell in Suffolk to be followed by a series of further PWR stations. Furthermore a

string of PWRs on the North coast of France is important in the context of accidental releases especially for Southern England. For instance, Gravelines PWR near Calais is only 30 kilometres further away from London than Sizewell. Hypothetical accidents leading to large releases were specified for the Sizewell enquiry and are discussed in section (2.3.1). These are compared with less severe accidents to both PWRs and gas cooled Magnox reactors which have a higher probabilty of occurrence. Finally the accident at Chernobyl is discussed. Here a substantial release of radionuclides, caused by a combination of operator errors and design faults, dispersed over Russia, Scandinavia and Europe.

Dispersion of released material is modelled using the Gaussian plume treatment, a semi-empirical model which does not include along wind dispersion. Dry deposition, in which pollutant is removed at the ground without being associated with precipitation, is included. Wet deposition is simulated using the standard washout model. In this manner, nuclear accident release inventories and their dipsersion and deposition which together constitute release scenarios are modelled and their consequences evaluated.

2.2 Modelling Theory

2.2.1 Accidental releases

For the Sizewell enquiry, the Central Electricity Generating Board specified hypothetical accidents to a PWR with inventory given in table(2.1). These were based on an analysis carried out by Westinghouse in which they identified a wide spectrum of accident sequences. Those leading to a degraded core were grouped into twelve categories called UK1 to UK12, each with an assigned frequency of occurrence and with a particular release pattern of radioactive material. They are summarised in table(2.2).

Table 2.1 Inventory of radionuclides for PWR (from Clarke, 1979)

Nuclide	Inventory (Bq)	Half-life	Nuclide	Inventory (Bq)	Half-life
^{58}Co	3.08 10^{16}	70.8 d	^{131m}Te	3.47 10^{17}	30.0 h
^{60}Co	1.14 10^{16}	5.27 y	^{132}Te	4.85 10^{18}	78.2 h
^{85}Kr	2.17 10^{16}	10.7 y	^{131}I	3.39 10^{18}	8.04 d
^{85m}Kr	9.25 10^{17}	4.48 h	^{132}I	4.96 10^{18}	2.30 h
^{87}Kr	1.70 10^{18}	76.3 min	^{133}I	6.81 10^{18}	20.8 h
^{88}Kr	2.34 10^{18}	2.84 h	^{134}I	7.84 10^{18}	52.6 min
^{86}Rb	7.96 10^{15}	18.6 d	^{135}I	6.40 10^{18}	6.61 h
^{89}Sr	3.37 10^{18}	50.5 d	^{133}Xe	6.85 10^{18}	5.25 d
^{90}Sr	1.75 10^{17}	29.1 y	^{135}Xe	1.67 10^{19}	9.09 h
^{91}Sr	4.37 10^{18}	9.48 h	^{134}Cs	3.85 10^{17}	2.06 y
^{90}Y	1.82 10^{17}	2.67 d	^{136}Cs	1.33 10^{17}	13.2 d
^{91}Y	4.51 10^{18}	58.6 d	^{137}Cs	2.29 10^{17}	30.0 y
^{95}Zr	5.88 10^{18}	65.5 d	^{140}Ba	6.14 10^{18}	12.7 d
^{95}Nb	5.81 10^{18}	35.1 d	^{140}La	6.32 10^{18}	40.3 h
^{97}Zr	5.88 10^{18}	16.9 h	^{141}Ce	5.92 10^{19}	32.5 d
^{99}Mo	6.44 10^{18}	66.02 h	^{143}Ce	5.44 10^{18}	33.0 h
^{99m}Tc	5.55 10^{18}	6.02 h	^{144}Ce	3.59 10^{18}	285 d
^{103}Ru	5.25 10^{18}	39.4 d	^{143}Pr	5.40 10^{18}	13.6 d
^{105}Ru	3.51 10^{18}	4.44 h	^{147}Nd	2.36 10^{18}	11.0 d
^{105}Rh	3.18 10^{18}	1.47 d	^{239}Np	7.32 10^{19}	2.36 d
^{106}Ru	1.30 10^{18}	368 d	^{238}Pu	3.17 10^{15}	87.7 y
^{127}Sb	2.93 10^{17}	3.89 d	^{239}Pu	1.11 10^{15}	2.41 10^{4} y
^{129}Sb	9.95 10^{17}	4.31 h	^{240}Pu	1.06 10^{15}	6550 y
^{127}Te	2.85 10^{17}	9.35 h	^{241}Pu	3.21 10^{17}	14.4 y
^{127m}Te	4.37 10^{16}	109 d	^{241}Am	2.06 10^{14}	432 y
^{129}Te	9.40 10^{17}	69.6 min	^{242}Cm	6.62 10^{16}	163 d
^{129m}Te	1.67 10^{17}	33.6 d	^{244}Cm	2.75 10^{15}	18.1 y

Table 2.2 Release categories and their characteristic parameters (from Clarke, 1979)

Release category	Frequency of occurrence (y^{-1})	Time before release[1] (h)	Duration of release (h)	Energy of release (10^6 Btu/h)	Elevation of release (m)	Warning time[2] (h)	Fraction of core inventory released to environment[3]							
							Xe-Kr	Organic I	Inorganic I-Br[4]	Cs-Rb	Te-Sb	Ba-Sr	Ru[5]	La[6]
1	2.4 10^{-6}	1	3	0.3	10	0	9 10^{-1}	7 10^{-1}	7 10^{-1}	3 10^{-1}	3 10^{-1}	6 10^{-3}	2 10^{-3}	4 10^{-3}
2	4.0 10^{-10}	1	0.5	20	10	0	9 10^{-1}	6 10^{-3}	7 10^{-1}	4 10^{-1}	3.5 10^{-1}	5 10^{-3}	2 10^{-3}	3 10^{-3}
3	2.4 10^{-6}	1	0.5	20	10	0	8 10^{-1}	6 10^{-3}	6 10^{-1}	6 10^{-1}	1 10^{-1}	8 10^{-3}	2 10^{-3}	2 10^{-3}
4	5.0 10^{-10}	2	1	6	10	1	8 10^{-1}	6 10^{-3}	3 10^{-1}	2 10^{-1}	2.5 10^{-1}	2 10^{-3}	1.5 10^{-3}	3 10^{-3}
5	8.0 10^{-6}	8	0.5	20	10	4	1 10^{0}	7 10^{-3}	6 10^{-2}	3 10^{-1}	3 10^{-1}	4 10^{-3}	3 10^{-3}	6 10^{-3}
6	4.2 10^{-6}	12	0.5	20	10	8	9 10^{-1}	6 10^{-3}	9 10^{-1}	2 10^{-1}	4 10^{-2}	2 10^{-3}	7 10^{-3}	7 10^{-3}
7	1.2 10^{-6}	1	0.5	20	10	0	8 10^{-1}	6 10^{-3}	8 10^{-3}	2 10^{-3}	4 10^{-5}	3 10^{-5}	8 10^{-5}	8 10^{-5}
8	2.8 10^{-10}	5	0.5	0.3	10	4	8 10^{-1}	6 10^{-3}	6 10^{-3}	5 10^{-5}	1 10^{-5}	7 10^{-7}	2 10^{-7}	2 10^{-6}
9	3.2 10^{-6}	2	10	0	0	1	3 10^{-1}	2 10^{-3}	8 10^{-4}	8 10^{-5}	1 10^{-3}	9 10^{-5}	7 10^{-5}	1 10^{-5}
10	4.2 10^{-6}	2	10	0	0	1	6 10^{-3}	2 10^{-5}	2 10^{-5}	1 10^{-5}	2 10^{-5}	1 10^{-5}	1 10^{-5}	2 10^{-7}
11	6.2 10^{-7}	2	long[7]	0	10	1	6 10^{-2}	3 10^{-5}	3 10^{-5}	3 10^{-5}	3 10^{-5}	3 10^{-5}	2 10^{-5}	4 10^{-7}
12	5.1 10^{-7}	2	long[7]	0	10	1	5 10^{-3}	3 10^{-5}	8 10^{-5}	1 10^{-5}	2 10^{-7}	1 10^{-7}	4 10^{-9}	6 10^{-9}

Also associated with each accident are release duration, energy and height. These parameters are needed to calculate the dispersion of the release.

Two much less severe accidents considered are a PWR design basis accident and a Magnox single channel melt and depressurisation accident. Their release inventories are given in tables(2.3) and (2.4) respectively. They are assumed to have a one hour duration of release and the same energy and elevation of release as UK1.

The World's largest nuclear power station accident took place at Chernobyl in 1986. By analysing the pattern of contamination it is possible to make an assessment of the quantities of particular radionuclides released. ApSimon et al(1987) used the MESOS numerical long range transport model to simulate the dispersal of radioactivity across Europe. By comparing measured depositions against model results they were able to make an estimate of the fraction of the ^{131}I and ^{137}Cs inventories released. These results could be compared with the values presented by the Soviet authorities at the IAEA meeting in Vienna in August, 1986. The release patterns used to model the Chernobyl accident are discussed further in section 2.3.3.

2.2.2 Dispersion

In modelling the dispersal of released material the recommendations of the Working Group on Atmospheric Dispersion were followed (Clarke, 1979). This was a group set up to review developments in atmospheric dispersion modelling and provide practical guidance on modelling of dispersion of radioactive releases to the atmosphere. They recommended that to represent a release of radioactive material from an isolated stack and its subsequent dispersion over land in constant meteorological conditions, a Gaussian plume diffusion model should be used. This is a semi-empirical treatment which provides a fairly easy calculation of plume

Table 2.3 Source term for a PWR design basis accident (from Taylor, 1986)

Nuclide	Activity released (Bq)
^{131}I	$1.85.10^{12}$
^{132}I	$5.18.10^{12}$
^{133}I	$8.14.10^{12}$
^{134}I	$6.29.10^{12}$
^{135}I	$3.63.10^{12}$
^{134}Cs	$2.15.10^{11}$
^{137}Cs	$2.70.10^{11}$
^{85m}Kr	$1.07.10^{11}$
^{85}Kr	$2.55.10^{9}$
^{87}Kr	$9.25.10^{10}$
^{88}Kr	$1.07.10^{11}$
^{131m}Xe	$2.33.10^{10}$
^{133m}Xe	$2.78.10^{10}$
^{135m}Xe	$9.25.10^{10}$
^{133}Xe	$1.48.10^{12}$
^{135}Xe	$3.40.10^{11}$
^{138}Xe	$4.07.10^{11}$

Table 2.4 Source term for a Magnox single channel melt and depressurisation accident (from Taylor, 1986)

Nuclide	Activity released (Bq)
^{85}Kr	$3.22.10^{12}$
^{88}Kr	$3.04.10^{14}$
^{89}Sr	$4.10.10^{11}$
^{90}Sr	$2.64.10^{10}$
^{103}Ru	$6.01.10^{12}$
^{106}Ru	$1.63.10^{12}$
^{129m}Te	$3.13.10^{12}$
^{132}Te	$5.61.10^{13}$
^{131}I	$3.85.10^{13}$
^{132}I	$5.69.10^{13}$
^{133}I	$8.20.10^{13}$
^{135}I	$7.64.10^{13}$
^{133}Xe	$8.21.10^{14}$
^{138}Xe	$6.82.10^{14}$
^{137}Cs	$3.37.10^{12}$
^{140}Ba	$7.10.10^{11}$

dispersal not allowed by the more complicated models which represent better the physical processes of turbulent diffusion.

The distribution is characterized by standard deviations σ_y, σ_z in the horizontal and vertical directions respectively. It is given by

$$C(x,y,z) = \frac{Q}{2\pi u_{10}\sigma_y\sigma_z} \exp\left(-\frac{1}{2}\left(\frac{y^2}{\sigma_y^2} + \frac{(z-h)^2}{\sigma_z^2}\right)\right). \qquad (2.1)$$

In this expression, Q represents either the total ammount released (units Bq) or the release rate (Bq/s). Correspondingly C represents time integrated air concentration in the former case (Bqs/m^3) or air concentration in the latter (Bq/m^3). u_{10} is the wind speed at 10m above the ground(m/s) and h is the height of the release.

It is necessary to take account of a plume from an elevated source reaching the ground below and an inversion layer above, between which it will be trapped. It is sufficient to regard the plume as being reflected from ground and inversion layer, at height A,to produce virtual sources at heights

$$z = -h \text{ and } z = \pm 2mA \pm h \qquad (m = 1, 2, 3, \ldots\ldots)$$

and hence an expression for the air concentration for $\sigma_z < A$;

$$C(x,y,z) = \frac{Q}{2\pi u_{10}\sigma_y\sigma_z} \exp\left(-\frac{y^2}{2\sigma_y^2}\right) F(h, z, A). \qquad (2.2)$$

where

$$F(h, z, A) = \exp\left(\frac{-(z-h)^2}{2\sigma_z^2}\right) + \exp\left(\frac{-(z+h)^2}{2\sigma_z^2}\right) \qquad (2.3)$$

$$+\exp\left(\frac{-(2A+z-h)^2}{2\sigma_z^2}\right)+\exp\left(\frac{-(2A-z+h)^2}{2\sigma_z^2}\right)$$

$$+\exp\left(\frac{-(2A+z+h)^2}{2\sigma_z^2}\right)+\exp\left(\frac{-(2A-z-h)^2}{2\sigma_z^2}\right)$$

taking the first six terms for F(h, z, A). Once the vertical dispersion, σ_z, becomes greater than the depth of the boundary layer, the vertical concentration distribution effectively becomes uniformly distributed throughout the mixing layer. Here

$$C(x,y,z)=\frac{Q}{\sqrt{2\pi}\,u_{10}\,A\,\sigma_y}\exp\left(\frac{-y^2}{2\sigma_y^2}\right). \qquad (2.4)$$

Meteorological conditions have been classified by Pasquill(1961) into 6 categories, A - F, in order of increasing atmospheric stability. Typical values of 10m wind speed, u_{10}, and mixing layer depth, A, for these stability categories are given in table(2.5).

The vertical standard deviation of the cloud, σ_z, at a given distance from the source, x, is a function of atmospheric stability, downwind distance and ground roughness. Hosker(1974) derived an analytic formula for σ_z in each stability category given by

$$\sigma_z=\frac{a\,x^b}{1+c\,x^d}\,f(z_0,x) \qquad (2.5)$$

where

$$f(z_0,x)=\ln\left(f\,x^g\left(1+(h\,x^j)^{-1}\right)\right) \quad \text{if } z_0 \geq 0.1\text{ m} \qquad (2.6)$$

and

$$f(z_0,x)=\ln\left(f\,x^g\left(1+(h\,x^j)\right)^{-1}\right) \quad \text{if } z_0 < 0.1\text{ m} \qquad (2.7)$$

Table 2.5 Typical values of wind speed and depth of mixing layer (from Clarke, 1979)

Stability category	Typical wind speed at 10m (m/s)	Typical mixing layer depth (m)
A	1	1300
B	2	900
C	5	850
D	5	800
E	3	400
F	2	100

and the appropriate values of a,b,c,d,f,g,h,j for stability categories A - F are given in table (2.6). To simplify calculation, a value for the roughness length, z_0, of 0.1m was chosen.

For along-wind distances of up to 100km, the dispersion of the plume in the horizontal plane with horizontal standard deviation, σ_y, can be regarded as a result of turbulent diffusion with standard deviation σ_{yt} and wind direction fluctuations with standard deviation σ_{yw}. The expression for σ_y given by

$$\sigma_y^2 = \sigma_{yt}^2 + \sigma_{yw}^2 \tag{2.8}$$

is due to Moore(1976). The expression for σ_{yw} used is

$$\sigma_{yw} = 0.065\ x/(7\,T/u_{10})^{1/2}\ . \tag{2.9}$$

and is discussed more fully in the first report of the Working Group (Clarke, 1979). The expression for σ_{yt} is derived from a graph of values calculated by Gifford(1968) given in the first report and plotted against x for each stability category. The graphs plotted on log-log paper are very nearly straight lines and so

$$\sigma_{yw} = \exp(k_1 \ln x + k_2) \tag{2.10}$$

can be written where the gradient k_1 has the value 0.933 for all stability categories A - F and the intercept is given in table(2.7).

For distances greater than 100 km, the fourth report of the Working Group on Atmospheric Dispersion (Jones,1981b) recommends a model for modelling atmospheric dispersion which is not constrained to be a

Table 2.6 Coefficients given by Hosker(1974) to derive the vertical standard deviation of the plume for various stability categories (from Clarke, 1979)

Stability Category	a	b	c	d
A	0.112	1.06	$5.38.10^{-4}$	0.815
B	0.130	0.950	$6.52.10^{-4}$	0.750
C	0.112	0.920	$9.05.10^{-4}$	0.718
D	0.098	0.889	$1.35.10^{-3}$	0.688
E	0.0609	0.895	$1.96.10^{-3}$	0.684
F	0.0638	0.783	$1.36.10^{-3}$	0.672

Roughness correction factor coefficients	f	g	h	j
z_0 = 0.1 m	2.72	0	0	0

Table 2.7 Coefficients in expression for standard deviation of lateral dispersion

Stability category	A	B	C	D	E	F
k_2	-1.147	-1.434	-1.744	-2.197	-2.533	-3.011

continuous extension of the original model which is most applicable for distances up to 100km. Plume width θ is defined as

$$\theta = \theta_t + \theta_w \tag{2.11}$$

where θ_t is the width due to turbulent spreading given by

$$\theta_t = x^{-0.16} \tag{2.12}$$

and θ_w is the width due to systematic changes of wind direction. Probabilities are calculated that θ_w is less than a given angle as a function of release duration and distance from the source averaged over all weather conditions. The angle less than that experienced by 68% of trajectories is

$$\theta_w = (T/12 \, (x / 5.10^5)^{-0.125} (0.6)) \tag{2.13}$$

where T is the duration of the release in hours. The expression

$$\begin{aligned} \theta &= \theta_w + \theta_t \\ &= (T/12 \, (x/5.10^5)^{-0.125} (0.6) + x^{-0.16}) \end{aligned} \tag{2.14}$$

was used to evaluate σ_y from

$$\sigma_y = x \tan (\theta/2). \tag{2.15}$$

This new value for σ_y was employed in the Gaussian plume diffusion model at distances greater than 100km.

Effective source height h includes plume rise dh, so that $h = h_c + dh$ where h_c is the height of the release. This has been calculated by employing the

formulae proposed by Briggs(1972). In neutral conditions,

$$h_c = \frac{1.6\, F_b^{1/3} x_f^{2/3}}{u} \qquad (2.16)$$

where F_b is the buoyancy flux, x_f is the distance at which plume rise stops and u is wind speed at the average height of the plume. The approximation due to Briggs is made that

$$x_f = 10\, h_c. \qquad (2.17)$$

In stable conditions,

$$h_c = 2.6 \left(\frac{F_b}{u\, s'}\right)^{1/3} \qquad (2.18)$$

where s' is a stability parameter. This is discussed further by Jones(1983). Allowance is made for plume spread due to the plume rise,h_c, by altering vertical standard deviation to

$$\sigma_z^2 = \sigma_{zd}^2 + h_c^2/12. \qquad (2.19)$$

2.2.3 Deposition

2.2.3.1 Dry deposition

Dry deposition of pollutant results from its transport to the vicinity of the ground surface by turbulent eddies in the air followed by crossing of the surface layers by a variety of processes depending on the form of the pollutant. A detailed review of these effects has been provided by Underwood(1983a). Dry deposition can be characterized by a deposition velocity, v_g, defined as the ratio of downward flux of pollutant to ground to

the concentration in air at ground level, C. Thus the dry deposition rate D_d is given by

$$D_d = v_g C. \tag{2.20}$$

Dry deposition is incorporated into the Gaussian plume by using a source depletion model. In this model, loss of pollutant material is felt uniformly throughout the cloud, leaving the Gaussian vertical profile unaltered. This is simulated by assuming that the effective source strength, Q, is reduced to a modified source strength, Q^*, given by

$$Q^* = Q\,(\exp(F_d(x)))^{v_g/u} \tag{2.21}$$

where

$$F_d(x) = -\sqrt{\frac{2}{\pi}} \int_0^x dx' \frac{1}{\sigma_z} \left(\exp\left(\frac{-h^2}{2\sigma_z^2}\right) + \exp\left(\frac{-(h+2A)^2}{2\sigma_z^2}\right) + \exp\left(\frac{-(h-2A)^2}{2\sigma_z^2}\right)\right) \text{ if } \sigma_z < A \tag{2.22}$$

and

$$F_d(x) = F_d(x_c) - \frac{x - x_c}{A} \qquad \text{if } \sigma_z \geq A \tag{2.23}$$

in which $\sigma_z(x_c) = A$.

2.2.3.2 Wet Deposition

The washout model involves the assumption that a certain fraction, Λ, of pollutant material in air is deposited instantaneously at the ground each second in precipitation. Λ is known as the washout coefficient and is expressed mathematically as

$$\Lambda(x,y) = \frac{D_r(x,y)}{\int C(x,y,z)\,dz} \tag{2.24}$$

where D_r is the wet deposition rate.

The total ammount of material, Q', remaining in a Gaussian plume with continuous rainfall at a constant rate is then given by

$$\frac{dQ'}{dt} = -\Lambda Q' \ . \tag{2.25}$$

In a rainband between distances x_0 and x_1 the effective source strength Q'_w due to wet deposition is

$$Q'_w = \begin{cases} Q & \text{for } 0 \le x \le x_0 \\ Q\,e^{-\Lambda(x-x_0)}\,1/u & \text{for } x_0 \le x \le x_1 \\ Q\,e^{-\Lambda(x_1-x_0)}\,1/u & \text{for } x_1 \le x. \end{cases} \tag{2.26}$$

Activity concentration in air is calculated from equations(2.2) and (2.4) with Q replaced by Q^* to include depletion due to dry deposition and Q replaced by $Q^* Q'_w / Q$ to include both dry and wet deposition. Thus

$$C(x,y,z) = \frac{Q^* Q'_w}{2\pi\sigma_y\sigma_z u_{10} Q} \exp\left(\frac{-y^2}{2\sigma_y^2}\right) F(h,z,A) \quad \text{if } \sigma_z < A \tag{2.27}$$

and

$$C(x,y,z) = \frac{Q^* Q'_w}{\sqrt{2\pi}\,A\,u_{10}\,\sigma_y\,Q} \exp\left(\frac{-y^2}{2\sigma_y^2}\right) \quad \text{if } \sigma_z \ge A \tag{2.28}$$

Dry deposition rate is given by

$$D_d(x,y) = v_g\ C(x,y,z=0) \tag{2.29}$$

and wet deposition rate by

$$D_r(x,y) = \frac{\Lambda Q^* Q'_w}{\sqrt{2\pi}\ u_{10}\ \sigma_y\ Q} \exp\left(\frac{-y^2}{2\sigma_y^2}\right). \tag{2.30}$$

2.2.4 Emergency reference levels and dose commitments

Emergency reference levels

The emergency reference levels (ERLs) considered are given in table (2.8). These have been set by the International Commission for Radiological Protection. A wide range of actions is considered from restriction of milk supplies, which occurred following the Windscale fire in 1957, to evacuation, which was carried out in the close-in region of Chernobyl.

Conversion of emergency reference level dose rates to depositions

The National Radiological Protection Board have developed models for the transfer of radionuclides through the foodchain and into the body. Using these models it was possible to make conversions from ERLs to their corresponding depositions for the pathways of interest (ingestion of milk, inhalation of ground gamma radiation) by referring to the relevant tables set out in the NRPB reports on DOSE-MARC (Charles et al,1982) and FOOD-MARC (Linsley et al,1982). The deposition calculated for each particular pathway was then related to the reference level deposition for a unit release of each of the accidents under consideration. In all cases considered here, the dose due to deposition of the release from a particular accident is dominated by a small number of radionuclides. It is therefore necessary simply to calculate the reference level deposition using data for

Table 2.8 Emergency reference levels and counter measures as recommended by the International Commission for Radiological Protection

Dose(mSv)	Pathway	Action
5	Ingestion of milk	Restriction of milk
5	Inhalation of ground gamma	Consideration should be given to sheltering
25	Inhalation of ground gamma	Sheltering should have started
100	Inhalation of ground gamma	Consideration should be given to evacuation
500	Inhalation of ground gamma	Evacuation should have started

those radionuclides identified as being significant. Sample calculations are given in appendix(B).

2.3 Results and discussion

For the hypothetical accidents, the dry deposition velocities used were those used by Kelly and Clarke(1982) in their consequence assessment for a PWR at Sizewell. They are 10^{-2} m/s for inorganic iodine and 10^{-3} m/s for elements which are all in particulate form such as caesium. For the Chernobyl accident the deposition velocities used in the MESOS analysis of the accident were chosen(ApSimon et al,1987). They are 3.10^{-3} m/s for iodine and 10^{-3} m/s for caesium. The washout coefficient for all accidents was defined by the empirical relation

$$\Lambda = \Lambda^0 J^{0.8} \tag{2.31}$$

where J is the precipitation rate in mm/hr and $\Lambda^0 = 5.10^{-5}$.

2.3.1 Serious PWR accidents

The consequences of releases from the PWR accidents UK1-8 dispersing in dry conditions are illustrated in tables(2.9) and (2.10). The distances downwind along the peak of the Gaussian distribution and the areas for which the 5mSv restriction of milk ERL would be exceeded in category D conditions are given in table(2.9) for the eight accidents. Table(2.10) gives distances and areas for the 500mSv ground gamma ERL at which evacuation is recommended. It is clear from these results that the most serious accidents contaminate very large areas. The distance, $1.3.10^6$m, in table(2.9) for UK1 would represent a threat to the milk supplies of Rome due to a degraded core at Sizewell in a steady Northerly wind. This certainly represents an upper limit since not only is the wind assumed constant for such a long travel time but the emergency reference level is calculated for

Table 2.9 Patterns of contamination for serious PWR accidents, ERL of 5mSv whole body dose equivalent due to ingestion of milk, no rain

	UK1	UK2	UK3	UK4	UK5	UK6	UK7	UK8
Distance (m)	$1.3.10^6$	$1.6.10^6$	$1.5.10^6$	$1.1.10^6$	$7.9.10^5$	$3.4.10^5$	$3.1.10^5$	$2.6.10^5$
Area (m^2)	$3.8.10^{11}$	$2.8.10^{11}$	$2.6.10^{11}$	$1.5.10^{11}$	$6.3.10^{10}$	$1.0.10^{10}$	$8.6.10^9$	$6.0.10^9$

Table 2.10 Patterns of contamination for serious PWR accidents, ERL of 500mSv whole body dose equivalent due to inhalation of ground gamma radiation, no rain

	UK1	UK2	UK3	UK4	UK5	UK6	UK7	UK8
Distance (m)	$2.3.10^4$	$2.9.10^4$	$3.9.10^4$	$1.7.10^4$	$2.5.10^4$	$1.9.10^4$	$8.1.10^2$	0.0
Area (m^2)	$8.3.10^7$	$6.5.10^7$	$1.2.10^8$	$2.8.10^7$	$5.3.10^7$	$2.5.10^7$	$1.9.10^4$	0.0
Area evac (m^2)*	$1.2.10^8$	$1.4.10^8$	$1.0.10^8$	$5.1.10^7$	$8.1.10^7$	$1.8.10^7$	$8.0.10^6$	$7.5.10^6$

(* areas evacuated as calculated by Kelly and Clarke, 1982)

Table 2.11 Patterns of contamination for serious PWR accidents, ERL of 5mSv whole body dose equivalent due to ingestion of milk, 0.5 mm/hr rain from source

	UK1	UK2	UK3	UK4	UK5	UK6	UK7	UK8
Distance (m)	$4.8.10^5$	$5.2.10^5$	$5.0.10^5$	$4.2.10^5$	$3.6.10^5$	$2.4.10^5$	$2.3.10^5$	$2.0.10^5$
Area (m^2)	$6.5.10^{10}$	$4.4.10^{10}$	$4.1.10^{10}$	$3.2.10^{10}$	$1.8.10^{10}$	$6.9.10^9$	$6.3.10^9$	$3.7.10^9$

the peak of the Gaussian distribution. If the total under the distribution is averaged over a width of $\pm 3\sigma_y$, which contains 99% of the total, the height becomes 0.42 of its original peak value. This is equivalent to increasing the ERL 2.4 times. For UK1 in the same conditions as above this reduces the distance at which the 5mSv milk ERL is exceeded to 1000 km. This is still an extremely long distance reflecting the seriousness of UK1. Table(2.10) shows that the areas corrseponding to 500mSv whole body dose due to ground gamma inhalation are in broad agreement with the areas of land evacuated as calculated by Kelly and Clarke(1987) which lends confidence to the results of these calculations. UK1-6 result in evacuation of large areas; at least 25 km^2 and up to 120 km^2 for UK3.

Wet deposition was included so as to investigate the possible change to areas exceeding emergency reference levels due to precipitation. A steady drizzle of 0.5 mm/hr affecting all the plume causes the distance downwind at which the 5mSv ERL for milk is exceeded to decrease (see table (2.11)). In the case of UK1 the distance is more than halved from 1300km to 480km. Rain is washing more pollutant out of the plume early on in its travel and so there is less available to be dispersed to further distances. However if the plume encounters precipitation for the first time late on in its travel this may result in the distance at which an ERL is exceeded being considerably increased. An illustration of this is given in figure(2.1). Here for the UK1 accident the 5mSv ERL for milk is exceeded out to a distance of 1300km in the absence of precipitation. With only a moderate fall of 2.5 mm/hr the ERL may be exceeded at 1900km. Another example is illustrated in fig (2.2). The 500mSv ground gamma ERL, the level at which ICRP recommends that evacuation should take place, is exceeded up to 20 km for UK1 in the absence of precipitation (see table (2.10)). This distance may be increased up to 100 km if there is 2.5 mm/hr precipitation at that distance.

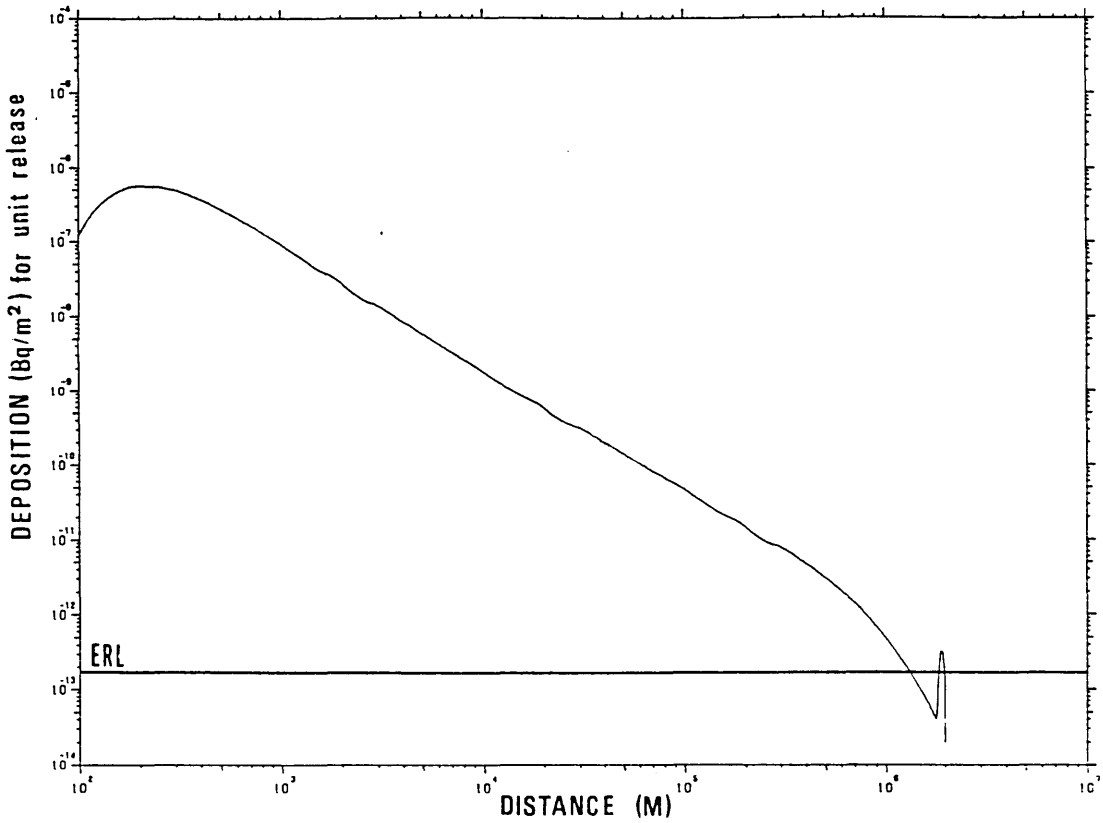


Figure 2.1 Distances out to which 5mSv ingestion of milk ERL is exceeded for UK1 accident

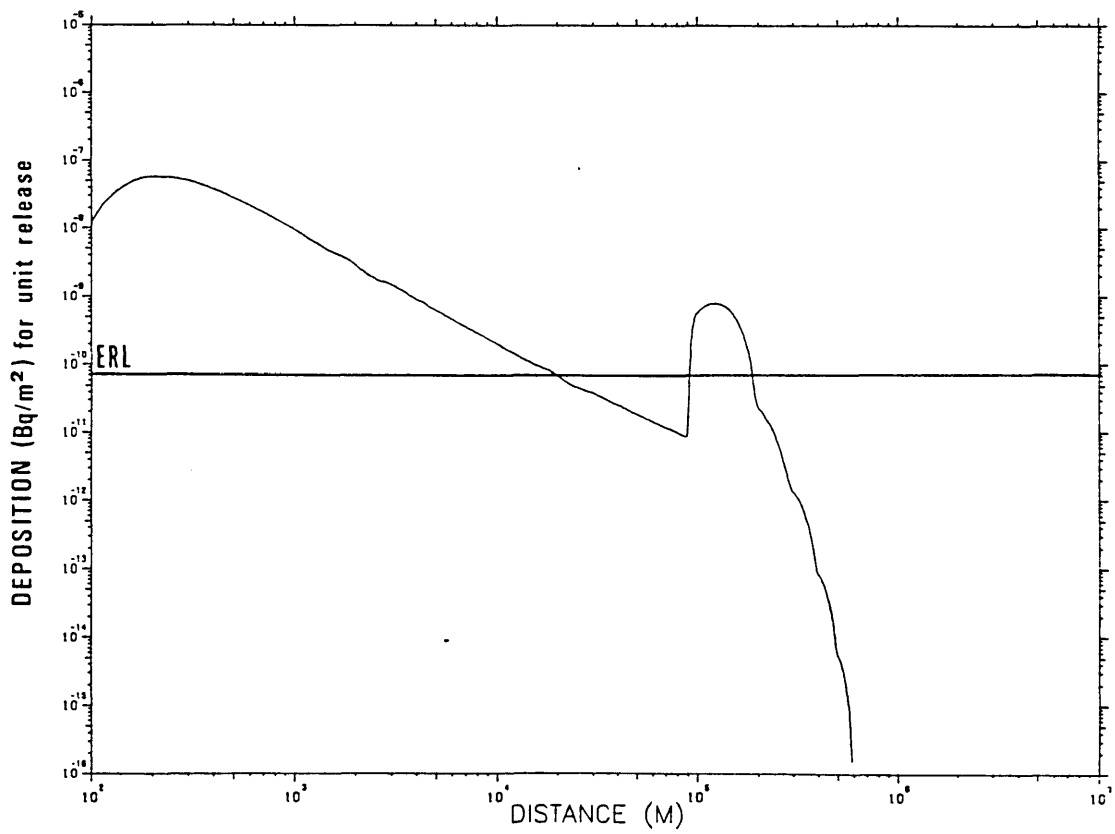


Figure 2.2 Distances out to which 500mSv inhalation of ground gamma ERL is exceeded for UK1 accident

2.3.2 PWR design basis and Magnox single channel melt and depressurisation accidents

These two much less severe accidents contaminate much smaller areas than the serious PWR accidents. Results are given in table(2.12) for the 5mSv restriction of milk ERL and in table (2.13) for the 5mSv whole body dose ground gamma ERL, the level at which the ICRP recommends that consideration should be given to sheltering. In the absence of rain, the 5mSv ingestion of milk ERL is exceeded no further than 540m for the PWR design basis accident and 3.1km for the Magnox accident. The 5mSv whole body dose equivalent due to ground gamma radiation, the level at which ICRP recommends consideration should be given to sheltering, is nowhere exceeded for either accident. It would appear that a PWR design basis accident would pose no threat to the general public outside the perimeter fence on a dry day.

This would still be the case if there was a light drizzle of 0.5 mm/hr. As shown in tables(2.14) and (2.15), the areas exceeding both the 5mSv restriction of milk and ground gamma emergency reference levels are little changed from the corresponding areas in dry conditions. However, a heavy storm in just the right place would change this picture. As shown in table(2.16), 25mm/hr of precipitation could cause the 5mSv milk ERL to be exceeded up to 2km from the release in a PWR design basis accident. There is a considerable increase in areas contaminated compared to the no-rain scenarios; for the PWR accident the area has increased twenty fold. There are also significant increases in the areas for the 5mSv ground gamma ERL. Table(2.17) shows that sheltering should be considered outside the perimeter fence of a PWR installation following a design basis accident in these conditions.

Table 2.12 Patterns of contamination for design basis accidents, ERL 5mSv whole body dose due to ingestion of milk, no rain

	PWR design basis	Magnox
Distance (m)	$5.4.10^2$	$3.1.10^3$
Area (m^2)	$2.5.10^4$	$1.1.10^6$

Table 2.13 Patterns of contamination for design basis accidents, ERL of 5mSv whole body dose due to ground gamma radiation, no rain

	PWR design basis	Magnox
Distance (m)	0	0
Area (m^2)	0	0

Table 2.14 Patterns of contamination for design basis accidents, ERL of 5mSv whole body dose due to ingestion of milk, 0.5 mm/hr rain from source

	PWR design basis	Magnox
Distance (m)	$6.1.10^2$	$4.1.10^3$
Area (m^2)	$3.5.10^4$	$1.8.10^6$

Table 2.15 Patterns of contamination for design basis accidents, ERL of 5mSv whole body dose due to ground gamma radiation, 0.5 mm/hr rain from source

	PWR design basis	Magnox
Distance (m)	0	$4.7.10^2$
Area (m^2)	0	$2.0.10^4$

Table 2.16 Patterns of contamination for design basis accidents, ERL of 5mSv whole body dose due to ingestion of milk, 25 mm/hr rain

	PWR design basis	Magnox
Rainfall rate	25 mm/hr from $5.4.10^2$ m	25 mm/hr from $3.08.10^3$ m
Distance (m)	$2.3.10^3$	$7.9.10^3$
Area (m^2)	$6.2.10^5$	$8.2.10^6$

Table 2.17 Patterns of contamination for design basis accidents, ERL of 5mSv whole body dose due to ground gamma radiation, 25 mm/hr rain from source

	PWR design basis	Magnox
Distance (m)	$1.7.10^3$	$3.3.10^3$
Area (m^2)	$2.8.10^5$	$1.4.10^6$

2.3.3 Chernobyl

The release from Chernobyl was simulated by using source terms calculated with the MESOS numerical long range transport model(ApSimon et al,1985). MESOS model results for air concentrations of the radionuclides ^{137}Cs and ^{131}I were compared with measurement (ApSimon et al, 1987). It was initially estimated that between 15 and 25 % of the ^{131}I and ^{137}Cs inventories had been released. This corresponded to 5 - 6 x 10^{16} Bq ^{137}Cs and 6 - 7.5 x 10^{17} Bq ^{131}I which agreed well with the values presented by USSR at the IAEA meeting in Vienna in August, 1986. The scenario adopted for the MESOS runs was that of a higher release persisting for the first two days reducing by a factor 3 on the 3rd day and a factor 10 on the fourth day. Therefore about 5/6 of the total is released over the first two days. This corresponds to approximately 4.10^{16} Bq ^{137}Cs and 5.10^{17} Bq ^{131}I.

Later, MESOS was used to make further estimates of the release(ApSimon and Wilson, 1987b). Source terms for ^{137}Cs, ^{131}I and ^{103}Ru were derived by using results from MESOS in multiple linear regression onto observations of air concentrations. The quantities calculated are the fractions of the release capable of being transported over long distances since only data from outside USSR were used. For the first 48 hours of the release (21-00 25/4 - 21-00 27/4) it was estimated that $1.4.10^{16}$ - $2.0.10^{16}$ Bq ^{137}Cs and $1.3.10^{17}$ - $2.3.10^{17}$ Bq ^{131}I were released.

Measurements were available for deposition of ^{137}Cs from the Chernobyl release over Sweden(Persson et al, 1987). It was therefore possible to assess the applicability of the modelling carried out by simulating the wet deposition of the Chernobyl release over Sweden. The approximate travel time for the release of 26 and 27th April to Sweden was two days and therefore wet deposition was associated with precipitation on 28 and 29th

April. Precipitation recorded over Sweden on these days is shown in figure(2.3). The maximum is 25 mm and a large area in Eastern Sweden exceeds 10mm.

In model runs the assumption was made that 12 hours of the release affected the area concerned. Precipitation rates chosen were 2 mm/hr and 1 mm/hr giving totals of 24mm and 12mm respectively. These correspond roughly to the two measured values quoted above. The latter source term estimates described above were used as these are appropriate to material capable of travelling long distances. The corresponding quantities released in 12 hours are $3.5.10^{15}$ to $5.0.10^{15}$ Bq ^{137}Cs. The peak value of the Gaussian profile is unrepresentative of the whole distribution. Instead the value averaged over ± 3 standard deviations of the median was taken. This is equivalent to 0.42 of the peak. The distance between the area of Sweden affected and Chernobyl is approximately 1300km. At this distance predictions of ^{137}Cs deposition for the two precipitation rates are shown in table(2.18). Comparison with measured depositions (see figure(2.4)) shows that agreement is fairly good. The peak measured deposition is 85 kBq/m^2. The area for which precipitation is greater than 10mm lies roughly within the area for which deposition is greater than 15 kBq/m^2. Although the model results agree broadly with measured depositions, there is a small region in Eastern Sweden where the concentrations of caesium in rain were considerably higher than predicted here using the washout model. This is discussed further in Chapter 6.

It should be noted that the decision to use 12 hours of the release in this calculation as compared to another figure is not significant. Provided the total quantity of precipitation remains unchanged, the deposition is virtually independent of the duration of release taken. For instance doubling the ammount released by increasing duration of release to 24

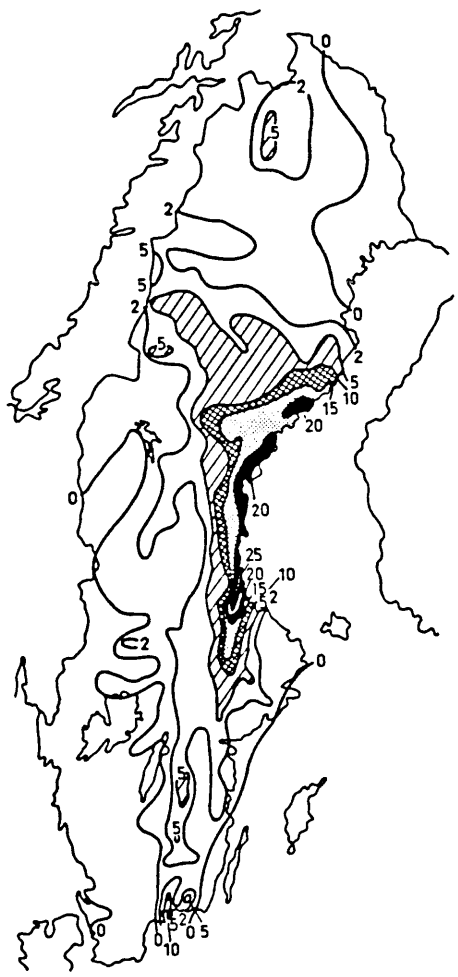


Figure 2.3 Recorded volumes of precipitation over Sweden for the period April 28 06 UTC to April 30 06 UTC(from Persson et al, 1987).

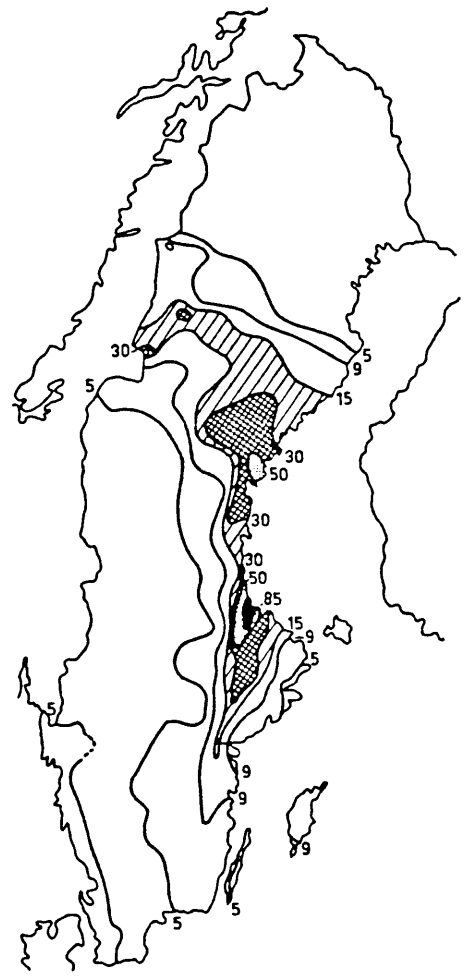


Figure 2.4 Estimated deposition of ^{137}Cs (kBq/m^{-2}) over Sweden(from Persson et al, 1987).

Table 2.18 Predicted total Cs deposition in Sweden(kBq/m^2)

Total ppn (mm)	12	24
Qty Cs released. (Bq)		
$3.5.10^{15}$	28.5	57.0
$5.0.10^{15}$	39.9	79.8

hours would require halving precipitation rate to 1mm/hr for a 24 mm total. Halving precipitation rate approximately halves deposition for a unit release. Therefore total deposited stays the same.

In order to assess the close-in consequences of the Chernobyl release, the first estimates for source terms described above were used. These agree well with values presented at the IAEA meeting in Vienna which were based on measurements made in USSR. 48 hours of the release were assumed to affect this area. As described earlier, for the initial estimates this corresponds to 5/6 of the total release. Without precipitation the 25mSv sheltering ERL due to ground gamma is exceeded out to 47 km but the 500mSv evacuation ERL is nowhere exceeded. Only a small quantity of precipitation changes this picture. In figure(2.5) variation of deposition with distance is shown. 2 mm/hr precipitation from 10 to 30 km causes the 500mSv ERL to be exceeded comfortably. It should be remembered that 2mm/hr for 48 hours represents a very high total of precipitation equal to 96mm. A more reasonable total of 12mm is equivalent to 0.25mm/hr for 48 hours. If this precipitation is present beyond 10kms from the source, the 500mSv evacuation ERL is exceeded out to 26km. In the event, the population was evacuated from a zone within a radius of 30km from the power station(Working document for Chernobyl post accident review meeting,1986). For the dose received due to ground gamma radiation, calculation with the Gaussian plume indicates that this was over cautious in completely dry conditions where only sheltering is strictly necessary. In fact, gravitational settling of coarse debris, which is not included in this treatment, gave greater deposition. In any case, only small quantities of precipitation would have justified evacuation due to deposition of the lighter particles alone.

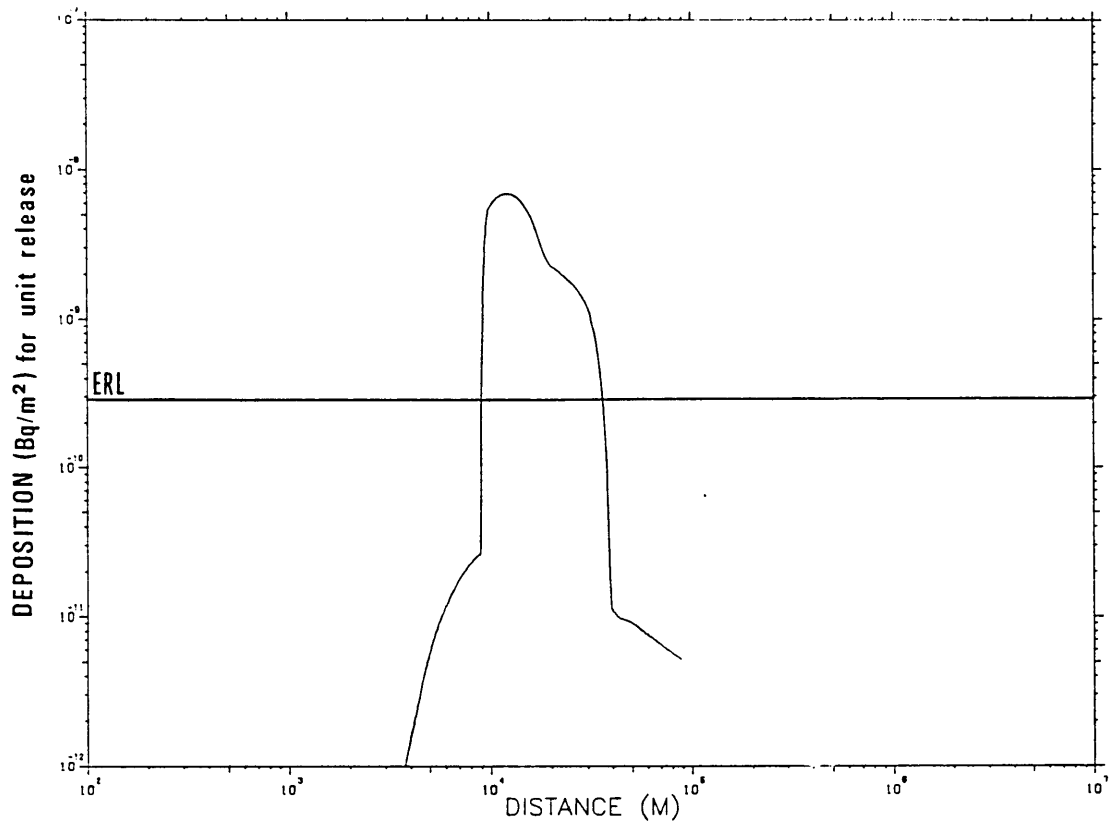


Figure 2.5 Comparison of modelled deposition from Chernobyl wtih 500 mSv inhalation of ground gamma ERL, 2 mm/hr precipitation rate from 10 to 30 km

2.4 Summary and conclusions

In this chapter, established techniques have been used to evaluate some of the possible consequences of nuclear accidents. Release scenarios for both hypothetical accidents and Chernobyl have been discussed. Dispersion modelling based on a Gaussian plume treatment has been employed with dry and wet deposition included. Wet deposition has been described by the traditional washout model. Levels of dose have been calculated using models of radionuclide uptake by plants and animals developed by the NRPB and these have been evaluated with reference to emergency reference levels recommended by the ICRP. It has been shown that for all the accidents considered, the interaction of precipitation with released material may cause major changes to areas exceeding particular ERLs as compared to dry conditions. Light precipitation may cause a decrease in the contaminated area by depleting the plume near to the source and allowing less material to travel to longer distances. Alternatively, heavy precipitation may cause an ERL to be exceeded that would otherwise not have been exceeded. If there is a large population affected, the consequences could be very serious and despite the low probability of occurrence could be significant in probabilistic risk assessment.

This modelling work also shows how the pattern of deposition is likely to be patchy. Where there is precipitation, radionuclides are removed more readily from the atmospheric boundary layer. The consequences to individuals affected by wet deposition may be very different to those people resident in areas which remained dry. Although the overall consequences felt by the total population may not be greatly changed by precipitation, there is likely to be significantly increased contamination felt by those individuals subject to precipitation. The incorporation of wet deposition is therefore crucial in determining the most severe consequences felt by subsections of the population.

There are problems with the techniques of modelling used here. The interaction of the washout model with a Gaussian plume leads to a sharp peak of deposition where the released material first encounters a band of precipitation. As shown by ApSimon and Simms(1987) this may give unrealistically high values of deposition. On the other hand, as discussed in chapter 1, the washout model may underestimate deposition in those circumstances in which rainout processes and concentration mechanisms are operative.

In the succeeding three chapters, more detailed models of the wet deposition of radionuclides, based more closely on the physics and chemistry of the processes in operation, are developed. These may subsequently be used to calculate wet deposition of dispersed material encountering storm systems. The techniques described in this chapter may then serve as the basis for the evaluation of accident consequences, with the washout model replaced by these storm models. This is considered in chapter 6.

3 1D Model

3.1 Introduction

The subject of cloud modelling owes much to the pioneering study of Kessler(1969) and the modelling described in this and the succeeding two chapters is no exception. Kessler developed a cloud model which was based on the conservation equations for air and water mass and he provided parametrisations for the microphysical processes involved, such as those which lead to the formation of cloud and rain. In order to study the motions and distributions of pollutant materials in storm systems, Kessler's one dimensional cloud model has been enhanced and extended to include the transport of aerosol and gaseous materials. In his study Kessler also described modelling in two dimensions. In chapter 5, the one dimensional model described in this chapter is extended to two dimensions rather differently, so as to describe better the dynamics found in various types of storm systems.

Modelling in 1D has dynamic limitations but it has some advantages over modelling in two or three dimensions. It is easier to gain an understanding of the importance of the microphysical processes involved without the distracting complications of working in higher dimensions. It is also considerably cheaper in computational resources, which allows more attention to be given to the sensitivity of results to the parameter values chosen.

In this chapter the 1D cloud model and the incorporation of particulate pollutants is discussed. First the model equations in their general form are derived from the basic conservation equations in section 3.2.1. These are reduced to their 1D form in section 3.2.2. The parametrisations used to describe the cloud microphysical processes are discussed in section 3.3.1

and cloud model runs and sensitivity studies are made in section 3.3.2. The incorporation of aerosol pollution into the model is described in section 3.4. In certain circumstances, convective storm systems can transport large quantities of pollutant from the boundary layer of the atmosphere to the upper troposphere. Therefore efficiencies with which storm systems both deposit material on the ground in rain and export material to the upper layers of the atmosphere are discussed.

3.2 Model Description

3.2.1 General Form

All mesoscale atmospheric models are founded on the principles of conservation of mass, heat, motion, water and other gaseous and aerosol materials. These have been derived from first principles by Pielke(1984) and can be expressed as follows.

Conservation of mass :

$$\frac{\partial \rho}{\partial t} + \underline{\nabla} . \rho \underline{V} = 0 . \tag{3.1}$$

Conservation of heat :

$$\frac{\partial \theta}{\partial t} + \underline{V} . \underline{\nabla} \theta = S_{\theta} . \tag{3.2}$$

Conservation of motion :

$$\frac{\partial \underline{V}}{\partial t} + \underline{V} . \underline{\nabla} . \underline{V} = - \frac{1}{\rho} \underline{\nabla} p - g \underline{k} - 2 \underline{\Omega} \Lambda \underline{V} . \tag{3.3}$$

Conservation of water :

$$\frac{\partial q_n}{\partial t} + \underline{V} . \underline{\nabla} q_n = S_{q_n} , \qquad n = 1, 2, 3. \tag{3.4}$$

Conservation of other gaseous and aerosol materials :

$$\frac{\partial \chi_m}{\partial t} + \underline{V} . \underline{\nabla} \chi_m = S_{\chi_m} , \qquad m = 1, 2....., M . \tag{3.5}$$

In equations (3.1) to (3.5), the symbols stand for the follwing

ρ : density of air

θ : potential temperature

S_θ : source/sink term for heat

$\underline{V}$: velocity of air

p : air pressure

g : acceleration due to gravity

$\underline{\Omega}$: angular velocity of rotation of Earth

$\underline{k}$: unit vector

q_1 : ratio of mass of solid form of water to mass of air in same volume

q_2 : ratio of mass of liquid form of water to mass of air in same volume

q_3 : ratio of mass of vapour form of water to mass of air in same volume

S_{qn} (n = 1,2,3) : source/sink terms for solid,liquid,vapour forms of water respectively

χ_m (m = 1,2,..,M): masses of other gaseous and aerosol material expressed in units of mass of substance to mass of air in same volume

$S_{\chi m}$ (m = 1,2,..,M): source/sink terms for gaseous and aerosol material

In fully dynamic models the full set of conservation equations is solved and the air motions arise as solutions. However in the modelling studies described here, air motions are predetermined and are provided as input to the model. As long as air motions satisfy the continuity equation(3.1), only the conservation equations for water(3.4) and pollutant material(3.5) need be solved.

Water and pollutant mass are reexpressed in units of mass of material per unit volume of air by defining variables Q_n ; n = 1,2,3 and P_m ; m = 1,2,..M, where

$$Q_n = \rho q_n \qquad n = 1, 2, 3 \tag{3.6}$$

$$P_m = \rho \chi_m \qquad m = 1, 2, ..., M. \tag{3.7}$$

Multiplying (3.1) by q_n gives

$$q_n \frac{\partial \rho}{\partial t} + q_n \underline{\nabla} . (\rho \underline{V}) = 0 \qquad (3.8)$$

and multiplying (3.4) by ρ gives

$$\rho \frac{\partial q_n}{\partial t} + \rho \underline{V} . \underline{\nabla} q_n = \rho S_{q_n} . \qquad (3.9)$$

Adding (3.8) and (3.9) gives

$$\frac{\partial}{\partial t} (\rho q_n) + \underline{\nabla} . (q_n \rho \underline{V}) = \rho S_{q_n} \qquad (3.10)$$

or

$$\frac{\partial Q_n}{\partial t} + \underline{\nabla} . (Q_n \underline{V}) = S_{Q_n} \quad , \qquad n = 1, 2, 3. \qquad (3.11)$$

Similarly (3.5) becomes

$$\frac{\partial P_m}{\partial t} + \underline{\nabla} . (P_m \underline{V}) = S_{P_m} \quad , \qquad m = 1, 2, ..., M. \qquad (3.12)$$

In warm colud (> 0^0 C), only the vapour and liquid forms of water are present. The approach of Kessler(1969) is taken here by splitting cloud water into a monodisperse population of cloud droplets that move with the air motions and a spectrum of rain drops that fall with terminal velocity V_t relative to the air. Thus in addition to the conservation equation for vapour

$$\frac{\partial Q_3}{\partial t} + \underline{\nabla} . (\underline{V} Q_3) = S_{Q_3} , \qquad (3.13)$$

there are two conservation equations for cloud water,

$$\frac{\partial Q_{2c}}{\partial t} + \underline{\nabla} . (\underline{V} Q_{2c}) = S_{Q_{2c}} \tag{3.14}$$

where Q_{2c} is mass of cloud droplets and

$$\frac{\partial Q_{2r}}{\partial t} + \underline{\nabla} . (\underline{V} Q_{2r}) = S_{Q_{2r}} \tag{3.15}$$

where Q_{2r} is mass of rain drops. In modelling calculations, a single variable is used to describe both saturation deficit and cloud droplet mass. This is given by q_c (in units mass of water per unit volume of air) and is defined by

$$q_c = Q_{2c} + Q_3 - Q_s \tag{3.16}$$

where Q_s is saturation vapour density. Thus if air is saturated

$$Q_3 = Q_s$$

$$q_c = Q_{2c} \geq 0$$

and if air is unsaturated

$$Q_{2c} = 0$$

$$q_c = Q_3 - Q_s < 0.$$

Adding (3.13) and (3.14) gives

$$\frac{\partial}{\partial t} (q_c + Q_s) + \underline{\nabla} ((q_c + Q_s) \underline{V}) = S_{Q_{2c}} + S_{Q_3} . \tag{3.17}$$

Assuming that saturation vapour density is a function of height only, i.e.

$$\frac{\partial Q_s}{\partial t} = \frac{\partial Q_s}{\partial x} = \frac{\partial Q_s}{\partial y} = 0 \tag{3.18}$$

leads to

$$\frac{\partial q_c}{\partial t} + \underline{\nabla} . (q_c \underline{V}) + \frac{\partial Q_s}{\partial z} w + Q_S \underline{\nabla} . \underline{V} = S_{Q_{2c}} + S_{Q_3} \tag{3.19}$$

where

$$\underline{V} = \begin{bmatrix} u \\ v \\ w \end{bmatrix} .$$

Now from (3.1) and assuming $\rho = \rho(z)$

$$0 = \rho \underline{\nabla} . \underline{V} + w \frac{\partial \rho}{\partial z} , \tag{3.20}$$

$$\underline{\nabla} . \underline{V} = - \frac{w}{\rho} \frac{\partial \rho}{\partial z} = - w \frac{\partial}{\partial z} \ln \rho . \tag{3.21}$$

Employing this in (3.19) gives

$$\frac{\partial q_c}{\partial t} + \underline{\nabla} . (q_c \underline{V}) = w (Q_S \frac{\partial}{\partial z} \ln \rho - \frac{\partial Q_S}{\partial z}) + S_{Q_{2c}} + S_{Q_3} . \tag{3.22}$$

The source/sink terms S_{Q2c}, S_{Q3} are

$$S_{Q2c} = - (\text{cloud -> rain}) + (\text{vapour -> cloud}) - (\text{cloud -> vapour}) ,$$
$$S_{Q3} = + (\text{rain -> vapour}) - (\text{vapour -> cloud}) + (\text{cloud -> vapour})$$

so that

$$S_{qc} = S_{Q2c} + S_{Q3} = - (\text{cloud -> rain}) + (\text{rain -> vapour}) . \tag{3.23}$$

Following Kessler(1969), the terms involving Q_S in (3.22) are defined as the generating function G where

$$G = Q_S \frac{\partial \ln \rho}{\partial z} - \frac{\partial Q_S}{\partial z} . \tag{3.24}$$

In an updraught, wG provides a source for q_c, decreasing the saturation deficit if $q_c < 0$ and allowing condensation of water vapour if $q_c > 0$.

Since precipitation has a fall speed relative to the air, one of the terms in S_{Q2r} in (3.15) results from the gain and loss of precipitation due to its fall through the air. The assumption is made that rain falls with the terminal velocity of the median raindrop,$-V_t$. Thus S_{qr} is defined by

$$S_{q_r} = S_{Q_{2r}} + \frac{\partial}{\partial z} (V_t q_r) \tag{3.25}$$

and (3.15) becomes

$$\frac{\partial q_r}{\partial t} + \underline{\nabla} . (q_r \underline{V}) + \frac{\partial}{\partial z} (V_t q_r) = S_{q_r} \tag{3.26}$$

where

$$q_r = Q_{2r} \tag{3.27}$$

and

$$S_{qr} = (\text{cloud -> rain}) - (\text{rain -> vapour}) . \tag{3.28}$$

The final forms for the conservation of water used in these modelling studies are

$$\frac{\partial q_c}{\partial t} + \underline{\nabla} . (q_c \underline{V}) = w G + S_{q_c} , \tag{3.29}$$

$$\frac{\partial q_r}{\partial t} + \underline{\nabla} . (q_r \underline{V}) + \frac{\partial}{\partial z}(V_t q_r) = S_{q_r} \qquad (3.30)$$

where

Sqc = - (cloud -> rain) + (rain -> vapour) ,

S_{qr} = (cloud -> rain) - (rain -> vapour) .

A similar development for pollutant material in air, cloud and rain (in units mass of pollutant per unit volume of air) yields

$$\frac{\partial P_a}{\partial t} + \underline{\nabla} . (P_a \underline{V}) = S_{P_a} , \qquad (3.31)$$

$$\frac{\partial P_c}{\partial t} + \underline{\nabla} . (P_c \underline{V}) = S_{P_c} , \qquad (3.32)$$

$$\frac{\partial P_r}{\partial t} + \underline{\nabla} . (P_r \underline{V}) + \frac{\partial}{\partial z}(V_t P_r) = S_{P_r} \qquad (3.33)$$

where S_{Pa}, S_{Pc}, S_{Pr} are the source/sink terms for pollutant material in air, cloud and rain respectively.

3.2.2 1D form of conservation equations

The continuity equation (3.21) is

$$\frac{\partial u}{\partial x} + \frac{\partial v}{\partial y} + \frac{\partial w}{\partial z} = - w \frac{\partial \ln \rho}{\partial z} .$$

The conservation equation for cloud water, (3.29),

$$\frac{\partial q_c}{\partial t} + \frac{\partial (q_c u)}{\partial x} + \frac{\partial (q_c v)}{\partial y} + \frac{\partial (q_c w)}{\partial z} = w G + S_{q_c}$$

becomes

$$\frac{\partial q_c}{\partial t} + u\frac{\partial q_c}{\partial x} + v\frac{\partial q_c}{\partial y} + w\frac{\partial q_c}{\partial z} = q_c\, w\frac{\partial \ln \rho}{\partial z} + w\,G + S_{q_c} . \qquad (3.34)$$

Assuming q_C is a function of height only, the 1D equation becomes

$$\frac{\partial q_c}{\partial t} + w\frac{\partial q_c}{\partial z} = q_c\, w\frac{\partial \ln \rho}{\partial z} + w\,G + S_{q_c}$$

from which

$$\frac{\partial q_c}{\partial t} + \frac{\partial}{\partial z}(w\,q_c) = q_c\left(\frac{\partial w}{\partial z} + w\frac{\partial \ln \rho}{\partial z}\right) + w\,G + S_{q_c} . \qquad (3.35)$$

Similarly, the 1D form for precipitation becomes

$$\frac{\partial q_r}{\partial t} + \frac{\partial}{\partial z}((V_t + w)\,q_r) = q_r\left(\frac{\partial w}{\partial z} + w\frac{\partial \ln \rho}{\partial z}\right) + S_{q_r} . \qquad (3.36)$$

The 1D forms of the conservation equations for pollutant material are

$$\frac{\partial P_a}{\partial t} + \frac{\partial}{\partial z}(w\,P_a) = P_a\left(\frac{\partial w}{\partial z} + w\frac{\partial \ln \rho}{\partial z}\right) + S_{P_a} , \qquad (3.37)$$

$$\frac{\partial P_c}{\partial t} + \frac{\partial}{\partial z}(w\,P_c) = P_c\left(\frac{\partial w}{\partial z} + w\frac{\partial \ln \rho}{\partial z}\right) + S_{P_c} , \qquad (3.38)$$

$$\frac{\partial P_r}{\partial t} + \frac{\partial}{\partial z}((V_t + w)\,P_r) = P_r\left(\frac{\partial w}{\partial z} + w\frac{\partial \ln \rho}{\partial z}\right) + S_{P_r} . \qquad (3.39)$$

These equations are solved by numerical means. The finite difference technique used is the Lax method (Lax, 1954). This is described in

appendix(A) together with its implementation for 1D modelling.

3.3 Cloud Model

Unlike the cloud droplet population, the raindrop population is described by a size spectrum and terminal fall velocity. These must be suitably parametrised as detailed below.

Raindrop distribution

Following Kessler(1969), the raindrop distribution is described by

$$N = N_0 e^{-\lambda D} \tag{3.40}$$

where N is the number of raindrops per unit volume of air per unit diameter dD. This negative exponential distribution is based on observations made by Marshall and Palmer(1948) of rain at the Earth's surface. Underwood(1983b) has reviewed experimental data on raindrop distributions. He concludes that in general the Marshall-Palmer distribution over-predicts the number of small drops, characterized by the parameter N_0 , observed in precipitation. Also the shape of the distribution can change both with rainfall type and with time during a particular rain event. Waldvogel(1974) found that during continuous rain the parameters in a Marshall-Palmer fit had variations

$$10^6 < N_0 < 5.10^7 \ m^{-4}$$

and

$$2.10^3 < \lambda < 5.10^3 \ m^{-1} .$$

λ is related to precipitation quantity q_r by

$$q_r = \int_0^\infty \frac{\pi \rho_w}{6} D^3 N_0 e^{-\lambda D} dD \quad , \tag{3.41}$$

where ρ_w is the density of water. From (3.41),

$$\lambda = 42.1\, N_0^{1/4}\, q_r^{-1/4} \ . \tag{3.42}$$

Velocity of raindrops

Kessler(1969) provided a formula for terminal velocity of raindrops based on the experimental results of Gunn and Kinzer(1949). It is given by

$$V_t = -K\left[\frac{\rho_0}{\rho}\right]^{1/2} D^{1/2} \tag{3.43}$$

with K = 130. The variation of air density with height can be approximated by a negative exponential. The hydrostatic approximation stated as

$$\rho = \rho_0 \left[\, 1 + \frac{\alpha z}{T_0} \,\right]^{-\frac{(1+\alpha R)}{\alpha R}} \tag{3.44}$$

where α is the vertical gradient of temperature T and R is the gas constant for air can be approximated by

$$\rho = \rho_0 \left[\exp\left[\frac{\alpha z}{T_0} \right] \right]^{-\frac{(1+\alpha R)}{\alpha R}}$$

or

$$\rho = \rho_0\, e^{-kz}. \tag{3.45}$$

$k = 10^{-4}\ m^{-1}$ is a suitable value. From (3.43),

$$V_t = -K\, e^{kz/2}\, (2R)^{1/2}. \tag{3.46}$$

where R is the radius of the raindrop. The assumption is made that all

raindrops fall with the terminal velocity of the raindrop with median volume radius, R_0. This has been derived by Kessler(1969) and is given by

$$R_0 = 0.044\, N_0^{-1/4}\, q_r^{1/4}. \tag{3.47}$$

Inserting (3.47) into (3.46) gives

$$V_t = -38.3\, N_0^{-1/8}\, q_r^{1/8}\, e^{kz/2} \tag{3.48}$$

3.3.1 Parametrisation of microphysical processes

In warm cloud($T > 0^oC$), water vapour, cloud water and rain water are converted from one form to another by the microphysical processes illustrated in figure(3.1). As moist air rises above its saturation level, water vapour condenses to form cloud droplets (wG). It would take much longer than is observed for cloud droplets to grow by condensation alone that they would be of sufficient size to fall out of cloud as rain drops. Instead cloud droplets coalesce to form precipitation sized drops and this process is known as autoconversion (AC). The process by which falling raindrops collect cloud droplets is known as accretion (CC). Rain drops evaporate in subsaturated air (EP). Thus the source/sink terms in (3.35) and (3.36) are given by

$$S_{qc} = EP - AC - CC \tag{3.49}$$

$$S_{qr} = -EP + AC + CC. \tag{3.50}$$

The parametrisations of these processes are described below.

Water substance

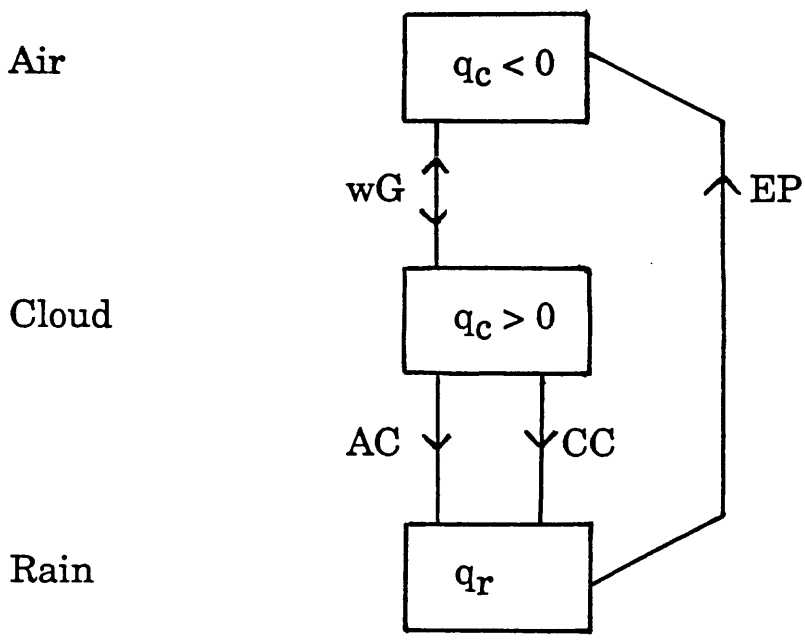


Figure 3.1 Microphysical processes for water substance

Condensation of water vapour and evaporation of cloud (wG)

The generating function G is parmaterised so as to represent the decline of moisture availabilty with height in the atmosphere. Kessler(1969) suggested a linear function

$$G = A + B z \quad (A > 0, B < 0) \tag{3.51}$$

and provided representative values for a tropical atmosphere of

$$A = 10^{-3}\, g\, m^{-4},\ B = -10^{-7}\, g\, m^{-5}.$$

Fisher(1982), noting that the rate of release of water due to condensation in an adiabatically ascending air parcel expressed as a mixing ratio (g water/ g air) is approximately a function only of temperature T at the condensation level of the column, expressed the generating function as

$$G = \rho\, G'(T). \tag{3.52}$$

Density of air, ρ, is given by (3.45) with $\rho_0 = \rho(z = 0) \sim 1.2\ kg/m^3$. G'(T) lies between 1 and $2 \times 10^{-6}\, g\, g^{-1}\, m^{-1}$. The two forms of G are little different since

$$G = \rho\, G'(T) = \rho_0\, G'(T)\, e^{-kz} \sim \rho_0\, G'(1 - kz)$$

which is a linear function of the same gradient as Kessler's. The linear form of the generating function is the one that is used here.

Autoconversion (AC)

Kessler(1969) provided a parametrisation for autoconversion which is based largely on intuitive reasoning and which is given by

$$AC = \begin{cases} k_1 (q_c - a) & \text{for } q_c > a \\ 0 & \text{otherwise} \end{cases} \qquad (3.53)$$

a is the threshold for cloud water content beneath which no autoconversion takes place and AC increases with increasing q_c according to the rate constant, k_1.

Berry and Reinhardt(1974) studied the problem more rigorously and their form for autoconversion as expressed by Easter and Hales(1984) is

$$AC = 5.5.10^9 \, q_c^2 \, m_c^{5/3} \left[1 - \left[\frac{2.35.10^{-9}}{m_c} \right]^{4/3} \right] . \left[1 - \left[\frac{2.04.10^{-9}}{m_c} \right]^{1/3} \right] . \qquad (3.54)$$

In this equation, q_c is in g/m^3 and

$$m_c = \frac{q_c}{10^6 \, N_c} \qquad (3.55)$$

where N_c is the number of cloud droplets per cubic cm. Here N_c is taken to be the number of cloud condensation nuclei.

The two forms of AC are compared in section (3.3.2) where their influence on precipitation development and their variation with the parameters k_1, a and N_c are studied. Autoconversion is most important in the early stages of precipitation development.

Accretion (CC)

The parametrisation of accretion common to many cloud models is derived by Kessler(1969). In that derivation, the assumption is made that the

efficiency with which a raindrop collects a cloud droplet encountered in its path, E_r, is independent of the diameter of the raindrop. Accretion is given by

$$CC = 6.96.10^{-4} E_r N_0^{1/8} q_c q_r^{7/8} e^{kz/2} \qquad \text{for } q_c > 0 . \tag{3.56}$$

Evaporation (EP)

Kessler(1969) obtained a parametrisation for evaporation of raindrops in subsaturated air based upon results given in the Smithsonian Meteorological Tables(1958). It is given by

$$EP = -1.93.10^{-6} N_0^{7/20} q_c q_r^{13/20} \qquad \text{for } q_c < 0 . \tag{3.57}$$

3.3.2 Cloud model results and sensitivity studies

The basic form of updraught velocity chosen for the runs is described by the formula

$$w = w_{max} \sin (\pi z / H) \tag{3.58}$$

where H is the height of the domain and w_{max} is the maximum updraught velocity at z = H/2. This form was chosen so as to give a continuous function that has positive values throughout the domain $0 \leq z \leq H$, that is symmetrical and has zero values at the top (z = 0) and bottom (z = H) of the domain.

Initially a standard run was made with parameters set to the values given in table(3.1). The dynamic parameters of updraught height, H, and velocity w_{max} are chosen to represent a moderately intense convective storm. Cloud and precipitation developments are shown in figures(3.2) and (3.3) for the base run. At first cloud water content increases via condensation

Table 3.1 Cloud model parameter values for standard run

Parameter	Value
G	$2.16.10^{-3}(1 - 10^{-4} z)$
H	10 km
w_{max}	5 m/s
N_c	500 cc^{-1}
E_r	1.0
$q_c(z,t=0)$	-2 (1 - z/H)
$q_r(z,t=0)$	0

with the largest increase coincidant with maximum updraught velocity in the middle of the domain(see figure(3.2), t = 800 s). Once sufficient cloud water has formed, autoconversion becomes significant resulting in depletion of cloud water to produce precipitation in a central region of the domain(fig 3.3, t = 1200 s). There are maxima in cloud water content above and beneath this central region. The lower maximum is depleted by accretion of cloud droplets by rain falling from above. Cloud water higher up is lost mainly by horizontal divergence. By T = 4000 s, cloud and rain have reached their steady state profiles with net production and loss of water in the cloud balancing out. The final ground level precipitation quantity is approximately 8 g/m^3. A higher value for G of $G = 3.10^{-3}.(1 - 10^{-4}.z)$ gives a ground level precipitation quantity slightly higher at 10 g/m^3 but the overall development is very much the same (see figures (3.4) and (3.5)).

Updraught velocity is crucial in determining the quantity of precipitation. Ground level precipitation rates for four updraught velocities, (w_{max} = 0.5, 1, 5, 10 m/s), are shown in figure(3.6). There is a 50-fold increase in precipitation for a 20-fold increase in updraught velocity. These quantities,

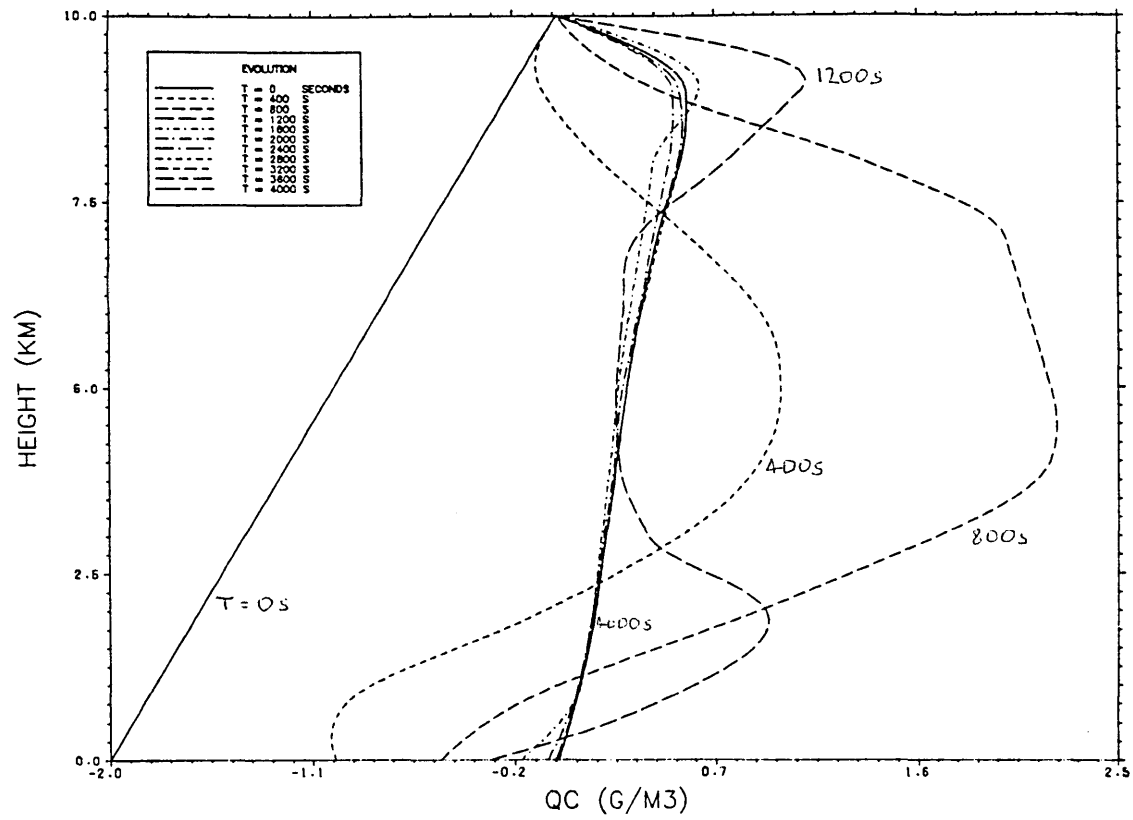


Figure 3.2 Cloud water development, $G = 2.16.10^{-3}(1 - 10^{-4}z)$

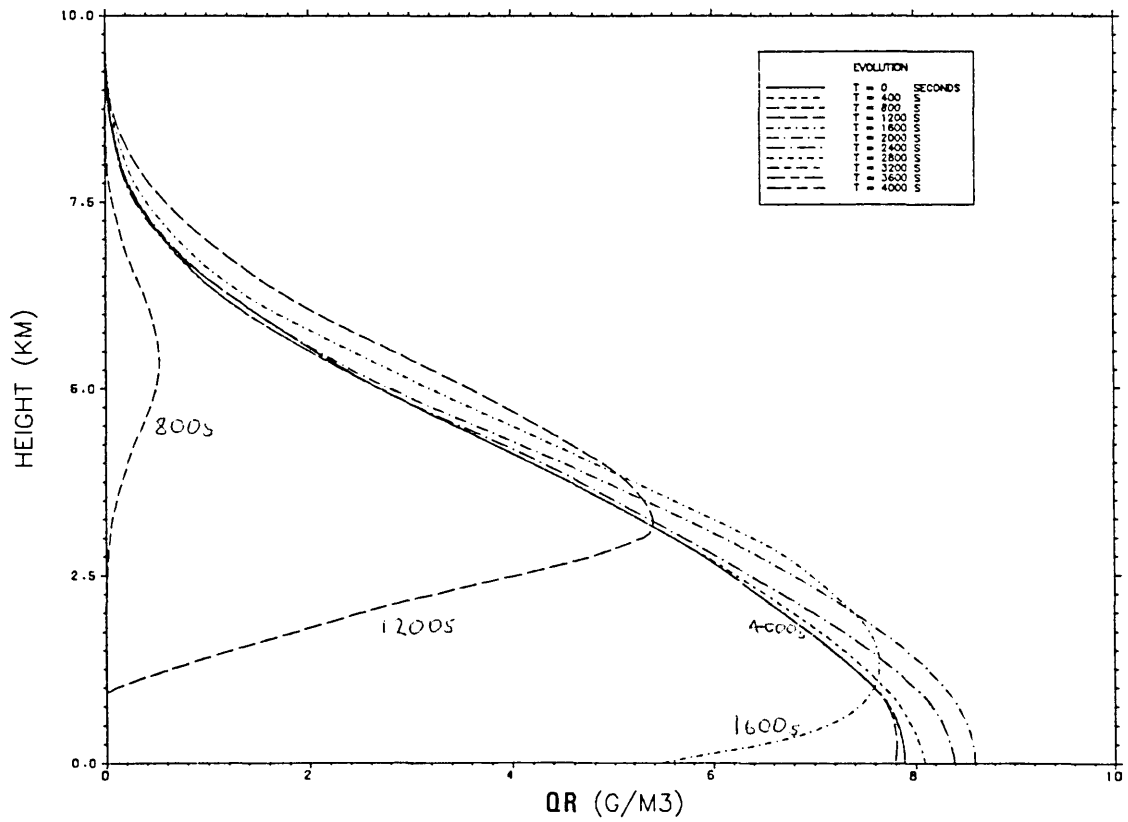


Figure 3.3 Rain water development, $G = 2.16.10^{-3}(1 - 10^{-4}z)$

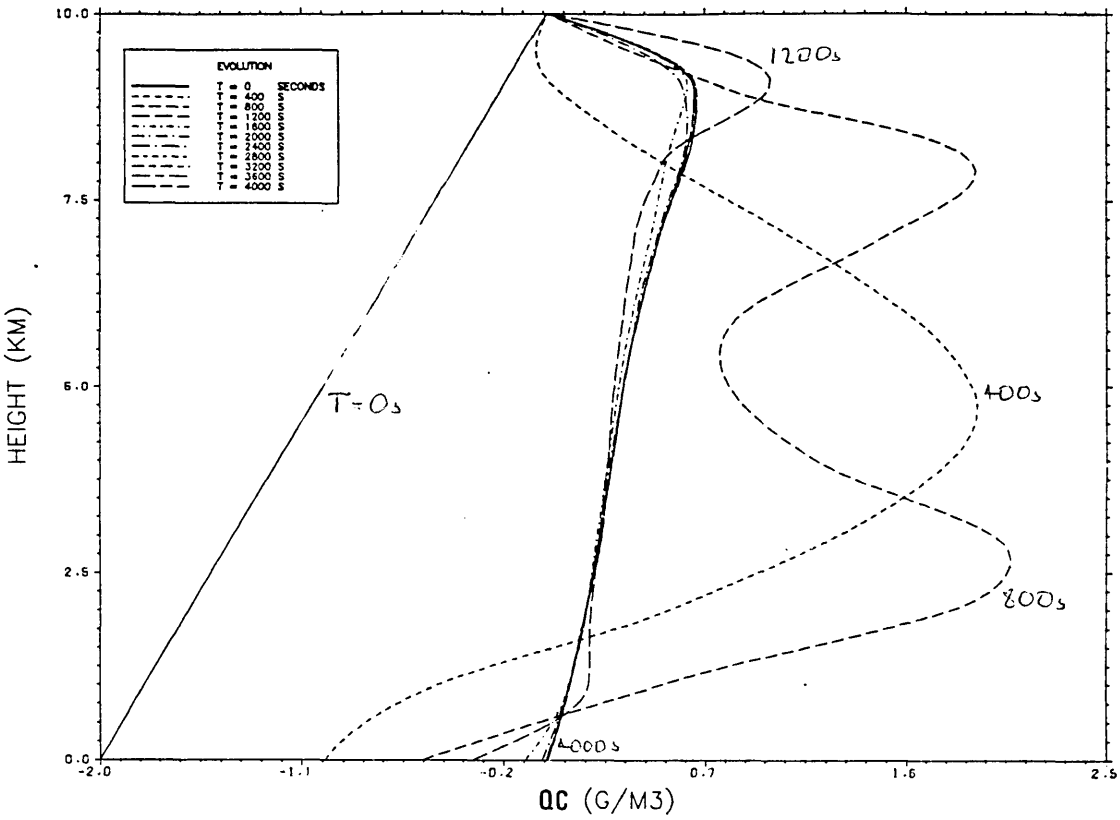


Figure 3.4 Cloud water development, $G = 3.10^{-3}(1 - 10^{-4}z)$

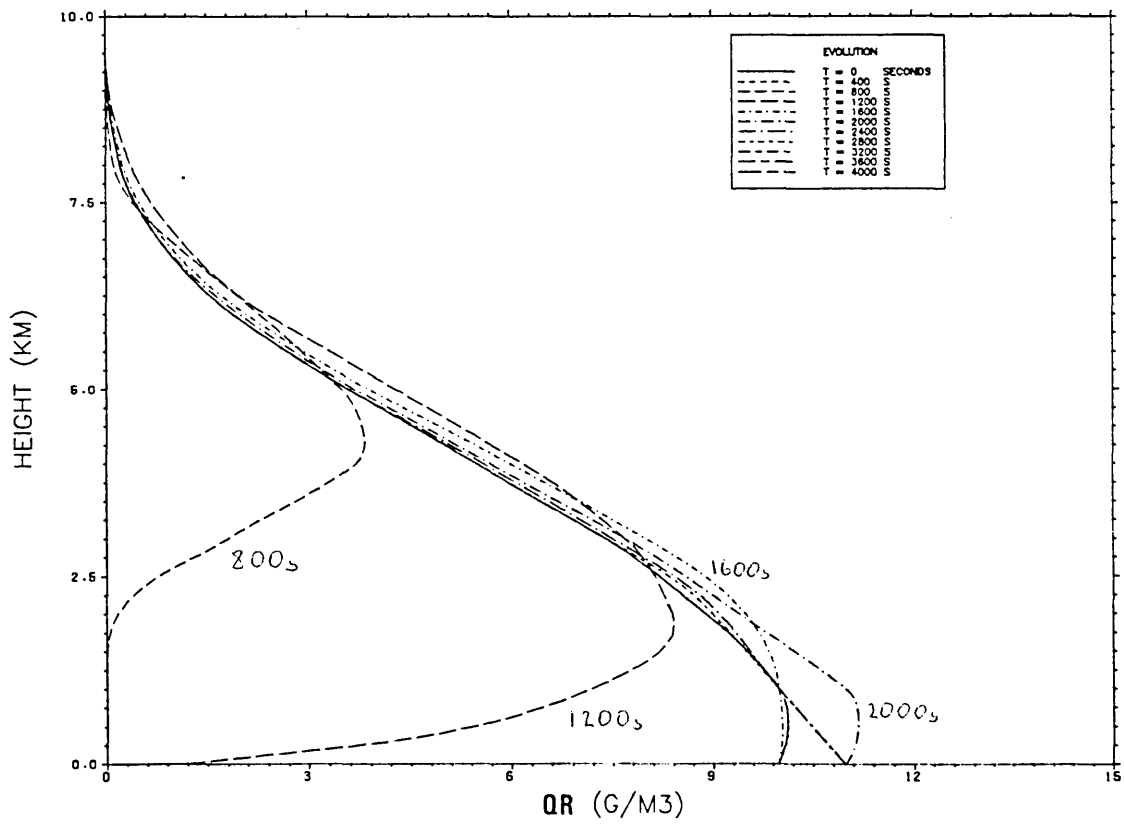


Figure 3.5 Rain water development, $G = 3.10^{-3}(1 - 10^{-4}z)$

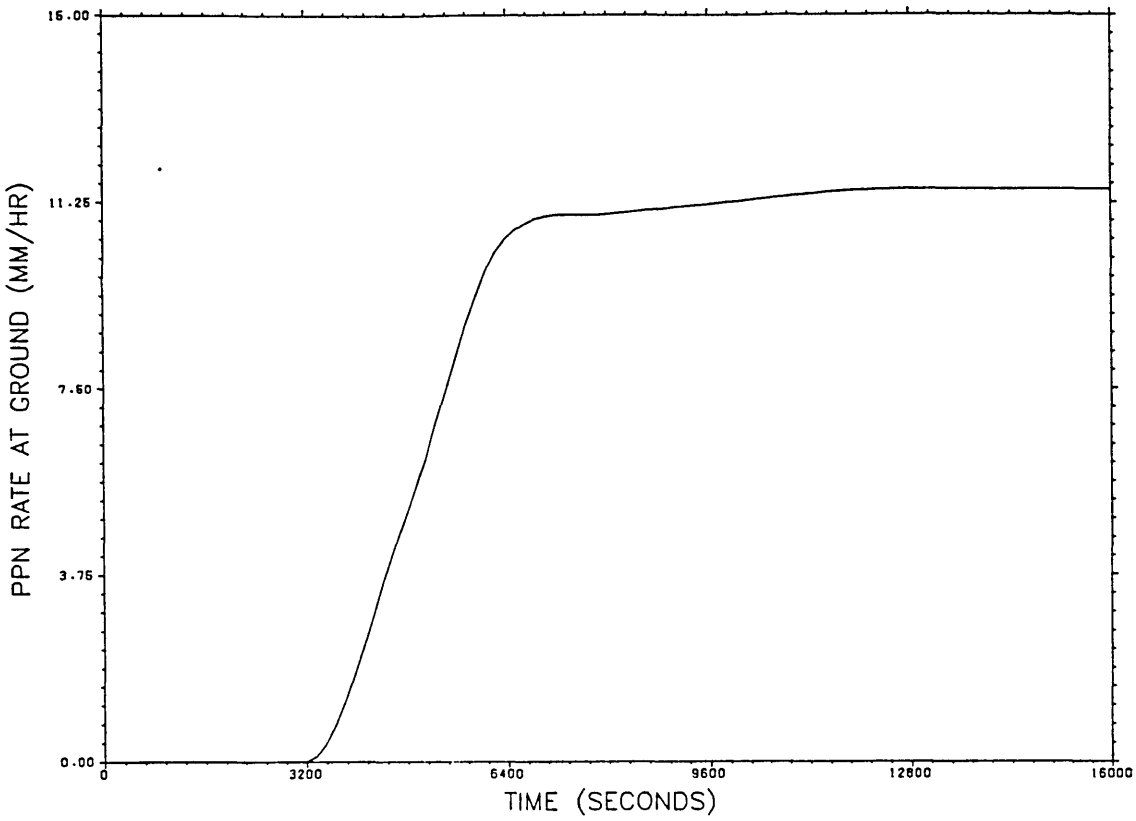


Figure 3.6a Development of precipitation rate at ground w_{max} = 0.5 m/s

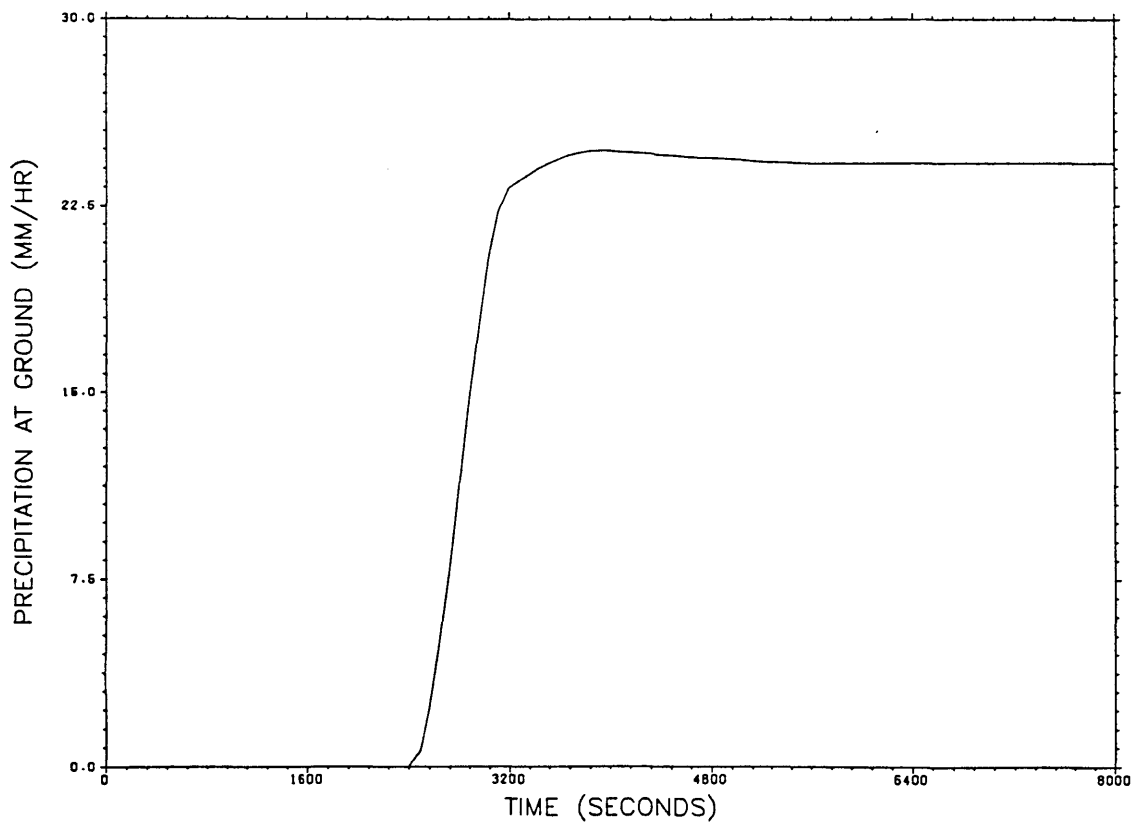


Figure 3.6b Development of precipitation rate at ground w_{max} = 1 m/s

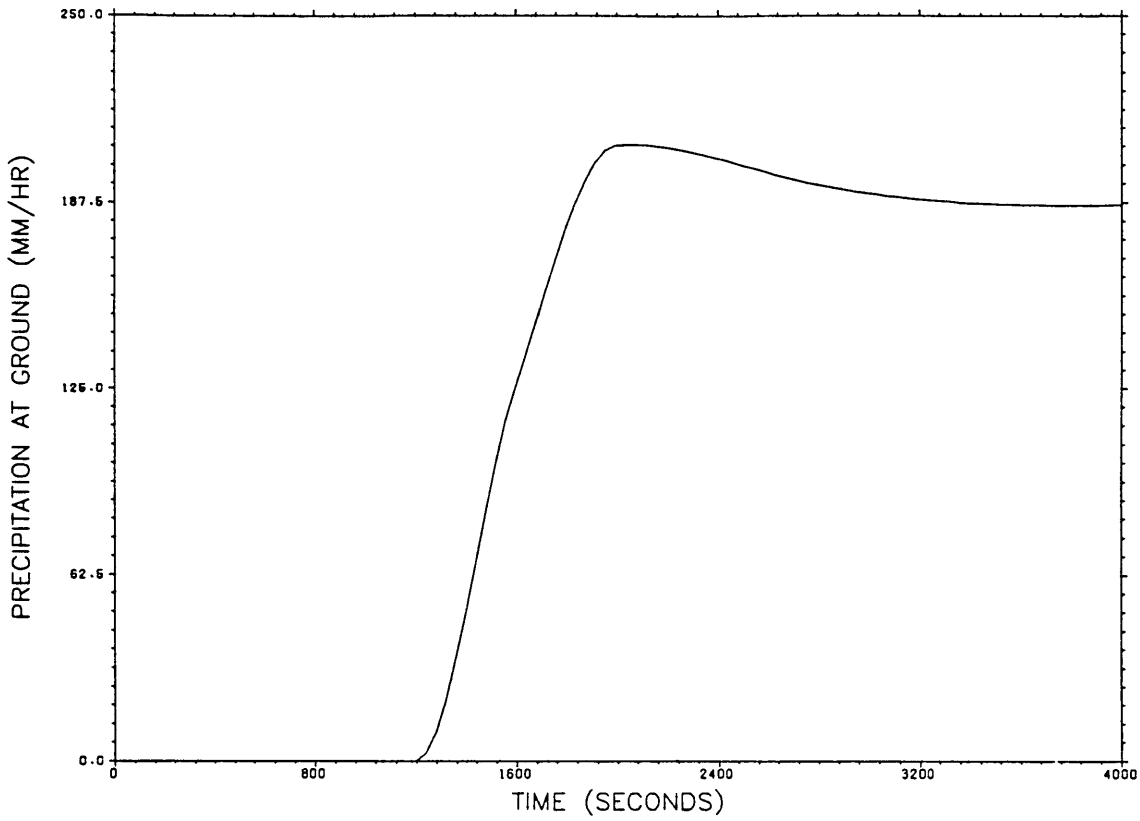


Figure 3.6c Development of precipitation rate at ground w_{max} = 5 m/s

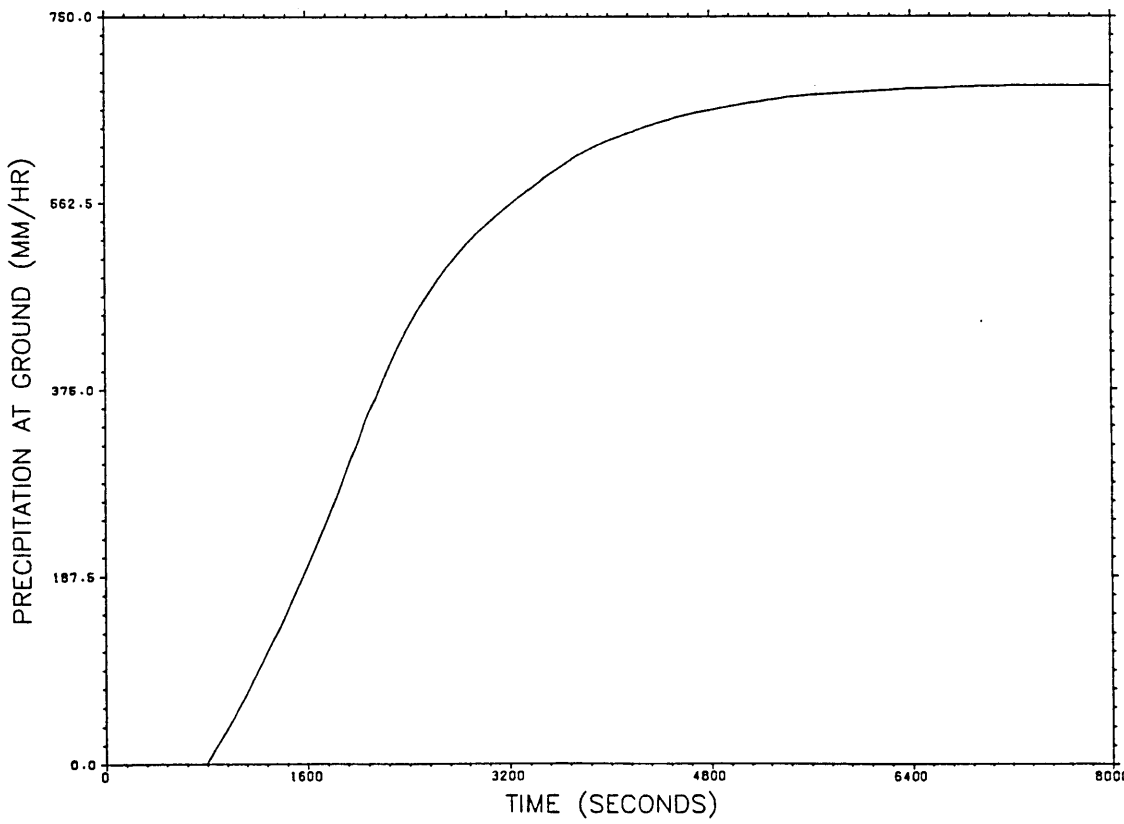


Figure 3.6d Development of precipitation rate at ground w_{max} = 10 m/s

especially for larger velocities, are extremely high and would very rarely be seen. These high figures reflect the artificiality of modelling in one spatial dimension. Updraughts of this magnitude could not be sustained with such high precipitation quantities. The buoyancy of the air would be reduced. The 1D nature of the domain results in rain falling into the updraught and thus collecting large amounts of cloud water. In fact this would lead to termination of the updraught when rain evaporates in subsaturated air cooling it. Long lived convective storms can only be sustained by a 3D structure in which updraught and downdraught flows twist around each other. However the simple nature of 1D modelling means that important processes can be studied with relative ease and cheapness before more realistic 2D studies are undertaken.

Autoconversion is most important in the early stages of precipitation development. Two parametrisations for AC are described above and these have been compared. The Berr y and Reinhardt parametrisation, based more closely on the physics of the process, gives very similar cloud and precipitation development for N_c varying by orders of magnitude. The cloud evolutions for $N_c = 50$ and $N_c = 5000$ cc^{-1}, shown in figures(3.7) and (3.9), show a slight variation but the precipitation developments (figures (3.8) and (3.10)) are very similar. The same is true for Kessler's more intuitive parametrisation. A larger a (see figures (3.11) to (3.14)) allows greater build up of cloud content and a longer delay before precipitation is formed. However , the steady state precipitation profiles are the same for both a = 0.1 and 1.0 and are little different from the results using the Berry and Reinhardt parametrisation. This latter parametrisation, with $N_c = 500$/cc was chosen for further runs.

The raindrop distribution for a particular precipitation quantity is specified by N_0. The influence of this parameter on cloud development is illustrated

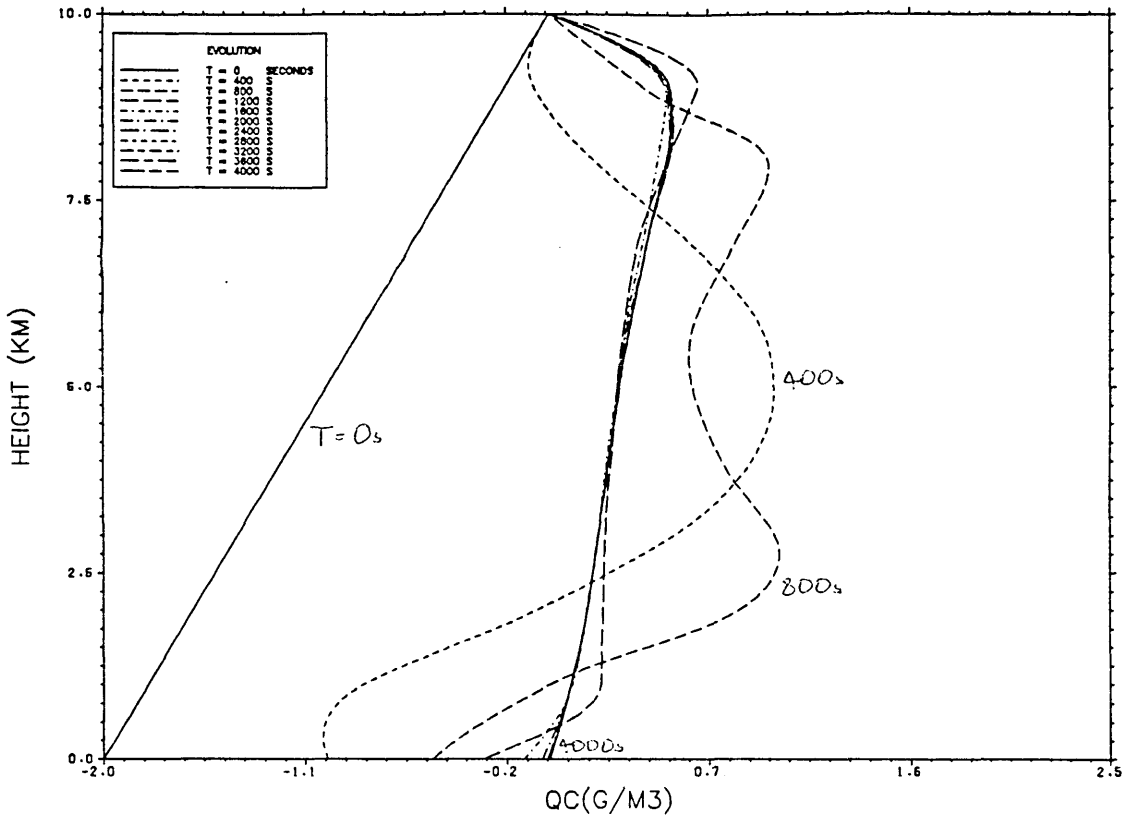


Figure 3.7 Cloud water development, $N_c = 50\ cc^{-1}$

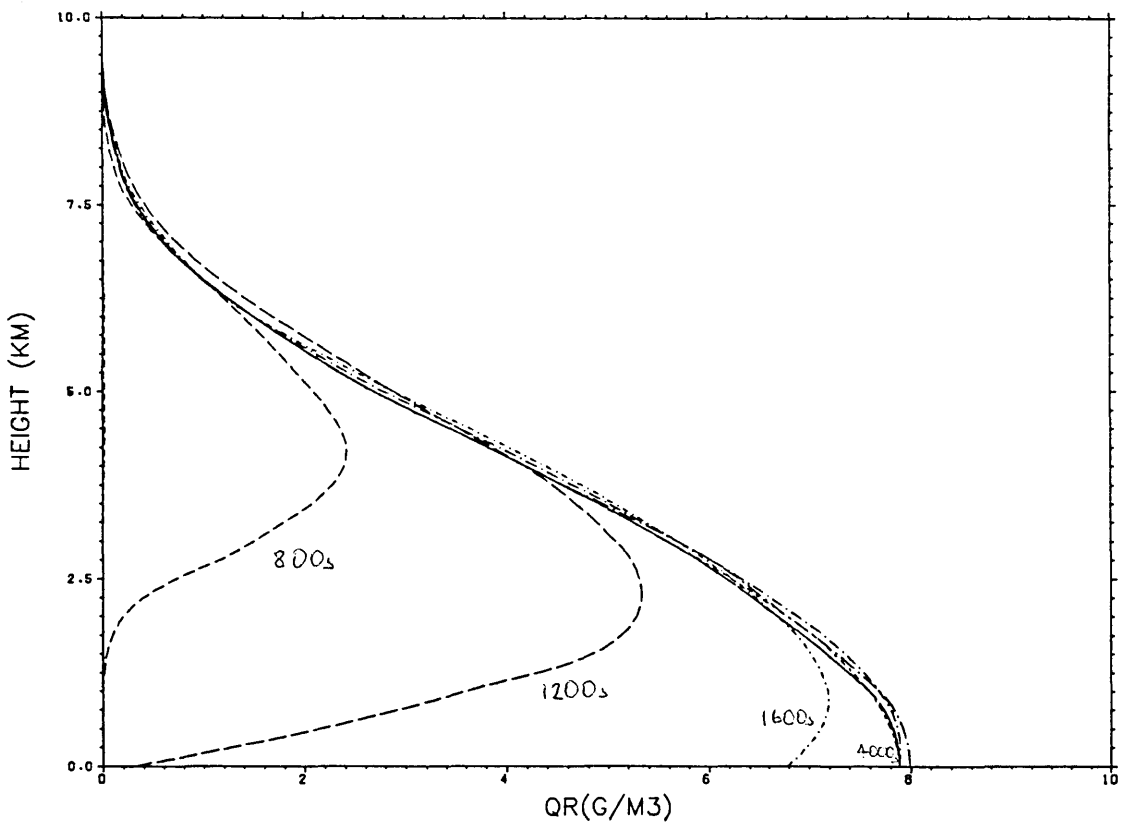


Figure 3.8 Rain water development, $N_c = 50\ cc^{-1}$

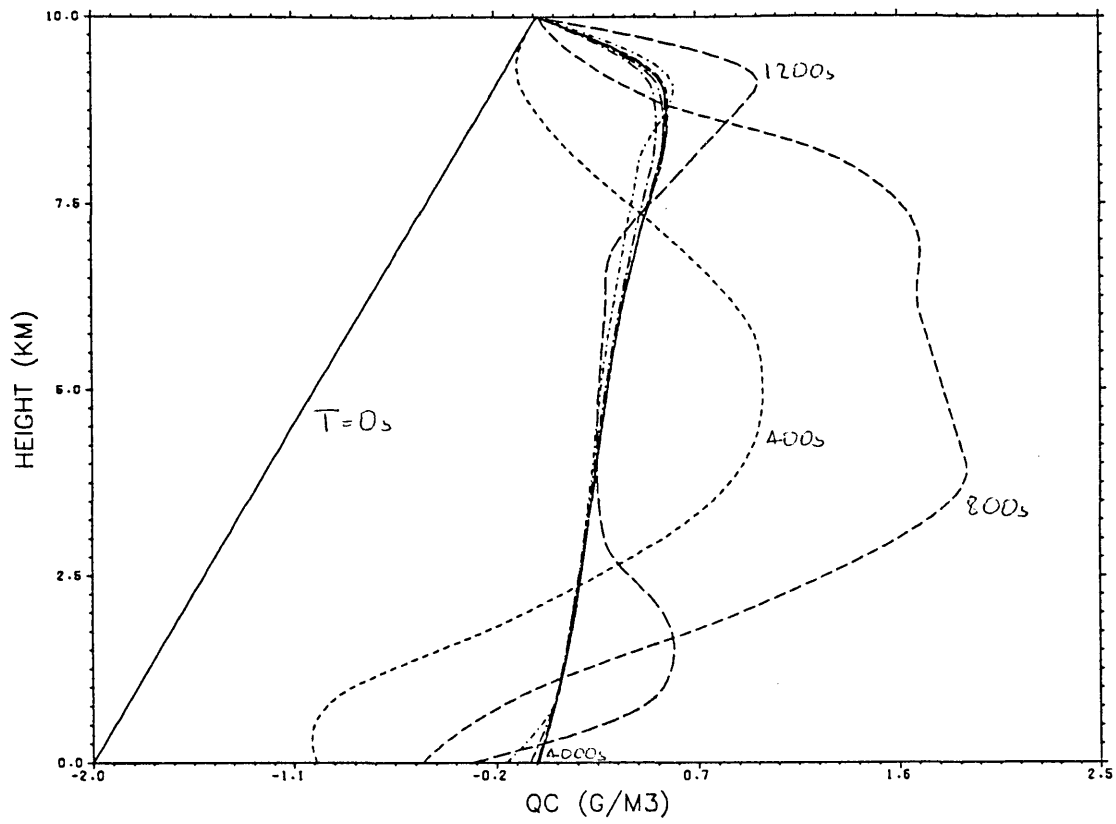


Figure 3.9 Cloud water development, $N_c = 5000\ cc^{-1}$

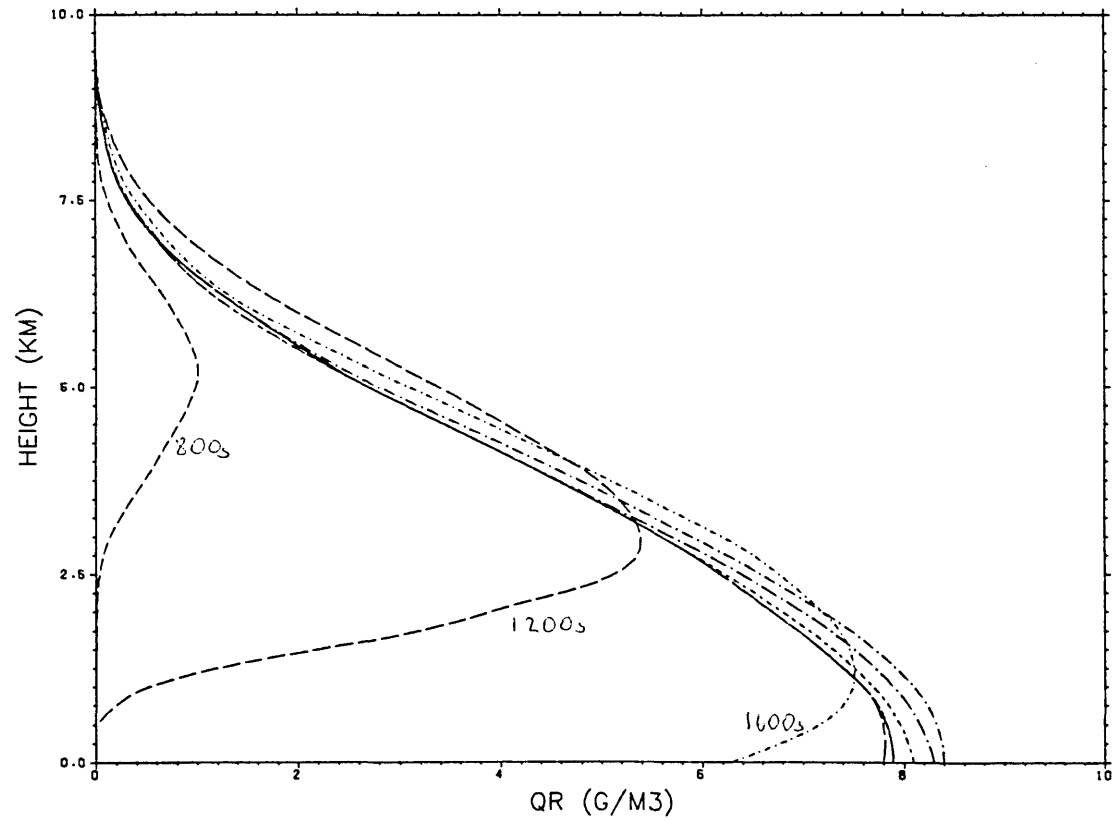


Figure 3.10 Rain water development, $N_c = 5000\ cc^{-1}$

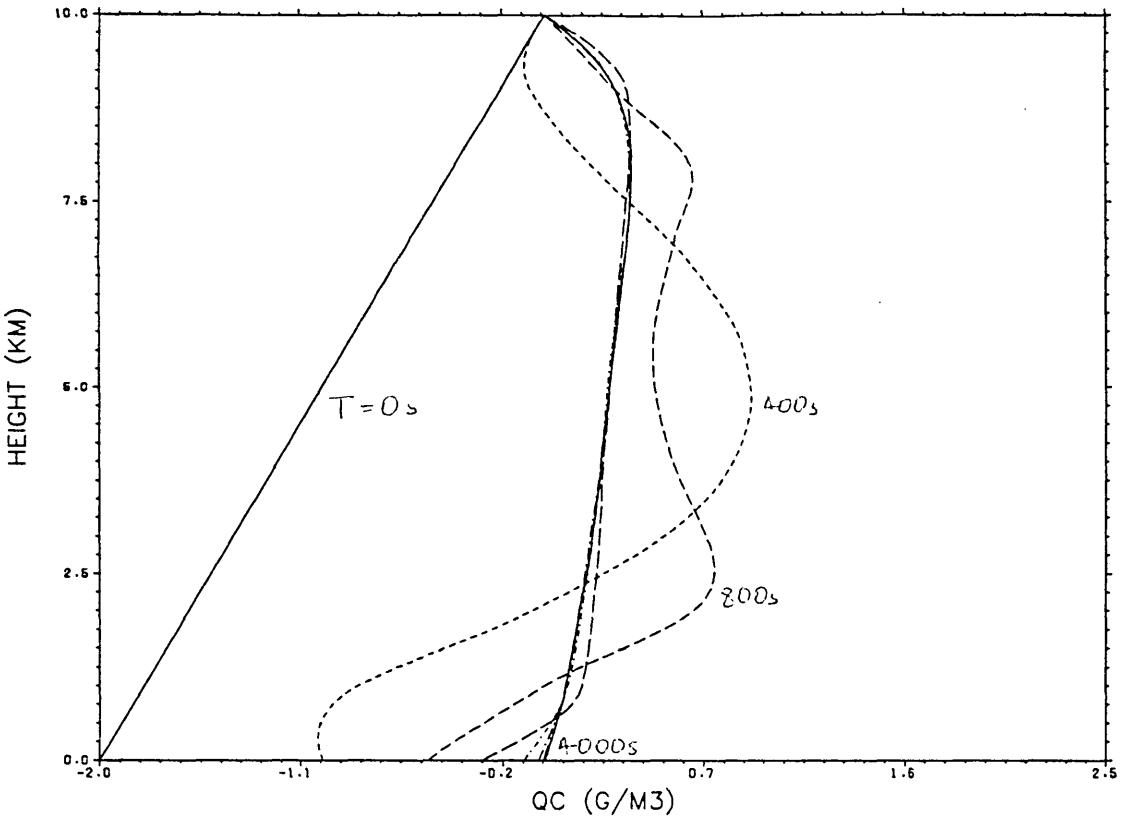


Figure 3.11 Cloud water development, a = 0.1 g/m^3

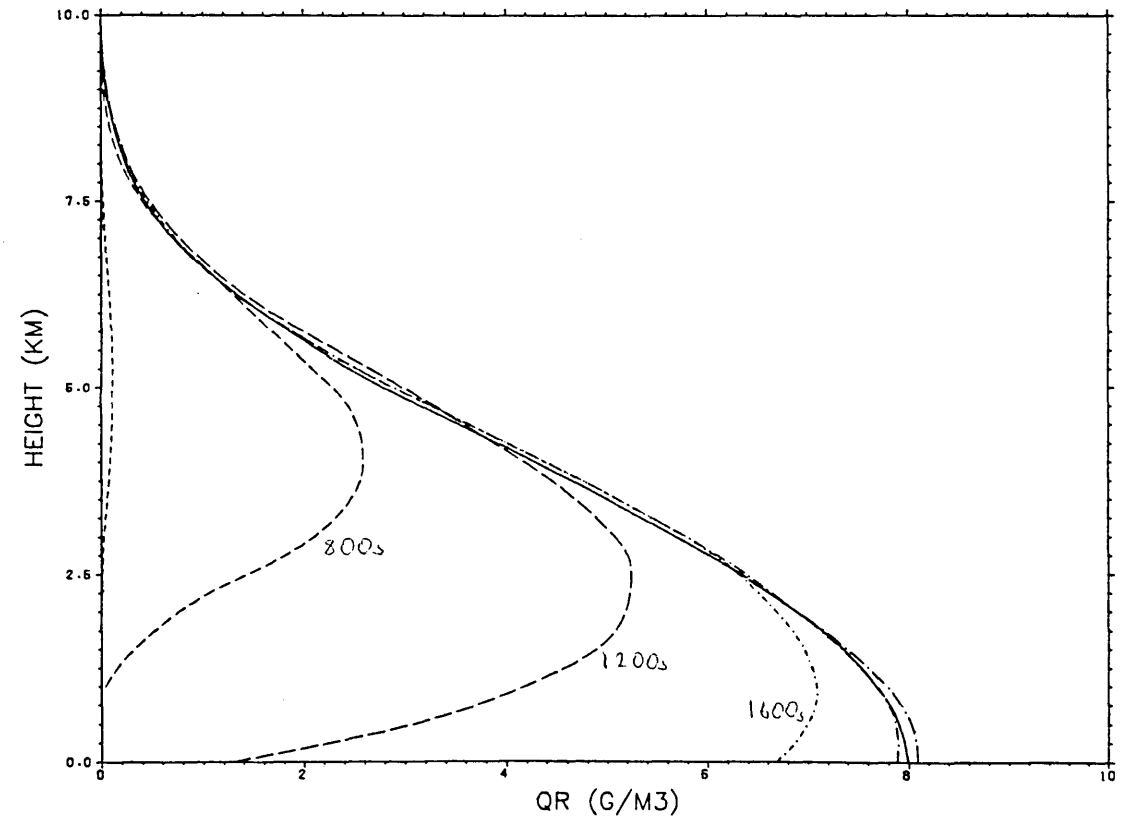


Figure 3.12 Rain water development, a = 0.1 g/m^3

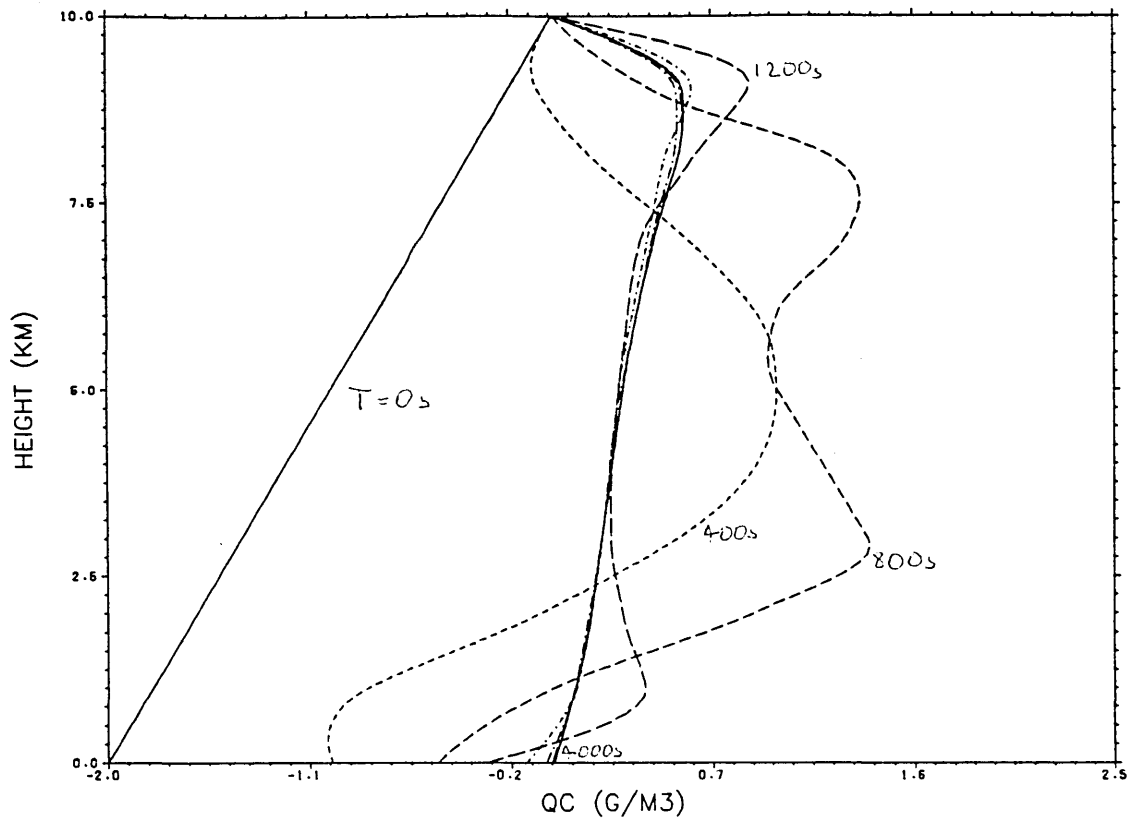


Figure 3.13 Cloud water development, a = 1.0 g/m^3

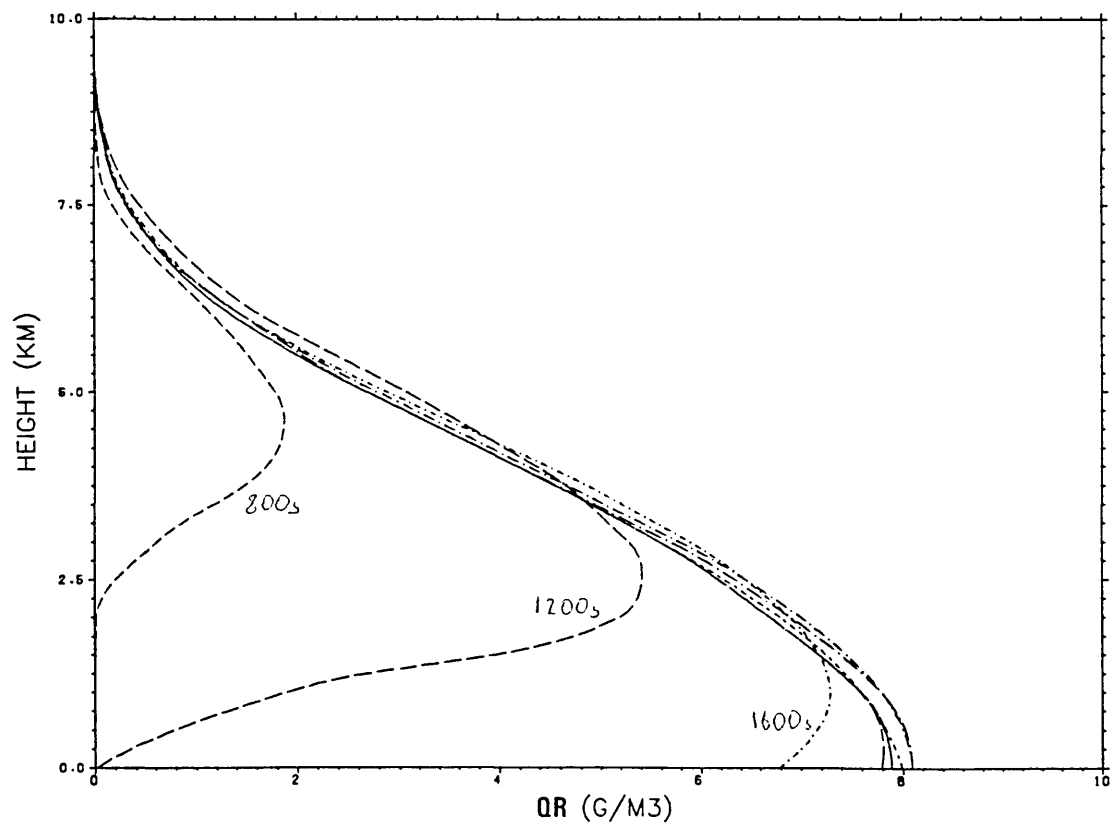


Figure 3.14 Rain water development, a = 1.0 g/m^3

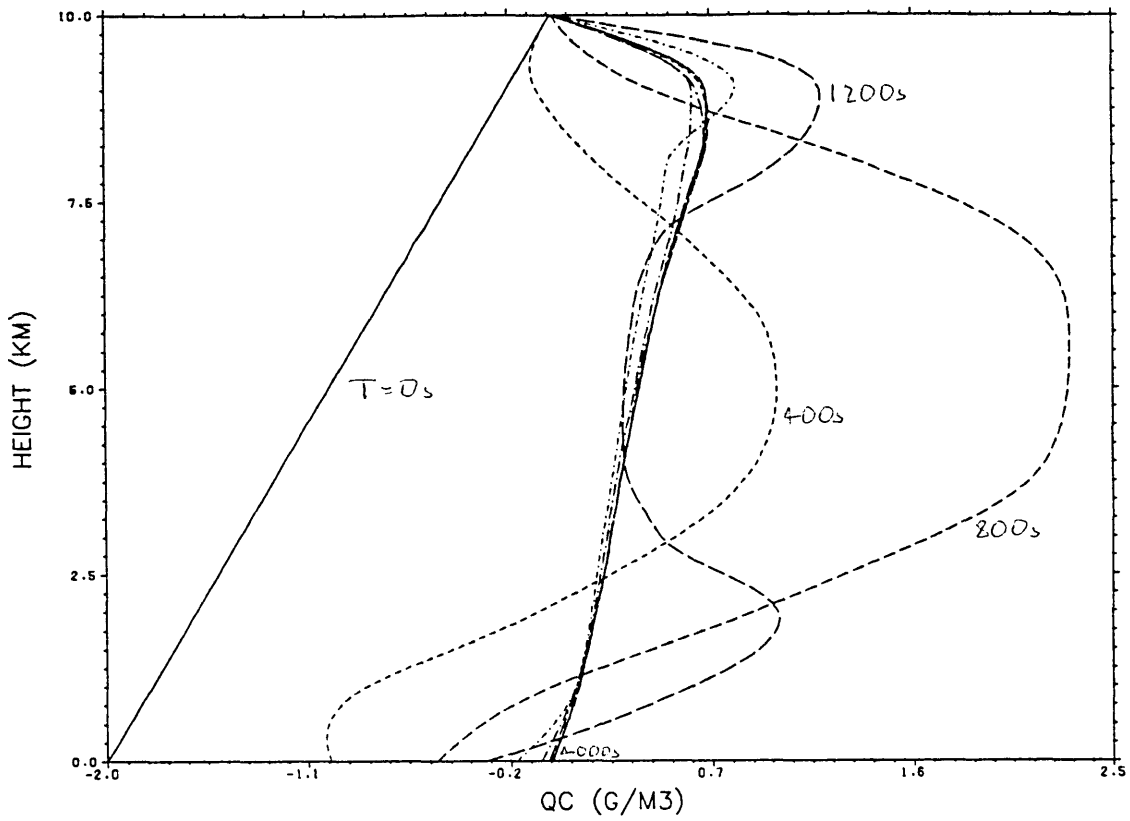


Figure 3.15 Cloud water development, $N_0 = 5.10^6$ m^{-4}

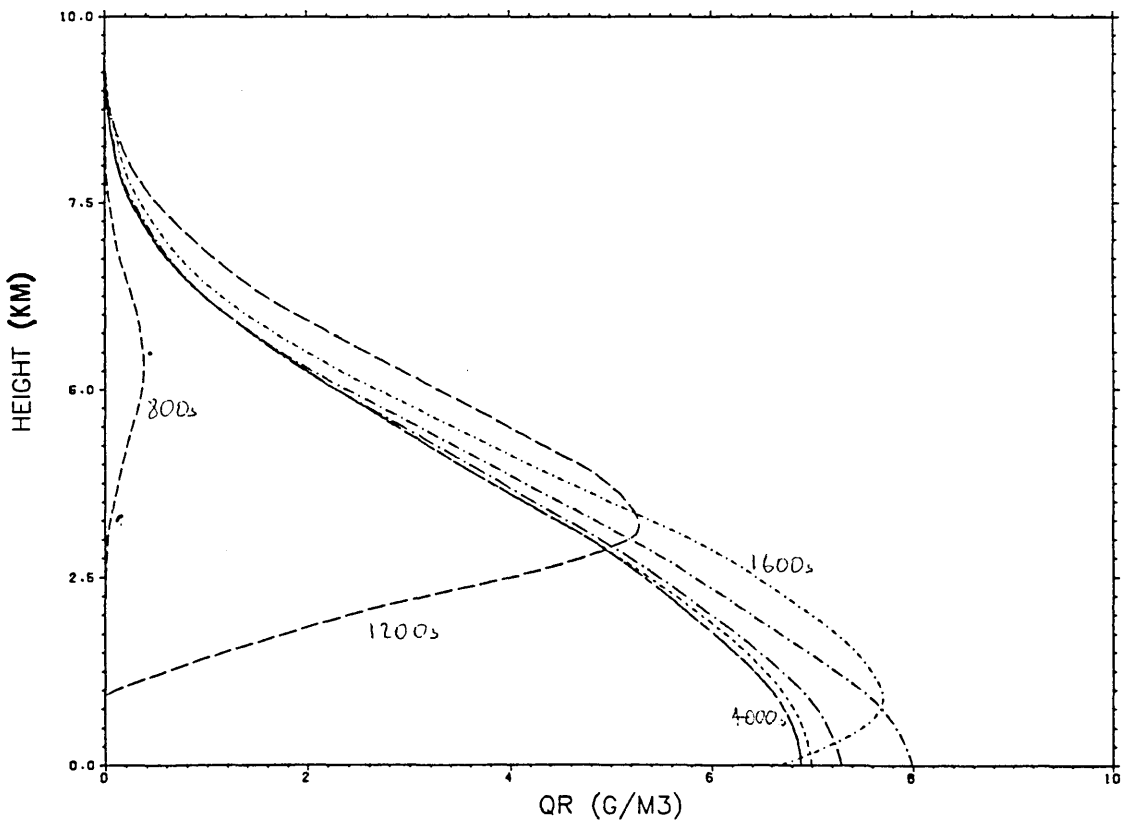


Figure 3.16 Rain water development, $N_0 = 5.10^6$ m^{-4}

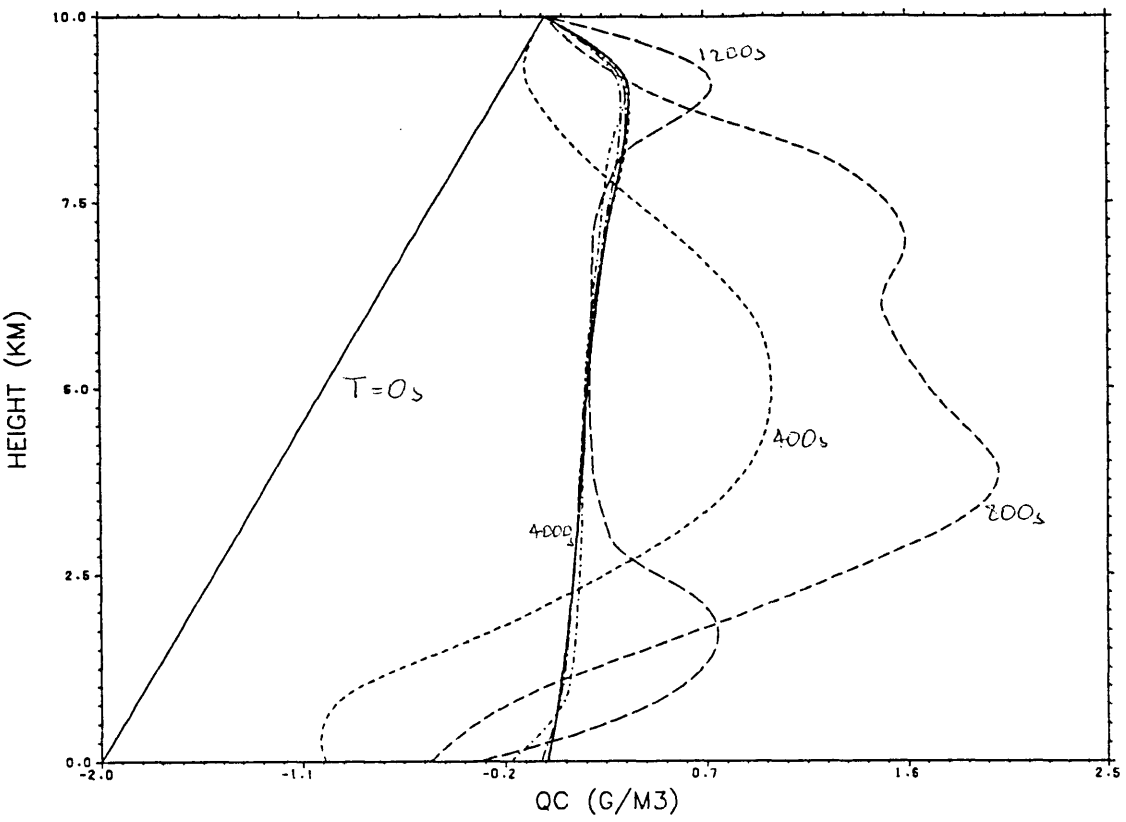


Figure 3.17 Cloud water development, $N_0 = 5.10^7$ m^{-4}

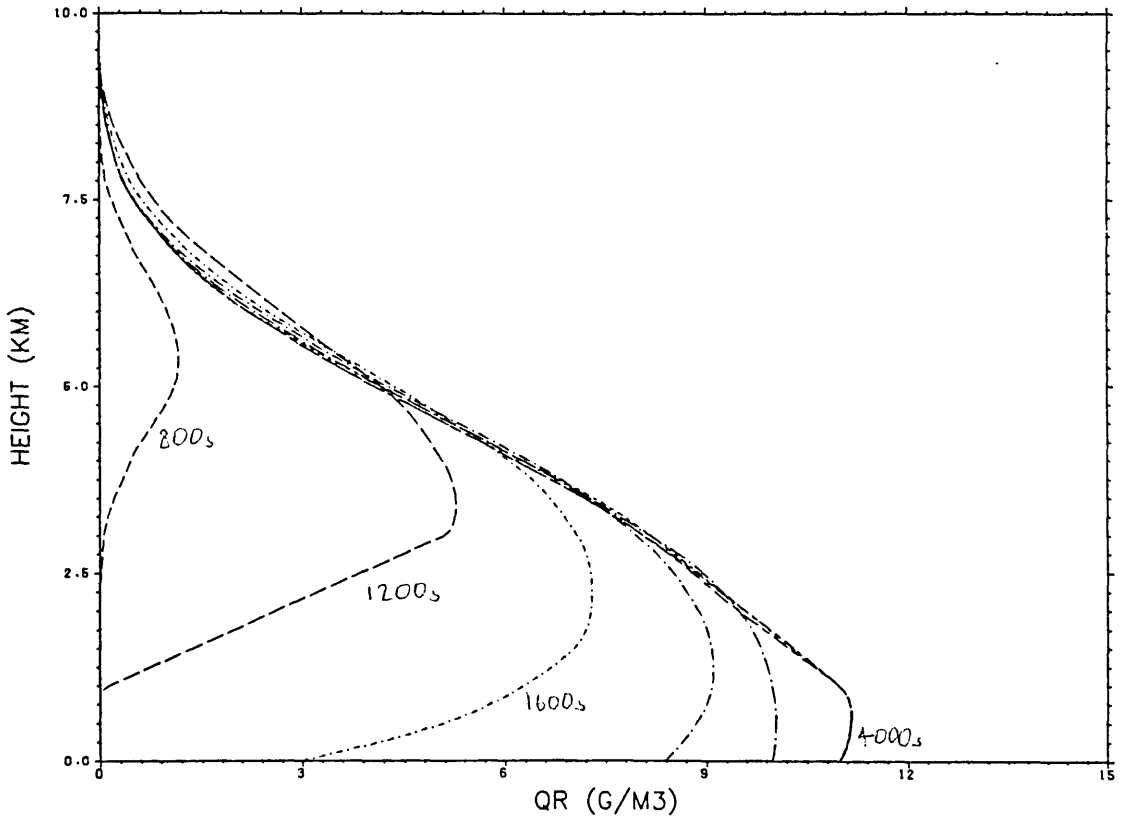


Figure 3.18 Rain water development, $N_0 = 5.10^7$ m^{-4}

in figures(3.15) to (3.18) for $N_0 = 5.10^6$ and $N_0 = 5.10^7$. Steady state precipitation profiles are affected and the variation of ground level precipitation quantity with N_0 is shown in table(3.2). The intermediate value of $N_0 = 10^7$ has been chosen for future runs.

Table 3.2 Variation of ground level steady state precipitation quantities with raindrop distribution

N_0 (m^{-4})	$q_r(0)$ (g/m^3)
5.10^6	~7
1.10^7	~8
5.10^7	~11

3.4 Cloud model incorporating particulate pollution

To include particulate pollution in the model, the equations(3.37) to (3.39) must be solved in addition to the cloud water conservation equations,(3.35) and (3.36). The source/sink terms describing the microphysical processes are parametrised as described below.

3.4.1 Parametrisation of microphysical processes

Particulate material in air, cloud and rain is converted from one form to another by the microphysical processes illustrated in figure(3.19). If particles are hygroscopic they can act as nuclei for cloud condensation (NUC), whereas if they are hydrophobic they cannot. Both hygroscopic and hydrophobic particles may be collected by falling raindrops (IMP). In addition, particulate material may be transferred by following the water mass. Particulate material in cloud water that evaporates is released to air(EPC). Material is transferred from cloud water to rain water when there is autoconversion or accretion (MPP). Evaporation of rain drops

Particulate pollution

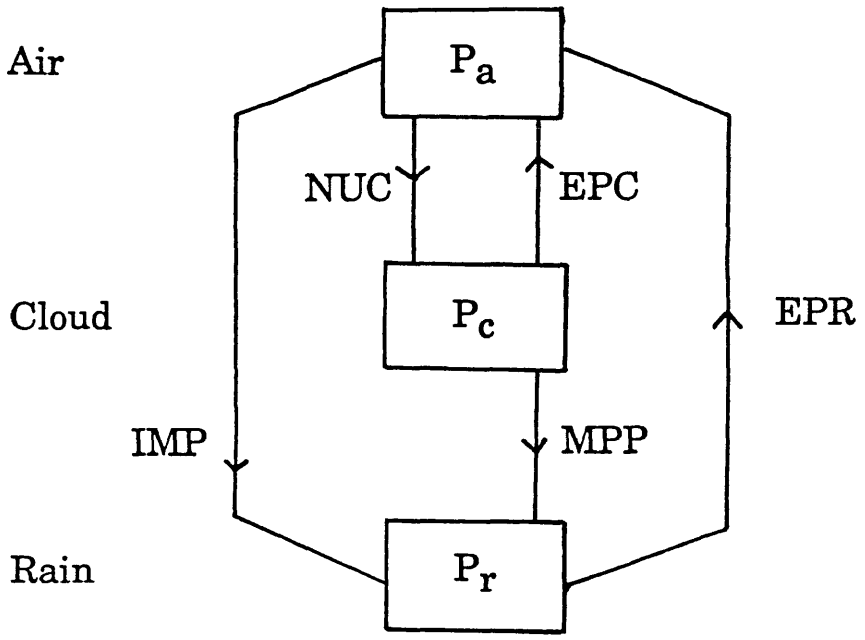


Figure 3.19 Microphysical processes for particulate pollution

causes particulate material in rain to be transferred to the air (EPR). The source/sink terms in (3.37) to (3.39) are given by

$$S_{Pa} = - IMP + EPR - NUC + EPC \tag{3.59}$$

$$S_{Pc} = - EPC - MPP + NUC \tag{3.60}$$

$$S_{Pr} = MPP - EPR + IMP \tag{3.61}$$

Nucleation (NUC)

Nucleation is parametrised by assuming that a certain fraction, E_{nuc}, of particulate material at cloud base is taken up in cloud water by nucleation. Aircraft measurements of sulphate scavenging (Ten Brink et al, 1987) indicate that for hygroscopic particles this factor is close to unity.

The cloud base grid point, j_{cb}^{τ}, at time $t = \tau$ is the lowest grid point for which $q_c(j,\tau) > 0$. Nucleation at cloud base is given by

$$\begin{aligned} &P_c \rightarrow P_c + E_{nuc} P_a \ , \\ &P_a \rightarrow P_a - E_{nuc} P_a \qquad \text{at } j = j_{cb}^{\tau} . \end{aligned} \tag{3.62}$$

In the case where cloud base is descending as cloud forms in previously subsaturated air, care is taken to ensure that nucleation takes place at each grid point through which cloud base descends. Thus if

$$\begin{aligned} j_{cb}^{\tau} &= \text{cloud base at time } t = \tau \\ \text{and } j_{cb}^{\tau+1} &= \text{cloud base at time } t = \tau+1 \end{aligned}$$

then at time $t = \tau+1$

$$\begin{aligned} &P_c \rightarrow P_c + E_{nuc} P_a \ , \\ &P_a \rightarrow P_a - E_{nuc} P_a \qquad \text{for } j_{cb}^{\tau+1} \leq j < j_{cb}^{\tau} . \end{aligned} \tag{3.63}$$

An alternative approach to parametrising nucleation scavenging is to specify the absolute quantity of material nucleated at cloud base. Easter and Hales(1984) calculate this quantity, P_{Anuc}, by

$$P_{Anuc} = N_c \rho_A 4/3 \pi r_A^3$$

where N_c, the number of cloud condensation nuclei, is a fixed constant and ρ_A and r_A are the density and radius respectively of the aerosol particles whose size distribution is assumed to be monodisperse. They specify nucleation as occurring where cloud first forms at a grid point. There,

$$P_a \rightarrow P_a - P_{Anuc}$$
$$P_c \rightarrow P_c + P_{Anuc} .$$

This approach was not chosen here since it does not allow the number of available cloud condensation nuclei to vary with the quantity of particulate material present in the air. This decision is supported by the aircraft measurements of Ten Brink et al(1987) referred to above, which show that a high proportion of aerosol material in air is removed via the nucleation mechanism. A second problem with this approach is that nucleation is only allowed when cloud first forms at a grid point. It seems more realistic to allow particulates passing through cloud base of established cloud to act as cloud condensation nuclei. Cloud is continually forming (wG) as air rises above the saturation level and for cloud droplets to form, particles in that air must act as cloud condensation nuclei.

Impaction (IMP)

Aerosol particles may be collected by falling raindrops. This can be parametrised in exactly the same way as for accretion with the same assumption being made that the efficiency with which a raindrop collects a

particle encountered in its path, E_A, is independent of the diameter of the raindrop. Thus

$$IMP = 6.96.10^{-4} E_A N_0^{1/8} P_a q_r^{7/8} e^{kz/2} . \quad (3.64)$$

This expression is related to the washout coefficient, Λ, defined in Chapter 2. The rate at which volume is swept out by a falling raindrop, radius R_i, falling at speed, V_i, is $\pi R_i^2 V_i$. Therfore the rate of takeup of particulate material by the raindrop is

$$\frac{\delta P_{a_i}}{\delta t} = - \pi R_i^2 E_{A_i} V_i P_a$$

where E_{Ai} is the average efficiency with which particles of total mass P_a per unit volume are caught. Integrating over the raindrop distribution gives the total rate of loss of particulate material in air

$$\frac{dP_a}{dt} = + \int_0^\infty \frac{\delta P_a}{\delta t} N(R)\, dR$$

$$= - \int_0^\infty \pi R^2 V(R) E_A(R) N(R)\, dR\, P_a$$

$$= - \Lambda Pa \quad (3.65)$$

where

$$\Lambda = \int_0^\infty \pi R^2 V(R) E_A(R) N(R)\, dR \quad (3.66)$$

is the washout coefficient. Substituting $N(R) = 2N_c e^{-2\lambda R}$ and $V(R) = 130\, e^{kz/2} (2R)^{1/2}$ into (3.64) and assuming E_A is independent of R gives

$$\frac{dP_a}{dt} = - 6.96.10^{-4} E_A N_0^{1/8} q_r^{7/8} e^{kz/2} P_a \ . \qquad (3.67)$$

Thus an alternative form for Λ is

$$\Lambda = 6.96.10^{-4} E_A N_0^{1/8} q_r^{7/8} e^{kz/2} \ . \qquad (3.68)$$

An expression for rainfall rate, J, in mm/hr has been derived by Kessler for $N_0 = 10^7$ m^{-4} and is given by

$$J = 18.35 q_r^{9/8}. \qquad (3.69)$$

For J = 1 mm/hr,

$$q_r = \left[\frac{J}{18.35} \right]^{8/9} = 0.075 \text{ g/m}^3 \ .$$

Thus $\Lambda_0 = \Lambda(J = 0) = 5.4.10^{-4}. E_A$, assuming $N_0 = 10^7$, z = 0. Values for E_A of 0.1 and 0.2 give Λ as $5.4.10^{-5}. J^{7/9}$ and $1.08.10^{-4}. J^{7/9}$ respectively. This is in good agreement with the recommendations of a report by Jones(1985) which were that Λ should be of the form $\Lambda = a.J^b \ s^{-1}$ with $3.10^{-5} < a < 3.10^{-4}$ and $0.7 < b < 0.9$.

A detailed review of the literature on the scavenging of particles by raindrops has been carried out by Underwood(1983b). For particles smaller than 0.1μ in diameter, collection is principally by the mechanisms of Brownian diffusion whereas for particles larger than 1μ it is by inertial impaction. In between, many processes of comparable magnitude may contribute to the low overall collection efficiencies observed. They include wake capture, phoretic processes and turbulence and electrical effects as well as Brownian diffusion and inertial impaction.

For micron sized particles, inertial impaction is the dominant collection

mechanism. These particles have sufficient inertia to deviate from the flow streamlines around raindrops and be collected. Beard and Grover(1974) have made sophisticated calculations of collection efficiencies for raindrop radii $40 < R < 600\ \mu$ and particle radii $a \geq 1\mu$. They present their results in graphical form and have also derived an interpolation scheme for these results as well as for the potential flow case which applies for larger raindrops with $600 < R < 3000\ \mu$. Results are shown in figures(3.20) and (3.21), taken from Beard and Grover(1974), and comparisons are shown with the theoretical results of Mason(1971) and experimental results. Beard and Grover conclude that previous results for $R \leq 300\mu$ were too low. It is more useful to calculate curves of E_A against R for different particle radii, a. These are shown in figure(3.22) for particles of density $\rho_A = 2300$ kg/m^3 (C), figure(3.23) for $\rho_A = 3675$ kg/m^3 (CsOH) and figure(3.24) for $\rho_A = 4510$ kg/m^3 (CsI).

Calculation of IMP including the variation of E with R gives, from (3.66),

$$\begin{aligned} IMP &= \int_0^\infty \pi R^2\, V(R)\, E_A(R)\, N(R)\, dR \\ &= \int_0^\infty \pi R^2\, 130 \sqrt{2R}\, l N_0\, e^{-2\lambda P}\, E_A(R)\, dR \\ &= 130\, \pi \sqrt{2}\, l \int_0^\infty R^{5/2}\, e^{-2\lambda R}\, E_A(R)\, dR \end{aligned} \qquad (3.70)$$

where from (3.42), $\lambda = 2.4.10^3\, q_r^{-1/4}$. Graphs of $R^{5/2}.\ e^{-2\lambda R}$ for qr = 0.1, 0.5 and 1.0 g/m^3 (J = 1.38, 8.41 and 18.35 mm/hr) are shown in figure(3.25).

Comparison of figures(3.22) to (3.24) and (3.25) shows that a large part of the integral

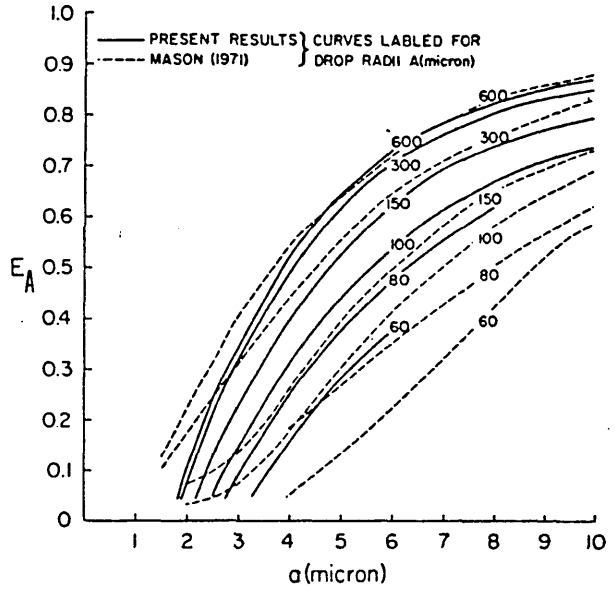


Figure 3.20 Comparison of collection efficiency, E_A, determined from interpolation scheme with values from Mason(1971) (from Beard and Grover, 1974)

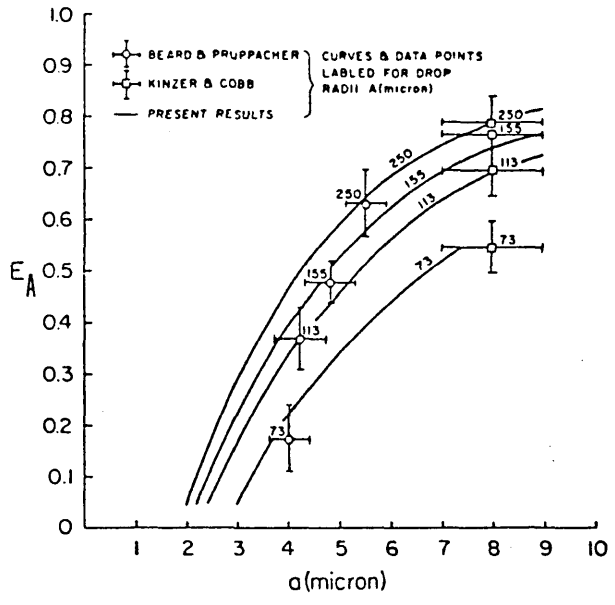


Figure 3.21 Comparison of collection efficiency, E_A, determined from interpolation scheme with experiments involving particles with $\rho_A = 1 g/cm^3$ (from Beard and Grover, 1974)

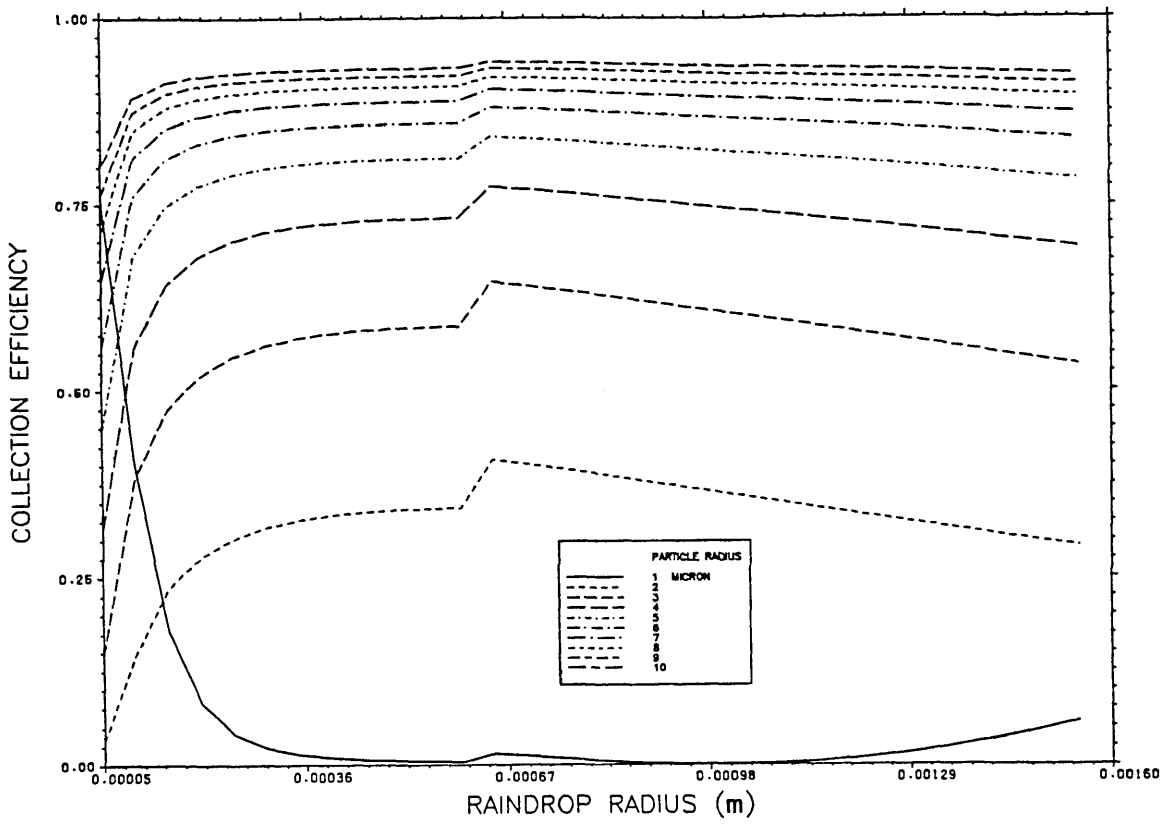


Figure 3.22 Collection efficiencies for particles of density of carbon (ρ_A = 2250 kg/m^3)

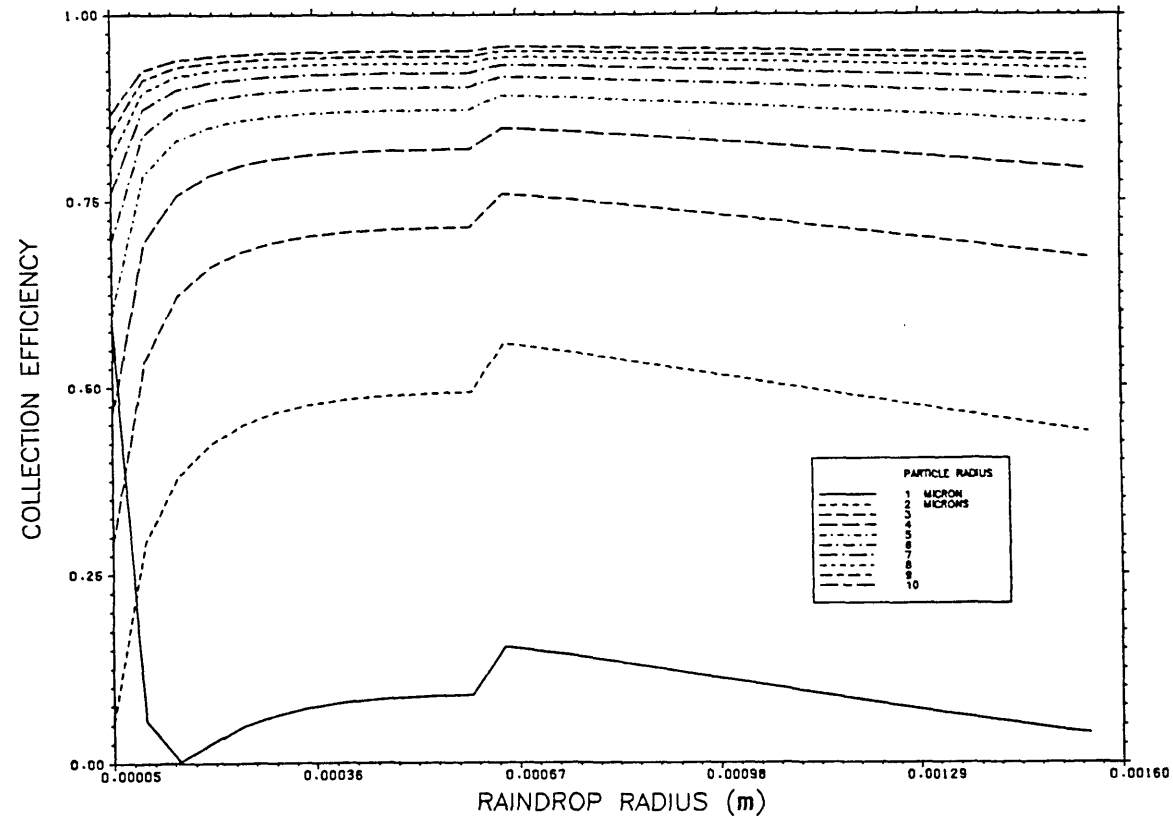


Figure 3.23 Collection efficiencies for particles of density of caesium hydroxide (ρ_A = 3675 kg/m^3)

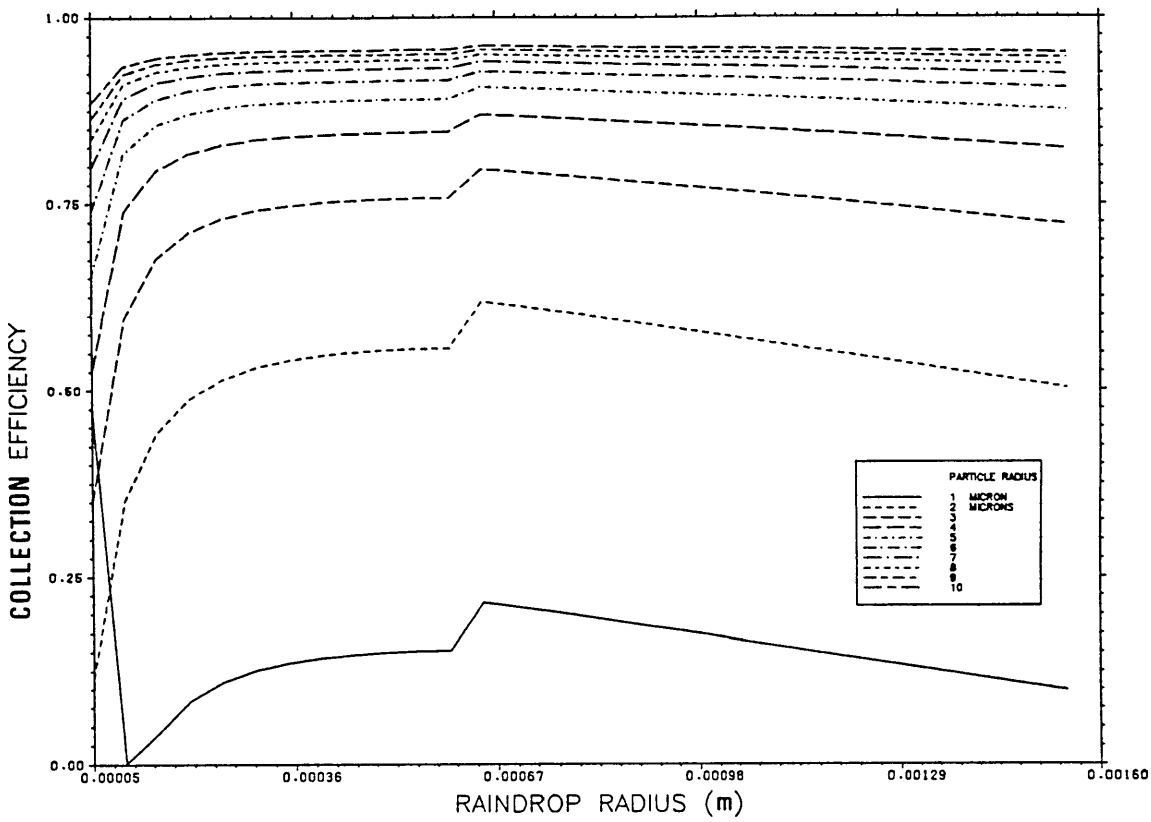


Figure 3.24 Collection efficiencies for particles of density of caesium iodide (ρ_A = 4510 kg/m^3)

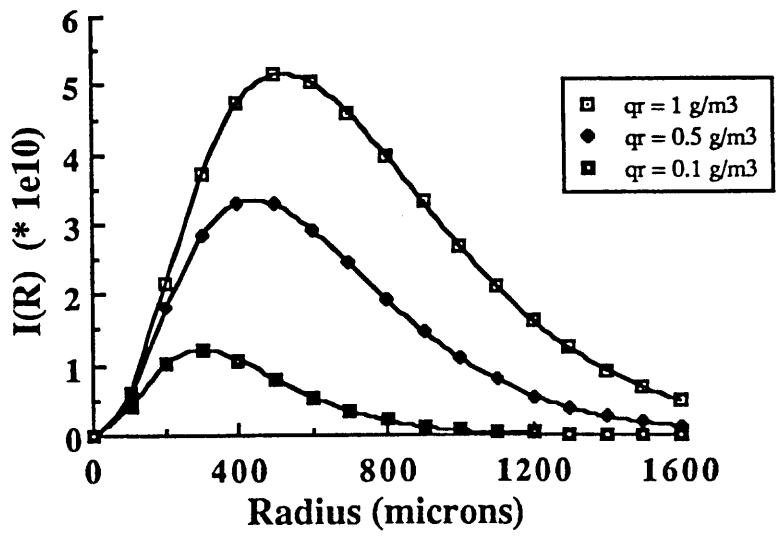


Figure 3.25 Variation of I(R) = $R^{5/2}e^{-2\lambda R}$ with raindrop radius, R

$$\int_0^{\infty} R^{5/2} e^{-2\lambda R} E_A(R)\, dR$$

is given by integrating over the range $0 < R < 1600\mu$. From figures(3.22) to (3.24) of collection efficiencies of C, CsI and CsOH particles, based on Beard and Grover's interpolation scheme, approximate average values for E_A have been derived and are given in table(3.3). The values of E_A for 1μ radius CsOH and CsI particles of 0.1 and 0.15 respectively yield values for Λ^0 of $5.4.10^{-5}$ and $8.1.10^{-5}$.

Table 3.3 Collection efficiencies based on Beard and Grover's (1974) interpolation scheme averaged across raindrop spectrum

Radius(μ)	C	CsOH	CsI
1	small	0.1	0.15
2	0.3	0.5	0.55
3	0.55	0.7	0.75

Evaporation of cloud (EPC)

Particulate material remaining in cloud water is assumed to be immediately released to air on total evaporation of cloud. Aircraft measurements support this assumption (Ten Brink et al, 1987). At those grid points for which $q_c < 0$

$$P_a \rightarrow P_a + P_c \ ,$$
$$P_c \rightarrow 0 \ . \qquad (3.71)$$

Conversion from cloud to rain by microphysical processes (MPP)

The proportion of particulate in cloud converted to particulate in rain is assumed to be the same as the proportion of cloud water converted to rain water by the microphysical processes of autoconversion and accretion.

$$MPP = \begin{cases} \dfrac{AC + CC}{q_c} P_c & \text{for } q_c > 0 \\ 0 & \text{otherwise} \end{cases} \qquad (3.72)$$

Evaporation of rain (EPR)

The proportion of particulate in rain released to air due to evaporation is the same as the proportion of rain that evaporates in subsaturated air.

$$EPR = \frac{EP}{q_r} P_r . \qquad (3.73)$$

3.4.2 Pollutant material budget

As for the pure cloud simulations, the updraught velocity is described by

$$w = w_{max} \sin(\pi z/H)$$

with an initial saturation deficit of

$$q_c = q_{cmin}(1 - z/H)$$

where q_{cmin} may be negative.

Particulate pollution has an initial profile

$$P_a = \begin{cases} P_{amax} \sin\left[\dfrac{2\pi z}{H}\right] & 0 \le z \le \dfrac{H}{2} \\ 0 & \dfrac{H}{2} \le z \le H \end{cases} \qquad (3.74)$$

Since the model formulation is completely linear, the absolute magnitude of P_{amax} is not important.

As cloud develops in the updraught, particulate material is scavenged as a result of the microphysical processes described above. Its fate can be followed by calculating a mass balance. Adding (3.37), (3.38) and (3.39) and integrating over the height of the model domain and the duration of the updraught gives

$$\int_0^H dz \left[P_a + P_c + P_r \right]_0^T + \int_0^T dt \left[wP_a + wP_c + (V_t+w)P_r \right]_0^H$$

$$= \int_0^T dt \int_0^H dz \left(\frac{\partial w}{\partial z} + w \frac{\partial \ln \rho}{\partial z} \right) (P_a + P_c + P_r) \qquad (3.75)$$

Since $w(z = 0) = w(z = H) = V_t(z=H) = 0$, this simplifies to

$$\int_0^H dz \left[P_a + P_c + P_r \right]_0^T - \int_0^T dt\, V_t\, P_r |_{z=0} = \int_0^T dt \int_0^H dz \left(\frac{\partial w}{\partial z} + w \frac{\partial \ln \rho}{\partial z} \right) (P_a + P_c + P_r) .$$

(3.76)

The term on the right hand side of (3.76), which can be rewritten

$$\int_0^T dt \int_0^H dz \left(\frac{\partial w}{\partial z} + w \frac{\partial \ln \rho}{\partial z} \right) (P_a + P_c + P_r) = -\int_0^T dt \int_0^H dz \left(\frac{\partial u}{\partial x} + \frac{\partial v}{\partial y} \right) (P_a + P_c + P_r) ,$$

from the continuity equation(3.21), represents the total horizontal divergence of material. Below the level of non-divergence, z_{nd}, where this term is positive, there is horizontal convergence of material and above the level of non-divergence, where it is negative, there is horizontal divergence. The mass balance can be expressed as

$$M_{in} = M_{out} \tag{3.77}$$

where M_{in} is the total particulate mass in and M_{out} is the total mass out during time T and

$$M_{in} = \int_0^H dz\,(P_a + P_c + P_r)\,|_{t=0} + \int_0^T dt \int_0^{z_{nd}} dz\,(\frac{\partial w}{\partial z} + w\frac{\partial \ln \rho}{\partial z})\,(P_a + P_c + P_r) \tag{3.78}$$

and

$$M_{out} = \int_0^H dz\,(P_a + P_c + P_r)\,|_{t=T} - \int_0^T dt\, V_t\, P_r\,|_{z=0} - \int_0^T dt \int_{z_{nd}}^H dz\,(\frac{\partial w}{\partial z} + w\frac{\partial \ln \rho}{\partial z})\,(P_a + P_c + P_r)\ . \tag{3.79}$$

Of the total mass of particulate material that is present initially or enters the updraught via horizontal convergence below the level of non-divergence, part is deposited in rain, part is exported via horizontal divergence above the level of non-divergence and the rest remains. The efficiency of rainout, E_{ro}, and the efficiency of export, E_{exp}, are given by

$$E_{ro} = \frac{-\int_0^T dt\, V_t P_r |_{z=0}}{M_{out}} \qquad (3.80)$$

and

$$E_{exp} = \frac{-\int_0^T dt \int_{z_{nl}}^H dz \left(\frac{\partial w}{\partial z} + w\frac{\partial \ln \rho}{\partial z}\right)(P_a + P_c + P_r)}{M_{out}} \qquad (3.81)$$

3.4.3 Model results and sensitivity studies

The essential difference between hygroscopic and hydrophobic particles is that the former can act as cloud condensation nuclei whereas the latter cannot. This is simply represented by

$E_{nuc} = 0$ for hydrophobic particles

$E_{nuc} \neq 0$ for hygroscopic particles.

The standard value for E_{nuc} for hygroscopic particles was taken to be 0.9. This represents almost complete nucleation sacavenging in accordance with the aircraft measurements of Brink et al. E_{nuc} was not set to unity so as to avoid numerical problems that can arise when the quantity of air pollutant in a grid box suddenly becomes zero.

The evolutions of hygroscopic material in air, cloud and rain water for the standard model run with parameter values as given in table(3.4) are shown in figures(3.26) to (3.28). Where cloud first forms, particulate material in air is lost to cloud water with peaks remaining above and beneath the cloud(see figure(3.26) at t = 400s). The lower peak is quickly lost by nucleation as the cloud base descends and impaction of remaining particles in air once precipitation starts to fall (figure(3.26) at t = 800s).

Table 3.4 Parameter values for standard cloud run including hygroscopic particulates (cloud parameters as in table (3.1))

Parameter	Value
E_{nuc}	0.9
E_A	0.1
T	4000 s

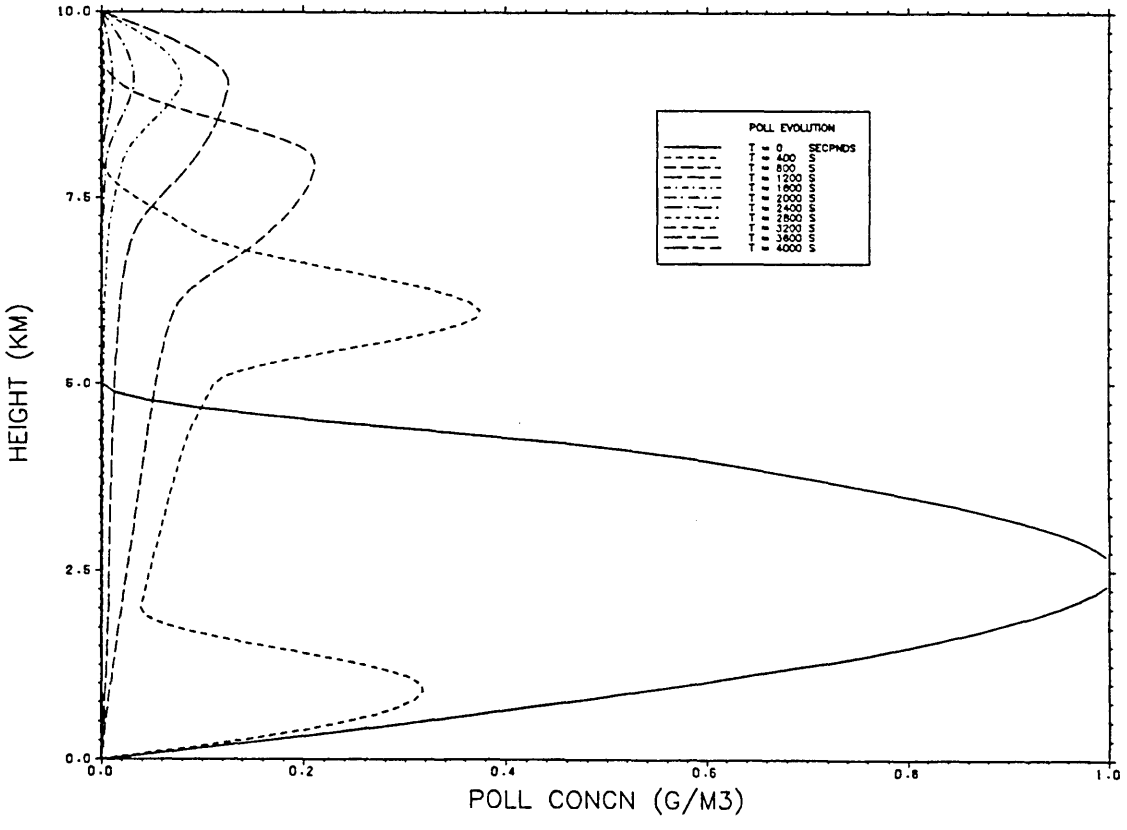


Figure 3.26 Development of particulate material in air - standard run

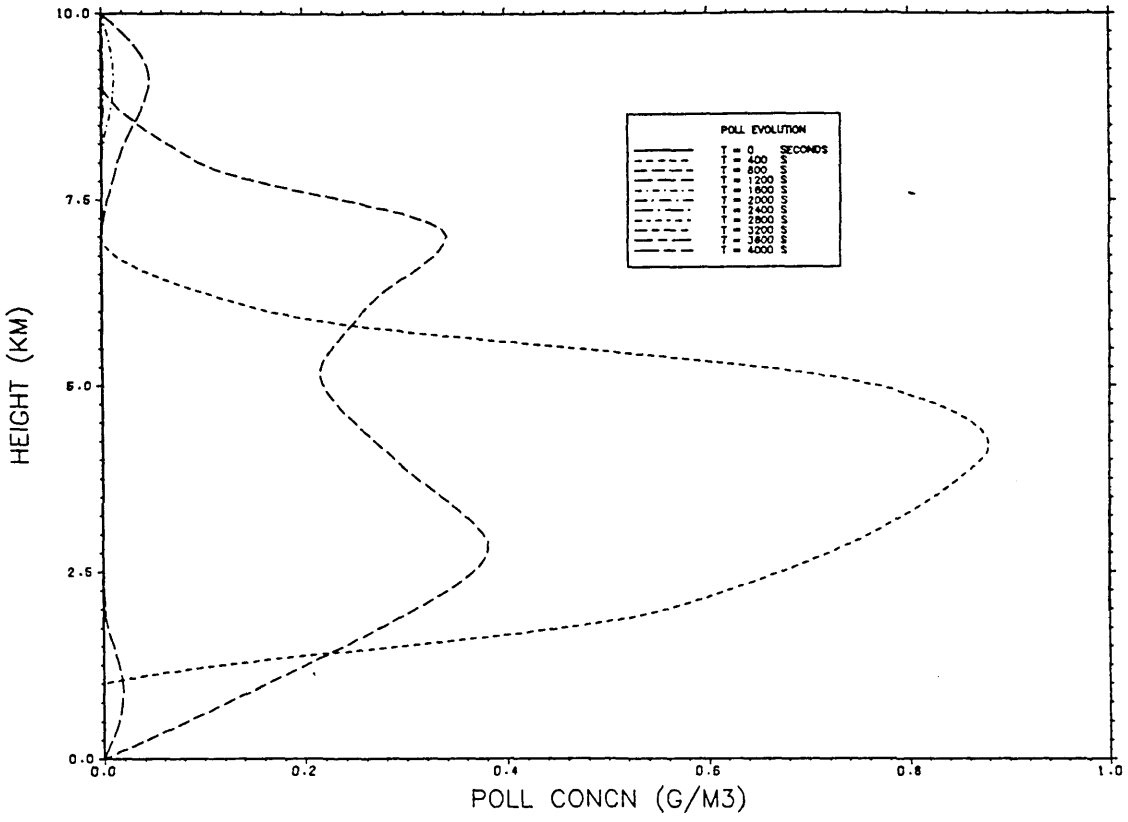


Figure 3.27 Development of particulate material in cloud water - standard run

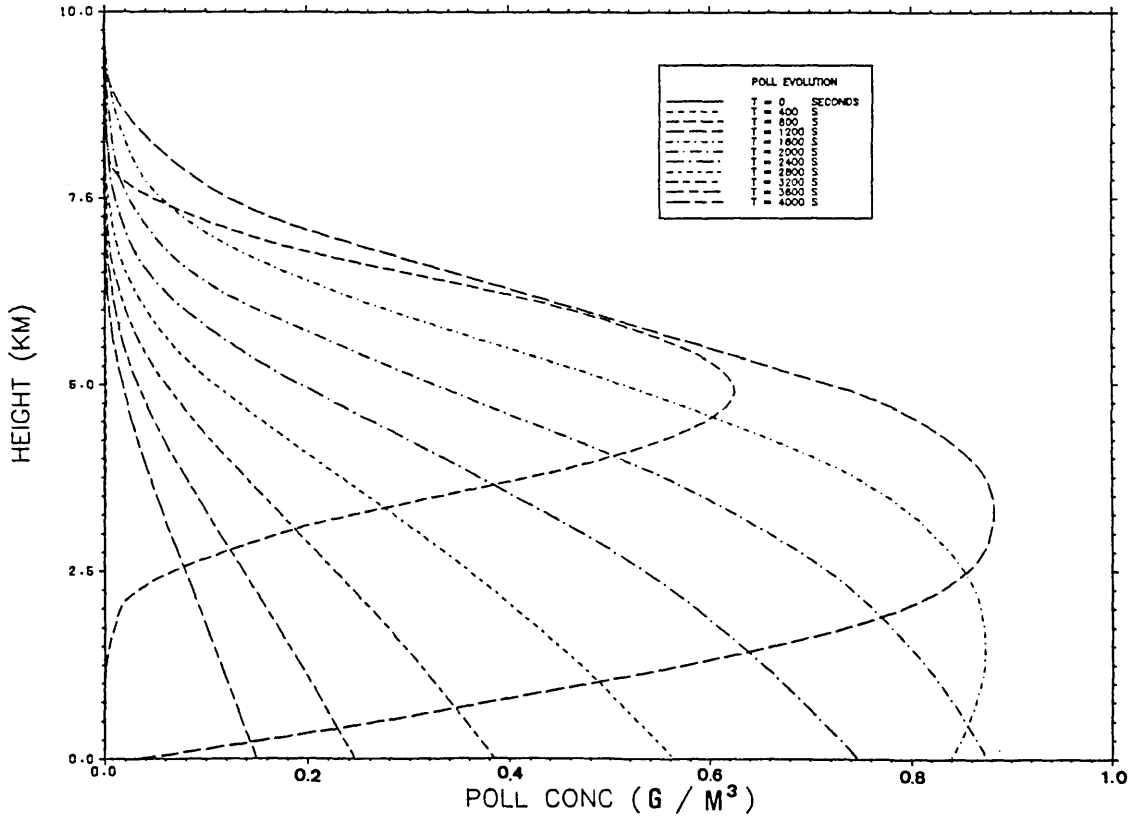


Figure 3.28 Development of particulate material in rain water - standard run

Particulates in air and cloud water near the top of the updraught are mostly swept out aloft by horizontal divergence. The quantities of most interest are the efficiencies with which pollution is rained out, E_{ro}, and swept out aloft, E_{exp}, which are given by equations(3.80) and (3.81).

Model runs were first made assuming air is incompressible, i.e. k = 0. This simplifies all calculations since all $\partial\rho/\partial z$ terms vanish, but for H = 10 km it is not a good app roximation.
($\rho(z = H) = \rho_0.e^{-kH} = \rho_0.e^{-1} = 0.37.\rho_0$).
The variations of E_{ro} and E_{exp} with updraught velocity for the standard run parameters and k = 0 are shown in figures(3.29) and (3.30). For very small updraught velocities (w_{max} < 0.5 m/s), cloud has barely formed by T = 4000s and the initial profile of air pollution remains relatively undisturbed with very little pollution being deposited in rain or exported at high level. For hygroscopic particles the efficiency of rainout increases sharply above w_{max} = 0.5 m/s with greater than 80% deposited at 1 m/s rising to 88% at 3 m/s. With larger updraught velocities the efficiency of rainout drops off as more pollution is swept up and out of the updraught before it can be deposited in rain. By w_{max} = 10 m/s, roughly equivalent am ounts are exported as rained out (~ 43%). For hydrophobic particles, rainout efficiencies are roughly 20% lower and efficiencies of export roughly 20% higher. Also the peak in E_{ro} is reached rather more gradually than for hygroscopic particles without such a sudden increase around w_{max} ~ 1 m/s.

Once runs had been made successfully with k = 0, compressibility was included by setting k = 10^{-4}. For both hygroscopic and hydrophobic particles, efficiencies of rainout are lower by 5 - 10 % than for the incompressible runs with efficiencies of export being 5 - 10 % higher. The overall pattern of wet deposition and export and their variation with

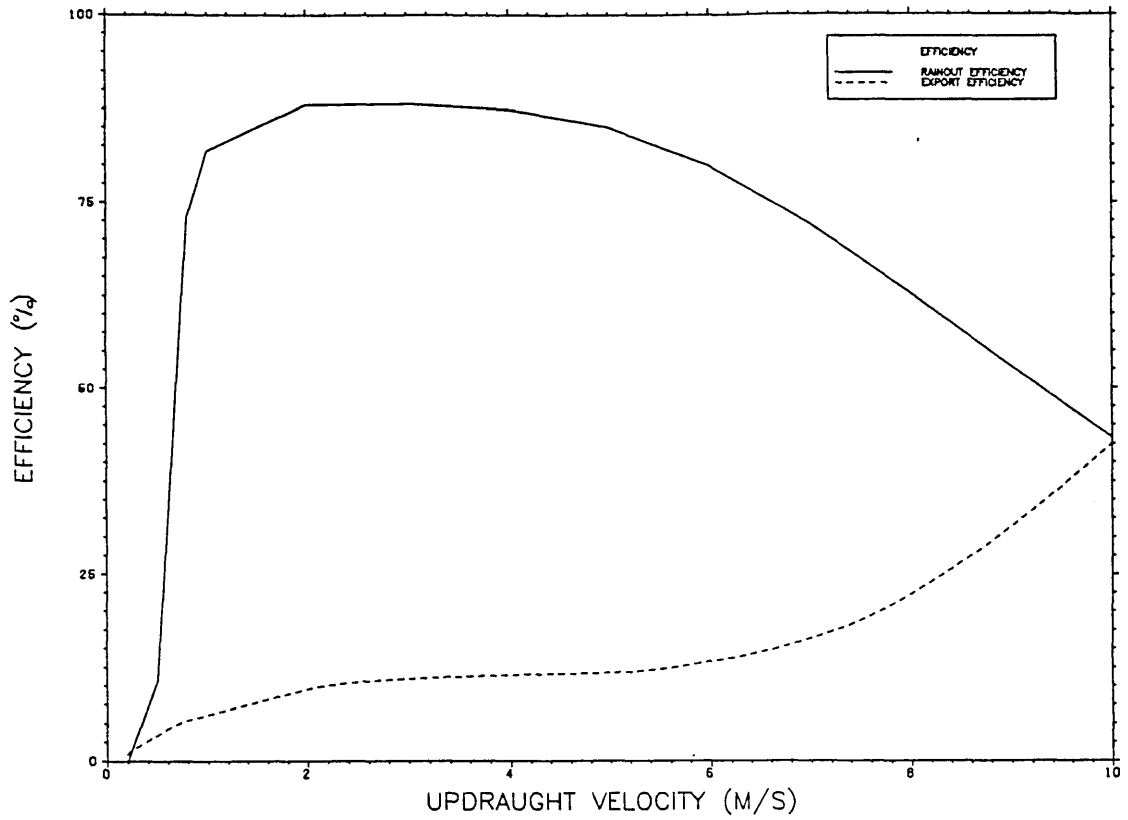


Figure 3.29 Rainout and export efficiencies for hygroscopic particles and standard run parameters, k = 0

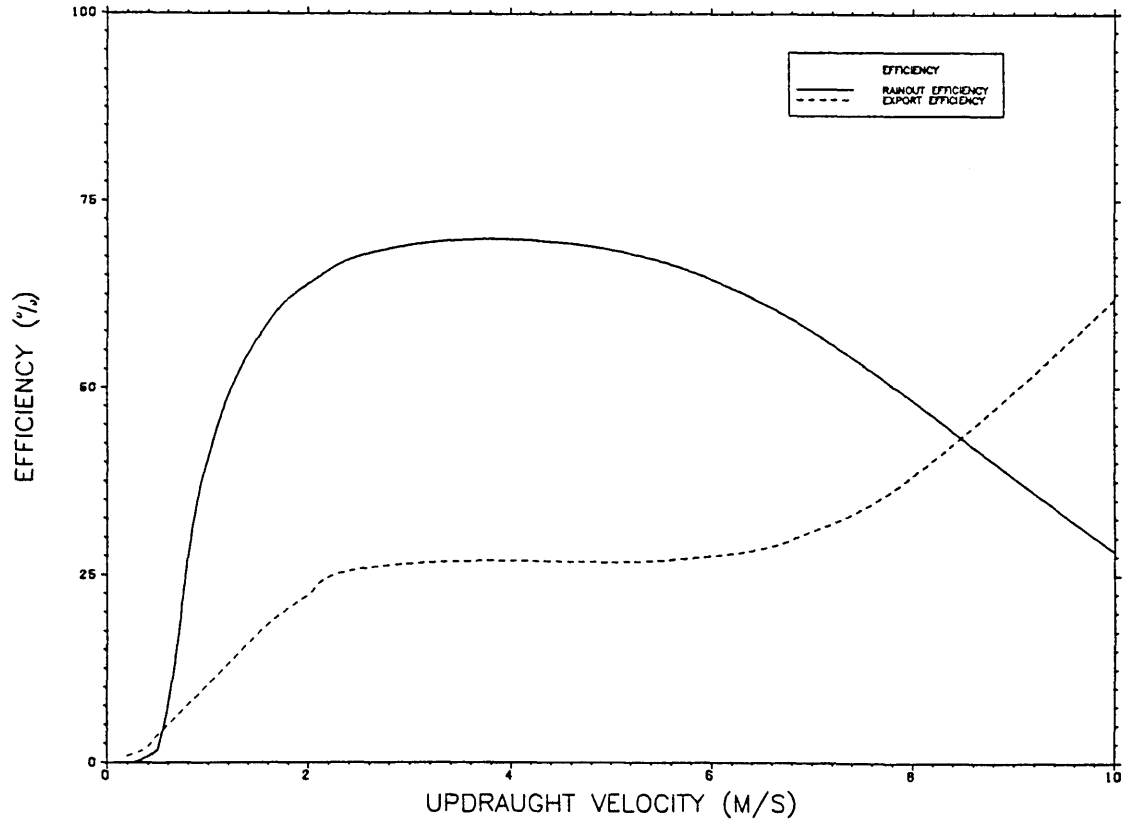


Figure 3.30 Rainout and export efficiencies for hydrophobic particles and standard run parameters, k = 0

updraught velocity remain the same (see figures (3.31) and (3.32)). Doubling impaction efficiency to 0.2 (figures (3.33) and (3.34)) reduces the difference between E_{ro} for hygroscopic and hydrophobic particles to 10%.

At T = 4000s, for a large range of updraught velocities, virtually all pollutant material is either rained out or exported aloft and virtually none is left in the domain at the conclusion of the model run. For a shorter run time of 2000 s, this is no longer the case and for w_{max} > 4 m/s the total rained out or exported aloft reduces to roughly 80% leaving 20% remaining (see figures(3.35) and (3.36)). It is still the case that efficiencies of rainout are about 20% higher for hygroscopic than for hydrophobic particles, although in this case the lower efficiencies mean that there is a doubling of E_{ro}. Exports aloft are increased by roughly 15% for hydrophobic particles compared to hygroscopic particles. For w_{max} = 10 m/s, 78% of hydrophobic material is exported aloft despite the high precipitation quantities. The ability of convective storms to transport material from the boundary layer to the higher layers of the atmosphere may lead to a reduction in wet deposition from that which might be expected from the washout model in certain circumstances.

3.5 Summary and conclusions

In this chapter, the one-dimensional cloud models of Kessler(1969) have been enhanced and extended to include the transport and scavenging of particulate pollution. The sensitivity of cloud model development to various microphysical parametrisations were studied before particulate pollutants were incorporated. Parametrisations of the important microphysical processes of nucleation and impaction scavenging were based on aircraft measurements, laboratory experiments and theoretical calculations. The model results of most interest are the efficiencies with which pollutant material is rained out in precipitation and exported from the model domain

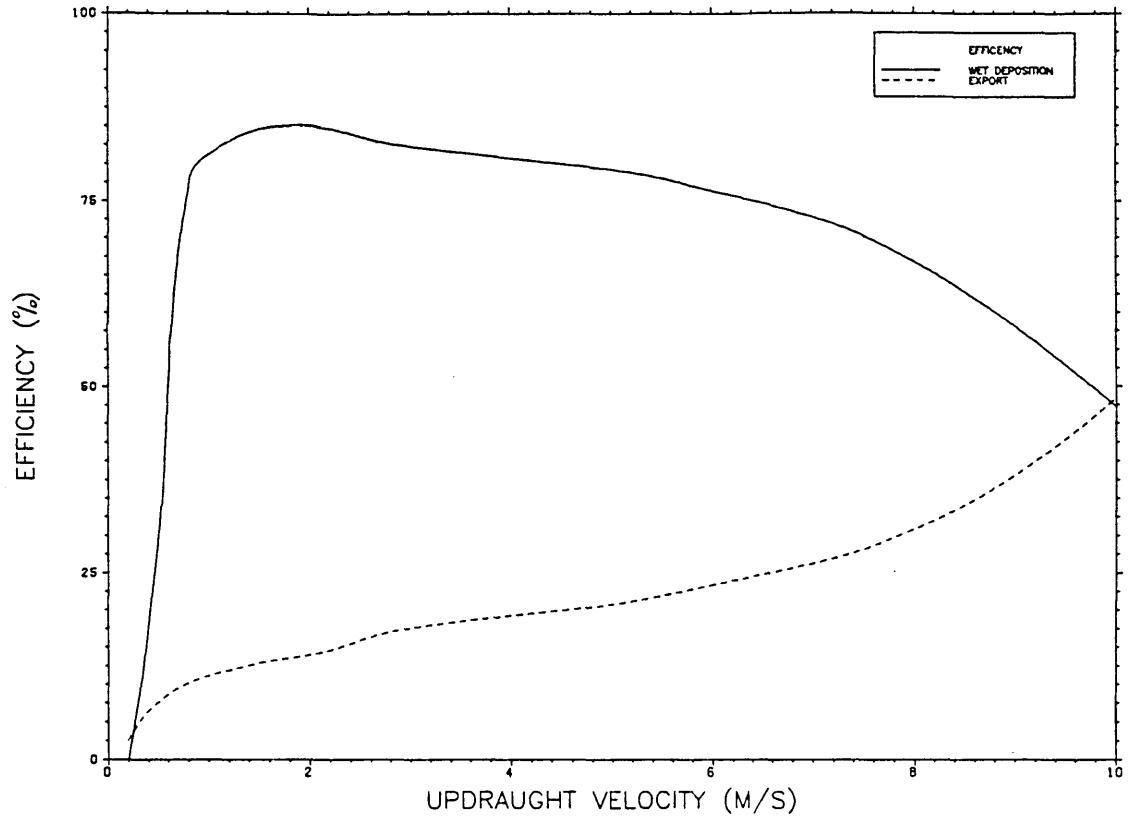


Figure 3.31 Rainout and export efficiencies for hygroscopic particles and standard run parameters, $k = 10^{-4}$

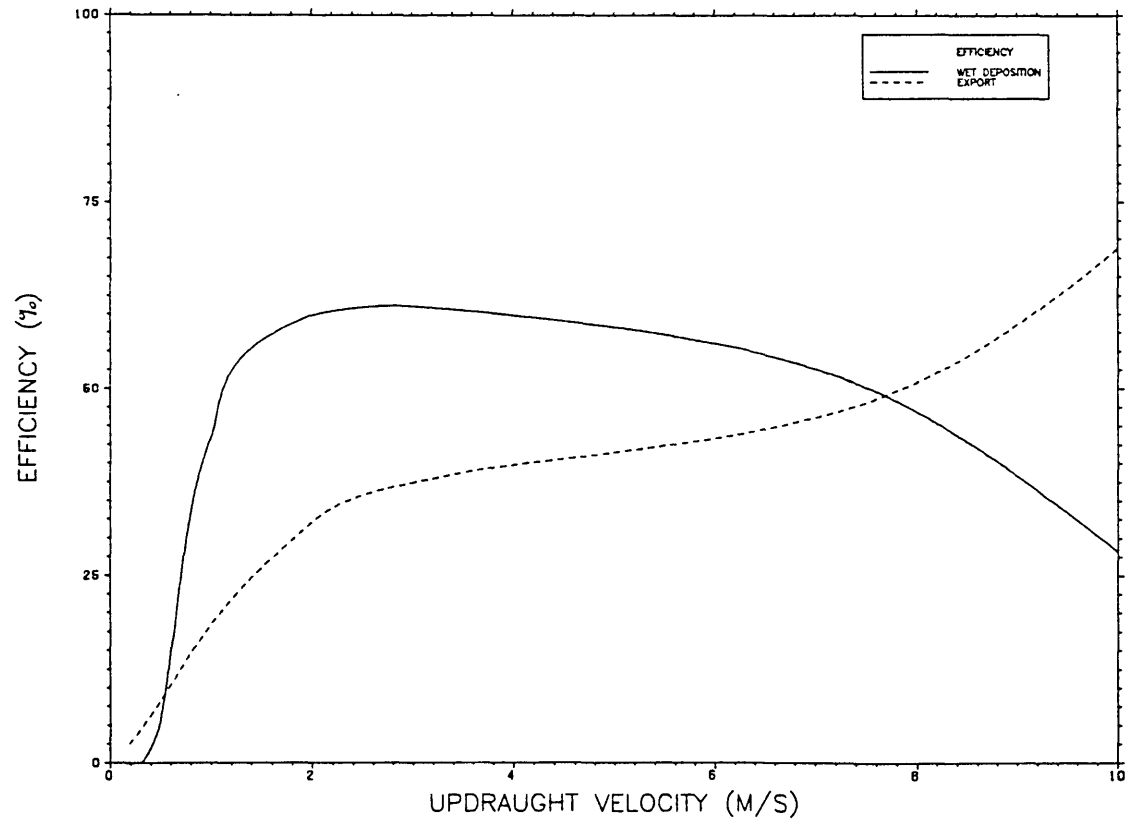


Figure 3.32 Rainout and export efficiencies for hydrophobic particles and standard run parameters, $k = 10^{-4}$

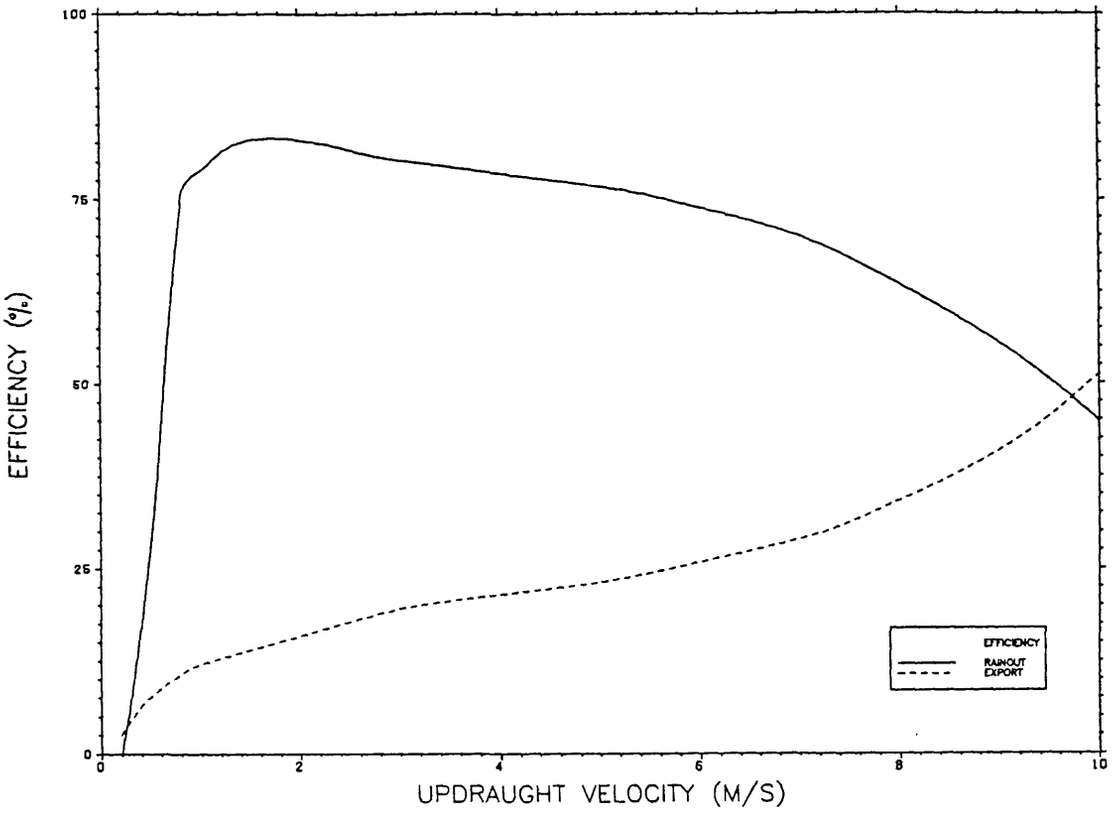


Figure 3.33 Rainout and export efficiencies for hygroscopic particles, $E_A = 0.2$, $k = 10^{-4}$

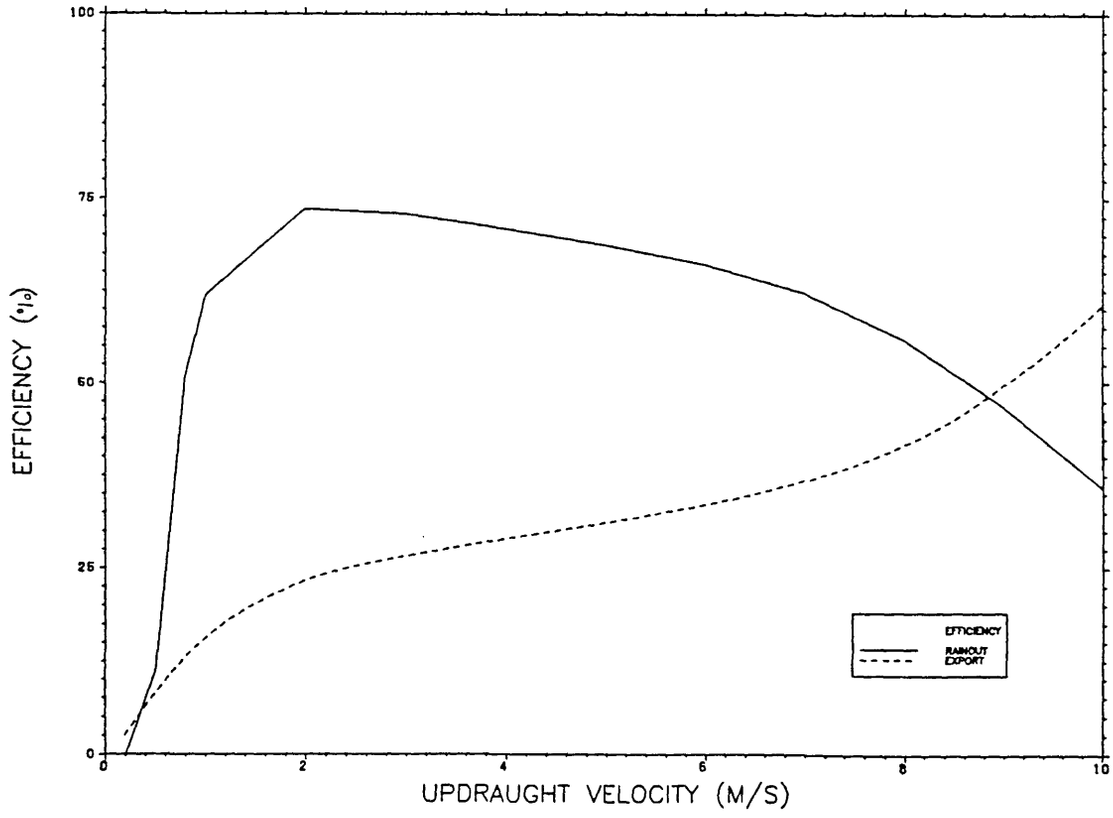


Figure 3.34 Rainout and export efficiencies for hydrophobic particles, $E_A = 0.2$, $k = 10^{-4}$

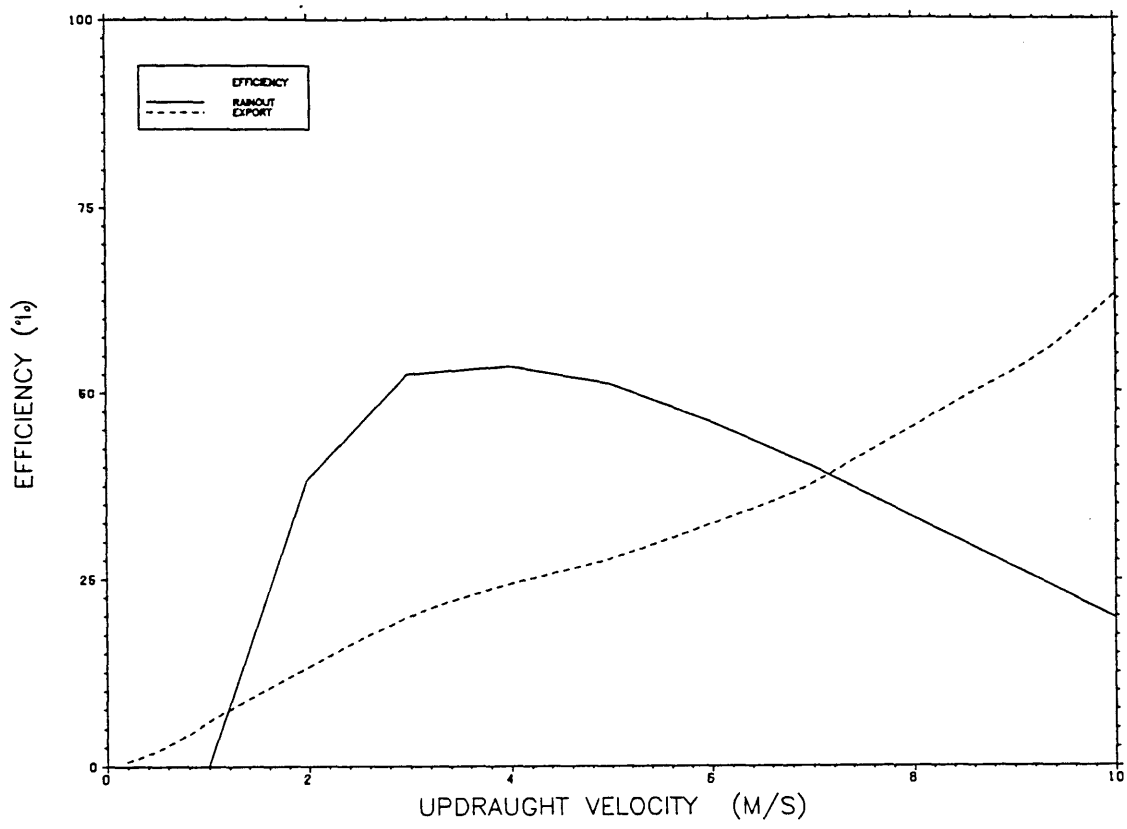


Figure 3.35 Rainout and export efficiencies for hygroscopic particles, $T = 2000s$, $k = 10^{-4}$

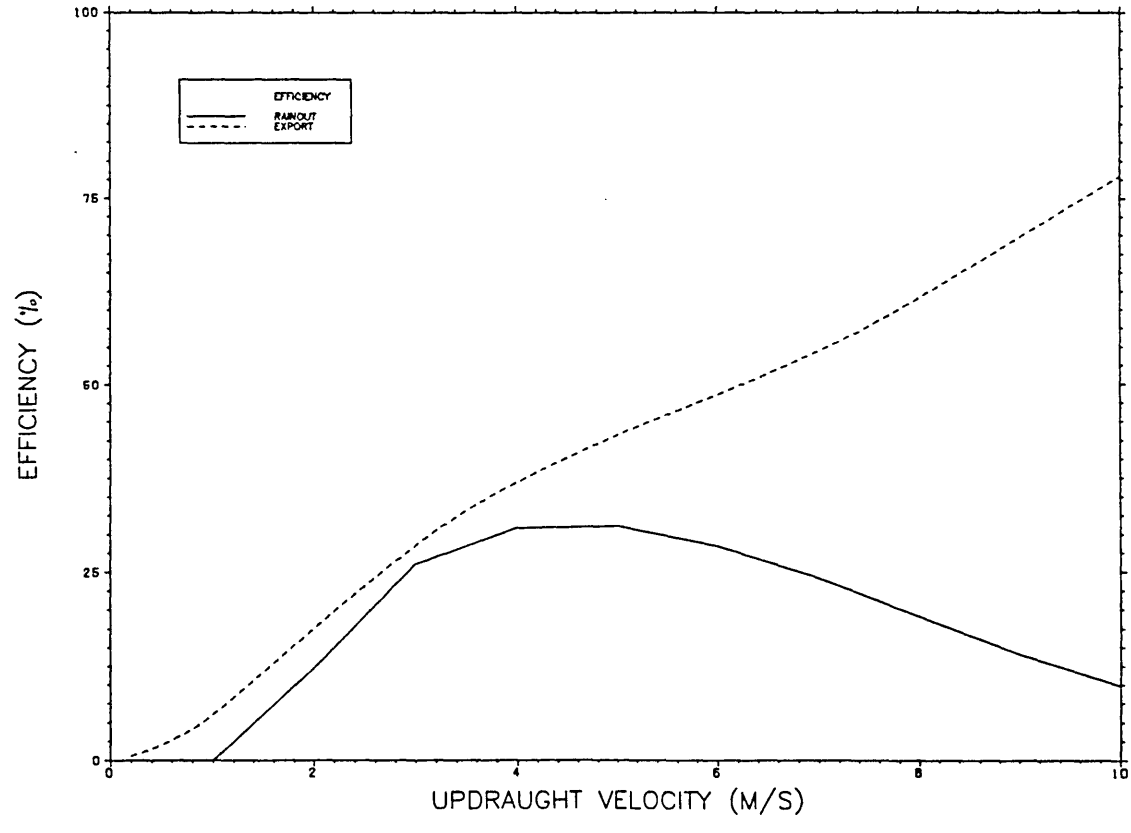


Figure 3.36 Rainout and export efficiencies for hydrophobic particles, $T = 2000s$, $k = 10^{-4}$

to upper layers of the atmosphere. These efficiencies show great variation with updraught velocity; for very small velocities precipitation is negligible and very little pollution can be transported aloft, whereas for large updraught speeds pollution is exported before it can be deposited in precipitation. Both hygroscopic and hydrophobic particles are deposited most efficiently in precipitation for updraught velocities between 1 and 6 m/s. Hygroscopic particles, which can be scavenged by nucleation, are deposited more efficiently than hydrophobic particles, the difference in efficiencies being about 20% for a large range of model parameters.

Modelling in one spatial dimension is limited dynamically. Only a single updraught can be simulated. Implicit in the formulation is convergence of air in the lower part of the domain and divergence higher up. Precipitation falls directly through the updraught that is generating cloud water droplets. Consequently the quantities of precipitation formed are unrealistically high and would lead to termination of the updraught due to negative buoyancy and evaporative cooling. In all the cloud modelling work described in this thesis, the dynamics is pre-specified and therefore such feedback mechanisms between microphysics and dynamics cannot be incorporated. However, better dynamical descriptions of many cloud systems can be acheived by modelling in two dimensions. Systems such as orographic cloud, cold fronts and long-lived convective storms are both multi-dimensional and steady state in nature. They are the subject of chapter 5.

In this chapter only particulate pollutants have been considered. Some part of the iodine release from a nuclear reactor accident is likely to be in gaseous form. Therefore to model the scavenging of this portion of the release, the chemistry of uptake of gases by cloud water drops needs to be incorporated. This chapter showed how overall efficiencies of deposition

and export of particulate pollution from a single updraught could be calculated in one dimension and sensitivities to model parameters investigated. Before going to the extra difficu lty and expense of modelling in two dimensions, the transport and scavenging of gaseous pollution is modelled in one dimension in the next chapter.

4 Chemistry

4.1 Introduction

A certain fraction of the iodine released in a nuclear accident is likely to be in gaseous form. Therefore the scavenging of gases in cloud systems and the chemistry of their behavour in air and in the aqueous phase should be considered. Little is known about the chemistry of iodine but the problems caused by 'acid rain' have led to a large research effort being directed into the scavenging of sulphur dioxide. Some cloud models have incorporated complex chemical schemes including sulphur dioxide and other important species such as carbon dioxide and ammonia (e.g. Seigneur and Saxena, 1988, Tremblay and Leighton, 1984, Hong and Carmichael, 1986). However the theoretical basis is the same, namely absorption from air to cloud water drops (or desorption to air from cloud water drops) until the gas in air and water is in equilibrium, followed by chemical reaction once in the aqueous phase. This may include oxidation to aerosol material allowing more gaseous material to be absorbed from air. Subsequent evaporation of the drop may lead to release of interstitial aerosol.

In many cloud models that incorporate chemical schemes the assumption is made that gases in air and cloud water are always in instantaneous equilibrium (e.g. Tremblay and Leighton, 1984, Hales, 1982). This is assumed in section(4.2). The basic theory of Henry's Law is reviewed in section(4.2.1) for both sulphur dioxide and iodine and the manner in which this is included in the dynamic model is described. A comparison is made in section(4.2.2) between model results and an analytic calculation in the special case of a small updraught velocity. This allows a check to be made on the accuracy of the numerical model. Results of more general modelling studies are discussed in section(4.2.3). A finite rate for absorption and desorption is included in the 1D model in section(4.3). The theory is

reviewed in section(4.3.1) and a calculation is made so as to allow incorporation of gaseous absorption and desorption by a population of raindrops into the bulk microphysical scheme. Results are discussed in section(4.3.2) and are compared with the instantaneous equilibrium results from section(4.2.3). Finally, the significance of these results to scavenging of iodine following an accidental release is discussed.

4.2 Gaseous scavenging assuming equilibrium

4.2.1 Basic theory

Sulphur dioxide scavenging

Sulphur dioxide present in air will be absorbed by water droplets in a cloud until they are saturated, when the sulphur dioxide in its aqueous and gaseous forms is in equilibrium. This equilibrium may be described by Henry's Law. The quantities of $S0_2$ in water, X_c, (in units g/m^3 water) and in air, G_a, (in units g/m^3 air) are related by

$$X_c = H\, G_a \tag{4.1}$$

where H is Henry's Law constant.

The solubility of the gas may be enhanced by chemical reaction in solution. Expression(4.1) relates only to the unreacted fraction of the gas and therefore a proportionately greater quantity of gas may enter into solution. For SO_2 the most important reaction occurring is

$$SO_2\,(aq) \overset{K1}{<=>} H^+ + HSO_3^- \tag{4.2}$$

where

$$K_1 = \frac{\left[H^+ \right]\left[HSO_3^- \right]}{\left[SO_2\,(aq) \right]} \tag{4.3}$$

at equilibrium and the square brackets denote concentrations. Following Postma(1970), an overall Henry's Law constant H' is defined by

$$H' = \frac{\text{total mass of } SO_2 \text{ in liquid}}{SO_2 \text{ concn in gas}}$$

$$= \frac{\left[SO_2(aq) \right] + \left[\text{dissoc. } SO_2 \right]}{\left[SO_2(gas) \right]}$$

$$= \frac{\left[SO_2(aq) \right] + \left[H^+ \right]}{\left[SO_2(gas) \right]}$$

$$= \frac{\left[SO_2(aq) \right] + K_1^{1/2} \left[SO_2(aq) \right]^{1/2}}{\left[SO_2(gas) \right]}$$

$$= H \left[1 + \frac{K_1^{1/2}}{\left[SO_2(aq) \right]^{1/2}} \right]$$

$$= H \left[1 + \frac{K_1}{\left[H^+ \right]} \right] \qquad (4.4)$$

Approximate values for H and K_1 in the temperature range 0 to 10^o C are 60 and 0.02 moles l^{-1} respectively (Hales (1978)). Following Fisher(1982), H' is specified by

$$H' = 60 \left(1 + \frac{0.02}{\left[H^+ \right]} \right)$$

$$\sim 1.2.10^{pH}. \qquad (4.5)$$

Once SO_2 is in solution, it oxidises to sulphate at a slow rate, k_t, which does not affect the instantaneous Henry' Law constant, H'. SO_2 in air also oxidises to sulphate but at a rather slower rate, k_a. $S0_2$ in solution is oxidised principally by ozone and hydrogen peroxide.

Iodine scavenging

Gaseous iodine behaves in a similar though more complex way to SO_2. Its behaviour has been reviewed by Underwood(1983b). Eggleton(1967) proposed the following series of reactions for iodine

		Reaction number
I_2 (gas phase)	$<=^{H}=>$ I_2 (aqueous)	1
$I_2(aq) + I^-$	$<=^{K1}=>$ I_3^-	2
$I_2(aq) + H_2O$	$<=^{K2}=>$ $H^+ + I^- + HIO$	3
$I_2(aq) + H_2O$	$<=^{K3}=>$ $H_2OI^+ + I^-$	4
$3I_2 + 3H_2O$	$<=^{K4}=>$ $IO_3^- + 5I^- + 6H^+$	5
HIO	$<=^{K5}=>$ $H^+ + IO^-$	6
$IO^- + I^- + H_2O$	$<=^{K6}=>$ $I_2OH^- + OH^-$	7
$IO_2^- + I^-$	$<=^{K7}=>$ $I_2O_2^{2-}$	8

Over pH values and iodine concentrations of interest, the last three reactions are unimportant. Reaction no 5 can be considered the net result of no 3 and

$$3HIO <==> 2I^- + 3H^+ + IO_3^-.$$

This latter reaction is slow and may not reach equilibrium. It therefore limits the extent to which no 5 takes place. The overall Henry's Law constant calculated by Eggleton(1967) is

$$H' = H\left[1 + \frac{1}{[I_2(aq)]}\left[1 + 2K_1[I_2(aq)]\right]\frac{K_2}{[H^+]} + K_3^{1/2}\left[\frac{1}{[I_2(aq)]} + K_1\right]^{1/2}\right] \quad (4.6)$$

where

$$K_1 = \frac{[I_3^-]}{[I_2(aq)][I^-]}$$

$$K_2 = \frac{[H^+][I^-][HIO]}{[I_2(aq)]}$$

$$K_3 = \frac{[H_2OI^+][I^-]}{[I_2(aq)]} .$$

Calculations of H' based on formula(4.6) with equilibrium constants calculated at 25^0 C are shown in figure(4.1). Also shown are modified results calculated assuming the iodate reaction reaches equilibrium.

Gittus et al(1982) reviewed iodine scavenging in the context of spray removal in PWR accidents. Theoretical predictions of Lin(1975) at 25^0 C and pH = 7 together with experimental measurements made by Pelletier and Hemphill(1979) over a pH range of 4 to 11 are shown in figure(4.2). From theoretical and experimental considerations, Underwood concludes that values for H' exceeding 10^4 may be difficu lt to substantiate at the low gas concentrations relevant to acccidental releases to the atmosphere.

Iodine in solution in the (-1) oxidation state may be oxidised by both O_3 and H_2O_2 (Jenkin(1987))

$$I^- + O_3 + H^+ \rightarrow HOI + O_2$$

$$I^- + H_2O_2 + H^+ \rightarrow HOI + H_2O$$

General gaseous scavenging

With the assumption that gaseous material present in air, cloud and rain water is instantaneously in equilibrium, their concentrations are related by

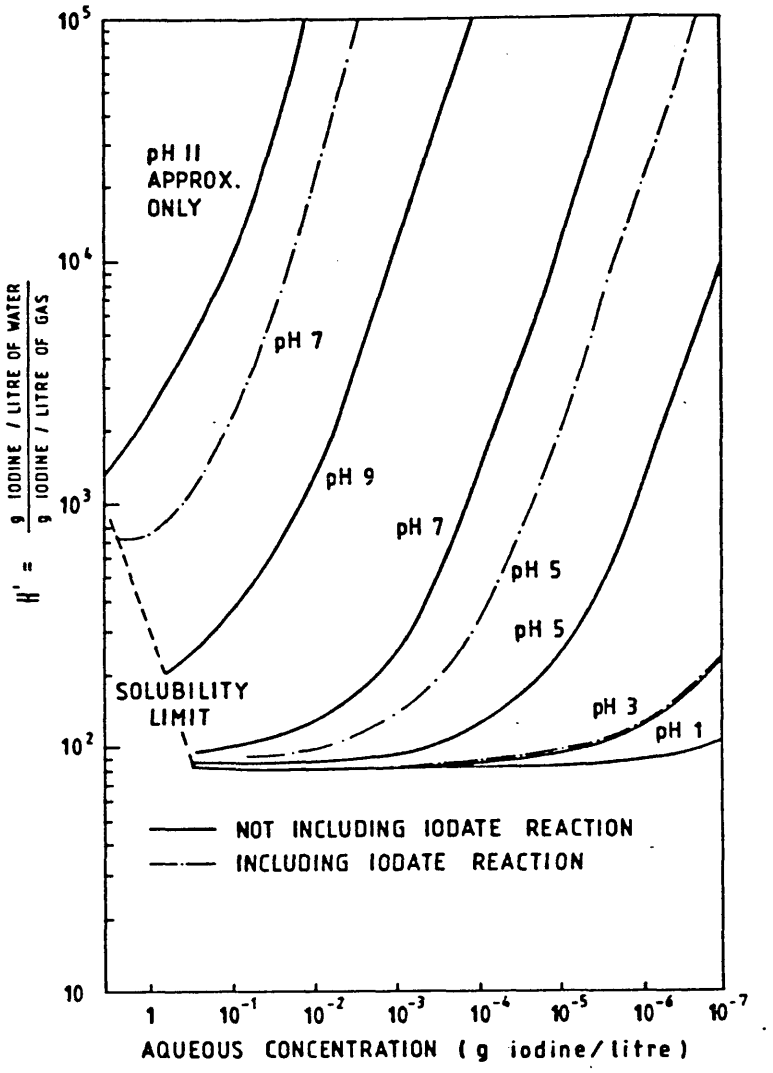


Figure 4.1 Henry's Law coefficient, H', for molecular iodine at 25° C (from Eggleton, 1967)

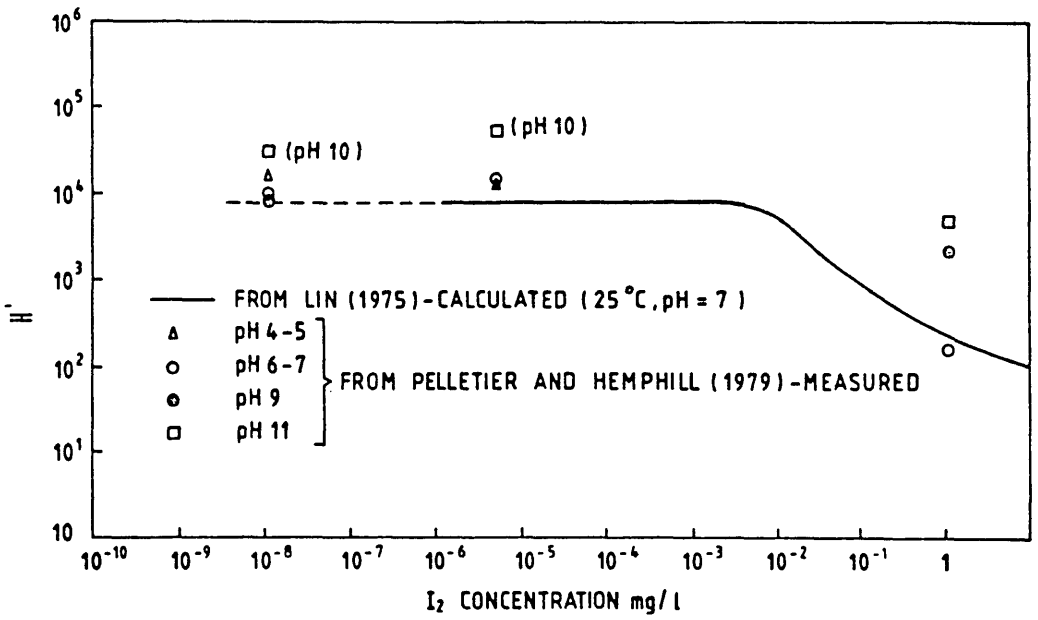


Figure 4.2 Variation of Henry's Law coefficient, H', with iodine concentration (from Gittus et al, 1982)

$$X_c = H' G_a \tag{4.7}$$

$$X_r = H' G_a \tag{4.8}$$

where X_c, X_r are the concentrations in cloud and rain respectively in units g/m^3 water. These are related to their concentrations in units g/m^3 air (G_c,G_r) by

$$G_c = \frac{X_c q_c}{\rho_w} \quad , \quad G_r = \frac{X_r q_r}{\rho_w} . \tag{4.9}$$

Thus for gaseous material to be in equilibrium

$$G_c = \frac{H' q_c G_a}{\rho_w} \quad \text{and} \quad G_r = \frac{H' q_r G_a}{\rho_w} . \tag{4.10}$$

4.2.2 Comparison of numerical calculation with analytic calculation in the limiting case of a very low updraught velocity

In the special case of small updraught velocities it is possible to calculate the efficiency of a precipitation system at scavenging SO_2 by mainly analytic means. This was acheived by Fisher(1982). A comparison can be made between scavenging effficiencies calculated by these means and by employing the 1D numerical model. This can serve as a check on the accuracy of the computational scheme.

The net sink term for loss of SO_2 due to absorption by cloud and rain water followed by oxidation to sulphate is

$$-\frac{(q_c + q_r) H' k_t G_a}{\rho_w} .$$

By neglecting the vertical advection terms in the 1D continuity equations for q_c and q_r (equations(3.35) and (3.36)) and assuming that autoconversion is unimportant, their steady state forms become

$$w\,G = CC \quad , \quad \frac{\partial}{\partial z}(V_t\,q_r) = CC. \tag{4.11}$$

The continuity equation for G_a is

$$\frac{\partial}{\partial z}(w\,G_a) = G_a\frac{\partial w}{\partial z} + w\,G_a\frac{\partial \ln \rho}{\partial z} - \frac{(q_c+q_r)\,H'\,k_t\,G_a}{\rho_w}. \tag{4.12}$$

Fisher defines the efficiency of the cloud at removing SO_2, β, as

$$\beta = \frac{\text{rate of removal of } SO_2 \text{ by cloud system}}{\text{rate of influx of } SO_2 \text{ to cloud system}}, \tag{4.13}$$

from which he writes

$$\beta = \frac{\int_0^H dz\,(q_c + q_r)\,H'\,\dfrac{k_t\,G_a}{\rho_w}}{w(z=0)\,G_a\,(z=0)}. \tag{4.14}$$

The assumption made here is that the horizontal divergence term $G_a\,\partial w/\partial z$ can be ignored. This is equivalent to considering only the central core of the updraught where streamlines have small horizontal components. Clearly, when the updraught velocity is constant, $\partial w/\partial z = 0$ and equation(4.14) holds exactly. If in addition the variation of density of air with height is neglected, equation(4.12) reduces to

$$\frac{\partial}{\partial z}(w G_a) = -(q_c + q_r) H' \frac{k_t G_a}{\rho_w} \tag{4.15}$$

Integrating over the height of the column,

$$w G_a|_{z=H} - w G_a|_{z=0} = -\int_0^H dz\,(q_c + q_r) H' \frac{k_t G_a}{\rho_w}$$

and (4.14) becomes

$$\beta = \frac{w G_a|_{z=0} - w G_a|_{z=H}}{w G_a|_{z=0}} . \tag{4.16}$$

For a symmetrical velocity distribution, with w(z = 0) = w(z = H),

$$\beta = 1 - \frac{G_a(z=H)}{G_a(z=0)} . \tag{4.17}$$

Fisher derives expressions for q_c and q_r from (4.11) with the generating function G = ρG'. A similar calculation for G = A - B z gives

$$q_c = \frac{683\, w\,(A - Bz)}{(w_* H)^{7/9}} \quad , \quad q_r = 0.235\,(H w_*)^{8/9} \tag{4.18}$$

where

$$w_* = \frac{1}{H}\int_z^H dz'\, w\,(A - Bz') . \tag{4.19}$$

The approximate balance between condensation and accretion breaks down near the top of the updraught column and in fact at z = H, q_c is infinitely large. Fisher calculates that (4.11) might hold reasonably well up to

$z = 0.9H$ and redefines β as

$$\beta = 1 - \frac{G_a(z=0.9H)}{G_a(z=0)} . \tag{4.20}$$

From (4.15), remembering the approximation $\partial w/\partial z = 0$ is being made,

$$\frac{1}{G_a}\frac{\partial G_a}{\partial z} = -\frac{(q_c + q_r)}{w}\frac{H' k_t}{\rho_w}$$

$$\text{from which} \quad G_a(z) = G_a(0) \exp\left[-\int_0^z dz' \frac{(q_c + q_r)}{w}\frac{H'k_t}{\rho_w} \right] . \tag{4.21}$$

Thus

$$\beta = 1 - \exp\left[-\int_0^{0.9H} dz' \frac{(q_c + q_r)}{w}\frac{H'k_t}{\rho_w} \right]$$

$$= 1 - \exp\left[-\frac{H'k_t}{\rho_w}\int_0^{0.9H} dz' \frac{(q_c + q_r)}{w} \right] \tag{4.22}$$

It is very expensive to run the numerical model until the pollutant quantities have reached steady state with small updraught velocities. A measure of the time taken to reach steady state, t_{ss}, for an updraught column of height, H, is given by

$$t_{ss} \sim \frac{2H}{w_{max}} \tag{4.23}$$

where w_{max} is the maximum updraught velocity (Fisher,1987). Thus for an updraught height of 10km and a maximum updraught velocity of 0.5 m/s, $t_{ss} \sim 40000$s. Therefore only a small number of runs were made to

compare with analytic calculations.

For an updraught with a constant vertical velocity, $\partial w/\partial z = 0$, and thus the analytic calculation should represent a good approximation to numerical modelling provided the variation of density of air with height, k, is set to zero. Three runs of the model were made with constant updraught velocities of 0.17, 0.5 and 1 m/s. Fig (4.3) shows a comparison between cloud and precipitation quantities calculated with the formulae(4.18) and the 1D model for $w_{max} = 0.5$ m/s. Agreement is good except for $z > 0.9$ H where, as expected, q_r calculated from (4.18) becomes large. This is because the approximation that there is a balance between condensation and accretion breaks down at the top of the column. The values for scavenging efficiency, β, defined in section (4.2.2), calculated by the two methods are shown in table(4.1). Provided β is calculated from the model distribution of pollutant material in the column using $\beta = 1 - (G_a(0.9\ H) / G_a(0))$, agreement is good. Including scavenging in the top tenth of the column increases β slightly.

These results give confidence that the computational scheme has been implemented correctly. The results from the model are close to those calculated by an analytic calculation possible for small updraught velocities. Numerical modelling allows solutions for larger updraught velocities as well as throughout the depth of the updraught.

With a variable updraught velocity, the agreement between results from the two calculations is less good. This is due to the deletion of the horizontal divergence terms in the analytic formulation. In the numerical model, material comes into the updraught by horizontal convergence from below the level of non-divergence and above this level leaves the updraught by horizontal divergence. Removal efficiencies are lower as more material is

Table 4.1 Comparison of analytic and numerical calculations of cloud removal efficiencies of SO_2

	v_k	β	β_1	β_2
	0.17	0.58	0.62	0.57
	0.5	0.42	0.45	0.42
	1.0	0.35	0.38	0.36

Constant updraught

w_0	w_1	β	β_1	β_2
0.05	0.45	0.71	0.67	0.55
0.10	0.90	0.67	0.58	0.49

Variable updraught, $w = w_0 + w_1 \sin(\pi z/H)$

In both cases, $H' = 1.2.10^5$, $k_t = 2.8.10^{-4}$.

β is calculated analytically (see text)

$\beta_1 = (1 - G_a(H)/G_a(0))$

$\beta_2 = (1 - G_a(0.9\ H)/G_a(0))$

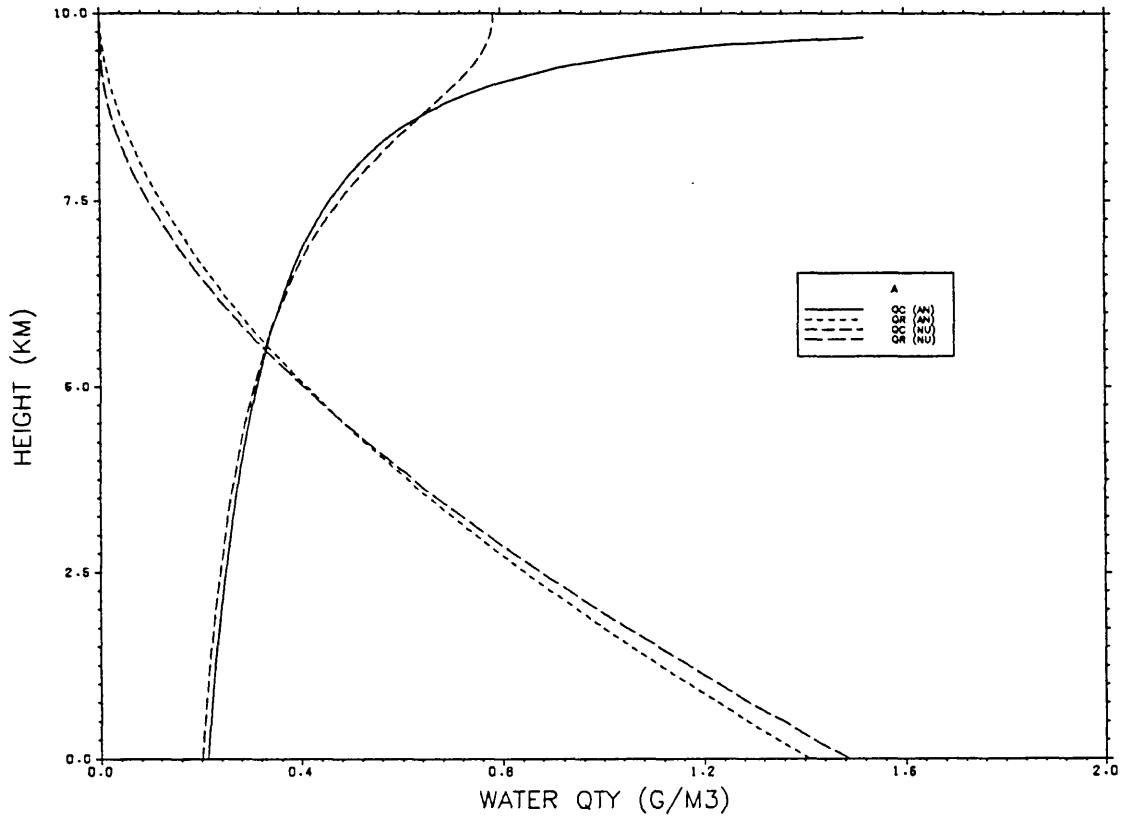


Figure 4.3 Comparison of numerically and analytically calculated cloud and rain water quantities at steady state for an updraught of height, 10km and maximum velocity, 0.5 m/s

able to leave the updraught by divergence before being scavenged by precipitation. In the 1D numerical model, quantities of cloud water and pollutant material may be thought of as representing their average values throughout the width of the updraught circulation at a particular height. Scavenging efficiency is therefore calculated for the whole of the system. In contrast, the analytic calculation only calculates the scavenging efficiency for the central core of the updraught where the streamlines are nearly vertical.

4.2.3 More general modelling studies

A schematic representation of the scavenging of gas by a precipitation system, assuming instantaneous equilibrium described by Henry's Law, is shown in figure(4.4). Gas in air, cloud and rain is maintained in equilibrium. Oxidation is allowed to occur in all three states. Aerosols are scavenged as described in Chapter 3 with nucleation, impaction and cloud microphysical processes all contributing to their redistribution.

The numerical procedure is broken down into three stages which are implemented at each time step. Firstly the new values of P_a, P_c, P_r, G_a, G_c, G_r are calculated from their previous values from the conservation equations

$$\frac{\partial P_a}{\partial t} + \frac{\partial}{\partial z}(w P_a) = P_a \left(\frac{\partial w}{\partial z} + w \frac{\partial \ln \rho}{\partial z}\right) + S_{P_a} \tag{4.24}$$

$$\frac{\partial P_c}{\partial t} + \frac{\partial}{\partial z}(w P_c) = P_c \left(\frac{\partial w}{\partial z} + w \frac{\partial \ln \rho}{\partial z}\right) + S_{P_c} \tag{4.25}$$

$$\frac{\partial P_r}{\partial t} + \frac{\partial}{\partial z}((V_t+w) P_r) = P_r \left(\frac{\partial w}{\partial z} + w \frac{\partial \ln \rho}{\partial z}\right) + S_{P_r} \tag{4.26}$$

$$\frac{\partial G_a}{\partial t} + \frac{\partial}{\partial z}(w G_a) = G_a \left(\frac{\partial w}{\partial z} + w \frac{\partial \ln \rho}{\partial z}\right) \tag{4.27}$$

$$\frac{\partial G_c}{\partial t} + \frac{\partial}{\partial z}(w G_c) = G_c \left(\frac{\partial w}{\partial z} + w \frac{\partial \ln \rho}{\partial z}\right) \tag{4.28}$$

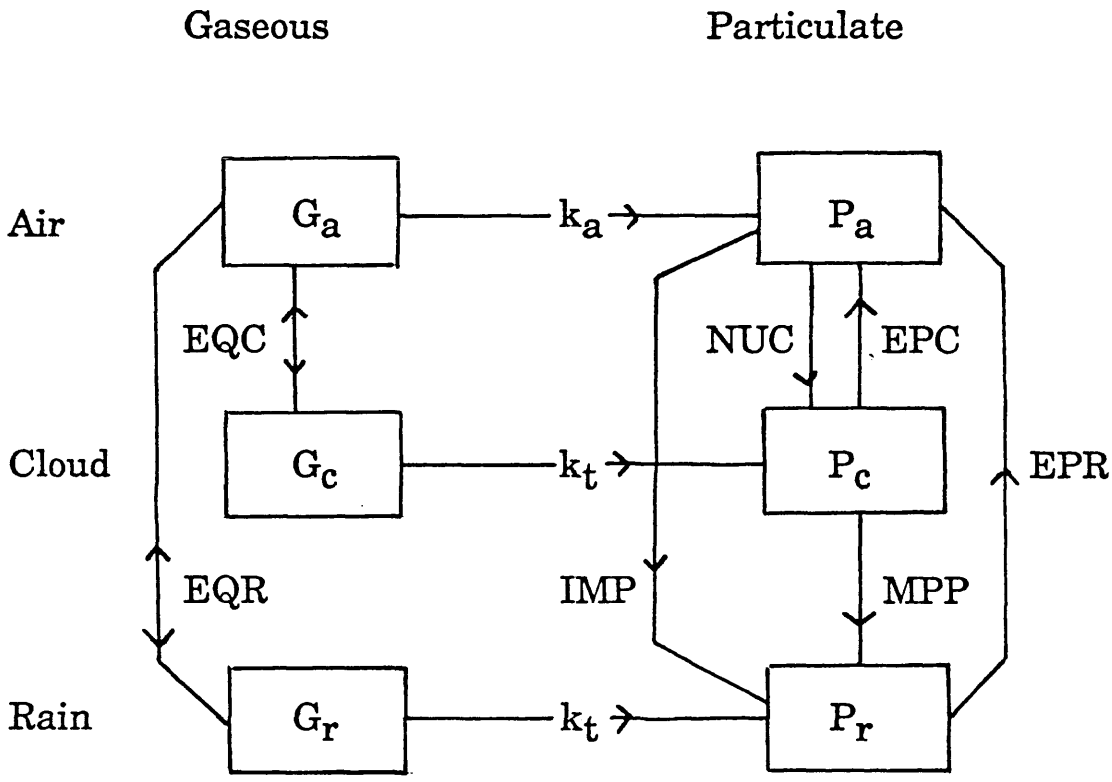


Figure 4.4 Microphysical processes for gaseous and particulate pollutants assuming instantaneous equilibrium for gases

$$\frac{\partial G_r}{\partial t} + \frac{\partial}{\partial z}((V_t+w)G_r) = G_r\left(\frac{\partial w}{\partial z} + w\frac{\partial \ln \rho}{\partial z}\right) \tag{4.29}$$

S_{Pa}, S_{Pc}, S_{Pr} are the source/sink terms for aerosol material given by (3.59) to (3.61) and discussed in detail in section(3.4.1).

Secondly, the total ammount of gas at each grid point is shared out amongst G_a, G_c, G_r to ensure chemical equilibrium. Since G_a, G_c, G_r must satisfy (4.10), the new values of these quantities are given by

$$G_{anew} = \frac{(G_a + G_c + G_r)}{\left[1 + \frac{H'}{\rho_w}(q_c + q_r)\right]} \tag{4.30}$$

$$G_{cnew} = \frac{(G_a + G_c + G_r)}{\left[1 + \frac{H'}{\rho_w}(q_c + q_r)\right]} \frac{H' q_c}{\rho_w} \tag{4.31}$$

$$G_{rnew} = \frac{(G_a + G_c + G_r)}{\left[1 + \frac{H'}{\rho_w}(q_c + q_r)\right]} \frac{H' q_r}{\rho_w} \tag{4.32}$$

Finally, the quantities of gas that oxidise in air, cloud and rain during the time step are calculated and are added to P_a, P_c, P_r and subtracted from G_a, G_c, G_r accordingly. Thus the final values for the quantities of gas in air, cloud and rain are

$$G_{anew} - G_{anew} k_a \, dt, \tag{4.33}$$

$$G_{cnew} - G_{cnew} k_t \, dt, \tag{4.34}$$

$$G_{rnew} - G_{rnew} k_t \, dt \tag{4.35}$$

where dt is the time step. Similarly the final quantities of aerosol are

$$P_{anew} + G_{anew}\, k_a\, dt, \tag{4.36}$$

$$P_{cnew} + G_{cnew}\, k_t\, dt, \tag{4.37}$$

$$P_{rnew} + G_{rnew}\, k_t\, dt. \tag{4.38}$$

Results and discussions : variation of rainout and export efficiencies with H' and k_t

The model was run for two storm durations; T = 4000 s and T = 2000 s. The efficiencies of rainout and export are shown in tables(4.2) and (4.3) for three values of H' ($1.2.10^4$ corresponding to a pH of 4 for SO_2, $1.2.10^5$ corresponding to a pH of 5 and $1.2.10^6$ corresponding to a pH of 6) and five oxidation rates varying from 0 to 2.10^{-3} s^{-1}. The efficiencies here refer to the total percentage of both gaseous and aerosol material removed.

For the lower H' of $1.2.10^4$ very little material is removed in precipitation. Efficiencies of rainout increase with oxidation rate. Thus at $k_t = 2.10^{-3}$, E_{ro} > 10%, but with no aqueous phase oxidation, E_{ro} is only 1.4%. With a higher H' of $1.2.10^5$, rainout efficiencies are much higher varying from 32.9 to 57.9 % over the range of oxidation rates. With H' = $1.2.10^6$, rainout efficiencies are all greater than 70%. A quick calculation confirms why so little is rained out for H' = $1.2.10^4$. From (4.10)

$$G_c = \frac{H'\, q_c\, G_a}{\rho_w} \quad \text{and} \quad G_r = \frac{H'\, q_r\, G_a}{\rho_w}.$$

If q_c, $q_r \sim 1$ g/m^3 and $\rho_w \sim 10^6$ g/m^3, then

$G_{c,r} \sim 0.01\, G_a$ for H' = $1.2.10^4$

and $G_{c,r} \sim 0.1\, G_a$ for H' = $1.2.10^5$.

Therefore at the lower H' only 2% of total pollutant material is in cloud

Table 4.2 Variation of efficiencies of rainout and export with pH and oxidation rate, T = 4000s, instantaneous equilib rium

		Rainout			Export		
k_t	pH	4	5	6	4	5	6
0		1.4	32.9	72.3	93.3	60.0	26.7
10^{-4}		3.5	35.5	72.9	91.5	58.2	26.2
$5x10^{-4}$		6.5	42.4	75.0	89.7	53.6	24.5
10^{-3}		8.5	49.0	76.8	87.5	48.6	23.0
$2x10^{-3}$		13.3	57.9	78.7	83.5	41.1	21.2

Table 4.3 Variation of efficiencies of rainout and export with pH and oxidation rate, T = 2000s, instantaneous equilibrium

		Rainout			Export		
k_t	pH	4	5	6	4	5	6
0		0.2	10.6	44.6	71.1	53.1	28.4
10^{-4}		1.1	12.4	45.6	70.3	52.1	27.9
$5x10^{-4}$		2.0	17.3	48.6	69.5	49.0	26.3
10^{-3}		3.0	22.5	51.4	68.6	45.7	24.9
$2x10^{-3}$		5.1	30.4	54.6	66.8	40.5	23.2

water at any one time. This figure rises to ~ 20% for H' = $1.2.10^5$ and to ~67% for H' = $1.2.10^6$.

Underwood(1983b) concludes (see section(4.2.1)) that H' for gaseous iodine is unlikely to exceed 10^4. This would indicate that very little would be scavenged by precipitation unless an appreciable part is oxidised in solution.

As the oxidation rate increases, the proportion of particulate material that remains in the model domain or has left it via deposition or export increases (see table(4.4). With zero oxidation rate and H' = $1.2.10^5$ there is no particulate material but for $k_t = 2.10^{-3}$ over half of the material is particulate for both T = 2000s and T = 4000 s. As more material is converted to particulate form so the scavenging efficiency rises. For particulate material alone, at T = 4000s and w_{max} = 5 m/s (see figure(3.31)) the scavenging efficiency is about 80%. For gaseous material alone with H' = $1.2.10^5$ and $k_t = 2.10^{-3}$ it is 30%. The efficiency of 57.9% for H' = $1.2.10^5$ and $k_t = 2.10^{-3}$, where half is particulate and half is gaseous, represents roughly an average of these two figures.

Table 4.4 Percentage of material gaseous(G) or particulate(P) in form (pH = 5)

T = 4000s	% G	%P	T = 2000s	%G	%P
0	100.0	0.0	0	100.0	0.0
10^{-4}	92.4	7.6	10^{-4}	94.5	5.5
$5x10^{-3}$	74.9	25.1	$5x10^{-4}$	81.3	18.7
10^{-3}	59.7	40.3	10^{-3}	68.2	31.8
$2x10^{-3}$	41.6	58.4	$2x10^{-3}$	49.8	50.2

The assumption that all gaseous material is instantaneously in equilibrium is only an approximation. It will take some time for water drops to absorb gas from air and to desorb gas to air. This effect might be sufficiently important to alter scavenging efficiencies significantly. This is explored in the next section.

4.3 Gaseous scavenging incorporating absorption and desorption

4.3.1 Theory

Gas in cloud water will not instantaneously come into equilbrium with gas in air. A finite time will be required for the water drop to absorb gas from the atmosphere until equilibrium is acheived. Conversely, if the raindrop contains more pollutant gas than the equilibrium value with respect to the surrounding air, gas will be desorbed. In this section, the discussion of gas scavenging given by Hales(1972) is used as a basis for the derivation of an expression for the absorption or desorption of gaseous pollutants by water drops.

For gaseous scavenging to occur, pollutant molecules must be first transported to the surface of the drop. Here they must cross the liquid-vapour interface before migrating into the interior of the drop. This can be modelled by splitting gas transfer into two steps; transfer of pollution to the drop surface through the surrounding gas (known as the gas phase step) and transfer of pollution into the interior of the drop (known as the liquid phase step). This is expressed as

$$N_0 = k_y(y_b - y_0) \tag{4.39}$$

$$N_0 = k_x(x_0 - x_b) \tag{4.40}$$

where N_0 is molar flux of pollutant passing into the drop through the liquid

vapour interface, k_y , k_x are gas,liquid phase mass transfer coefficients, y, x are mole fractions of pollutant in gas,liquid and subscripts o,b refer to interfacial and bulk conditions respectively. In the simplified film theory approach, the two steps occur across thin liquid and gaseous films on either side of the interface. From Fick's Law of diffusion

$$N_0 = c_y D_y \frac{\partial y}{\partial r}\Big|_{\text{drop surface}} = c_x D_x \frac{\partial x}{\partial r}\Big|_{\text{drop surface}} \tag{4.41}$$

where D_y, D_x are effective diffusivities in gas, liquid phases. This may be approximated in film theory by

$$N_0 = \frac{c_y D_y}{\delta_y}(y_b - y_0) = \frac{c_x D_x}{\delta_x}(x_0 - x_b) \tag{4.42}$$

where δ_y, δ_x are gas, liquid film thicknesses and c denotes the total concentration (in moles/m^3).

Since it is difficuilt to determine interfacial concentrations x_0, y_0, an overall mass transfer coefficient K_y is defined based on the overall concentration driving force betweeen the bulk gas and the bulk liquid. It is given by

$$N_0 = K_y(y_b - y_e) \tag{4.43}$$

where y_e is the mole fraction of pollutant material that would exist in the gas phase in equilibrium with the bulk liquid of mole fraction x_b. For systems obeying Henry's Law,

$$y = \frac{x}{H} \qquad \text{at equilibrium .} \tag{4.44}$$

Combining (4.39), (4.40) and (4.43) gives

$$\frac{1}{K_y} = \frac{1}{H k_x} + \frac{1}{k_y} \ . \tag{4.45}$$

Gas phase mass transfer occurs mainly by convection and diffusion. The mass transfer coefficient, k_y, can be estimated by the semi-empirical relation

$$Sh = 2 + 0.6\, Re^{1/2}\, Sc^{1/3} \tag{4.46}$$

where

$$Sh = \frac{2 k_y R}{D_y c_y} \quad , \quad Re = \frac{2 R |V|}{\upsilon} \quad , \quad Sc = \frac{\upsilon}{D_y} \ . \tag{4.47}$$

V is the terminal velocity of the drop and υ is the kinematic viscosity of air.

In the case where gas phase resistance dominates,

$$\frac{1}{K_y} \sim \frac{1}{k_y} \tag{4.48}$$

and

$$N_0 = \frac{D_y\, Sh}{2R} c_y \, (y_b - y_e) \ . \tag{4.49}$$

The rate of transfer of mass to drops of radius R, m (in units $g/m^3 s$) is given by

$$m = \frac{4 \pi R^2 D_y\, Sh}{2R} \, (G_a - G_e) \tag{4.50}$$

where G_e is the mass of pollutant in air (g/m^3) that would be in equilibrium with G_a. From section (4.2.1),

$$G_e = \frac{1}{H'} X_c = \frac{1}{H'} \frac{G_c \rho_w}{q_c} \tag{4.51}$$

$$G_e = \frac{1}{H'} X_r = \frac{1}{H'} \frac{G_r \rho_w}{q_r} . \tag{4.52}$$

Thus the rate of mass transfer to cloud droplets, m_c, is

$$m_c = 4 \pi R D \frac{Sh}{2} \left[G_a - \frac{G_c \rho_w}{H' q_c} \right] \tag{4.53}$$

and to rain, m_r, is

$$m_r = 4 \pi R D \frac{Sh}{2} \left[G_a - \frac{G_r \rho_w}{H' q_r} \right] \tag{4.54}$$

where D is the effective diffusivity in air. Liquid phase transfer can be modelled by first assuming that the interior of the drop is stagnant with transfer taking place by diffusion alone. Corrections can then be made to account for drop circulation and oscillation. Calculations made by Underwood(1983b) show that for iodine, its aqueous phase concentration in rainwater must be below 10^{-8} g/l before liquid phase resistance can be ignored, assuming stagnant drops. This implies an air concentration below 10^{-9} g/m^3 which would be exceeded up to 100 km from the source of an extreme PWR accident releasing 10kg I. In fact drop circulation and oscillation considerably reduce the liquid phase resistance. Underwood concludes that for molecular iodine, gas phase resistance dominates even close to extreme accidental releases.

The importance of modelling absorption/desorption

An estimate of the rate at which gaseous pollution is absorbed by cloud droplets and raindrops is made in this section. For raindrops, the rate of mass transfer is

$$m_r = 4\pi R D \frac{Sh}{2}\left[G_a - \frac{X_r}{H'} \right]$$

$$= 4\pi R D \frac{Sh}{2}\frac{1}{H'}(X^* - X_r) \qquad (4.55)$$

where X^* is the concentration of gas that would be in rain water at equilibrium (in units g/m^3 water).

$$\frac{4}{3}\pi R^3 \frac{dX_r}{dt} = 4\pi R D \frac{Sh}{2}\frac{1}{H'}(X^* - X_r),$$

$$\frac{dX_r}{dt} = \frac{3}{2}\frac{D\,Sh}{R^2}\frac{1}{H'}(X^* - X_r). \qquad (4.56)$$

If $X_r(t=0) = 0$, then

$$\frac{X_r(t)}{X^*} = 1 - \exp\left[-\frac{3\,Sh\,D}{2R^2\,H'}t \right]. \qquad (4.57)$$

The time taken for the concentration in the raindrop to reach 1-1/e of its saturation value, T_e, is given by

$$0.63 = 1 - \exp\left[-\frac{3\,Sh\,D}{2R^2\,H'}T_e \right]$$

from which

$$T_e = \frac{2R^2 H'}{3 Sh D} .$$

For $q_r = 1$ g/m^3, the median volume radius, R_0, is from (3.47), with $N_0 = 10^7$,

$$R_0 = 0.044 N_0^{-1/4} q_r^{1/4}$$
$$= 7.7.10^{-4} m$$

and from (3.48)

$$|V| = 38.3 (N_0)^{-1/8} q_r^{1/8} = 5.1 \text{ m/s.}$$

Inserting suitable values for υ and D at atmospheric pressure and 15°C of $1.3.10^{-5}$ m^{2}s^{-1} and $0.14.10^{-4}$ m^{2}s^{-1} respectively gives

$$Sh = 2\left[1 + 0.3\left[\frac{2|V|R}{\upsilon} \right]^{1/2} \left[\frac{\upsilon}{D} \right]^{1/3} \right]$$

$$= 16.4$$

A suitable value for H' for SO_2 at a pH of 5 is

$$H' = H(1 + K_1/[H^+]) = 60(1 + 0.02/10^{-5}).$$

Thus Te = 200 s. In this time the raindrop will fall 5.1 x 200 = 1020m. Thus the time taken for raindrops to absorb or desorb gaseous material may be significant.

A typical radius for a cloud droplet is 10^{-5}m (Rogers,1979). Since cloud droplets have negligible fall velocity, Sh = 2 and T_e = 0.28s. This is a much shorter time and for cloud droplets it is reasonable to assume instantaneous equilibrium.

Numerical modelling incorporating absorption/desorption by raindrops

In order to calculate the absorption/desorption of gas (GAD) by a population of raindrops, total mass q_r, (4.54) is integrated over the spectrum of raindrops to give

$$GAD = \int_0^\infty dR\, N(R)\, 4\, D\, \frac{Sh}{2}\, \pi\, R \left[G_a - \frac{G_r\, \rho_w}{q_r\, H'} \right]$$

$$= \left[G_a - \frac{G_r\, \rho_w}{q_r\, H'} \right] Z \qquad (4.58)$$

where

$$Z = \int_0^\infty dR\, 4\, D\, \frac{Sh}{2}\, \pi\, R\, N(R)$$

$$= \int_0^\infty dR\, 4\, D\, (1 + 0.3\, Re^{1/2}\, Sc^{1/3})\, \pi\, R\, N_0\, e^{-2\lambda R}$$

$$= \int_0^\infty 4\, D\, \pi\, R\, N_0\, e^{-2\lambda R}\, dR + \int_0^\infty 1.2\, D \left[\frac{2\sqrt{2}\, K e^{kz}\, \ell}{\upsilon} \right]^{1/2} \left[\frac{\upsilon}{D} \right]^{1/3} \pi\, N_0\, R^{7/4}\, e^{-2\lambda R}\, dR$$

$$= Z_1 + Z_2 \,. \qquad (4.59)$$

The first integral is

$$Z_1 = 4\, D\, \pi N_0\, \frac{1}{2\lambda} \int_0^\infty 2\, \lambda\, R\, e^{-2\lambda R}\, dR$$

$$= 4\, D\, \pi N_0\, \frac{1}{(2\lambda)^2}\, \Gamma(2) = 4\, D\, \pi\, N_0\, \frac{1}{(2\lambda)^2} \,. \qquad (4.60)$$

The second integral is

$$Z_2 = 1.2\,D\left[\frac{2\sqrt{2}\,K e^{kz/2}}{\upsilon}\right]^{1/2}\left[\frac{\upsilon}{D}\right]^{1/3}\frac{\pi N_0}{(2\lambda)^{11/4}}\int_0^{\infty}(2\lambda R)^{7/4}\,e^{-2\lambda R}\,d(2\lambda R)$$

$$= 1.2\,D\left[\frac{2\sqrt{2}\,K e^{kz/2}}{\upsilon}\right]\left[\frac{\upsilon}{D}\right]^{1/2}\left[\frac{\upsilon}{D}\right]^{1/3}\frac{\pi N_0}{(2\lambda)^{11/4}}\Gamma(11/4)\ . \qquad (4.61)$$

Employing (3.42) gives

$$Z_1 = 7.86.10^{-5}\,q_r^{1/2}$$

and

$$Z_2 = 3.20.10^{-4}\,e^{kz/4}\,q_r^{11/16}\ .$$

From (4.58),

$$GAD = \left[7.86.10^{-5}\,q_r^{1/2} + 3.20.10^{-4}\,e^{kz/4}\,q_r^{11/16}\right].\left[G_a - \frac{G_r\,\rho_w}{q_r\,H'}\right]\ . \qquad (4.62)$$

A representation of the scheme for gaseous scavenging used in this section is given in figure(4.5). It includes absorption or desorption of gas by raindrops, with the gas in air and cloud droplets being in instantaneous equilibrium. It is now necessary to include microphysical transfer of gas from cloud to rain as well as evaporative transfer from rain to air.

As before, the numerical procedure is broken down into three stages which are implemented at each time step. Firstly the new values of P_a, P_c, P_r, G_a, G_c, G_r are calculated from their previous values from the conservation equations

$$\frac{\partial P_a}{\partial t} + \frac{\partial}{\partial z}(w\,P_a) = P_a\left(\frac{\partial w}{\partial z} + w\frac{\partial \ln \rho}{\partial z}\right) + S_{P_a} \qquad (4.63)$$

$$\frac{\partial P_c}{\partial t} + \frac{\partial}{\partial z}(w\,P_c) = P_c\left(\frac{\partial w}{\partial z} + w\frac{\partial \ln \rho}{\partial z}\right) + S_{P_c} \qquad (4.64)$$

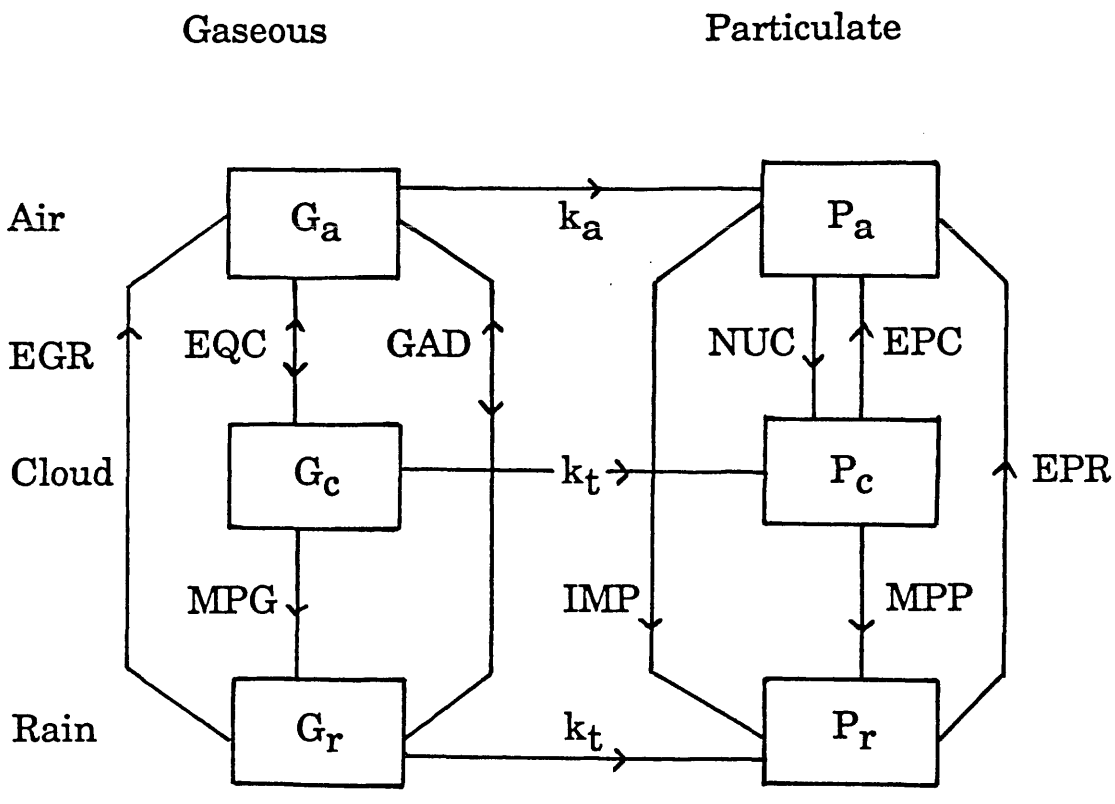


Figure 4.5 Microphysical processes for gaseous and particulate pollutants including absorption and desorption of gases to and from raindrops

$$\frac{\partial P_r}{\partial t} + \frac{\partial}{\partial z}((V_t+w)\,P_r) = P_r\left(\frac{\partial w}{\partial z} + w\frac{\partial \ln \rho}{\partial z}\right) + S_{P_r} \tag{4.65}$$

$$\frac{\partial G_a}{\partial t} + \frac{\partial}{\partial z}(w\,G_a) = G_a\left(\frac{\partial w}{\partial z} + w\frac{\partial \ln \rho}{\partial z}\right) + S_{G_a} \tag{4.66}$$

$$\frac{\partial G_c}{\partial t} + \frac{\partial}{\partial z}(w\,G_c) = G_c\left(\frac{\partial w}{\partial z} + w\frac{\partial \ln \rho}{\partial z}\right) + S_{G_c} \tag{4.67}$$

$$\frac{\partial G_r}{\partial t} + \frac{\partial}{\partial z}((V_t+w)\,G_r) = G_r\left(\frac{\partial w}{\partial z} + w\frac{\partial \ln \rho}{\partial z}\right) + S_{G_r} \tag{4.68}$$

Here the source/sink terms for gaseous material, S_{Ga}, S_{Gc}, S_{Gr} are given by

$$S_{Ga} = + \text{ EGR } - \text{ GAD} \tag{4.69}$$

$$S_{Gc} = - \text{ MPG} \tag{4.70}$$

$$S_{Gr} = - \text{ EGR } + \text{ MPG } + \text{GAD} \tag{4.71}$$

where

$$\text{MPG} = \begin{cases} \dfrac{AC + CC}{q_c} G_c & \text{for } q_c > 0 \\ 0 & \text{otherwise} \end{cases} \tag{4.72}$$

and

$$\text{EGR} = \frac{EP}{q_r} G_r \ . \tag{4.73}$$

Secondly, the ammount of gas in air and cloud at each grid point is shared out amongst G_a, G_c to ensure chemical equilibrium. G_a and G_c must satsify the first part of (4.10) and therefore their new quantities are

$$G_{anew} = \frac{(G_a + G_c)}{\left[1 + \dfrac{H'}{\rho_w} q_c\right]} \quad , \quad G_{cnew} = \frac{(G_a + G_c)}{\left[1 + \dfrac{H'}{\rho_w} q_c\right]} \frac{H' q_c}{\rho_w} \ . \tag{4.74}$$

Finally, the quantities of gas that oxidise in air, cloud and rain during the

time step are added to P_a, P_c, P_r and subtracted from G_a, G_c, G_r. The final values for the quantities of gas in air, cloud and rain are

$$G_{anew} - G_{anew} k_a dt \quad (4.75)$$

$$G_{cnew} - G_{cnew} k_t dt \quad (4.76)$$

$$G_{rnew} - G_{rnew} k_t dt \quad (4.77)$$

where dt is the time step. The final quantities of aerosol are

$$P_{anew} + G_{anew} k_a dt \quad (4.78)$$

$$P_{cnew} + G_{cnew} k_t dt \quad (4.79)$$

$$P_{rnew} + G_{rnew} k_t dt. \quad (4.80)$$

4.3.2 Results and discussion

The general pattern of variation of scavenging efficiency with H' and k_t is the same as for the simple equilibrium runs (see tables(4.5) and (4.6)). Efficiencies of rainout are slightly higher on the whole with the discrepancy increasing for decreasing oxidation rate, k_t. For the 4000s run with a zero oxidation rate and H' ~ $1.2.10^5$ the efficiency of rainout is 7% higher than for equilibrium. This at first sight seems suprising since there will be a delay in absorption of gas by raindrops from air. In fact an important route for eventual deposition of gas (as it is for particulate) is via microphysical collection of cloud water. Gas is assumed to be immediately in equilibrium in cloud water which is subsequently collected with high efficiency by falling raindrops. With small oxidation rates the situation may arise where raindrops are falling which contain more gaseous material than would be in equilibrium with the surrounding air. Desorption of gas from water to air takes place at a finite rate and the quantity of material reaching the ground may well be greater than would be calculated assuming instantaneous equilibrium.

Table 4.5 Variation of efficiencies of rainout and export with pH and oxidation rate, T = 4000s, gaseous absorption/desorption

pH=5 k_t	E_{ro}	E_{exp}	$k_t=5.10^{-4}$	pH	E_{ro}	E_{exp}
0	39.9	52.2		3.5	2.7	94.8
10^{-4}	41.9	51.2		4.0	6.1	89.4
$5x10^{-4}$	46.8	48.7		4.5	19.1	74.4
10^{-3}	51.4	45.8		5.0	46.8	48.7
$2x10^{-3}$	57.6	41.1		5.5	70.5	28.4
				6.0	78.6	21.2
				6.5	80.3	19.6

Table 4.6 Variation of efficiencies of rainout and export with pH and oxidation rate, T = 2000s, gaseous absorption/desorption

pH=5 k_t	E_{ro}	E_{exp}	$k_t=5.10^{-4}$	pH	E_{ro}	E_{exp}
0	17.2	49.0		3.5	1.1	71.9
10^{-4}	18.5	48.3		4.0	2.2	69.4
$5x10^{-4}$	22.1	46.3		4.5	7.2	61.7
10^{-3}	25.8	44.1		5.0	22.1	46.3
$2x10^{-3}$	31.2	40.6		5.5	42.4	30.6
				6.0	54.2	23.4
				6.5	57.6	21.5

The differences between results from the equilibrium and the absorption/desorption models are not great for these runs. This is not surprising since the scales for the updraught (T ~ 4000s, H = 10^4m) are a good deal larger than representative scales for absorption/desorption by raindrops calculated in section(4.3.1) (t ~ 200s, $\Delta z \sim 10^3$m). However the latter runs provide a more complete description, explicitly including microphysical uptake of gas in cloud by rain (MPG) and evaporation of raindrops releasing gas to air (EGR) as well as absorption and desorption (GAD). Further investigations were therefore carried out using this model into the variation of rainout and export efficiencies with updraught velocity.

With a pH of 5 and a high oxidation rate of 2.10^{-3}, the variation of rainout efficiency with updraught shows a pattern that is familiar from Chapter 3 (see figure(4.6)). This is a fairly sharp increase up to 2 m/s with a levelling of between 2 and 6 m/s and a gradual reduction above 6 m/s. The increase is less sharp than for hygroscopic particulate (c.f. figure(3.31)) suggesting that the gaseous part of the material has rounded off the curve. Figure(4.7) shows scavenging efficiency for purely gaseous material with a zero oxidation rate. Here there is a more gradual rise still to 2 m/s with the peak not reached until 6 m/s. Thus it would appear that for hygroscopic particulate material the peak in scavenging efficiency is reached very sharply before 2 m/s whereas the peak for gaseous material is reached much more gradually at 5 or 6 m/s. With both forms of material present the curve for total scavenging efficiency will be a combination of the two.

The variation of rainout and export efficiencies for a wide range of pH values for a particular oxidation rate ($k_t = 5.10^{-4}$) are shown in tables(4.5) and (4.6) for run durations of 4000 and 2000 seconds and rainout efficiencies are given in graphical form in figure(4.8). Both curves take the same form,

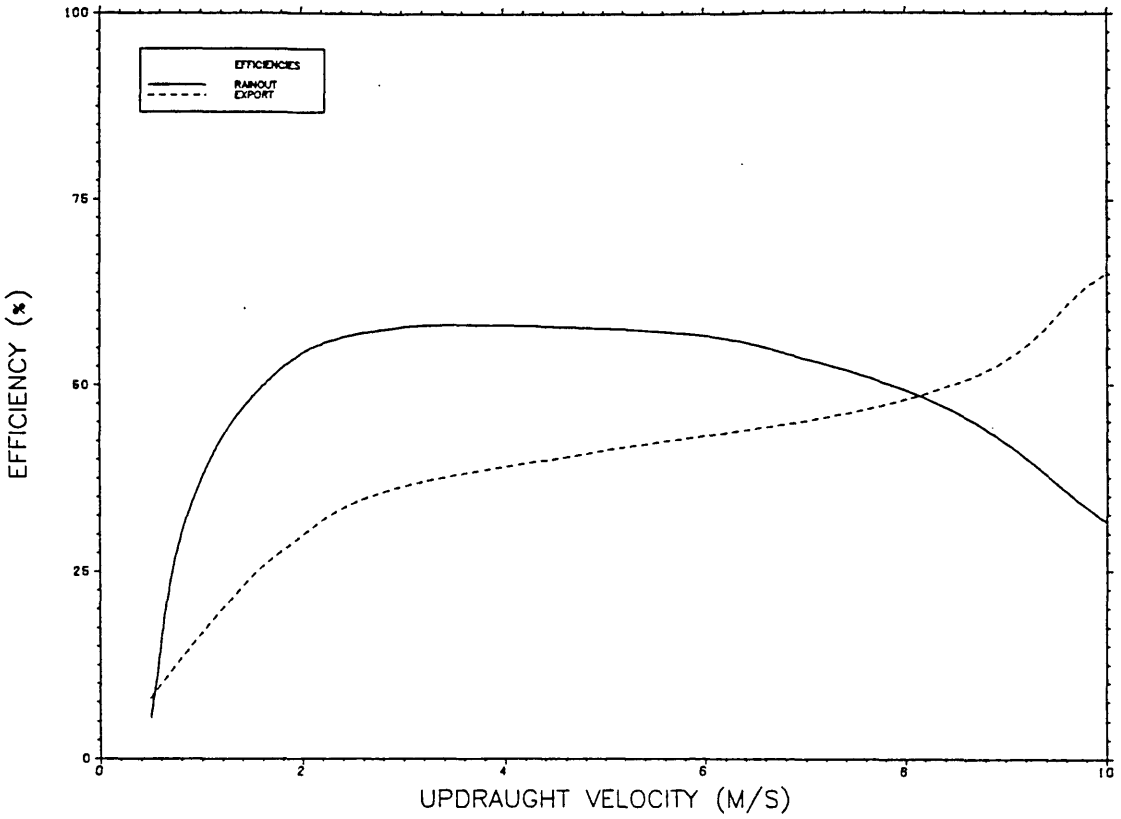


Figure 4.6 Rainout and export efficiencies for gaseous material, pH = 5, $k_t = 2.10^{-3}$

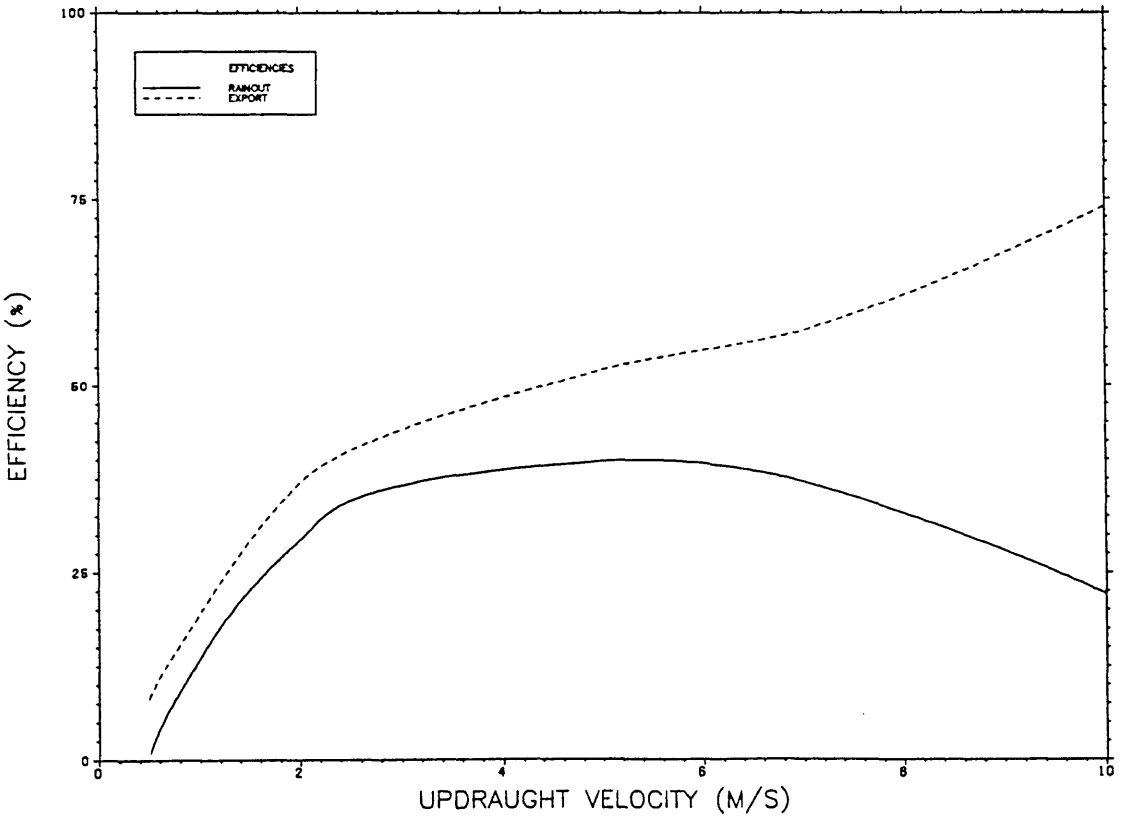


Figure 4.7 Rainout and export efficiencies for gaseous material, pH = 5, $k_t = 0$

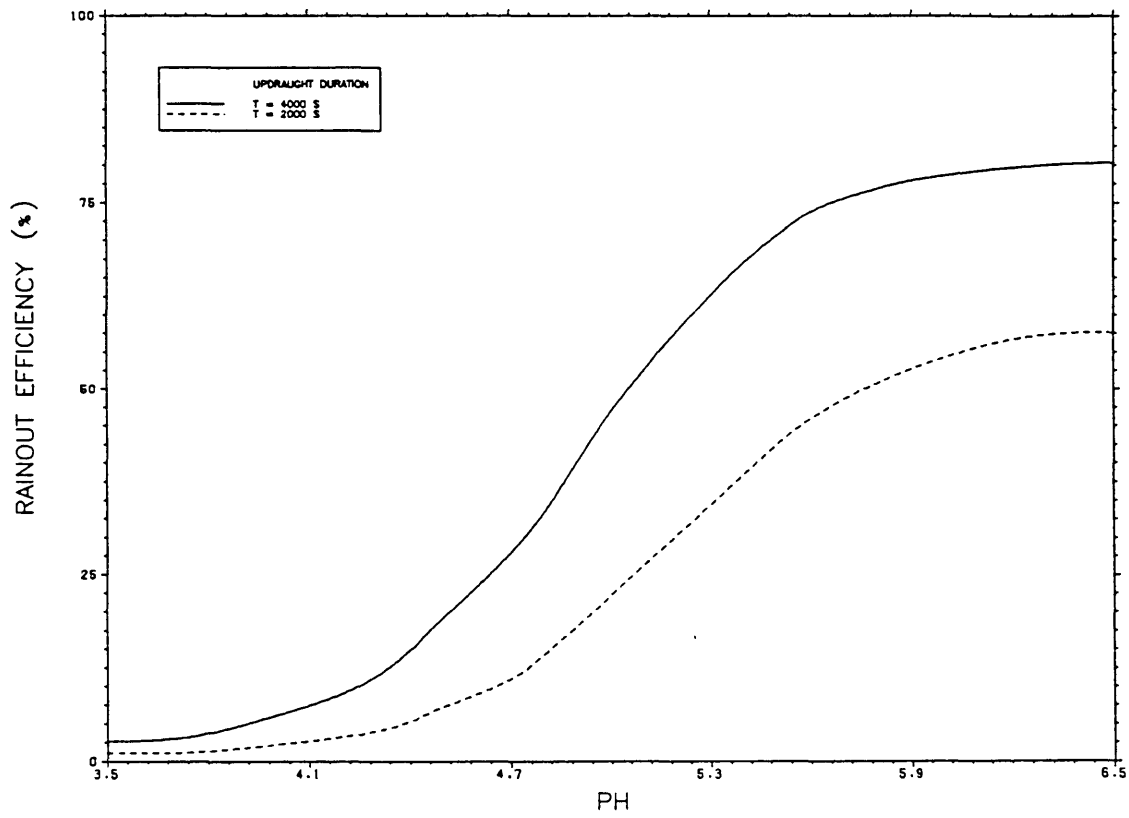


Figure 4.8 Variation of rainout efficiencies with pH

having just about reached their maximum at pH = 6.5. Most of the increase takes place between pH = 4 and pH = 6 or H' = $1.2.10^4$ to $1.2.10^6$. Beneath the lower limit rainout efficiencies are very small, emphasising again that gaseous iodine is unlikely to be removed very greatly in precipitation unless an appreciable part is able to oxidise to a particulate form.

4.4 Summary and conclusions

The absorption and desorption of gaseous material by cloud and raindrops and its oxidation to form aerosol material have been modelled within the framework of the one-dimensional model. Since much more is known about the chemistry of sulphur dioxide scavenging than iodine,theory and results for both gases were used in this chapter. A check on the computational accuracy of the model was made possible by comparing model results with an analytic calculation of sulphur dioxide scavenging in the limiting case of a very small updraught velocity. Agreement was good, lending confidence that the computational scheme is performing properly.

Modelling of gaseous scavenging was first carried out assuming that all gas was in instantaneous equilibrium between air and both cloud and raindrops. Later modelling included a finite rate for absorption and desorption by raindrops; the time taken for absorption to or desorption from cloud droplets was found to be insignificant. There was relatively little difference between overall rainout and export efficiencies calculated by the two methods. Results for the latter method were generally slightly larger than the former. This can be explained by the delay time for saturated drops falling through clean air to lose some of their pollutant burden.

Model runs were made for a variety of Henry's Law constants and oxidation rates. For the small Henry's Law constants predicted for

atmospheric concentrations of iodine released from a nuclear accident, the ammount of iodine taken up by cloud water is expected to be small unless it has an appreciable aqueous phase oxidation rate. Data collected following the Chernobyl accident indicated that iodine was deposited in precipitation as readily as caesium. Since a large proportion of the Chernobyl release of iodine was in gaseous form, it would appear that gaseous iodine was scavenged as efficiently as particulate caesium. This would suggest that either the Henry's rate constants for iodine are higher than predicted or that iodine oxidises at a very fast rate once in solution. More work on the chemistry of iodine is required to address this problem.

5 2D Model

5.1 Introduction

One-dimensional modelling is limited in its ability to represent the dynamic structures of precipitation systems. A 1D model may readily simulate a single updraught or downdraught column, but by only employing the vertical dimension rain is forced to fall through its generative updraught. This occurs in short-lived convective showers where the updraught is cut off by evaporative cooling as rain falls through subsaturated air. However, as discussed in Chapter 1, most systems are intrinsically two or three-dimensional. In frontal situations, updraught flows overlie downdraughts and in convective situations, updraught and downdraught twist around each other in a complex three-dimensional arrangement. Horizontal as well as vertical coordinates are required to model dynamics adequately.

In 1D modelling it is a simple matter to represent the dynamics by specifying an equation for the air velocity $\underline{V}$. However, in two and three dimensions it is rather more difficuilt to take this approach and almost all two and three-dimensional cloud models solve the full set of conservation equations to derive the air velocity. An example of such a model is that of Tremblay(1987) who combined the chemical scheme previously incorporated in a 1D updraught (Tremblay and Leighton(1984)) with a 3D dynamic model. Another cloud model incorporating pollutant transport and scavenging is the 3D dynamic model of Chaumerliac, Nickerson and Rosset (1983) which was used for sensitivity studies in the 2D simulation of an orographic cloud (Chaumerliac and Rosset, 1987). One of the most sophisticated and expensive to run of these types of models is described in its 2D form by Pruppacher(1987). It was adapted from an entrainment parcel formulation in which cloud water and aerosol pollution are

represented by continuous spectra and SO_2 gas scavenging is incorporated (Flossman, Hall and Pruppacher, 1985).

In this chapter, model development is extended to 2D by specifying velocity fields analytically. Kessler(1969) took this approach in extending his 1D cloud model to two dimensions. In his velocity field, air circulates clockwise around the domain to represent overturning air. Modelling of SO_2 scavenging in frontal systems was extended in a similar manner from 1D (Fisher, 1982) to 2D by Fisher and Clark(1986). In their velocity field, convergent air feeds in below and divergent air escapes aloft. Although the shape of their circulation suggests a convective situation it is applied to a frontal situation in which there are small updraught velocities. Here, it is aimed to apply appropriate 2D flow fields to describe schematically the dynamics of particular storm systems.

5.2 Model Descrip tion

The two-dimensional forms of the conservation equations(3.29) to (3.33) are

$$\frac{\partial q_c}{\partial t} + \frac{\partial}{\partial x}(u q_c) + \frac{\partial}{\partial z}(w q_c) = w G + S_{q_c} \tag{5.1}$$

$$\frac{\partial q_r}{\partial t} + \frac{\partial}{\partial x}(u q_r) + \frac{\partial}{\partial z}((V_t+w) q_r) = S_{q_r} \tag{5.2}$$

$$\frac{\partial P_{ia}}{\partial t} + \frac{\partial}{\partial x}(u P_{ia}) + \frac{\partial}{\partial z}(w P_{ia}) = S_{ia} \tag{5.3}$$

$$\frac{\partial P_{ic}}{\partial t} + \frac{\partial}{\partial x}(u P_{ic}) + \frac{\partial}{\partial z}(w P_{ic}) = S_{ic} \tag{5.4}$$

$$\frac{\partial P_{ir}}{\partial t} + \frac{\partial}{\partial x}(u P_{ir}) + \frac{\partial}{\partial z}((V_t+w) P_{ir}) = S_{ir}\ , \tag{5.5}$$

As before, P_{ia}, P_{ic} and P_{ir} are the masses of the ith pollutant in air, cloud and rain respectively (in g pollutant / m^3 air). S_{ia}, S_{ic} and S_{ir} are the source/sink terms due to the physiochemical processes responsible for the transport of pollutant between air, cloud and rain.

The specified air velocity must satisfy the 2D version of the continuity equation,(3.21),

$$\frac{\partial}{\partial x}(\rho u) + \frac{\partial}{\partial z}(\rho w) = 0. \tag{5.6}$$

This can be acheived by specifying a stream function, ψ, such that

$$u = \frac{1}{\rho}\frac{\partial \psi}{\partial z} \quad , \quad w = -\frac{1}{\rho}\frac{\partial \psi}{\partial x} . \tag{5.7}$$

The flow field given by Fisher and Clark(1986) to simulate frontal uplift is described by the stream function

$$\psi = \frac{1}{\pi} \sin \pi z \sin\left[\frac{\pi x}{2}\right] \tag{5.8}$$

which is defined on the domain $0 \leq z \leq 1$, $-1 \leq x \leq 1$. Streamlines are shown in figure(5.1). A transformation of coordinates needs to be made to produce a velocity field on a domain of height H and length L. In this case, the flow is symmetrical about $x = 0$ and only the solution for $x \geq 0$ need be considered. Thus (5.8) becomes

$$\psi = \frac{v_k}{\pi} \sin\left[\frac{\pi z}{H}\right] \sin\left[\frac{\pi x}{2L}\right] . \tag{5.9}$$

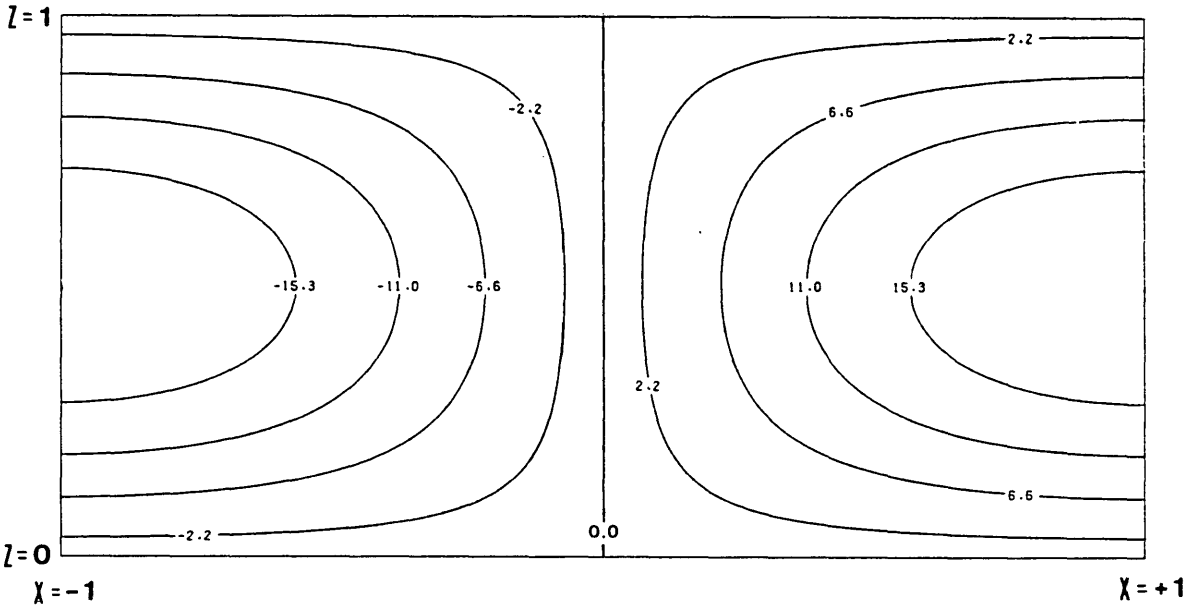


Figure 5.1 Field of streamlines for two-dimensional updraught circulation

The multiplicative constant, v_k, gives maximum velocities, for $\rho = \rho_0$, of

$$|u_{max}| = \frac{v_k}{H} \quad , \quad |w_{max}| = \frac{v_k}{2L} \; . \tag{5.10}$$

A further flow field is derived in order to represent the important configuration of an updraught overlying a downdraught. By squaring the previous function, (5.8), to give

$$\psi = \frac{1}{2}\left[\frac{1}{\pi} \sin \pi z \sin(\pi x/2) \right]^2 , \tag{5.11}$$

an updraught and downdraught are produced. By adding a shearing term the updraught is made to lean over the downdraught;

$$\psi = \frac{1}{2}\left[\frac{1}{\pi} \sin \pi z \sin (\pi x/2) + Kz \right]^2 . \tag{5.12}$$

By a transformation of coordinates to define the flow on the domain $0 \leq z \leq H$, $0 \leq x \leq L$, (5.12) becomes

$$\psi = \frac{v_k}{2}\left[\frac{1}{\pi} \sin\left[\frac{\pi z}{H} \right] \sin\left[\pi\left[\frac{x}{L} - \frac{1}{2} \right] \right] + \frac{Kz}{H} \right]^2 . \tag{5.13}$$

5.3 Orographic precipitation

5.3.1 Description of orographic precipitation

The importance of the spatial distribution of precipitation to accident consequence analysis has been discussed above. For this reason alone,orographic precipitation is worthy of consideration. A mountaineer

knows only too well that he is more likely to encounter rain or snow walking in Britain's mountains than he is walking to work in a lowland part of the country. By analysing autographic rain gauge measurements, Smith(1981) showed that both annual duration and quantity of precipitation increase with altitude. He derived an expression linking duration, D (hours/year), at altitude h (m), with sea-level duration, S (hrs/yr), which is given by

$$D = S + 0.9\,h\,. \tag{5.14}$$

In addition he showed that there is a good correlation between annual rainfall ammounts, R (mm/year), and duration and he derived an empirical relation given by

$$R = D\,(1.25 - 1.15\,D' + 36.5\,D'^{2}) \tag{5.15}$$

where $D' = D.10^{-4}$. Thus elevation enhances the quantity and duration of precipitation.

Precipitation on high ground is also likely to be heavier than in low lying areas. It can be shown from (5.15) that the average rainfall rate, R/D (mm/hr), increases with D and hence with altitude. Highland areas have an average of up to 2 mm/hr of rainfall compared to 1.3 mm/hr in lowland areas. This comes about largely through the seeder-feeder mechanism which is operative in frontal conditions when there is a covering of stratus clouds. Moist surface air is forced to rise when it meets high ground and where it reaches its saturation level, cloud is formed. There is usually insufficient time for the droplets on the hill cloud to coalesce to form precipitation sized drops. Instead they are swept out by raindrops falling from high level stratus cloud which acts as the seeder to the feeder cloud

beneath. By this process, rainfall rates at the ground are enhanced by an ammount related to the quantity of cloud water in the hill cloud.

Clearly, wet deposition can be increased on elevated terrain since altitude enhances both duration and intensity of precipitation. In addition to this, there is the possibility of a further enhancement to wet deposition. Aerosol particles in air passing through cloud base can act preferentially as cloud condensation nuclei with the likelihood that a high proportion of aerosol mass will be taken up by cloud water. Attached to cloud droplets, aerosol particles are collected by falling raindrops with much greater efficiency than unattached particles. Since most of the mass of aerosol pollution in the boundary layer of air passing over the hill is taken up by the feeder cloud and efficiently scavenged by raindrops from the seeder clouds, the increase in deposition is likely to be greater than the increase in precipitation. Thus there are three components to the influence of orographic precipitation on deposition. The quantity of precipitation is enhanced at altitude, its intensity is also enhanced and the efficiency of scavenging by precipitation of particulate pollution within orographic cloud is greater than for particulate in cloud free air.

5.3.2 Calculation of possible enhancement

A quantitative estimate of the possible enhancement to precipitation and deposition by the seeder-feeder mechanism is calculated here. It is assumed that all particulate mass entering cloud base is taken up in cloud water by nucleation. The scavenging coefficients for the rainout of particulate in the hill cloud, Λ_r, by accretion and the washout of particulate outside the hill cloud, Λ_w, are given by

$$\Lambda_r = 1/q_c\,(CC) = 6.96.10^{-4}\,E_r\,N_0^{1/8}\,q_r^{7/8} \qquad (5.16)$$

from (3.56). From (3.64),

$$\Lambda_w = 1/P_a\,(\mathrm{IMP}) = 6.96.10^{-4}\, E_A\, N_0^{1/8}\, q_r^{7/8}\,. \qquad (5.17)$$

The assumption is made here that density of air is close to its value at $z = 0$ and therefore $e^{kz/2} \sim 1$. Taking $N_0 = 10^7$, $E_r = 1$ and $E_A = 0.1$, a value appropriate to micron sized particles, gives

$$\Lambda_r = 5.2.10^{-3}\, q_r^{7/8}$$

and $\Lambda_w = 5.2.10^{-4}\, q_r^{7/8}$.

A suitable value for the rainfall rate from the seeder cloud is $J = 1$ mm/hr which from (3.69), i.e.

$$J = 18.35\, q_r^{9/8},$$

is equivalent to $q_r = 0.075$ g/m^3. As this precipitation falls through the feeder cloud it will collect cloud water at a rate given by

$$\frac{dq_r}{dt} = (CC) = 5.2.10^{-3}\, q_r^{7/8}\, q_c\,. \qquad (5.18)$$

The velocity of rainfall is, from (3.48), given by

$$V(q_r) = -\,5.09\, q_r^{1/8}. \qquad (5.19)$$

Therefore, the rate of change of precipitation mass with height is

$$\frac{dq_r}{dz} = \frac{1}{V(q_r)}\frac{dq_r}{dt} = -\,\frac{5.2.10^{-3}\, q_r^{7/8}\, q_c}{5.09\, q_r^{1/8}}\,. \qquad (5.20)$$

Taking q_c constant throughout the height, H, of the feeder cloud and integrating,

$$\int_{q_r(0)}^{q_r(H)} \frac{dq_r}{q_r^{3/4}} = -\,1.2.10^{-3}\, q_c\, H\,.$$

Thus

$$(q_r(0))^{1/4} - (q_r(H))^{1/4} = 2.55.10^{-4}\, q_c H$$

and

$$q_r(0) = (2.55.10^{-4}\, q_c H + (0.075)^{1/4})^4 \quad . \qquad (5.21)$$

The experimental field studies carried out on Great Dunn Fell in Cumbria (Carruthers and Choularton,1986) have provided data for values of liquid water content in orographic cloud. Taking a suitable value for q_c of 0.4 g/m^3 and setting H = 800m gives

$$q_r(0) = 0.134 \text{ g/m}^3$$

from which

$$J = 1.91 \text{ mm/hr.}$$

Hence rainfall rate has been roughly doubled from 1 to 2 mm/hr.

It is to be expected that deposition will have more than doubled. Outside the feeder cloud, the washout coefficient is

$$\Lambda_w = 5.2.10^{-4}\,(0.075)^{7/8}$$
$$= 5.3.10^{-5}\ s^{-1}$$

giving an effective washout coefficient for 1 mm/hr of

$$\Lambda_w^0 = \Lambda_w / J = 5.3.10^{-5}\ s^{-1}(\text{mm/hr})^{-1}.$$

Inside the feeder cloud,

$$\Lambda_r = 5.2.10^{-3}\, qr^{7/8}.$$

The quantity of precipitation varies from 0.075 g/m^3 at the top of the cloud to 0.134 g/m^3 at the bottom. The effective washout coefficient is $\Lambda_r^0 = \Lambda_r / J$ which is also

$$\Lambda_r^0 = \frac{\Lambda_r}{18.35\, q_r^{9/8}} = 2.8.10^{-4}\, q_r^{-1/4} \quad .$$

Thus Λ_r increases from $5.3.10^{-4}$ s^{-1} at the top of the cloud to $9.0.10^{-4}$ at the

ground and Λ^0_r decreases from $5.3.10^{-4}$ $s^{-1}(mm/hr)^{-1}$ at cloud top to $4.6.10^{-4}$ $s^{-1}(mm/hr)^{-1}$ at the ground.

These calculations indicate that in more detailed modelling studies, an approximate doubling of precipitation rate due to orographic enhancement might be expected. Also an enhancement to deposition rate for micron sized particles, as measured by an effective washout coefficient Λ_0, of an order of magnitude is predicted.

5.3.3 Description of modelling

The feeder-seeder can be simulated within the framework of the two-dimensional model. As a result of air being forced to rise in flowing over a hill, water vapour condenses and the feeder cloud is formed. Rain water falls from the seeder cloud above and collects cloud water as it falls to the hill surface. This is modelled as follows.

The windfield over the hill is expressed by the stream function

$$\psi = \frac{v_k}{2}\left[\frac{1}{\pi}\sin\left[\frac{\pi z}{H}\right]\sin\left[\pi\left[\frac{x}{L}-\frac{1}{2}\right]\right] - \frac{K z}{H}\right]^2 \qquad (5.22)$$

on the domain $0 \leq x \leq L$, $0 \leq z \leq H$. Since orographic cloud is a fairly low-level phenomenon and the height of the domain is at most 1km, the approximation is made that density of air is constant. Thus continuity can be written

$$\frac{\partial u}{\partial x} + \frac{\partial w}{\partial z} = 0 \qquad (5.23)$$

where

$$u = \frac{\partial \psi}{\partial z} \quad , \quad w = -\frac{\partial \psi}{\partial x}. \tag{5.24}$$

In this case,

$$u = \frac{v_k}{H}\left[\frac{1}{\pi}\sin\left[\frac{\pi z}{H}\right]\sin\left[\pi\left[\frac{x}{L}-\frac{1}{2}\right]\right] - \frac{Kz}{H}\right].\left[\cos\left[\frac{\pi z}{H}\right]\sin\left[\pi\left[\frac{x}{L}-\frac{1}{2}\right]\right] - K\right]$$

and (5.25)

$$w = -\frac{v_k}{L}\left[\frac{1}{\pi}\sin\left[\frac{\pi z}{H}\right]\sin\left[\pi\left[\frac{x}{L}-\frac{1}{2}\right]\right] - \frac{Kz}{H}\right].\left[\sin\left[\frac{\pi z}{H}\right]\cos\left[\pi\left[\frac{x}{L}-\frac{1}{2}\right]\right]\right].$$

(5.26)

The surface of the hill is defined by a streamline

$\psi = \psi_h$

and rainfall rates and deposition rates at the ground are calculated there. A windfield is illustrated in figure(5.2) for the parameters

$v_k = 50000$, $K = 0.5$, $L = 1$ km, $H = 3$ km and $\psi_h = 100$.

The seeder cloud is generated by

$$\frac{dq_c}{dt}\Big|_{condn} = w\,G \ . \tag{5.27}$$

The feeder cloud is simulated by a pre-specified rainfall distribution falling through the top boundary of the domain. The boundary condition is

$$q_r(x, z=H, t) = Q_{sc}, \tag{5.28}$$

where Q_{sc} is the seeder cloud rainfall quantity in g/m^3.

The boundary layer of air running over the hill lies between the streamlines $\psi = \psi_h$ and $\psi = \psi_t$ where ψ_t is the streamline that runs up to

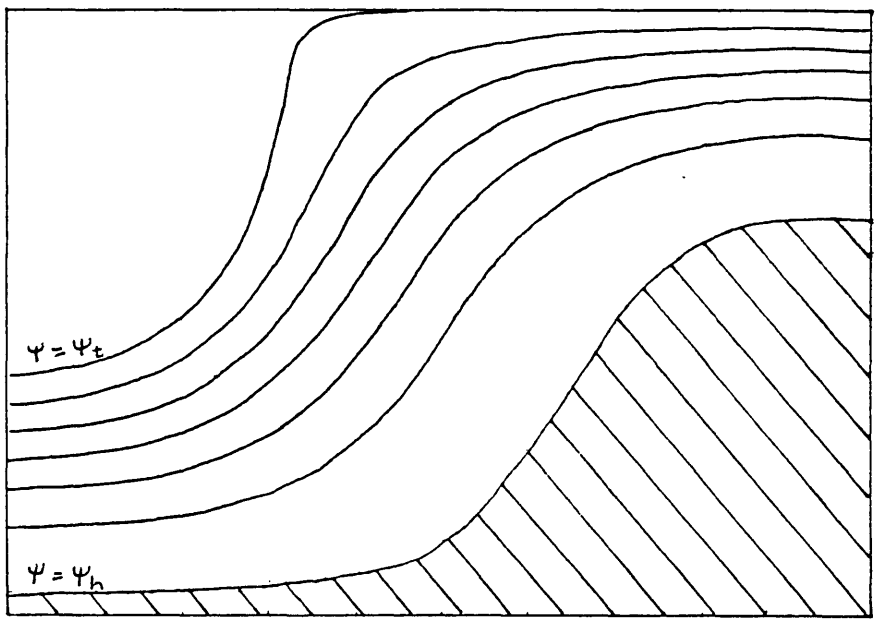


Figure 5.2 Field of streamlines for two-dimensional orographic circulation - standard run

the top boundary from the left hand edge and along the top boundary to the right hand edge (see fig (5.2)). Pollution feeds into this layer from the left hand edge. This is represented by a boundary condition which is taken to be

$$X_a(x=0,z) = \begin{cases} X_{in} \sin\left[\dfrac{\pi z}{z_t}\right] & \text{for } 0 \le z \le z_t \\ 0 & \text{otherwise} \end{cases} \qquad (5.29)$$

where z_t satsifies

$$\psi(x=0, z_t) = \psi_t \qquad \text{and } z_t < H. \qquad (5.30)$$

X_{in} is the maximum pollutant concentration in the incoming air in g/m^3. There is no cloud at the left hand boundary and so

$$X_c(x=0, z) = 0. \qquad (5.31)$$

5.3.4 Results and discussion

First, a standard run was made in which model parameters took suitable values to represent the dynamic and microphysical characteristics of an orographic situation. Later, further runs were made to test the sensitivity of precipitation rate and deposition rate to the variation of these parameters.

Standard run

The parameter values chosen are shown in table(5.1). The hill surface ($\psi = \psi_h$) and streamlines are shown in figure(5.2). The height of the hill is 675m and at its steepest point the slope is at 37^0 to the vertical. The geometry has been chosen thus so as to represent a hill such as Great Dunn Fell in the Pennines. The maximum updraught velocity is 6.1 m/s and the average inflow velocity for the streamlines which pass over the hill is 17.3 m/s. This

Table 5.1 Parameter values for standard orographic run

	Parameter	Value
Dynamic parameters	H	1000 m
	L	3000 m
	v_k	50000
	K	0.5
	ψ_h	100
Microphysical parameters	E_{nuc}	0.9
	E_A	0.1
	Er	1.0
	N_c	300 cm^{-3}
Seeder cloud	Q_{sc}	0.075 g/m^3

represents quite a windy day and is equivalent to force 7 on the Beaufort scale. A high efficiency of 90% of nucleation is assumed. A value for E_A of 0.1 is taken so as to represent the scavenging of particles of 1μ radius(see section (3.4.1)). 100% efficiency for cloud collection is taken and a value for N_c, the number of cloud condensation nuclei, is set at 300 cm^{-3}, a value typical of the measurements taken at Great Dunn Fell (Carruthers and Choularton, 1986). The value for the precipitation quantity falling from the seeder into the top of the feeder cloud is equivalent to a rainfall rate of 1 mm/hr.

Since hill cloud is likely to persist longer than the time taken for pollutant material to process through it, the model is run without pollution until the cloud and rain profiles have reached a steady state. Pollution is then processed through the system until pollutant profiles in air, cloud and rain have reached a steady state. In the case of the standard run this took 1000 seconds. For all orographic runs, the numerical time and space steps are

Δt = 2s, Δz = 50m, Δx = 100m. The small time step is necessitated by the Courant condition required for the space steps.

The steady state precipitation rate at the hill surface is shown in figure(5.4). The peak value is 2.14 mm/hr representing an enhancement of 1.14 mm/hr of the seeder rainfall rate by the feeder cloud. Steady state deposition rate at the hill surface is also shown in figure(5.4). Since all scavenging processes are linear, the input of particulate in air specified by X_{in} is set nominally to be $X_{in} = 1$ g/m^3. It can be seen that deposition has increased dramatically more than precipitation rate, going from $1.18.10^{-2}$ g/m^{3}s at the domain edge outside the hill cloud to $3.38.10^{-1}$ g/m^{3}s at peak value. Thus there is an enhancement to the deposition rate of a factor 28 which is equivalent to 14 times the increase in precipitation rate. An effective washout coefficient weighted by the rainfall rate, J, can be calculated from

$$\Lambda_0 = \frac{\Lambda}{J} = \frac{1}{J} \frac{D_r}{\int_0^{z_t} X_a \, dz} . \qquad (5.32)$$

Λ_0 increases from $4.6.10^{-5}$ outside the hill cloud where only washout is operating to $6.3.10^{-4}$ at its maximum value. Its variation is shown in figure(5.3). Its average value over the hill is $4.3.10^{-4}$ s^{-1} which is close to the value of $4.6.10^{-4}$ s^{-1} derived in the calculation made in section(5.3.2). It is interesting to note that a high proportion of material is swept right through the model domain without being deposited in rain. At steady state, only 19% of the influx of pollutant is deposited at the ground whereas 81% flows over the hill summit and through the right hand boundary.

These results show how the rainout processes operating in the hill cloud

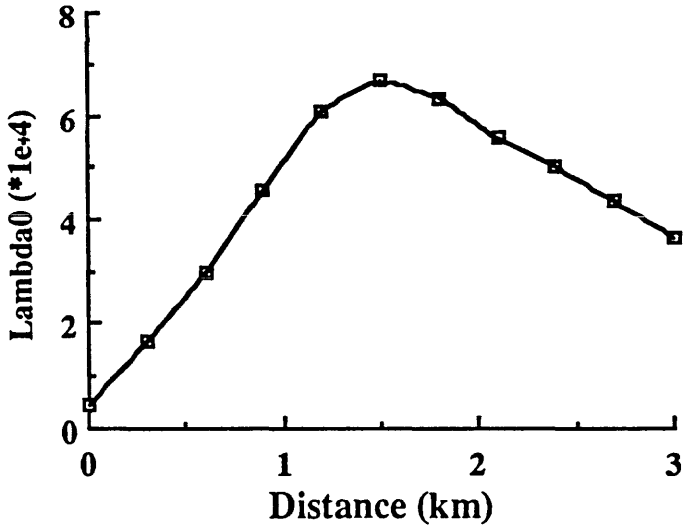


Figure 5.3 Effective washout coefficient for orographic run number 1

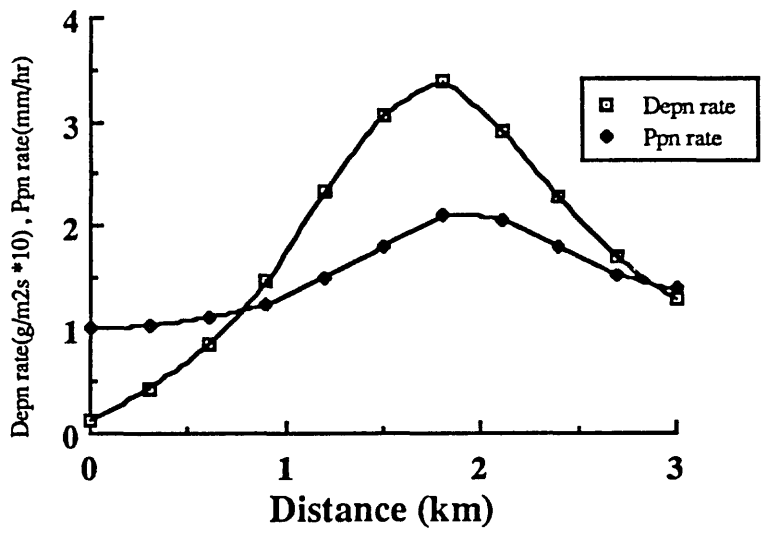


Figure 5.4 Steady state deposition and precipitation rates for orographic run number 1

can dramatically increase deposition rate over its value outside, where scavenging takes place entirely due to washout. The enhancement calculated in the standard run is likely to be near to the upper end of the spectrum of possible results. 1μ particles have a lower efficiency of impaction scavenging than larger particles and efficiency of nucleation has been set to a high value as has the efficiency of collection of cloud droplets by rain drops. Therefore, sensitivity studies were caried out to see how the orographic enhancements to precipitation and deposition rate vary with model parameters.

Sensitivity studies

The values taken by the model parameters varied in the sensitivity studies are given in table(5.2). The standard run (no. 1) is included for comparison. The 2D model is expensive to run and so the number of runs has to be limited but it is still possible to gain a useful insight into the influence of the principle dynamic and microphysical parameters.

Table 5.2 Orographic sensitivity studies : variation of model parameters

Run no.	Vel	Hill ht.	v_k	K	E_{nuc}	E_A	E_r
1	17.3	675	50000	0.5	0.9	0.1	1.0
2	11.5	675	33333	0.5	0.9	0.1	1.0
3	17.3	675	50000	0.5	0.9	0.1	0.6
4	17.4	400	30000	0.85	0.9	0.1	1.0
5	17.3	675	50000	0.5	0.9	0.2	1.0
6	17.3	675	50000	0.5	0.6	0.1	1.0

The variations of precipitation and deposition rates with distance along the hill for the five runs are shown in figures (5.5) to (5.9). Also the peak and average values for D_r, Λ, J, Λ_0 are calculated in table(5.3) so as to gauge the enhancement factors. The efficiencies with which the pollutant is deposited at steady state are given in table(5.4).

Lowering the overall velocity in the domain (run 2, see figure(5.5)) so that the average inflow velocity is 11.5 m/s reduces peak precipitation rate to 1.8 mm/hr but reduces the deposition rate less, thus raising Λ_0. Also, E_{r0} is higher than for the standard run. With a lower velocity, the pollutant material has a longer time in being swept over the hill during which it can be deposited. Reducing E_r to 0.6 (run 3, see figure(5.6)) reduces peak precipitation rate to 1.6 mm/hr and reduces deposition rate in proportion to give the same value for Λ_0. By changing v_k and K (run 4, see figure(5.7)) the height of the hill is lowered to 400m. In this run the maximum inflow velocity is kept the same as for the standard run, but the maximum updraught velocity is reduced to 5.5 m/s. As a result of this, peak precipitation rate is 2.0 mm/hr, slightly less than the standard run. Deposition rate is reduced more to give a smaller Λ_0, and as can be seen from figure(5.7) the peak has shifted towards the hill summit. The efficiency of rainout is decreased as the pollutant is swept more easily over the lower hill. Run 5 (see figure(5.8)) models larger particles by setting E_A = 0.2. Peak deposition rate is increased very slightly (~ 2%) but the major change is that minimum depsition rate at the domain left hand edge has doubled to $2.35.10^{-2}$ g/m^{2}s which is equivalent to $\Lambda_0 = 9.2.10^{-5}$ s^{-1}. Hence the overall enhancement factor at the peak is 14, which is a factor 7 times the increase in precipitation rate. In run 6 (see figure (5.9)), the nucleation efficiency is reduced to 0.6. Precipitation rate is the same as for the standard run but deposition rate is lowered so that its peak value is $4.3.10^{-4}$ g/m^{2}s. However this still represents an enhancement factor of 20 for 1μ

Table 5.3 Peak values of equivalent and effective washout coefficients, deposition and precipitation rates

Run no.	D_r	Λ	J	Λ^0
1	0.34	$1.3.10^{-3}$	2.1	$6.3.10^{-4}$
2	0.31	$1.2.10^{-3}$	1.8	$6.7.10^{-4}$
3	0.26	$1.0.10^{-3}$	1.6	$6.4.10^{-4}$
4	0.46	$1.1.10^{-3}$	2.0	$5.6.10^{-4}$
5	0.34	$1.3.10^{-3}$	2.1	$6.2.10^{-4}$
6	0.23	$9.0.10^{-4}$	2.1	$4.3.10^{-4}$

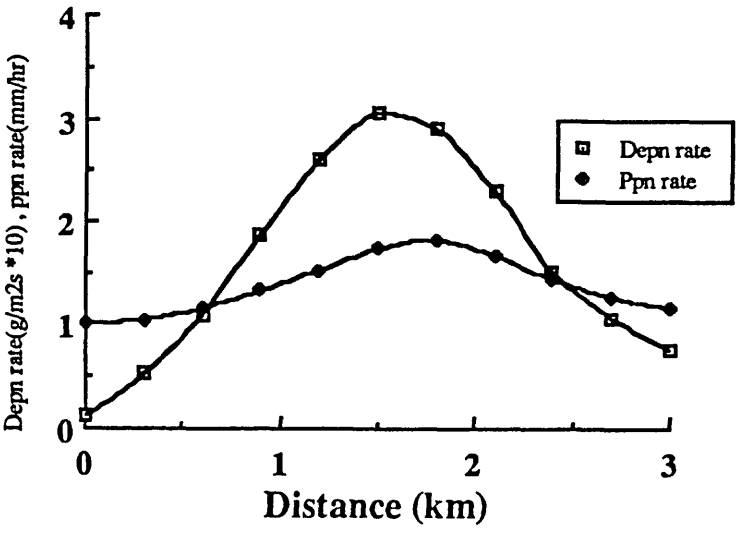


Figure 5.5 Steady state deposition and precipitation rates for orographic run number 2

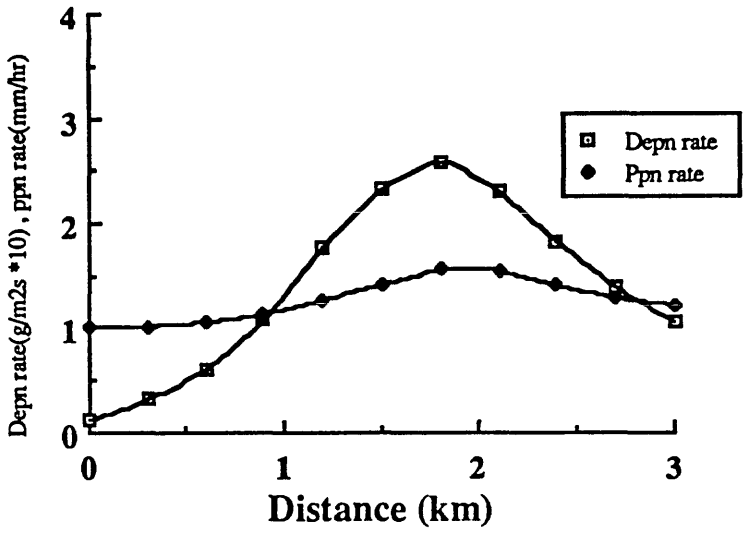


Figure 5.6 Steady state deposition and precipitation rates for orographic run number 3

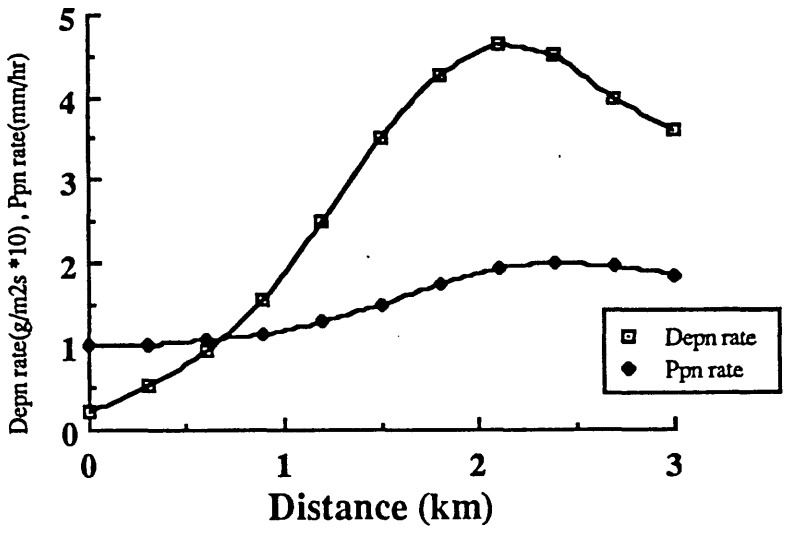


Figure 5.7 Steady state deposition and precipitation rates for orographic run number 4

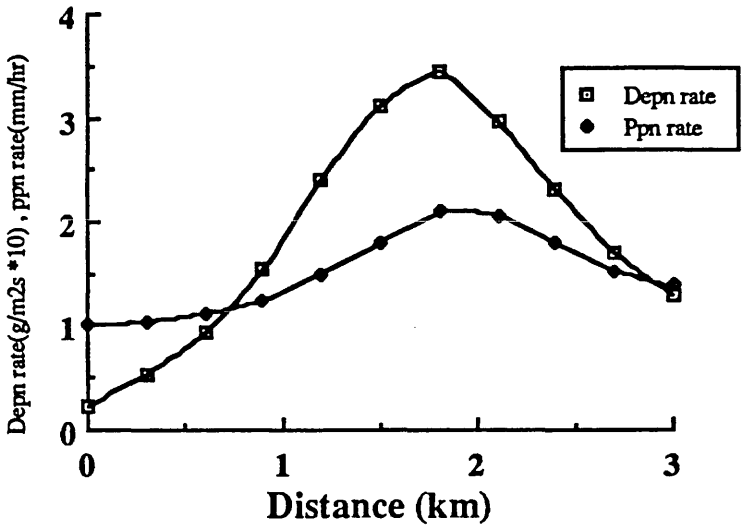


Figure 5.8 Steady state deposition and precipitation rates for orographic run number 5

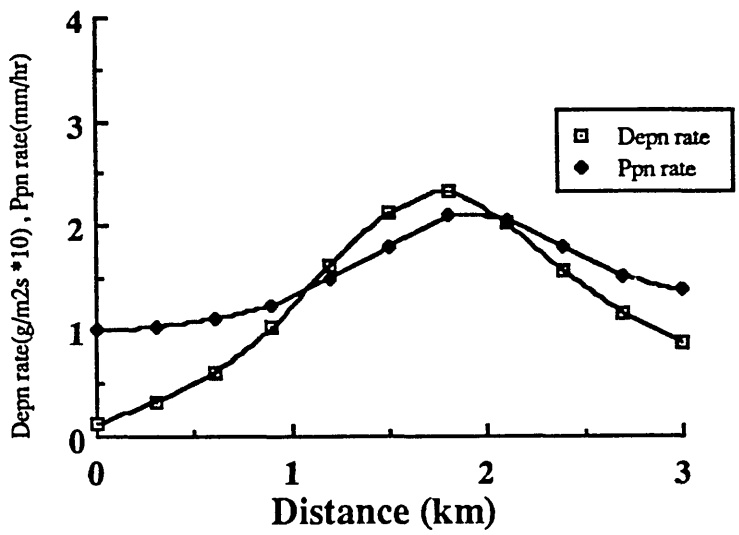


Figure 5.9 Steady state deposition and precipitation rates for orographic run number 6

Table 5.4 Efficiencies of rainout and export for orographic runs

Run no.	E_{ro}	E_{exp}
1	19	81
2	26	74
3	14	86
4	16	84
5	19	81
6	12	88

particles or 10 for larger particles which is 10 and 5 times the enhancement to precipitation rate respectively.

It is clear that orographic precipitation can considerably enhance deposition. Nucleation efficiency is the most important parameter although as discussed in section(3.4.1) it is likely to be close to unity. These studies indicate that a conservative estimate of the enhancement to the deposition rate over the hill is an order of magnitude for a doubling of the precipitation rate.

5.4 Cold Frontal Precipitation

5.4.1 Description of cold frontal precipitation

The rearward sloping cold frontal system discussed in Chapter 1 has particular relevance for wet deposition for two reasons. Firstly, frontal precipitation accounts for a high proportion of precipitation in mid-latitudes and although rearward sloping ascent is less common than forward sloping ascent, it is still frequently observed in Britain and elsewhere in Northern Europe. Secondly, a concentration mechanism is operative. Large volumes of air are drawn in to feed the steep updraught at

the cold frontal surface, producing a narrow band of heavy precipitation. This band of near vertical lifting is known as line convection and in the event of a pollutant release may give rise to a highly concentrated strip of wet deposition.

Line convection is essentially a two dimensional phenomenon and hence lends itself well to 2D modelling. Observational studies have been made by Browning and Harold(1970) using Doppler radar techniques. The flow for an instance of moderately intense line convection is shown in figure(5.10). Air typically rises 2 to 3 kilometres in its ascent over a horizontal distance of about 3 kilometres. Beneath the updraught flow of warm, moist air there is a weaker downdraught flow of cooler, drier air through which precipitation may fall and partially evaporate. The fate of pollutant drawn into these two airstreams is likely to be significantly different. Particulate pollution in the updraught may be taken up readily by cloud water as condensation nuclei and deposited in rain with high efficiency, whereas in the downdraught flow it can only be washed out by falling raindrops with much lower efficiency. An instance where the shortcomings of the washout model are especially apparent may occur if polluted air is feeding into the updraught and a receptor point lies beneath clean air in the downdraught. An attempt to calculate deposition there by applying a washout coefficient to measured air concentrations may produce unfortunately innacurate results.

5.4.2 Description of modelling

The rearward sloping cold front is simulated as follows. The updraught of warm air that rises sharply at the cold front and the downdraught of colder air that lies beneath it and behind the front can both be described by the stream function

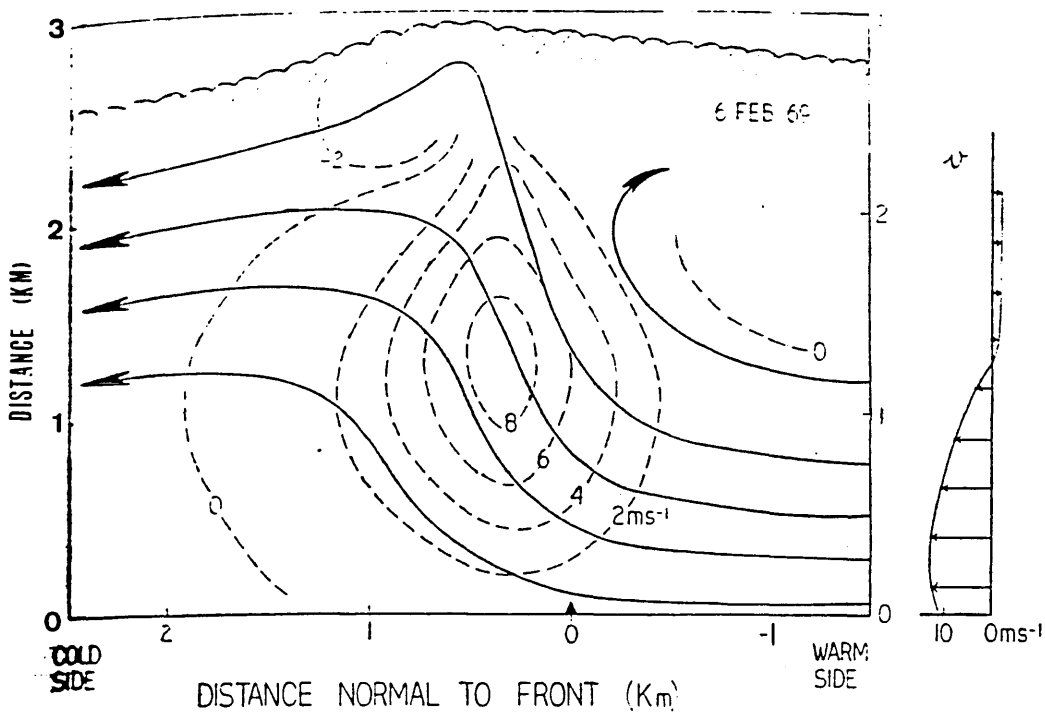


Figure 5.10 Transverse circulation at the surface cold front at 1124 on 6th February, 1969 (from Browning and Harold, 1970)

$$\psi = -\frac{v_k}{2}\left[\frac{1}{\pi}\sin\left[\frac{\pi z}{H}\right]\sin\left[\pi\left[\frac{x}{L}-\frac{1}{2}\right]\right]+\frac{Kz}{H}\right]^2 . \qquad (5.33)$$

This is defined on the domain $0 \leq x \leq L$, $0 \leq z \leq H$. The case studies described by Browning and Harold(1970) indicate that

$H = 3\,km$, $L = 3\,km$

are suitable values for the height and the length of the domain. The variation of density of air with height was considered significant in this case. Therefore the continuity equation is written

$$\frac{\partial}{\partial x}(\rho u) + \frac{\partial}{\partial z}(\rho w) = 0 \qquad (5.34)$$

where ρ is the density of air. This is parametrised by $\rho = \rho_0 e^{-kz}$ where $k = 10^{-4}$ and $\rho_0 = \rho(z = 0)$ is the air density at the ground. In order to factor out ρ_0, multiplying by $1/\rho_0$ gives

$$\frac{\partial}{\partial x}\left(\frac{\rho}{\rho_0}u\right) + \frac{\partial}{\partial z}\left(\frac{\rho}{\rho_0}w\right) = 0 \qquad (5.35)$$

where the stream function ψ is related to the air velocities by

$$u = \frac{\rho_0}{\rho}\frac{\delta\psi}{\delta z} \quad , \quad w = -\frac{\rho_0}{\rho}\frac{\delta\psi}{\delta x} . \qquad (5.36)$$

Therefore,

$$u = -e^{kz}\frac{v_k}{H}\left[\frac{1}{\pi}\sin\left[\frac{\pi z}{H}\right]\sin\left[\pi\left[\frac{x}{L}-\frac{1}{2}\right]\right]+\frac{Kz}{H}\right].\left[\cos\left[\frac{\pi z}{H}\right]\sin\left[\pi\left[\frac{x}{L}-\frac{1}{2}\right]\right]+K\right]$$

and (5.37)

$$w = e^{kz}\frac{v_k}{L}\left[\frac{1}{\pi}\sin\left[\frac{\pi z}{H}\right]\sin\left[\pi\left[\frac{x}{L}-\frac{1}{2}\right]\right]+\frac{Kz}{H}\right].\left[\sin\left[\frac{\pi z}{H}\right]\cos\left[\pi\left[\frac{x}{L}-\frac{1}{2}\right]\right]\right].$$

(5.38)

The boundary between the updraught and downdraught flows is given by the streamline

$\psi = 0.$

A windfield is illustrated in figure(5.11) for the parameters

$v_k = 60000$, $K = 0.25$, $H = 3$ km , $L = 3$ km.

The microphysical processes are parametrised as before with the boundary conditions as follows. The boundaries of the cloud correspond to the boundaries of the domain, where w = 0. Therefore

$$q_c(x = 0, z, t) = q_c(x = L, z, t) = q_c(x, z = 0, t) = q_c(x, z = H, t) = 0. \quad (5.39)$$

No rain falls from the top boundary or at the sides of the cloud;

$$q_r(x, z = H, t) = q_r(x = 0, z, t) = q_r(x = L, z, t) = 0. \quad (5.40)$$

Polluted air may feed into the updraught from the right hand edge or into the downdraught from the left hand edge.

Updraught

The flow of air that feeds up over the downdraught flow and behind the cold front is bounded by the streamlines

$\psi = 0$ and $\psi = \psi_t$

where ψ_t is the streamline which runs up to the top boundary from the right hand edge and along the top boundary to the left hand edge (see figure (5.11)). The pollution feeding into the flow is represented by the boundary condition

$$X_a(x = L, z) = \begin{cases} X_{rin}\sin\left[\dfrac{\pi z}{z_{tr}}\right] & \text{for } 0 \le z \le z_{tr} \\ 0 & \text{otherwise} \end{cases} \quad (5.41)$$

where z_{tr} satisfies

$$\psi(x = L, z_{tr}) = \psi_t \text{ and } z_{tr} < H \tag{5.42}$$

and where X_{rin} is the maximum pollutant concentration (in units g/m^3) in the incoming air in the updraught.

Downdraught

Incoming air in the downdraught flow has

$$u(x = 0, z) > 0.$$

The boundary condition for pollution feeding into this flow is

$$X_a(x = 0, z) = \begin{cases} X_{lin} \sin\left[\dfrac{\pi(z - z_{bl})}{(z_{tl} - z_{bl})}\right] & \text{for } z_{bl} \le z \le z_{tl} \\ 0 & \text{otherwise} \end{cases} \tag{5.43}$$

where z_{bl}, z_{tl} are defined by

$$u(x = 0, z_{bl}) = 0 \ , \ u(x = 0, z_{tl}) = 0 \text{ and } 0 < z_{bl} < z_{tl} < H \tag{5.44}$$

and X_{lin} is the maximum pollutant concentration feeding into the downdraught flow.

5.4.3 Results and discussion

The model was run with two different geometrical configurations which can both represent the situation of line convection. The dynamic variables for each are shown in table(5.5) and their streamlines are shown in figures(5.11) and (5.12). Circulation 1 (runs 1 and 2) has a larger region of downdraught flow and hence subsaturated air than circulation 2 (runs 3 to 6). Circulation 2, on the other hand, has a greater depth of air in the updraught flow which overlies this downdraught(1150m as against 650m). Maximum updraught flows are 5.0 m/s and 6.1 m/s respectively.

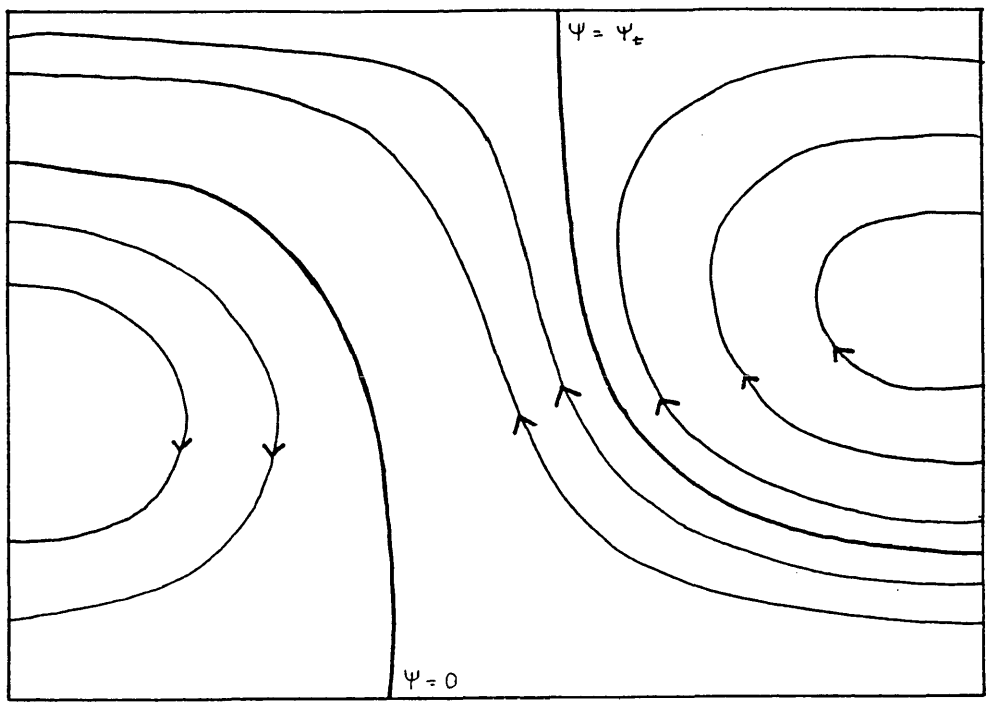


Figure 5.11 Field of streamlines for two-dimensional cold frontal circulation 1

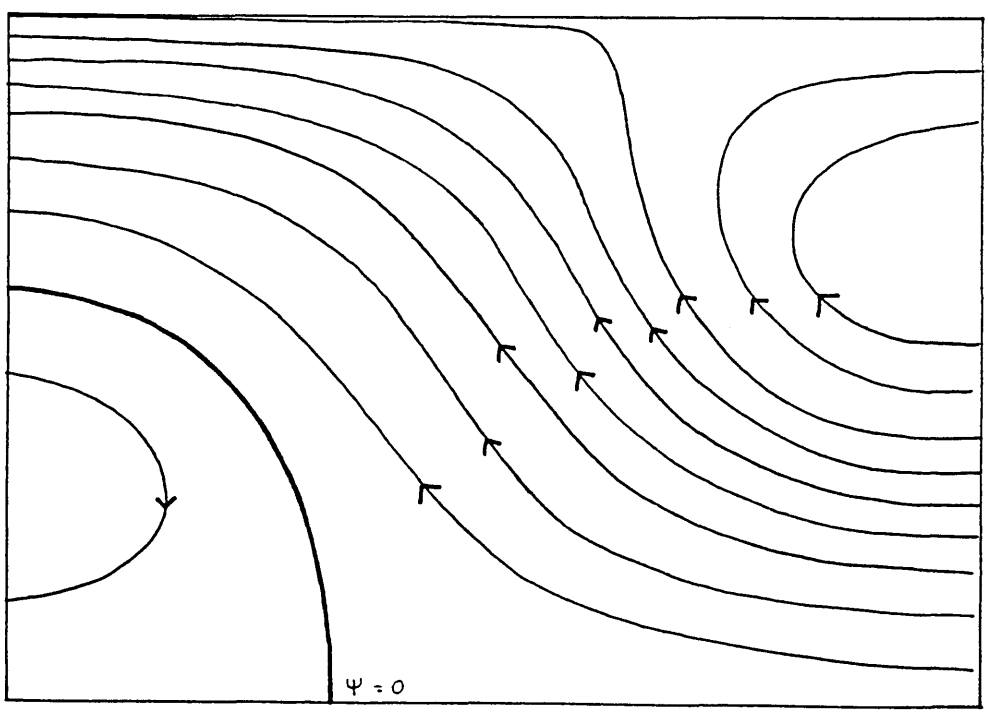


Figure 5.12 Field of streamlines for two-dimensional cold frontal circulation 2

Table 5.5 Model parameters for cold frontal runs

Run no.	v_k	K	E_{nuc}	E_A	E_r	wo/ro
1	60000	0.25	0.9	0.1	1.0	wo
2	60000	0.25	0.9	0.1	1.0	ro
3	50000	0.5	0.9	0.1	1.0	wo
4	50000	0.5	0.9	0.1	1.0	ro
5	50000	0.5	0.6	0.1	1.0	ro
6	50000	0.5	0.9	0.2	1.0	ro

Like the orographic situation, the rearward sloping cold front is regarded as a steady state phenomenon with pollutant processing through it. Thus the model is run first without pollutant until steady state cloud and rain profiles are reached. Standard runs for the two cases are specified by the microphysical parameters given for runs 1 to 4 in table (5.5). The steady state precipitation rates at the ground for these case are shown in figures (5.13) and (5.14). They have maxima of 16 and 25 mm/hr respectively. These values seem reasonably in line with the observations of Browning and Harold(1970), being between their measurements for peak precipitation during two instances of line convection of 10 and 65 mm/hr.

Particulate pollutants may feed into either the updraught or the downdraught flows and it is interesting to compare their fates. This is acheived by calculating the effective washout coefficient, Λ^0, defined as

$$\Lambda^0 = \Lambda / J^{0.8}$$

where

$$\Lambda = \frac{D_r}{\int X_a \, dz} .$$

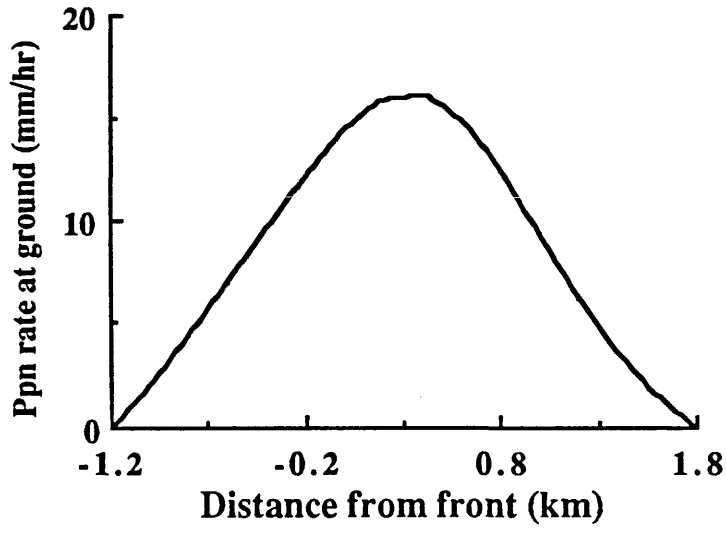


Figure 5.13 Steady state precipitation rate for cold frontal circulation 1

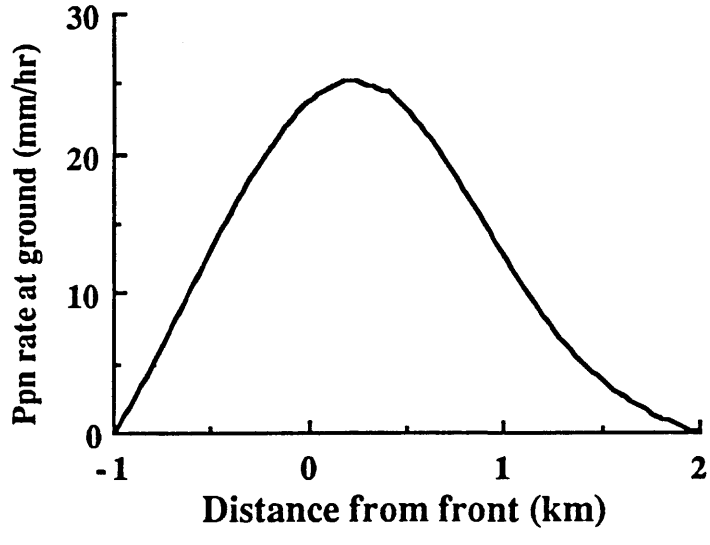


Figure 5.14 Steady state precipitation rate for cold frontal circulation 2

$J^{0.8}$ is appropriate in this case since precipitation rates are higher than for the orographic situation and it is to be expected that Λ should increase less than linearly with J.

The distributions of Λ^0 for the updraught and downdraught flows for circulation 1 are shown in figure (5.15). Particulates feeding into the downdraught are collected by impaction by falling raindrops. Here $\Lambda^0 \sim 5.10^{-5}$ which is the value to be expected for straightforward washout of micron sized pollutants. In the updraught flow, Λ^0 is rather higher, reaching a peak value of $2.2.10^{-4}$ and averaging $1.2.10^{-4}$. As for the orographic case, the deposition peak precedes the precipitation peak, but in the cold frontal situation there is a greater gap between the two peaks. At steady state, 70% of the material entering the frontal domain is deposited in rain whereas this figure is only 20% in the orographic case. More material is being depleted in the former case and therefore less is available for deposition further on in the flow. Hence the peak is brought further forward relative to the precipitation peak. Nevertheless, 30% of material passes right through the front and is available for deposition elsewhere.

Calculations of Λ^0 have also been made for circulation 2. Results are shown in figure(5.16) for both updraught and downdraught circulations and various microphysical parameters. Once again, particles feeding into the downdraught flow are collected by falling raindrops with a corresponding value for Λ^0 of about 5.10^{-5} (run 3). In the updraught flow, for the standard microphysical parameters, Λ^0 reaches a peak of $2.25.10^{-4}$ averaging $1.5.10^{-4}$ (run 4). This curve for Λ^0 does not dip as sharply towards the left hand side of the domain as in circulation 1, a consequence of the greater depth of updraught. Raising the impaction efficiency to 0.2 (run 6) causes a slight increase in Λ^0 over the whole domain giving it a peak value of $2.3.10^{-4}$. The most important parameter is nucleation

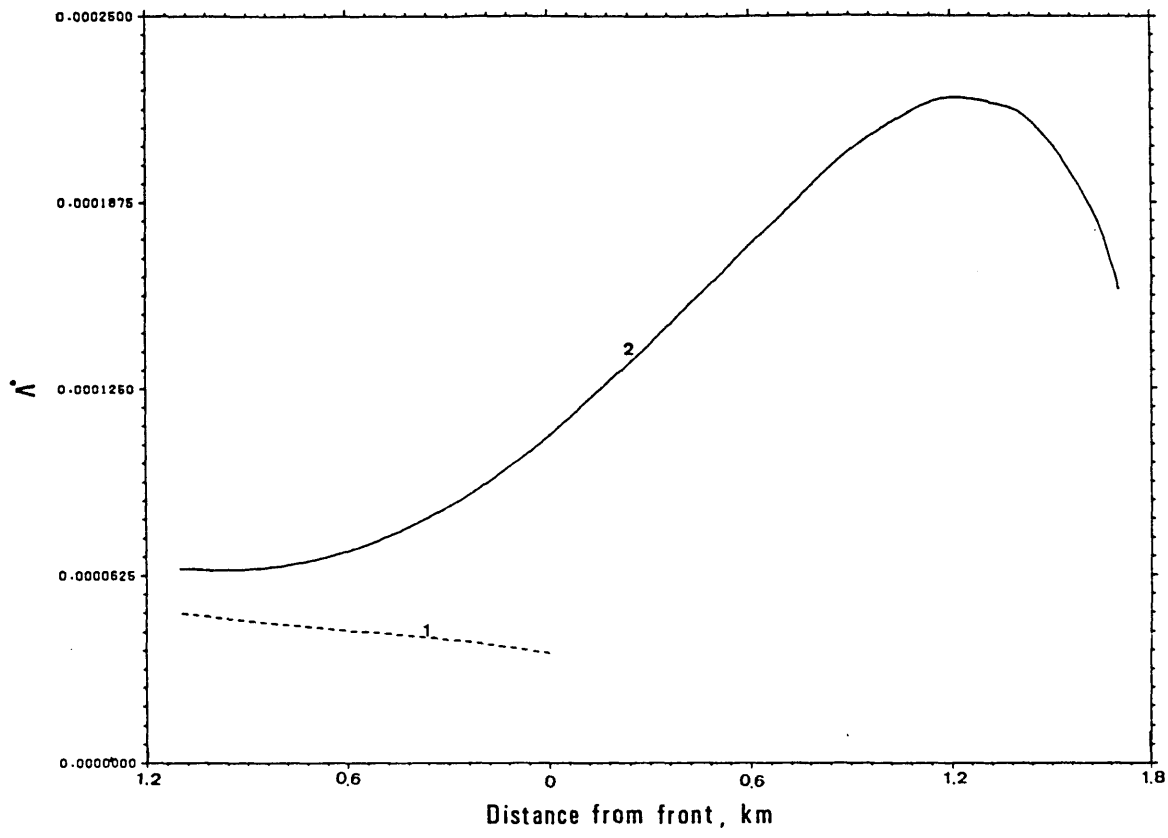


Figure 5.15 Effective washout coefficients for cold frontal circulation 1

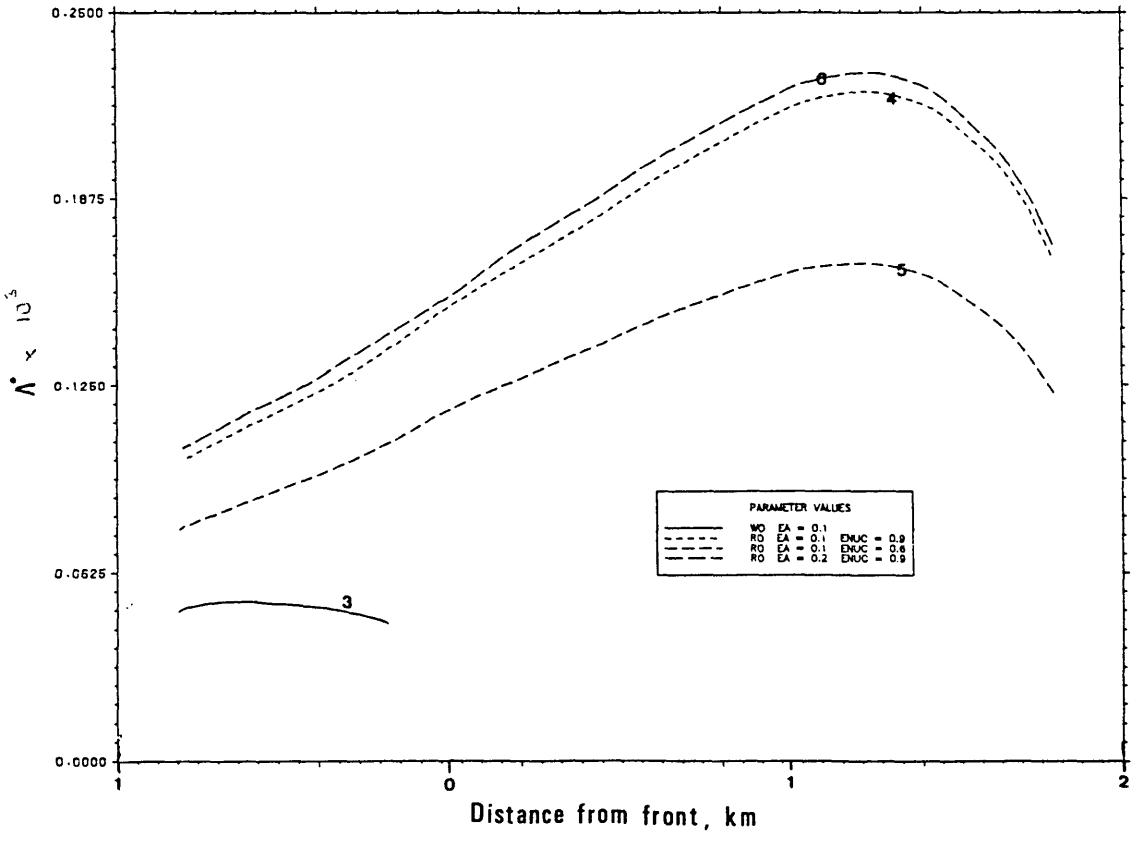


Figure 5.16 Effective washout coefficients for cold frontal circulation 2

efficiency. With a low value for E_{nuc} of 0.6 (run 5), the peak value of Λ^0 drops to $1.7.10^{-4}$.

5.5 Convective precipitation

5.5.1 Description of convective precipitation

Convective precipitation is more common in more Southerly regions of Europe than Britain. Nevertheless, especially in the Summer months, convective systems may play an important part in the production of wet deposition. Large volumes of boundary layer air are sucked into the updraught cores of convective systems with precipitation being deposited over relatively small areas. Such concentration mechanisms may lead to enhanced levels of contamination in precipitation and localised hot spots of deposition. An estimate of the approximate magnitudes of these concentration factors is made in section (5.5.2).

The literature of observational data on convective storms has been reviewed by Atkinson(1981). He identifies the classification given by Chisholm and Renick(1972) as being the most appropriate. They split storms into three types; single cell, multicell and supercell storms. Single cell storms are short lived (duration $T \leq 1$ hour), evolve in time and are usually about 5 to 10 km in horizontal extent. A schematic illustration of their life cycle is given in figure(5.17). Precipitation results from condensation of water vapour in moist air rising above its saturation level in the updraught. There is very little wind shear and hence precipitation falls through the updraught which leads to its termination.

A multicell storm consists of a sequence of evolving cells each of which has a life cycle as described above. The storm is the net result of the propagation of these cells along the storm direction. A schematic illustration is given in

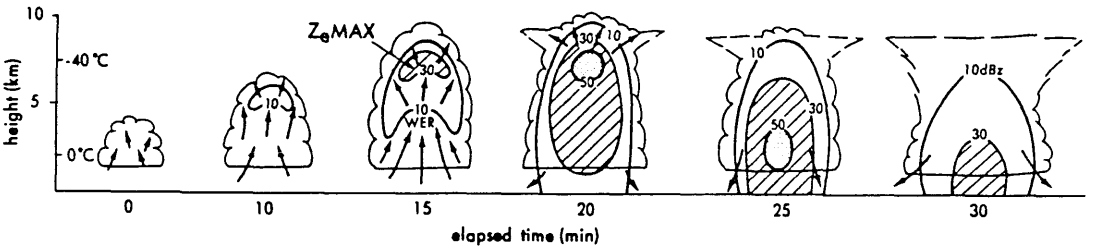


Figure 5.17 Schematic vertical cross sections through a single-cell storm at various stages of its life cycle. Contours of echo intensity labelled in dBz; arrows depict the major airflow components (from Atkinson, 1981).

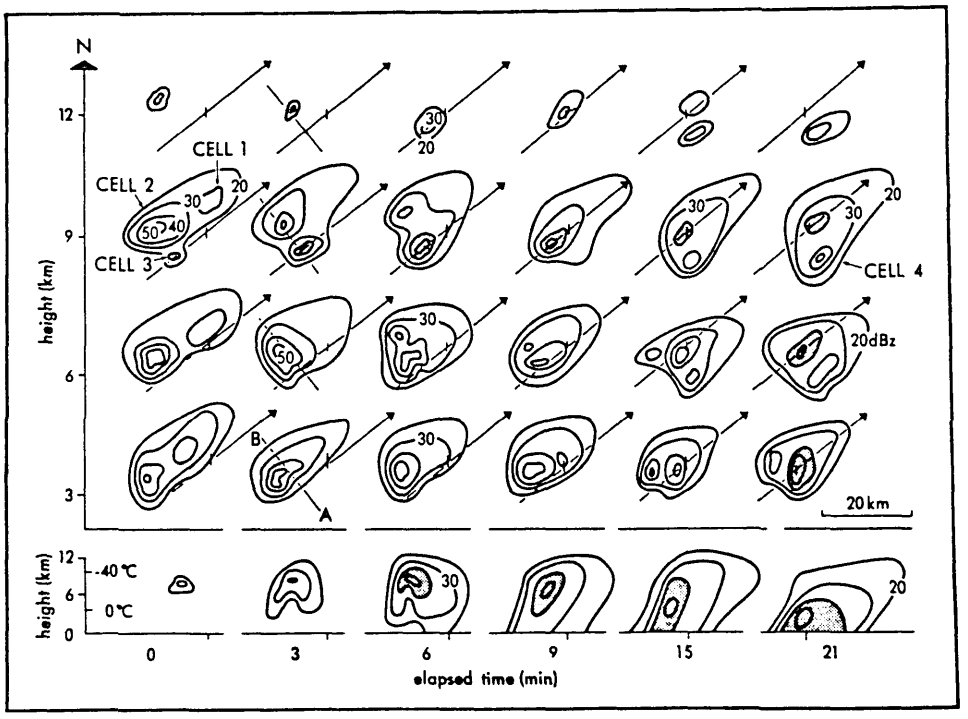


Figure 5.18 Schematic plan position indicator sections and vertical cross-sections for a multi-cell storm at various stages of its life cycle. The heavy arrows depict the direction of cell motion and are also geographical reference lines for the vertical cross-sections shown along the bottom of the figure (from Atkinson, 1981)

figure(5.18). As one cell is decaying, another next to it is reaching maturity and a third is just forming.

A supercell storm is a large single convective storm that is long lived and acheives a steady state. This is maintained by the pres ence of an updraught and downdraught in strong wind shear. Precipitation formed in the updraught falls into the downdraught allowing the continued existence of both circulations. The windfields are essentially three dimensional and illustrations of schematic models by Browning and Ludlam(1962) and Browning(1964) are given in figures(1.2) and (5.19). Browning and Ludlam(1962) also provided a 2D model (see figure(5.20)) which is rather like an untwisted and flattened version of the 3D models.

For the purpose of the modelling studies described in this thesis, convective storms are split into 2 types. They are convective showers which are equivalent to the single cell storms described above and convective storms which are equivalent to supercell storms. The multicell storms can be regarded as either a series of convective showers evolving at various places along the path of the storm or as a convective storm moving along the direction of the storm's movement. This duality of approach is similar to the schematic model of a multicell by Browning et al(1976) shown in figure(5.21). The model can be regarded either as an instantaneous view of a structure containing four cells at different stages of evolution or as showing four stages in the evolution of an individual cell.

5.5.2 Estimation of concentration factors

The modelling carried out in chapters 3 and 4 utilised a 1D representation of convective shower type circulations. This is shown schematically in figure(5.22). There is a single updraught with convergence of air in the lower part of the updraught and divergence aloft. Since the updraught is

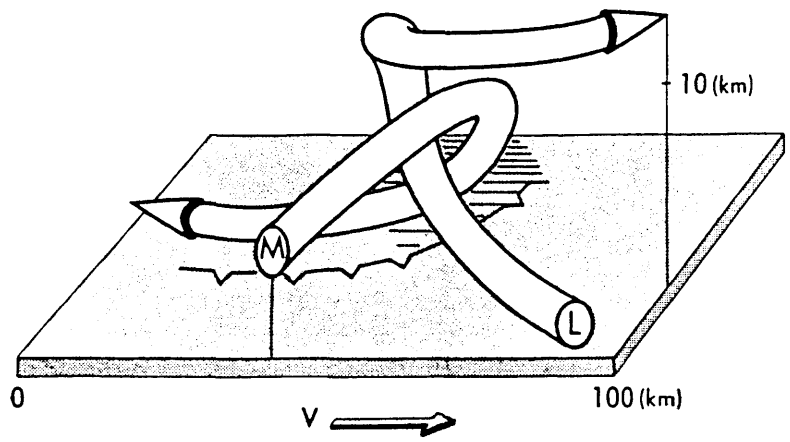


Figure 5.19 Three-dimensional airflow in severe storm that travels to the right of the winds in the middle troposphere. L(low) and M(middle) refer to the main levels of origin of updraught and downdraught respectively. Hatched area shows extent of surface precipitation; barbed line the position of surface gust front. V is storm velocity (from Atkinson, 1981).

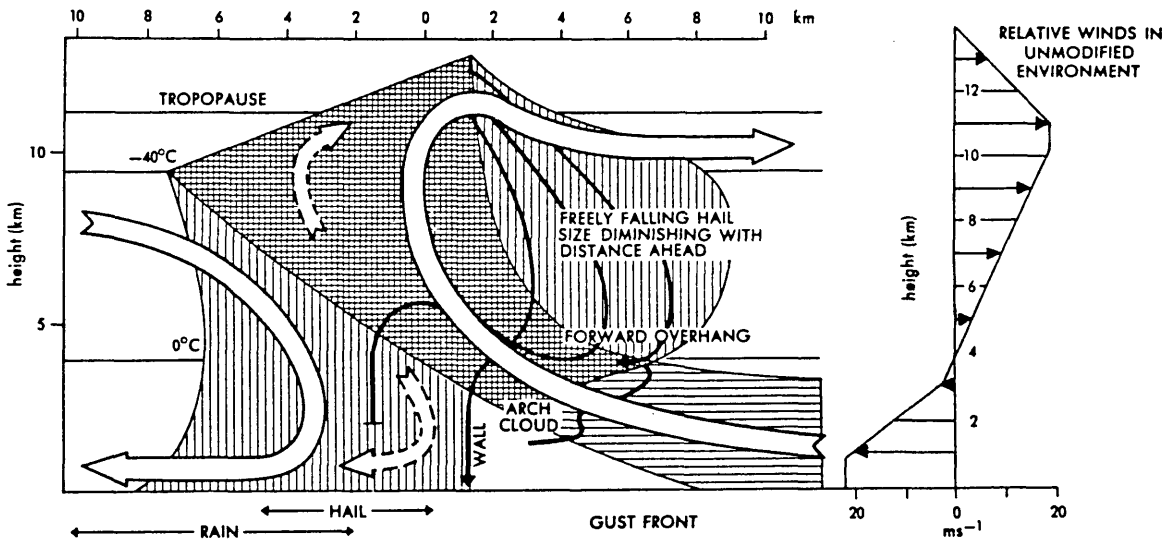


Figure 5.20 Two-dimensional schematic model of convective storm circulation. Horizontal shading shows updraught and vertical shading the bulk of the radar echo (from Atkinson, 1981)

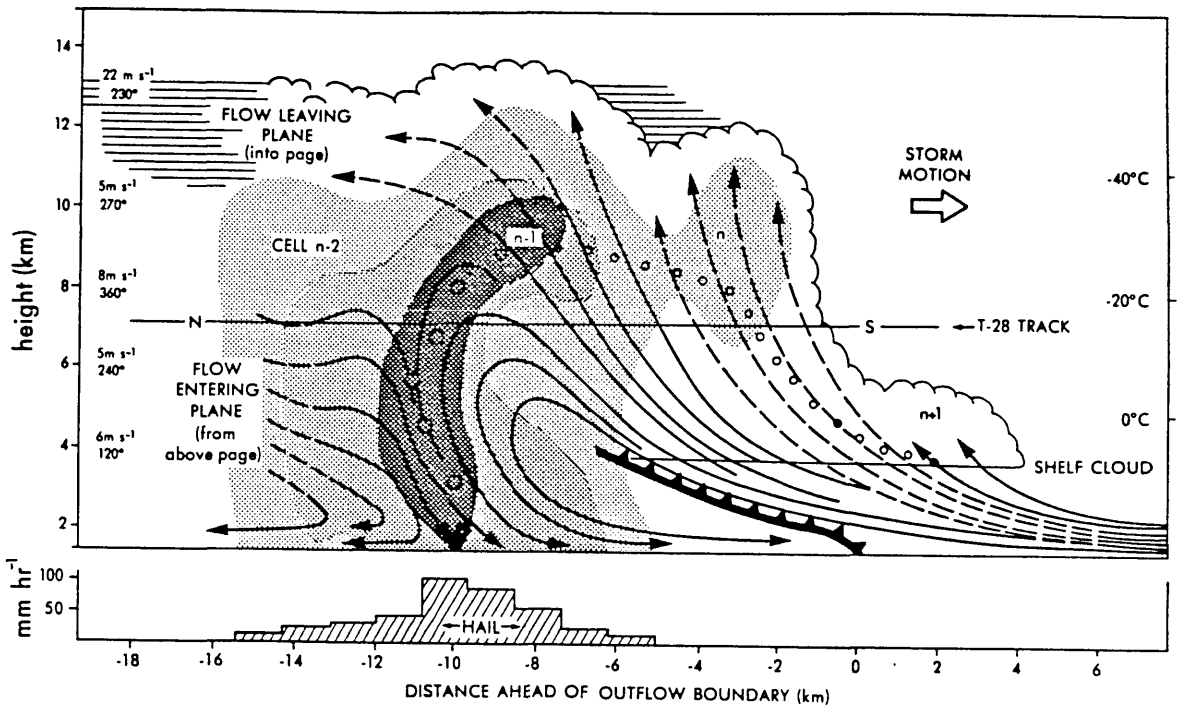


Figure 5.21 Schematic model of a severe multi-cell hailstorm showing a vertical section along the storm's direction of travel through a sequence of evolving cells (from Atkinson, 1981)

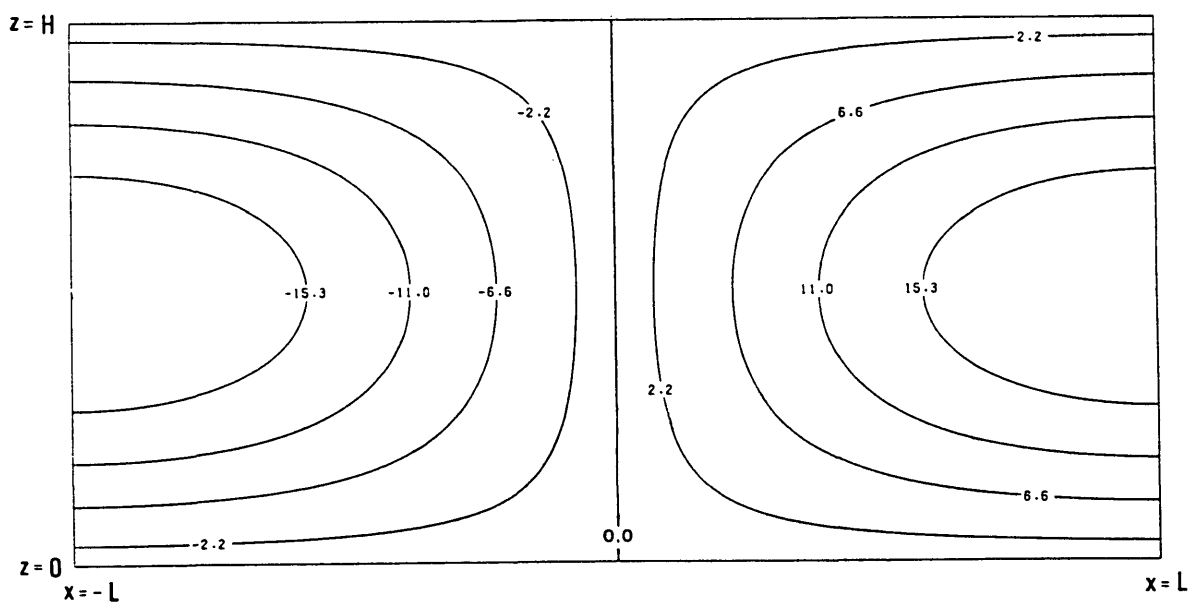


Figure 5.22 Field of streamlines for two-dimensional convective shower circulation

terminated by preicipation falling through it, it does not have time to reach a steady state. The efficiencies of convective showers at depositing gaseous and aerosol pollution in precipitation were studied in 1D in chapters 3 and 4 for different durations of storm life.

The 2D representation of this circulation is given by the stream function

$$\psi = -\frac{v_k}{\pi} \sin\left[\frac{\pi z}{H}\right] \sin\left[\frac{\pi x}{2L}\right] \tag{5.45}$$

from which air velocities are

$$u = -e^{kz} \frac{v_k}{H} \cos\left[\frac{\pi z}{H}\right] \sin\left[\frac{\pi x}{2L}\right] \tag{5.46}$$

$$w = e^{kz} \frac{v_k}{2L} \sin\left[\frac{\pi z}{H}\right] \cos\left[\frac{\pi x}{2L}\right] \tag{5.47}$$

defined on the domain

$0 \leq z \leq H$

$-L \leq x \leq L$ (see fig (5.22)).

This can be used as the basis for a calculation of the concentration factor, F, operative in convective showers.

The deposition, D_s, beneath a convective shower can be estimated from

$$D_s = \frac{Q\varepsilon}{A} \tag{5.48}$$

where Q is the total quantity of pollutant processed by the system, ε is its efficiency at depositing pollutant in precipitation and A is the area beneath the system over which wet deposition takes place. If the radius of the

system is L, then

$$D_s = \frac{Q\varepsilon}{\pi L^2} . \qquad (5.49)$$

This can be compared with the deposition, D_w, calculated assuming a washout coefficient acting over the whole area of the boundary layer from which the system's air is fed. This area is given by

$$A_0 = \frac{V}{H_b} \qquad (5.50)$$

where V is the volume of air drawn in and H_b is the height of the boundary layer. Assuming a washout coefficient, Λ, acting for the duration of the shower, T, on the same am ount of material, Q, the total deposition in this case is

$$D_w = \frac{QH_b}{V}(1-e^{-\Lambda t}) = \frac{Q}{A_0}(1-e^{-\Lambda t}) . \qquad (5.51)$$

The concentration factor, F, is the ratio between the depositions;

$$F = \frac{D_s}{D_w} = \frac{\varepsilon}{1-e^{-\Lambda t}} \frac{A_0}{A} \qquad (5.52)$$

where A_0/A is the areal concentration factor.

The unknown quantity is the volume of air drawn in, V. This can be calculated from the 2D model circulation given by eqs(5.45), (5.46) and (5.47). It is given by

$$V = T\,2\pi L \int_0^{H/2} dz \{ -u(x=L, z) \} \tag{5.53}$$

where H is the height of the updraught. Thus

$$V = T\,2\pi L \frac{v_k}{H} \int_0^{H/2} dz\, e^{kz} \cos(\pi z / H) \,. \tag{5.54}$$

By carrying out an integration by parts twice, the integral is solved to give

$$V = 2LT v_k \left[\frac{1}{1 + \frac{k^2 H^2}{\pi^2}} \right] . \left[e^{kH/2} - \frac{kH}{\pi} \right] \tag{5.55}$$

and taking $k = 10^{-4}$, $H = 10^4$, $k.H = 1$ gives

$$V = 2LT v_k 1.208$$

The areal concentration factor can now be calculated;

$$\frac{A_0}{A} = \frac{V}{H_b \pi L^2} = \frac{2T v_k}{\pi H_b L} 1.208 \,. \tag{5.56}$$

In order to illustrate the possible magnitudes of the areal and deposition ratios, suitable values for circulation parameters are taken to be

ε = 0.4

T = 2000 s

$v_k/2L$ = 5 m/s

H_b = 1000 m.

Then $A_0 / A = 15.4$ and with a washout coefficient of $\Lambda = 10^{-4}$ (with $\Lambda = 10^{-4} = 5.10^{-5}$ J this is equivalent to 30 mm/hr from shower being smeared out over A_0 at 2 mm/hr), $F = D_s / D_w = 34.0$. The concentration factor for deposition is over 30. Thus a dramatically higher level of deposition is occurring beneath the convective shower than would be predicted by applying a washout coefficient to the whole volume of air swept out by the updraught.

5.5.3 Description of modelling

A two-dimensional representation of the essentially three-dimensional motions in a long lived convective storm is produced as follows. The updraught and downdraught, untwisted in the manner of figure(5.20) are described by the stream function

$$\psi = -\frac{v_k}{2}\left[\frac{1}{\pi}\sin\left[\frac{\pi z}{H}\right]\sin\left[\pi\left[\frac{x}{L}-\frac{1}{2}\right]\right] + \frac{Kz}{H}\right]^2 . \qquad (5.57)$$

This is defined on the domain $0 \leq x \leq L$, $0 \leq z \leq H$. The variation of density of air with height is significant ($\rho(z = 10 \text{ km }) = \rho_0 e^{-1} = 0.37 \rho_0$) and so the continuity equation is

$$\frac{\partial}{\partial x}\left(\frac{\rho}{\rho_0} u\right) + \frac{\partial}{\partial z}\left(\frac{\rho}{\rho_0} w\right) = 0 . \qquad (5.58)$$

The stream function is related to air velocities by

$$u = \frac{\rho_0}{\rho}\frac{\partial \psi}{\partial z} \quad , \quad w = -\frac{\rho_0}{\rho}\frac{\partial \psi}{\partial x} . \qquad (5.59)$$

from which the air velocities take the same general form as the cold frontal model;

$$u = -e^{kz}\frac{v_k}{H}\left[\frac{1}{\pi}\sin\left[\frac{\pi z}{H}\right]\sin\left[\pi\left[\frac{x}{L}-\frac{1}{2}\right]\right]+\frac{Kz}{H}\right].\left[\cos\left[\frac{\pi z}{H}\right]\sin\left[\pi\left[\frac{x}{L}-\frac{1}{2}\right]\right]+K\right] \tag{5.60}$$

$$w = e^{kz}\frac{v_k}{L}\left[\frac{1}{\pi}\sin\left[\frac{\pi z}{H}\right]\sin\left[\pi\left[\frac{x}{L}-\frac{1}{2}\right]\right]+\frac{Kz}{H}\right].\left[\sin\left[\frac{\pi z}{H}\right]\cos\left[\pi\left[\frac{x}{L}-\frac{1}{2}\right]\right]\right]. \tag{5.61}$$

As for the cold frontal model, the boundaries of the cloud correspond to the boundaries of the domain where w = 0. Therefore

$$q_c(x=0,z,t) = q_c(x=L,z,t)$$
$$= q_r(x,z=0,t) = q_r(x,z=H,t) = 0. \tag{5.62}$$

No rain falls from the top boundary or the sides;

$$q_r(x,z=H,t) = q_r(x=0,z,t) = q_r(x=L,z,t) = 0. \tag{5.63}$$

The boundary between the updraught and the downdraught flow is given by the streamline

$$\psi = 0.$$

Pollution may feed into the updraught from the right hand edge or into the downdraught from the left hand edge.

Updraught

Incoming air in the updraught flow has

$$u(x=L,z) < 0.$$

Therefore the flow of air that feeds into the updraught from the right hand boundary is bounded by

$$z=0 \quad \text{and} \quad z=z_{in}$$

where $u(x=L,z_{in}) = 0$ and $0 < z_{in} < H$.

The pollution feeding into the flow is represented by the boundary condition

$$X_a(x=L,z) = \begin{cases} X_{rin}\sin\left[\dfrac{\pi z}{z_{in}}\right] & \text{for } 0 \le z \le z_{in} \\ 0 & \text{otherwise} \end{cases} \tag{5.64}$$

where X_{rin} is the maximum pollutant concentration in incoming air (in units g/m^3).

Downdraught

Incoming air in the downdraught flow has

$$u(x=0,z) > 0.$$

The boundary condition for pollution feeding into the flow is

$$X_a(x=0,z) = \begin{cases} X_{lin} \sin\left[\dfrac{\pi(z-z_{bl})}{(z_{tl}-z_{bl})}\right] & \text{for } z_{bl} \le z \le z_{tl} \\ 0 & \text{otherwise} \end{cases} \qquad (5.65)$$

where z_{bl}, z_{tl} are defined by

$$u(x=0,\ z_{bl}) = 0, \quad u(x=0, z_{tl}) = 0, \quad 0 < z_{bl} < z_{tl} < H \qquad (5.66)$$

and X_{lin} is the maximum pollutant concentration feeding into the downdraught.

5.5.4 Results and discussion

The set of dynamic variables first chosen to model a convective storm are given for runs 1 and 2 in table(5.6). The maximum updraught velocity is 10.1 m/s. Since the convective storm is a long lived entity that has reached a steady state, the same procedure was used as for cold frontal modelling. First the model was run without pollutant until steady state cloud and rain profiles were reached. With the microphysical parameters given for runs 1 and 2 in table(5.6), the profile of steady state precipitation that was produced is shown in figure(5.23). The peak value is about 30 mm/hr.

As for the cold frontal circulation the fate of pollution drawn into the storm via the updraught and downdraught circulations can be compared. For

Table 5.6 Model parameters for convective storm runs

Run no.	v_k	K	H	L	E_{nuc}	E_A	E_r	wo/ro
1	240000	0.25	9	6	0.9	0.1	1.0	ro
2	240000	0.25	9	6	0.9	0.1	1.0	wo
3	400000	0.25	10	10	0.9	0.1	1.0	ro
4	400000	0.25	10	10	0.9	0.1	1.0	wo
5	400000	0.25	10	10	0.9	0.2	1.0	ro
6	400000	0.25	10	10	0.6	0.1	1.0	ro

pollution entering the storm in the updraught (run 1), the pattern of deposition when it has reached steady state is shown in figure (5.24). This takes about 3000s. As before, the effective washout coefficients given by $\Lambda_0 = \Lambda / J^{0.8}$ can be calculated. Their distributions for pollutant material with the microphysical parameters given in table(5.6) is shown in figure(5.25). There is now much less difference between Λ_0 for updraught and downdraught circulations with the peak for the updraught being $7.5.10^{-5}$, only about 3/4 as much again as the peak of $4.3.10^{-5}$ for the downdraught. This is despite the fact that about 85 % of material entering the updraught is being deposited in rain. The high precipitation quantities ensure that values for Λ_0 are lower than the cold frontal circulation despite deposition rates being considerably higher.

The concentration mechanism that is operative will still lead to high levels of deposition. Large quantities of material are feeding into the storm in the high influx velocities and these are being deposited over small areas with high efficiencies. The consequences of this are discussed more fully in the next chapter.

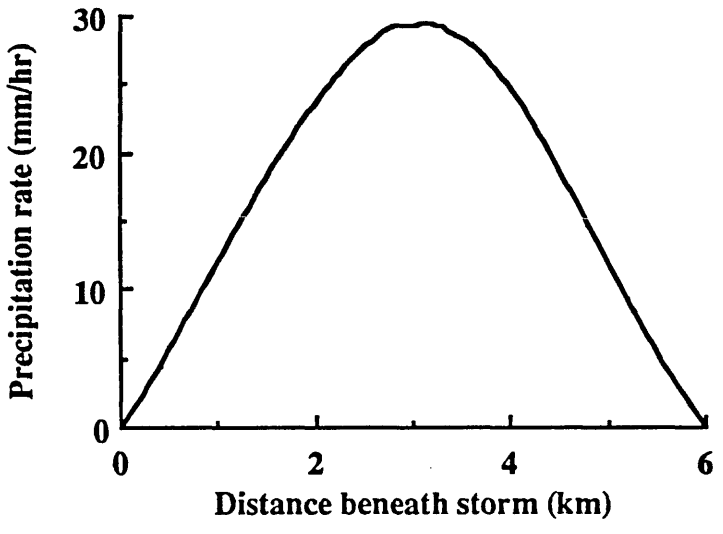


Figure 5.23 Steady state precipitation rate for first convective storm

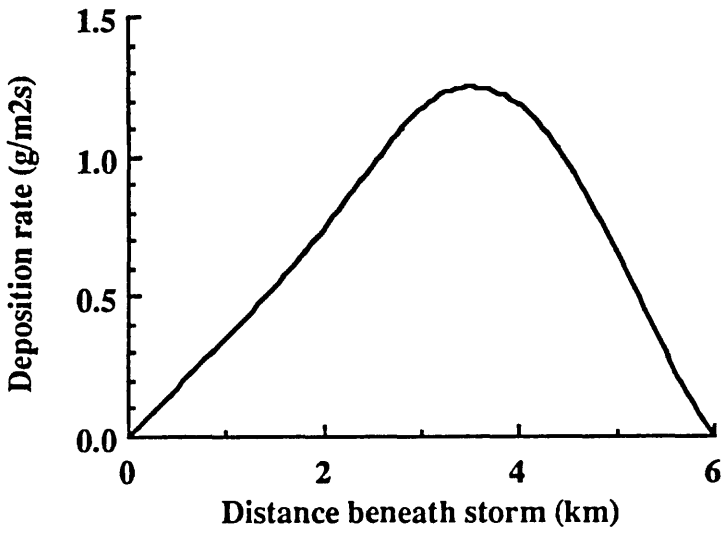


Figure 5.24 Steady state deposition rate for first convective storm

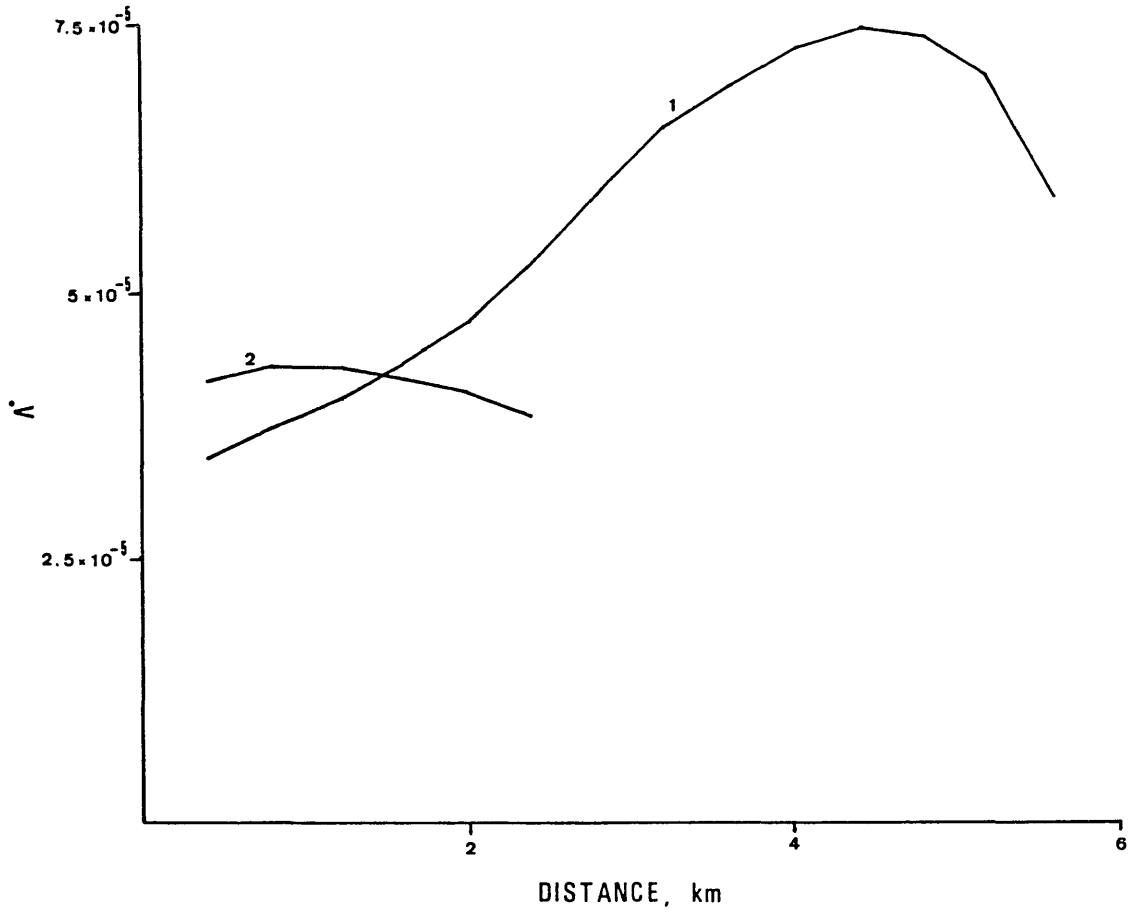


Figure 5.25 Effective washout coefficients for first convective storm

The studies of convective storms detailed by Ludlam(1980) indicate that the precipitation rates obtained in this first simulation are rather small and the studies of Chisholm and Renick(1972) cited by Atkinson(1981) show that the updraught velocities are rather low. Therefore a second set of dynamic variables was chosen and is given for runs 3 to 6 in table(5.6). The maximum updraught velocity is now 18.4 m/s. The domain size has been increased slightly to 10 x 10 km to be more in line with Browning and Ludlam's 2D conceptual model (see figure (5.20)).

The precipitation rate at the ground is shown in figure(5.26). The peak is now at 109 mm/hr which is more in line with the figures given by Ludlam(1980). The variation of Λ^0 for updraught and downdraught circulations and for various parameters are shown in figure(5.27). The distributions are familiar in shape to the distributions of Λ^0 for the previous circulation. In the higher precipitation, Λ^0 for material in the downdraught is now lower so that its maximum is $3.2.10^{-5}$. With the standard microphysical parameters, Λ^0 for material in the updraught is also lower peaking at $6.2.10^{-5}$. Increasing impaction efficiency increases Λ^0 slightly to a maximum of $6.4.10^{-5}$. This is reduced to $4.5.10^{-5}$ when nucleation efficiency is 0.6.

5.6 Summary and conclusions

In the two-dimensional modelling described in this chapter, simplified and schematic windfields have been used which are illustrative of the general characteristics of precipitation systems. This has been achieved by analytically specifying flow fields in which there are both updraught and downdraught circulations. They have been applied to simulate the dynamics appropriate to orographic, frontal and convective situations. Other windfields could be used that represent air flows better. For instance, velocities could be specified by the WAFT computer model which produces

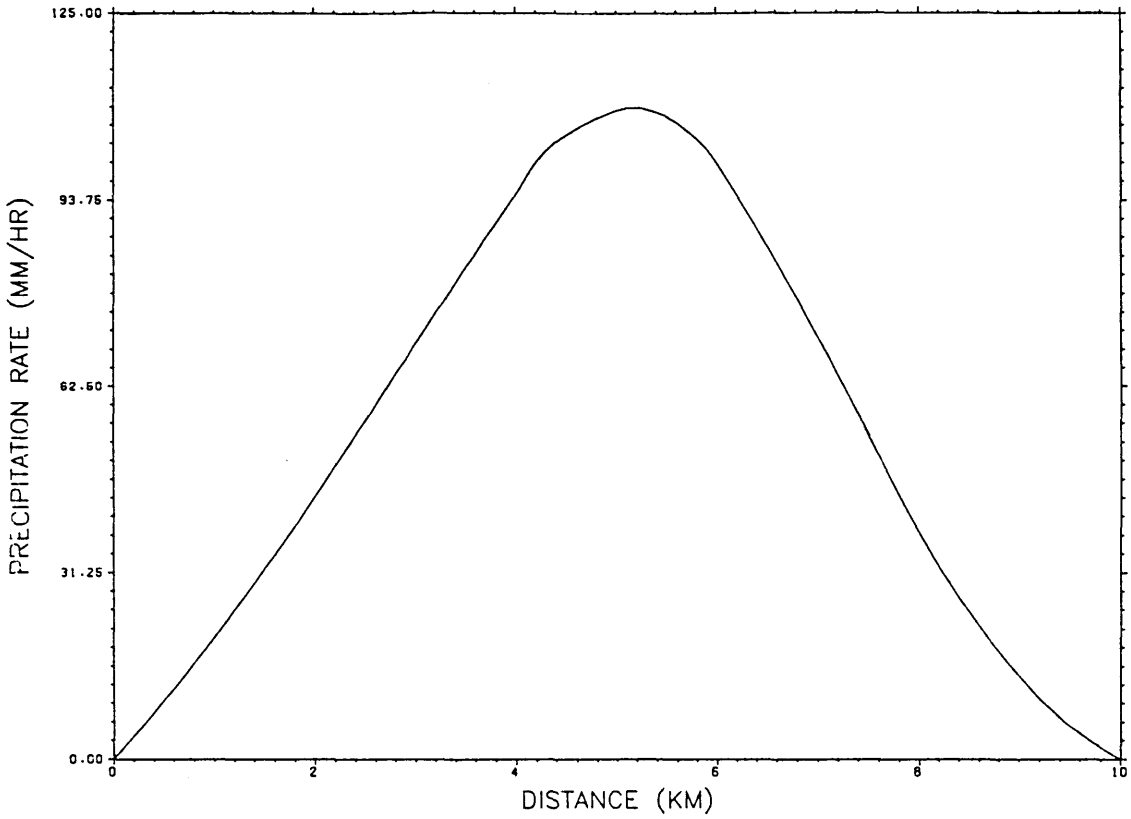


Figure 5.26 Precipitation rate for second convective storm

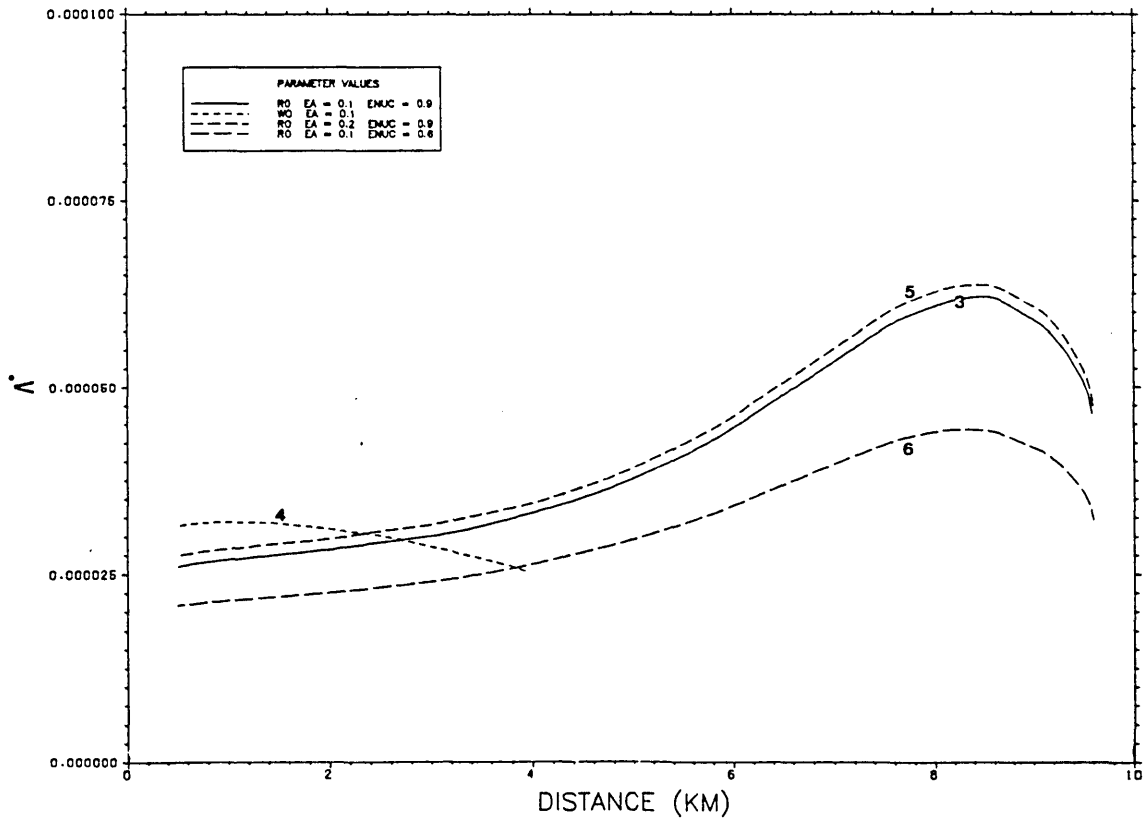


Figure 5.27 Effective washout coefficients for second convective storm

mass-consistent windfields for flow over complex terrain (Kitson, 1988). However, the analytically specified windfields used here have permitted model development before more complex and accurate windfields are introduced.

From the model runs, calculations have been made of the rainout and export efficiencies of aerosol pollutants as well as equivalent washout coefficients, Λ. This latter quantity provides a measure of the enhancement to deposition that has been acheived due to rainout processes within the cloud system. Orographic precipitation was modelled by simulating flow over a single hill with an input of precipitation from the top of the model domain to simulate the seeder cloud. The seeder-feeder mechanism resulted in an approximate doubling of the precipitation rate. However, deposition rate experienced a much greater enhancement, on average increasing by an order of magnitude. Line convection which is associated with a rearward sloping cold front was modelled, since it is essentially a two-dimensional phenomenon. The differing fates of pollution drawn into the updraught and downdraught flows could be compared by means of an effective washout coefficient, Λ^0, which is the equivalent washout coefficient, Λ, weighted by the precipitation rate. This was up to four times greater in the updraught flow than in the downdraught, although the greater overall precipitation rates beneath the former flow meant that the difference in deposition rates was greater. Although long-lived convective storms are three-dimensional phenomena they could be represented in two dimensions by untwisting the interlocking flows. It was again possible to compare the fates of pollutants in the updraught and the downdraught. Here, Λ^0 in the former case was increased by roughly 3/4 compared to the latter. However since precipitation rates were up to 100 mm/hr, deposition rates were considerably higher than in either of the two previous precipitation systems. Also large volumes of air feed into convective sytems

to feed their strong updraughts. An analytic calculation showed that a convective shower lasting about half an hour might produce as much as thirty times the deposition that would have been experienced if the same ammount of rain had fallen through the volume of boundary layer that is sucked into the core of the shower's updraught.

In this chapter, pollutant deposition in storm sytems has been measured by means of equivalent and effective washout coefficients, Λ and Λ^0. These have been compared with their values in those regions where pollutants are scavenged only by washout mechanisms so that the enhancements in deposition due to rainout processes may be assessed. In the context of accident consequence assessment it is necessary to calculate the absolute quantities of material deposited beneath storm systems. Therefore pollutant concentrations and volumes of air feeding into storms as well as the areas upon which material is deposited will influence depositions and hence consequences felt by affected populations. These effects are included in the next chapter. There, the cloud models developed in this chapter are used in conjuction with the techniques for calculating dispersion of released material and received doses from consequent depositions, which were described in chapter 2.

6 Application of cloud modelling studies to accident consequence analysis

6.1 Introduction

The range of possible consequences resulting from an accident at a nuclear power station were discussed in chapter 2. It was shown how emergency reference levels can be used to categorise the severity of an accident. By employing a Gaussian plume diffusion model, the distances from the plant and the areas within which emergency reference levels would be exceeded were calculated for various accidents. These included degraded core PWR accidents, design basis PWR and Magnox accidents and the accident at Chernobyl. Also, the possible enhancement due to wet deposition was calculated using the simple washout model. It was shown how even modest am ounts of precipitation can lead to emergency reference levels being exceeded much further away from the source and for larger areas than in dry conditions.

There are problems with modelling wet deposition by using a Gaussian plume with the washout model and these have been discussed by ApSimon and Simms(1986). Where the material in the plume first encounters a stationery rain band there is a sharp peak of deposition. A more realistic description of washout was developed by Simms(1988) by including the relative velocities of precipitation and pollution and the alongwind dispersion of pollutant material in a puff based model. However, rainout processes and concentration mechanisms were not explicitly included. The modelling described in the preceeding three chapters attempted to include these effects. The models that have been developed are used in this chapter to calculate the consequences resulting from wet deposition in those instances in which rainout processes and concentration mechanisms are important. The circumstances are investigated in which precipitation

leads to higher levels of deposition than would be predicted using a washout model such as RAINPATCH.

The analysis is split up into four stages which are illustrated in figure(6.1). First the quantities of the most important radionuclides released in the relevant accident are calculated. Next this material is allowed to disperse according to a Gaussian plume treatment until the storm system is encountered. The material processes through the storm system and the deposition at the ground is calculated, taking care to include any movement of the system relative to the ground. Finally the dose received by the exposed population is calculated and compared with appropriate emergency reference levels.

The physical forms of the radionuclides released have great relevance for these calculations. The two elements identified in chapter 2 as most important to consequence analysis are Cs and I. CsI may be the principal form of I released in severe reactor accidents and Cs is expected to be released as oxide, hydroxide or carbonate (Underwood, 1983b). All of these particulate compounds are very soluble in water and would act readily as cloud condensation nuclei. Some part of the iodine released may be in gaseous form, although the fraction will vary from accident to accident. Approximately 3/4 of the iodine released from Chernobyl was in gaseous form(ApSimon et al, 1987). Therefore, in the calculations made below, two scenarios have been chosen so as to cover the range of possibilities. In the first, all the iodine is assumed to be in hygroscopic particulate form such as CsI and in the second, 3/4 is assumed to be in gaseous form with the rest being hygroscopic particles. It was shown in chapter 4 that there is considerable uncertainty as to the efficiency with which gaseous iodine is likely to be scavenged. In this case therefore only scavenging of the particulate fraction is considered.

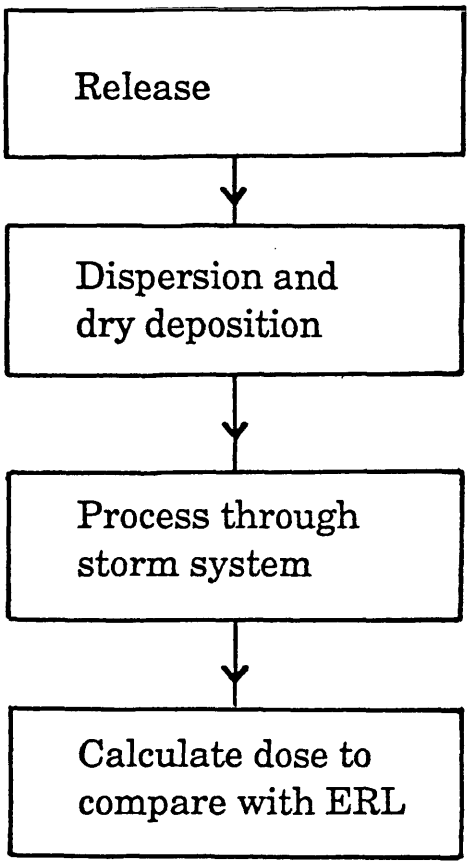


Figure 6.1 Schematic diagram of stages in analysis of consequences from accidental releases using storm models for wet deposition

The same dry deposition velocities are used here as in chapter 2. They are 10^{-3} m/s for particulate material such as caesium and 10^{-2} m/s for iodine released from hypothetical accidents and 3.10^{-3} m/s from Chernobyl.

6.2 Orographic precipitation

6.2.1 Discussion : observation and modelling

In temperate latitudes, orographic cloud is seen on an average of one day in three in hilly terrain (Wallace and Hobbs, 1977). As discussed in section 5.3, the quantity and duration of precipitation in hilly areas is greater than in lowland areas. The intensity of precipitation is enhanced by the seeder-feeder mechanism and deposition of hygroscopic particulate material is enhanced yet further by rainout processes. It is important to consider these effects when calculating the consequences of a nuclear accident to areas of high ground.

There are two further factors that emphasise even more the importance of orographic precipitation. Firstly, hill cloud is essentially a stationery phenomenon which may persist for a long time, possibly many hours. Pollution feeding into this cloud may be caught up in the system and be deposited on a relatively small patch of ground. Secondly, the orographic cloud may persist long enough for the whole of a release to process through it, all of which would be subject to wet deposition on the same area.

These two additional factors, special to orographic situations, make the task of relating cloud model depositions to consequences in terms of emergency reference levels fairly straightforward. Unlike frontal and convective situations, which are discussed below, there is no relative motion between storm system and ground. This would lead to a smearing out of the pattern of deposition and hence a reduction in the total deposition

received at an affected place beneath the storm. Also the longevity of orographic precipitation allows the assumption to be made that all short releases (duration three hours or less) are entirely processed by the system.

A simple conversion relates deposition rates from cloud model runs to reference level depositions. Suppose the deposition rate at a place on the hill is X Bq/m^2s for an average concentration feeding into the storm of 1 Bq/m^3. Then a total deposition of X Bq/m^2 would result from a time integrated air concentration of 1 Bqs/m^3. If a reference level corresponding to a unit release is Y Bq/m^2, then the corresponding time integrated air concentration is Y/X Bqs/m^3. For instance, for the UK1 accident the reference level deposition for a unit release corresponding to restriction of milk at 5mSv is $1.67.10^{-13}$ Bq/m^2. If the deposition rate at a point is 0.5 Bq/m^2s the reference level time integrated air concentration is $1.67.10^{-13}/0.5 = 3.34.10^{-13}$ Bqs/m^3. The distance along a Gaussian plume out to which this is exceeded can then be calculated. Results are discussed below for some of the hypothetical accidents specified in chapter 2. It should be borne in mind that an important assumption in the calculations for hypothetical accidents is that the whole of the release is able to process through the storm system. For the accidents considered, all of which have release durations of no more than three hours, this assumption seems justified.

6.2.2 Results

6.2.2.1 Serious PWR accidents

Two accidents have been chosen to represent the range of severe PWR melt down and depressurisation accidents. They are UK1 and UK8 whose characteristics are given in tables(2.1) and (2.2). They give respectively the most and least severe consequences of the eight accidents considered in

detail in chapter 2. Sensitivities of effects to the nature of the orographic cloud have been studied by calculating the alongwind distances up to which two emergency reference levels would be exceeded for the six orographic runs specified in table(5.2). The emergency reference levels considered are the 5mSv restriction of milk ERL and the 500 mSv ground gamma ERL at which the ICRP recommends that evacuation should have been initiated.

For UK1 and the 5mSv milk ERL, results are shown for the six cloud parameter sets assuming all iodine is released in particulate form in figure(6.2). As the deposition over the hill varies so the alongwind distance up to which an ERL is exceeded varies, with the greatest distance being at the point of maximum deposition. Where this mximum deposition occurs depends on the windfield and the terminal velocity of the drops. The drops' fall speed depends on their size spectrum which has been assumed to have a Marshall-Palmer distribution. The schematic windfield used for the orographic simulations has maximum updraught velocities near to the beginning of the hill and consequently the maximum deposition is downwind of this but still on the upward slope of the hill. The windfield is only an approximation to the flow of air over an orographic barrier. However, the model is able to predict the likely possible range of values of depostions and so can be used to model the range of downwind distances up to which particular ERLs could be exceeded on high ground.

Compared to dry deposition only, there are large increases in these distances. For 100% particulate iodine, the maximum is at about 3000km and the average for the six runs is 2500kms, whereas for dry deposition only the distance is 1300km. The highest downwind distances of the six runs are for run 4 which is the run with the lower hill height. Although this has a low value of Λ^0, there is still a higher deposition because a deeper layer of air is feeding into the system than in the other cases. With a

greater depth of air flowing over the hill, more material can be scavenged. The curve drops less sharply than the others towards the summit of the hill due to the height of the boundary layer narrowing less as it flows over the hill. The other runs show relatively little variation. Run 6 with a nucleation efficiency of 0.6 has the lowest overall distances. Run 2, which has an air velocity lower than the other runs of 10 m/s, has a peak which drops off more rapidly. For this run there is a greater depletion of the air pollution and hence there is less available for deposition at the right hand side of the model domain (26% rained out as compared to about 20% in the other cases). Runs 1 and 5 are almost exactly the same and only at the left hand edge is there a significant difference. Here the greater efficiency of impaction for scavenging of particles leads to higher deposition in run 5. For 25% particulate, the pattern of distances for the six runs is identical except that the highest peak is at 2400kms and the average for the six runs is at about 2000 kms. This is still a significant increase over the distance for dry deposition only which is at 1300km.

There is a similar pattern of curves for UK8 (see figure(6.3)). Here, for 100% particulate iodine, the distances are increased up to 1500 km with an average of about 1000km as compared to 260 km for dry deposition only. With 25% particulate iodine the alongwind distances have a maximum at 1070km and an average at about 600km.

The results for the downwind distances from UK1 accident for which the 500mSv ground gamma ERL is exceeded are given in figures(6.4). Some of these distances are extremely large and it is surprising that they are greater than those for the 5mSv iodine ERL. However the lower dry deposition of Cs (10^{-3} m/s) as compared to I (10^{-2} m/s) results in the Cs plume being depleted much more slowly. A long way away from the source this

Table 6.1 Depletion of Gaussian plume for two different dry deposition velocities; air concentrations for unit release (Bq/m^3)

Distance(km)	$v_g = 10^{-3}$	$v_g = 10^{-2}$
100	$6.6.10^{-9}$	$5.8.10^{-9}$
500	$1.3.10^{-9}$	$4.5.10^{-10}$
1000	$6.3.10^{-10}$	$7.1.10^{-11}$
2000	$2.7.10^{-10}$	$3.2.10^{-12}$
3000	$1.5.10^{-10}$	$1.9.10^{-13}$

difference has become quite considerable; from table(6.1) it can be seen that at 3000km the air concentrations are three orders of magnitude different.

It is extremely unlikely that the plume would travel such long distances along a constant trajectory without encountering some precipitation en route. However some relevant points emerge from these calculations. They demonstrate that the low dry deposition velocity of ^{137}Cs is an additional factor contributing to the severity of the consequences of its wet deposition at long distances from the source. If the released material does not encounter precipitation early on in its travel the consequences felt at greater distances are likely to be much more severe. UK1 is an extremely serious accident. During three hours it releases $2.4.10^{18}$ Bq ^{131}I and $1.1.10^{17}$ Bq ^{137}Cs. It is interesting to compare this discharge with that from Chernobyl. The estimates made by ApSimon et al(1987) and used in chapter 2 were $6\text{-}7.5.10^{17}$ Bq ^{131}I and $5\text{-}6.10^{16}$ Bq ^{137}Cs released over the first 48 hours. During that time wind trajectories from Chernobyl swung around considerably (see figure(6.6)) and thus only small fractions of the release were being dispersed to any one place more than a few hundreds of kilometres from the source. For instance Simms(1988) asssumed that 2 hours of the release affected Britain. On the other hand a release of three

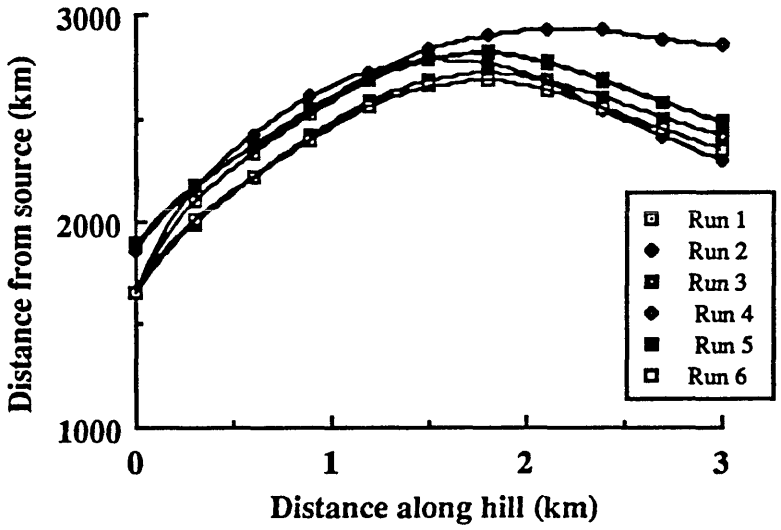


Figure 6.2 Downwind distances at which the 5mSv ingestion of milk ERL is exceeded for UK1 release and deposition in orographic precipitation

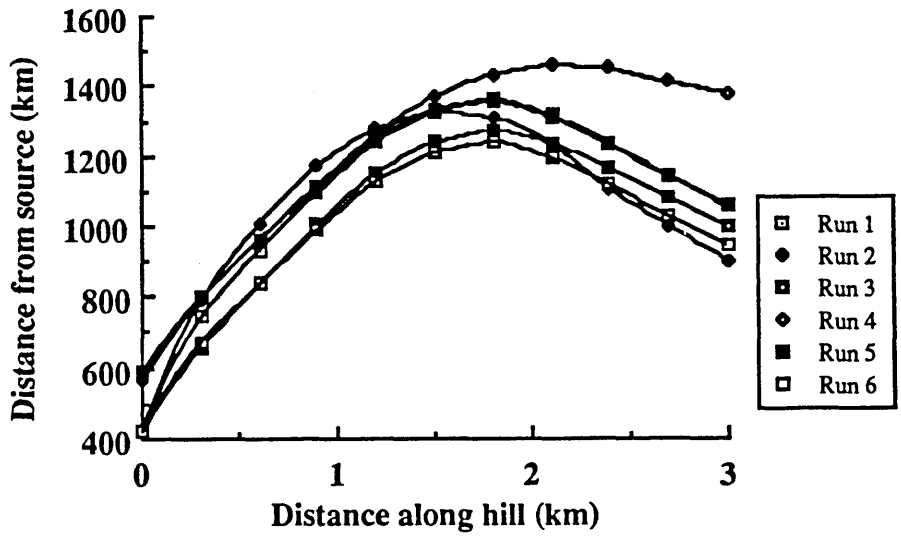


Figure 6.3 Downwind distances at which the 5mSv ingestion of milk ERL is exceeded for UK8 release and deposition in orographic precipitation

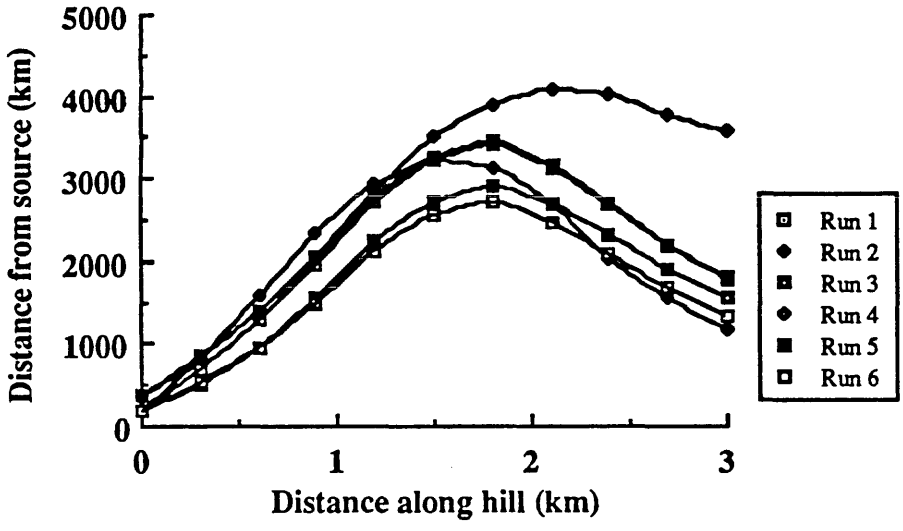


Figure 6.4 Downwind distances at which the 500mSv inhalation of ground gamma ERL is exceeded for UK1 release and deposition in orographic precipitation

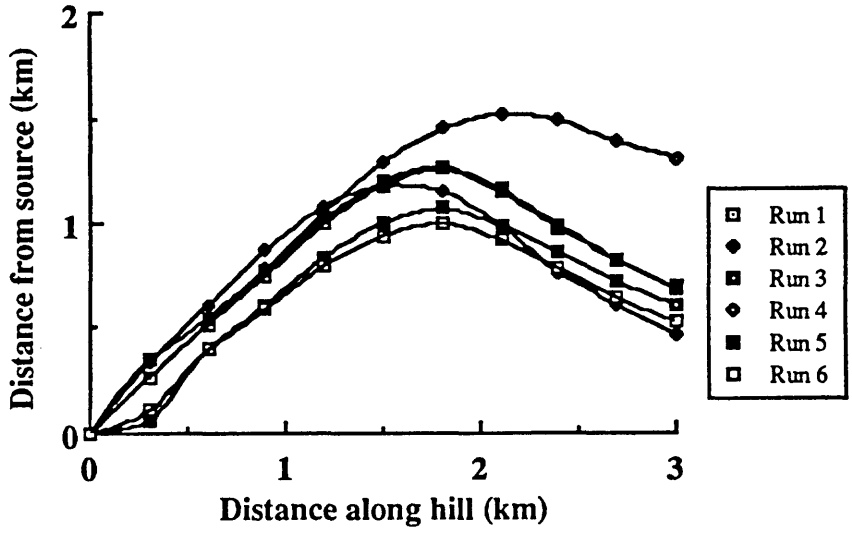


Figure 6.5 Downwind distances at which the 500mSv inhalation of ground gamma ERL is exceeded for UK8 release and deposition in orographic precipitation

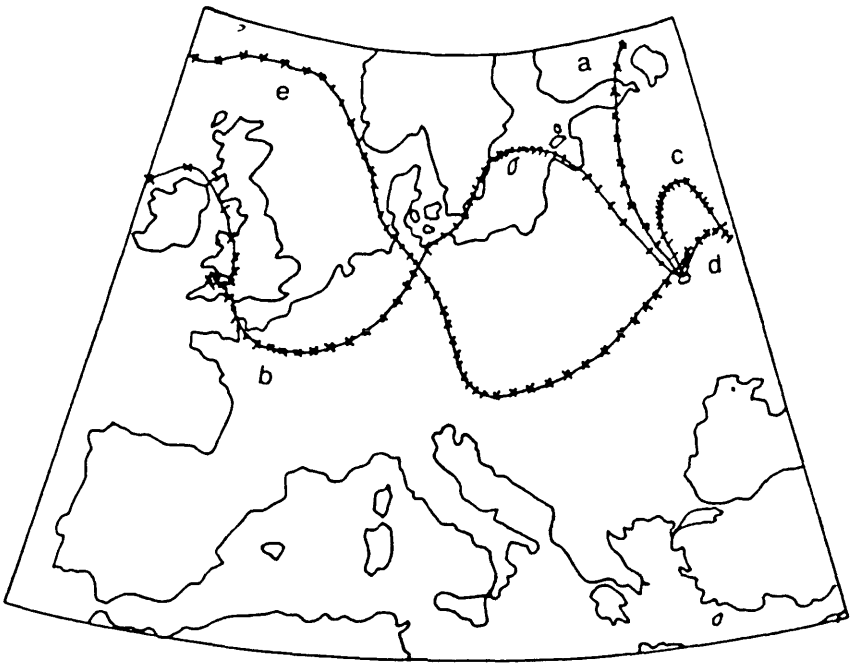


Figure 6.6 Specimen trajectories originating from Chernobyl;
(a) at 12.00h GMT, 25 April 1986
(b) at 12.00h GMT, 26 April 1986
(c) at 12.00h GMT, 27 April 1986
(d) at 12.00h GMT, 28 April 1986
(e) at 12.00h GMT, 29 April 1986
(from ApSimon et al, 1987)

hours duration may follow roughly a single trajectory. Therefore the whole of the UK1 release may come to affect an area many hundreds or even thousands of kilometres downwind.

UK8 releases very small ammounts of Cs ammounting to only 5.10^{-6} of the total inventory (see tables (2.1) and (2.2)). Therefore the alongwind distances at which the 500mSv ground gamma ERL are exceeded are very much smaller than for UK1. They are shown in figures(6.5) for the six orographic cases and they average about 1 km. Whereas in the absence of wet deposition this ERL is not exceeded at all, evacuation may be necessary outside the perimeter fence if the release were to feed immediately into an orographic precipitation system.

6.2.2.2 Magnox and PWR design basis accidents

Two emergency reference levels are chosen to categorise these less severe accidents. They are the 5mSv restriction of milk ERL and the 5mSv ground gamma ERL at which ICRP recommends that consideration should be given to sheltering. Downwind distances up to which the first of these ERLs is exceeded are shown in figures(6.7) and (6.8) for 100% of iodine in hygroscopic particulate form. The ERL is exceeded up to between 2 and 7 km from the PWR accident with 100% particulate and between 1 and 3 km with 25% particulate. These compare with a distance of 540m in the absence of precipitation. For the Magnox accident the distances are greater being between 10 and 40 km and 5 and 20 km for the 100 and 25 % particulate cases respectively. With dry deposition only, the corresponding distance is 3km. The distances out to which the 5mSv ground gamma ERL would be exceeded are shown in figures(6.9) and (6.10) for the two accidents. In the absence of precipitation this ERL is nowhere exceeded(see table(2.13)). The effect of orographic precipitation is to cause the ERL to be exceeded up to 5km from the PWR accident and up to 18km for the Magnox

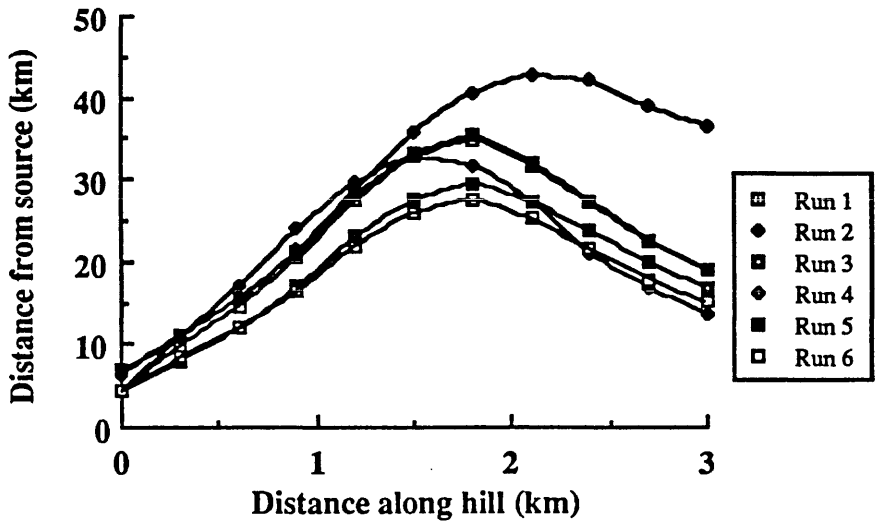


Figure 6.7 Downwind distances at which the 5mSv ingestion of milk ERL is exceeded for Magnox single channel melt and depressurisation accident and orographic deposition

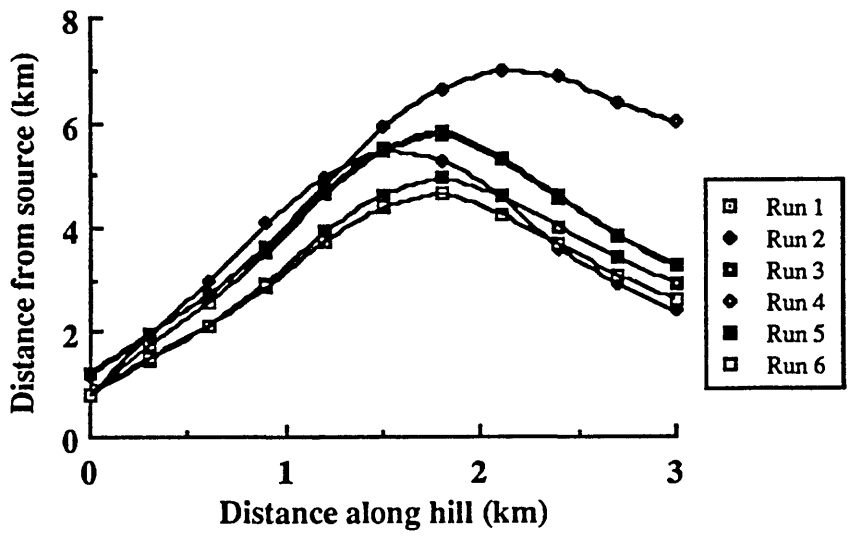


Figure 6.8 Downwind distances at which the 5mSv ingestion of milk ERL is exceeded for PWR design basis accident and orographic deposition

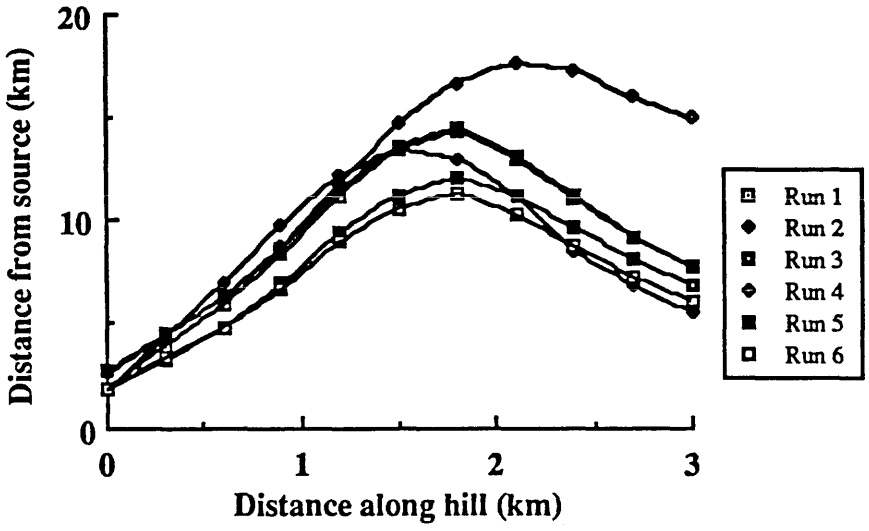


Figure 6.9 Downwind distances at which the 5mSv inhalation of ground gamma ERL is exceeded for Magnox single channel melt and depressurisation accident and orographic deposition

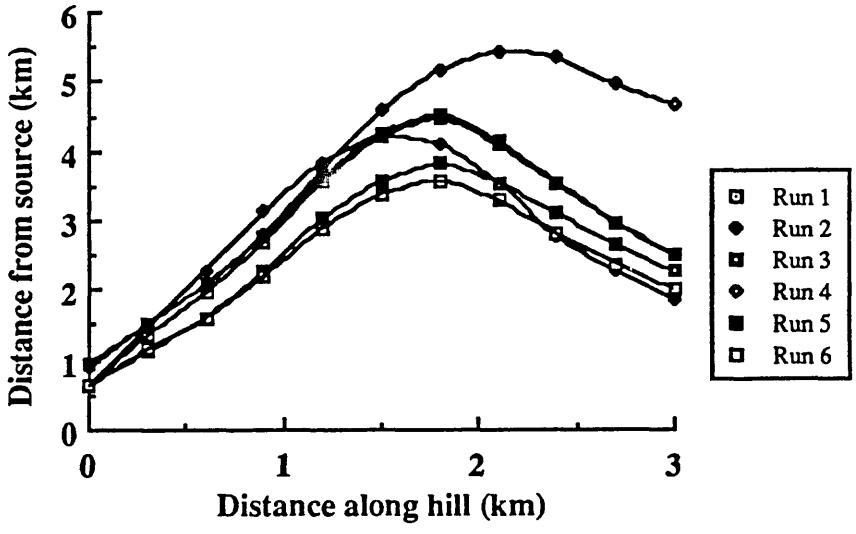


Figure 6.10 Downwind distancves at which the 5mSv inhalation of ground gamma ERL is exceeded for PWR design basis accident and orographic deposition

accident.

Once again, deposition in precipitation is relatively more significant for caesium than for iodine. Not only does the higher deposition velocity of iodine mean that it is dry deposited more than caesium but also the caesium is depleted less making more available for wet deposition further away from the source. Thus, although there is an order of magnitude less caesium released than iodine in both accidents, the 5mSv inhalation of ground gamma ERL is exceeded up to the distances exceeded by the 5mSv ingestion of milk ERL.

6.2.2.3 Chernobyl

In the aftermath of the Chernobyl accident, orographically enhanced precipitation was of particular importance to upland areas in Northern England and Wales. In this section the orographic model is used to calculate the likely range of values of depositions on high ground, so as to compare with measured values.

The contaminated precipitation fell on the weekend of the 3rd and 4th of May. It was associated with a frontal system that moved in a North-Easterly direction across Britain and whose passage is shown in figure(6.11). Rainfall accumulations estimated by Monk and Jonas(1986) for the period during which the cloud of radionuclides was passing over Britain are shown in figure(6.12). In Cumbria they are between 10 and 20 mm. Air concentrations of ^{137}Cs in air were typically 1 Bq/m^3. Assuming that this is the average air concentration feeding into the seeder-feeder system the deposition rate can be calculated for the six orographic runs discussed above. The total depositions can be calculated by integrating the deposition rate over the time required to produce the measured accumulations of

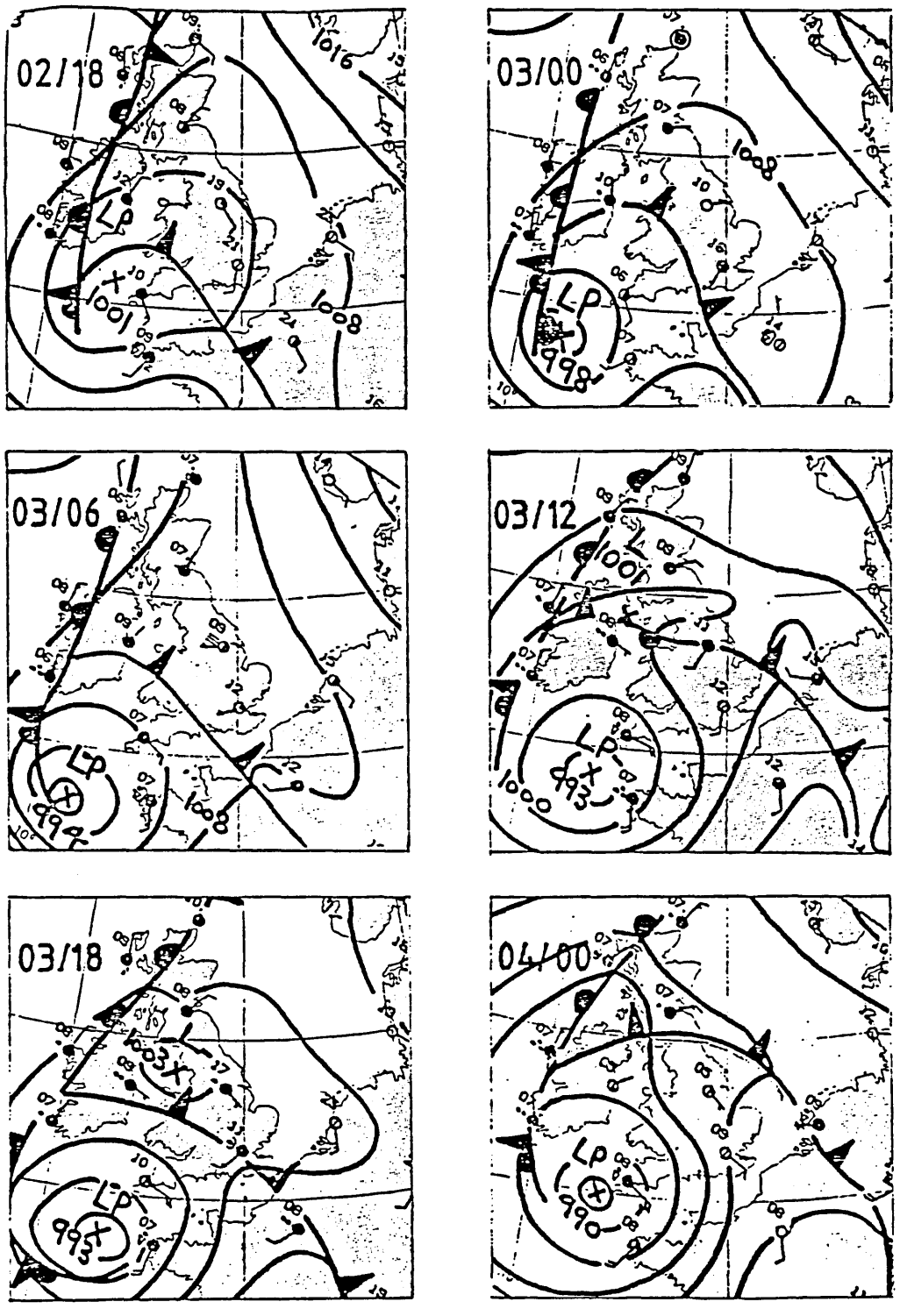


Figure 6.11 Sequence of surface analyses at 6h intervals showing frontal positions and isobars (4mb spacing) between 18 GMT 2 May and 00 GMT 4 May (from Monk and Jonas, 1986)



Figure 6.12 Rainfall accumulations (mm) during the passage of the Chernobyl cloud (from Monk and Jonas, 1986)

precipitation. Since the peak precipitation rates for the orographic cloud runs are about 2 mm/hr and the minimum rates are at 1 mm/hr, integration times of 10 and 5 hours were chosen. These represent peak accumulations of 20 and 10 mm respectively. The patterns of total deposition are shown in figure(6.13). Peak depositions range from 6 to 26 kBq/m^2. Values averaged over the hill range from 4 to 14 kBq/m^2. At the edge of the cloud, where there is washout only, depositions are 0.34 and 0.68 kBq/m^2. Observed values over Cumbria, as reported by Monk and Jonas(1986), were generally between 0.25 and 4 kBq/m^2 with peak values of 19 kBq/m^2. Thus the higher values can be explained by the orographic enhancement of deposition due to the seeder-feeder mechanism. Washout only would produce depositions of the order of 1 kBq/m^2. Therefore the patchy nature of deposition in Cumbria and its high measured values in small hot spots of contamination can be explained by the seeder-feeder mechanism producing enhanced levels of deposition on locally affected hillsides. Where hill clouds are not found and radionuclides are scavenged by precipitation falling from high level stratus, levels of deposition may be an order of magnitude lower.

6.3 Frontal precipitation

6.3.1 Discussion : observation and modelling

Frontal precipitation is the most common type of precipitation found in Northern Europe and Scandinavia. It is caused primarily by the ascent of warm conveyor belts of moist air that ascend ahead and roughly parallel to the cold front. Two archetypal models have been proposed by Browning(1983) to categorise the behaviour of the warm conveyor belt. If the conveyor belt has a component of flow towards the cold front it is termed rearward sloping. More commonly it moves away from the front and is termed forward sloping. Line convection which was

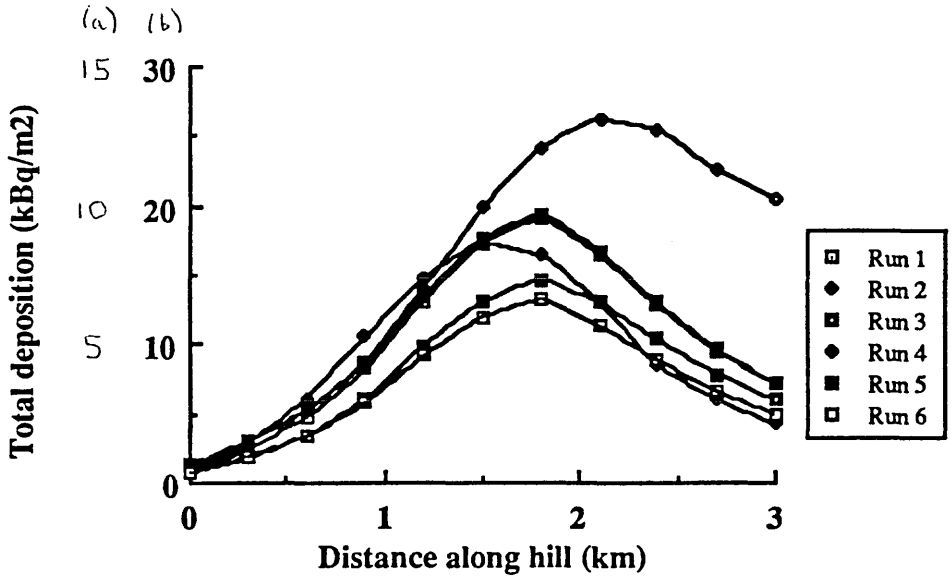


Figure 6.13 Predicted deposition from Chernobyl in orographic precipitation corresponding to peak accumulations of precipitation of (a) 10 mm and (b) 20 mm

modelled in chapter 5 is associated with rearward sloping ascent and occurs where the conveyor belt meets the frontal surface and rises sharply. Although it is not particularly common, it is an important phenomenon to study in the context of consequence assessment since a powerful concentration mechanism is operative. Large volumes of boundary layer are drawn into the system and intense rain is produced in a sharp band. Pollution in the incoming air may be deposited on a relatively small area with high efficiency. Once the air in the warm conveyor belt has left the area of line convection it continues to rise but at a much smaller updraught velocity, typically several tens of centimetres per second. This produces a much larger region of lighter precipitation. Again pollutant would be scavenged principally by rainout processes.

Forward sloping ascent may transport pollution many thousands of kilometres. Typically the warm conveyor belt ascends gradually until it reaches the surface warm front where it turns anticyclonically and overrides cold air ahead of the front. A schematic diagram of forward sloping ascent is shown in figure(6.14). The warm conveyor belt ascends gradually until it reaches the surface cold front where it turns anticyclonically and overrides flow of cold air ahead of the front. A flow of cold dry air rides over the warm conveyor belt leading to the generation of potential instability. Convective precipitation usually results and this often occurs at a sharply defined upper cold front. This is shown in figure(6.15) together with the overall precipitation distribution.

In chapter 5, line convection was modelled and this is discussed in detail in this section. Unlike the orographic system, the cold frontal system will move relative to the ground. All the calculations made so far have been made in the reference frame of the system. In order to calculate the deposition at the ground, the deposition from the line convection must be

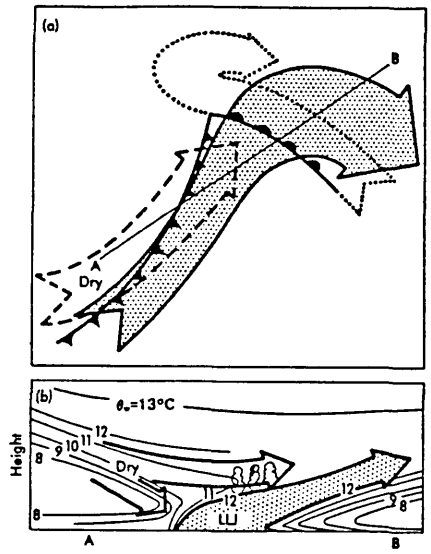


Figure 6.14 Schematic portrayal of airflow in a mid-latitude cyclone in which the warm conveyor belt is undergoing forward sloping ascent (from Browning, 1985)

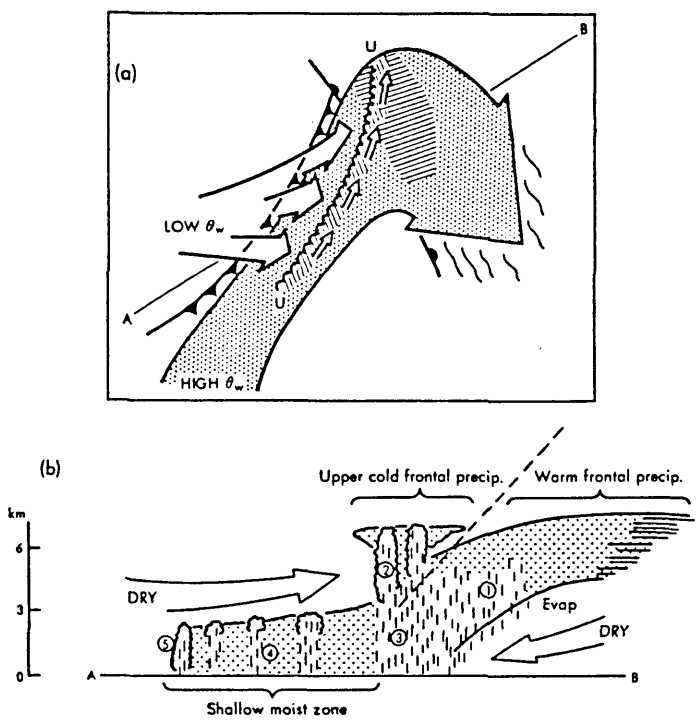


Figure 6.15 Schematic portrayal of the same situation as figure(6.14) with the warm conveyor belt undergoing forward sloping ascent but drawing attention to the split front characteristic and the overall precipitation distribution (from Browning, 1985)

smeared out over the ground as the front moves over it. Let v be the velocity of the system which is assumed constant. The total deposition at a point x on the ground as the frontal system moves over it can be calculated by imagining that the point moves relative to a stationery system with velocity -v (see figure(6.16)).

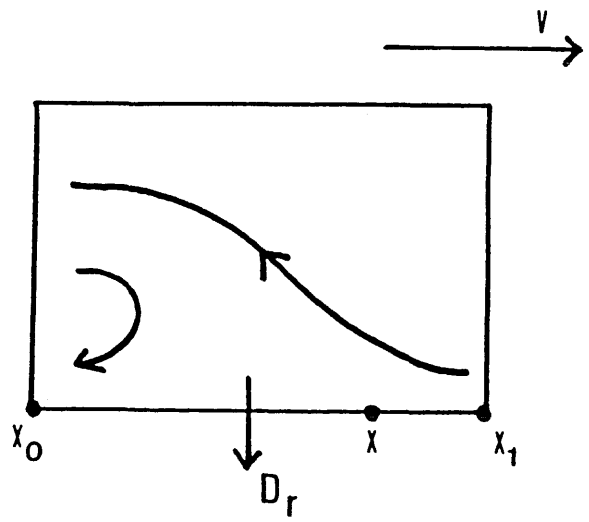


Figure 6.16 Schematic portrayal of calculation of deposition at the ground beneath moving system

Then

$$x = x_1 - v\,t. \tag{6.1}$$

The total deposition D_t is given by

$$D_t = \int_{t_0}^{t_1} dt\, D_r\,(x_1 - v\,t) \tag{6.2}$$

where t_0 is the time the system the system arrives above point x and t_1 is the time the system leaves.

Since $t = (x_1 - x)/v$, $dt = -(dx/v)$ and

$$D_t = -\int_{x_1}^{x_0} \frac{dx}{v} D_r(x)$$

$$= \frac{1}{v}\int_{x_0}^{x_1} dx\, D_r(x) \qquad (6.3)$$

since v is a constant.

The alongwind distances out to which emergency reference levels would be exceeded are calculated in a similar manner as for the orographic case. The essential difference is that the system is above a point on the ground only for time

$$T = L/v$$

where L is its length. Therefore if T_d is the duration of the release, at most only the fraction T / T_d of the release may process through the system to be deposited on one place on the ground. Therefore alongwind distances are calculated by increasing the reference level air concentrations by this ammount. The deposition rate used is the average along the length of the model domain, i.e.

$$\frac{1}{L}\int_{x_0}^{x_1} dx\, D_r(x) \qquad (6.4)$$

When integrated over time T this gives a total deposition of

$$\frac{T}{L}\int_{x_0}^{x_1} dx\, D_r(x)$$

$$= \frac{1}{v} \int_{x_0}^{x_1} dx \; D_r(x)$$

which is the same as (6.3) as required.

The width of the model domain used in the simulation in section(5.3) was 3km. This is a fairly typical value for the width of line convection(see table(6.2)). The velocity of the rearward sloping cold front analysed in detail

Table 6.2 Characteristics of six sharp surface cold fronts (from Browning, 1983)

	Case (a)	(b)	(c)	(d)	(e)	(f)
Velocity of front normal to its length ($m\ s^{-1}$)	5	8	11	19	11	10
Maximum wind speed within low level jet just ahead of front ($m\ s^{-1}$)	27	31	26	26	35	34
Decrease in wind speed above low level jet maximum ($m\ s^{-1}$)	9	7	9	>2	8	10
Height of low level jet maximum (km)	0.8	1.0	1.0	1.6	0.8	0.6
Wind speed at height of 1 km behind front ($m\ s^{-1}$)	-	9	6	16	9	9
Vector wind change across line convection ($m\ s^{-1}$)	19	14	15	13	12	12
Width of line convection (km)	2	2	2	4	2	3
Change in θ_w across front (^{o}C)	6	5	3	3	3	3
Change in 1000–700 mb thickness across front (m)	23	15	18	20	12	11
Maximum pressure kick at front (mb)	1.2	1.9	0.8	1.7	1.6	0.8
Depth of line convection (km)	2.5	2.8	2.5	>2.5	>2.8	2.4

by Browning and Harold(1970) was 12 m/s and the front that affected the Chernobyl release travelled across Southern Britain with a speed of 5 m/s (Monk and Jonas, 1987). In these calculations three values have been chosen to represent the range of frontal velocities; they are 5, 10 and 15 m/s. A three kilometre width implies that these give above ground durations of 600, 300 and 200 seconds respectively.

6.3.2 Results

6.3.2.1 Serious PWR accidents

UK1 and UK8 were chosen to represent the range of severe PWR accidents. Calculations of alongwind distances out to which the 5mSv milk ERL and the 500mSv ground gamma ERL would be exceeded have been made for six sets of cloud model parameters which are given in table(5.5). Cloud model results for these parameter sets were discussed in section(5.4.3). Results are given in tables(6.3) to (6.5) for UK1 and in tables (6.6) to (6.8) for UK8. From table(6.3) it can be seen that alongwind distances for the 5mSv iodine ERL assuming that 100% of the iodine is in particulate form are increased only where the pollutant material is in the updraught flow. Values vary considerably with the frontal velocity and have a minimum of 1355km and a maximum of 2053km. For a particular velocity there is considerably less variation. The smallest distance is for run 2 which has smaller updraught velocities and a smaller influx of air than the other three,runs 4, 5 and 6. The variation of dynamic parameters is seen to be more important than the variation of microphysical parameters. Run 5 with a smaller nucleation efficiency gives the lowest distance of the three but it is only about 100km less than the other two and is still 200km more than for run 2. Distances for the two cases where pollutant material is being drawn into the downdraught flow (runs 1 and 3) differ by about 100km. They are smaller than the distance for dry deposition only, 1300 km, indicating that in these cases dry deposition would be the most important deposition mechanism.

Table 6.3 UK1 - distances out to which 5 mSv milk ERL exceeded (100 % iodine in particulate form) (km) - dry depn. only 1300km

Run no.	5 m/s	10 m/s	15 m/s
1	1183	973	855
2	1714	1486	1355
3	1005	804	694
4	2037	1802	1667
5	1923	1691	1556
6	2053	1817	1681

Table 6.4 UK1 - distances out to which 5 mSv milk ERL exceeded (25 % iodine in particulate form) (km) - dry depn. only 1300 km

Run no.	5 m/s	10 m/s	15 m/s
1	755	573	475
2	1244	1031	911
3	601	435	349
4	1550	1327	1199
5	1441	1221	1096
6	1565	1340	1213

Table 6.5 UK1 - distances out to which 500 mSv ground gamma ERL exceeded (km) - dry depn. only 23 km

Run no.	5 m/s	10 m/s	15 m/s
1	67.3	40.9	31.0
2	247.6	125.1	95.4
3	44.6	28.2	21.2
4	654.8	321.5	214.1
5	467.7	229.8	153.4
6	683.6	337.0	223.9

Table 6.6 UK8 - distances out to which 5 mSv milk ERL exceeded (100 % iodine in particulate form) (km) - dry depn. only 260 km

Run no.	5 m/s	10 m/s	15 m/s
1	507	353	277
2	953	754	645
3	375	248	188
4	1245	1031	911
5	1140	931	815
6	1259	1044	924

Table 6.7 UK8 - distances out to which 5 mSv milk ERL exceeded (25 % iodine in particulate form) (km) - dry depn. only 260 km

Run no.	5 m/s	10 m/s	15 m/s
1	223	137	101
2	559	397	314
3	148	96	80
4	814	626	524
5	721	541	445
6	827	637	535

Table 6.8 UK8 - distances out to which 500 mSv ground gamma ERL exceeded (km) dry depn. only 0.00 km

Run no.	5 m/s	10 m/s	15 m/s
1	0.00	0.00	0.00
2	0.57	0.31	0.00
3	0.00	0.00	0.00
4	1.05	0.68	0.51
5	0.85	0.54	0.39
6	1.08	0.70	0.53

When only 25% of the iodine is in particulate form the pattern of results is similar except that all distances are decreased by 400 to 500 km. Consequently they are only greater than 1300km for runs 4, 5 and 6 with smaller frontal speeds.

Alongwind distances for UK8 are greater than that due to dry deposition alone (260 km) for a greater range of parameter values than for UK1. With 100% particulate iodine, distances for four of the six runs where pollution is in the downdraught flow exceed 260km although none do when only 25% is in particulate form. All other runs exceed 260km for both 100% and 25% particulate material. At shorter distances from the source of a release the dispersed material is less depleted by dry deposition and hence more is available to process through a storm system. Thus for emergency reference levels that are exceeded at shorter distances, wet deposition is likely to be more important, whereas dry deposition becomes more significant for those ERLs that are exceeded at longer distances.

As for orographic precipitation, there is potentially a large increase in alongwind distances at which the 500mSv ground gamma erl is exceeded for UK1. The values given in table(6.5) change relatively much more than for the 5mSv milk ERL, going up from 21.2km to 683.6km. Even at a particular velocity there is almost a trebling of distances for the rainout runs, e.g. at 5m/s from 247.6km to 683.6km. Because there is a smaller deposition velocity (vg = 10^{-3} m/s) alongwind concentrations change much more slowly (see table(6.1)). Consequently there is an enhanced sensitivity to changes in reference level inflow concentrations.

The 500mSv ground gamma ERL is exceeded at very small distances for UK8 as expected for an accident which releases very little Cs. From table(6.8) it can be seen that for all the downdraught cases the reference

level concentration is not reached at all and for updraught cases the maximum distance is just over 1km. Therefore this ERL may be exceeded just outside the perimeter fence in some circumstances.

6.3.2.2 Magnox and PWR design basis accidents

Tables(6.9) to (6.12) show that for both accidents the distances out to which the 5mSv milk erl would be exceeded are greater due to wet deposition from line convection than from dry deposition alone providing that the pollutant is drawn into the updraught flow. The maximum distance attained for the PWR accident is 3.3km and for the Magnox accident is 18.9 km which represent significant increases over the distances for dry deposition of 0.54 and 3.1 km respectively. Distances are shown in tables (6.13) and (6.14) for the 5mSv ground gamma ERL which is nowhere exceeded in the absence of precipitation for either accident. With pollution from the PWR accident drawn into the downdraught flow, the distances are not significant but if the source is the Magnox accident the ERL may be exceeded up to more than a kilometre away. When the pollution is drawn into the updraught flow distances are considerably greater, being up to 2.5 km for the PWR accident and 7.8 km for the Magnox accident.

6.3.2.3 Chernobyl

Contaminated frontal precipitation fell on Sweden on the 28th and 29th April, 1986. Measurements of cumulative precipitation quantities and total ^{137}Cs depositions (figures (2.3) and (2.4)) show a good correlation indicating that a large part of the total Cs deposition in Sweden was deposited in this frontal precipitation. The concentrations of Cs in precipitation calculated from these two figures average about 2 to 3 kBq/l. In section 2.3.3 it was possible to reach good agreement with these concentrations by modelling dispersion of material released at a suitable rate from Chernobyl by a Gaussian plume and its deposition in appropriate quantities of

Table 6.9 Magnox - distances out to which 5 mSv milk ERL exceeded (100 % iodine in particulate form) (km) - dry depn. only 3.1 km

Run no.	5 m/s	10 m/s	15 m/s
1	3.8	2.5	2.0
2	10.2	6.7	5.3
3	2.7	1.8	1.4
4	18.4	12.0	9.3
5	14.9	9.8	7.6
6	18.9	12.3	9.6

Table 6.10 Magnox - distances out to which 5 mSv milk ERL exceeded (25 % iodine in particulate form) (km) - dry depn. only 3.1 km

Run no.	5 m/s	10 m/s	15 m/s
1	1.7	1.1	0.9
2	4.4	3.0	2.3
3	1.2	0.8	0.6
4	7.9	5.2	4.1
5	6.4	4.3	3.4
6	8.1	5.3	4.2

Table 6.11 PWR design basis - distances out to which 5 mSv milk ERL exceeded (100% iodine in particulate form) (km) - dry depn. only 0.54 km

Run no.	5 m/s	10 m/s	15 m/s
1	0.69	0.43	0.28
2	1.85	1.24	0.97
3	0.46	0.00	0.00
4	3.23	2.16	1.71
5	2.66	1.78	1.40
6	3.31	2.22	1.75

Table 6.12 PWR design basis - distances out to which 5 mSv milk ERL exceeded (25 % iodine in particulate form) (km)

Run no.	5 m/s	10 m/s	15 m/s
1	0.00	0.00	0.00
2	0.82	0.52	0.38
3	0.00	0.00	0.00
4	1.44	0.96	0.75
5	1.19	0.78	0.60
6	1.48	0.98	0.77

Table 6.13 Magnox - distances out to which 5 mSv ground gamma ERL exceeded(km) - dry depn. only 0.0 km

Run no.	5 m/s	10 m/s	15 m/s
1	1.6	1.0	0.8
2	4.2	2.8	2.2
3	1.1	0.7	0.6
4	7.6	4.9	3.9
5	6.2	4.0	3.2
6	7.8	5.1	4.0

Table 6.14 PWR design basis - distances out to which 5 mSv ground gamma ERL exceeded (km) - dry depn. only 0.0 km

Run no.	5 m/s	10 m/s	15 m/s
1	0.49	0.00	0.00
2	1.40	0.92	0.71
3	0.28	0.00	0.00
4	2.47	1.63	1.28
5	2.02	1.34	1.05
6	2.53	1.68	1.32

precipitation by the washout model.

However, measurements reported by Persson et al(1987) indicate that although concentrations of Cs in precipitation were about 2 to 3 kBq/l over a large part of the country, they exceeded 8 to 16 kBq/l in a small region in Eastern Sweden (see figure(6.17)). Calculations have been made to see whether the cold frontal model can produce such enhanced concentrations. Concentrations in rain at the ground have been calculated for the six model runs assuming a unit influx and have been averaged over the width of the system. The results have then been normalised so that concentrations in rain falling when pollution is washed from the downdraught flow are between 2 and 3 kBq/l. They are shown in table(6.15). Enhancements are between 5 and 8 times for circulation 2 (runs 4, 5, 6) and about 4 times for circulation 1 (run 2). The results show that concentrations in excess of 16kBq/l are achievable where pollution feeds into the updraught flow and is deposited in rain as a result of rainout processes.

Table 6.15 Predicted ^{137}Cs concentration in cold frontal precipitation in Eastern Sweden

Run no.	Concn in rain (kBq/l)	
1	2.0	3.0
2	7.9	11.9
3	2.2	3.3
4	15.0	22.5
5	10.6	15.9
6	15.6	23.4

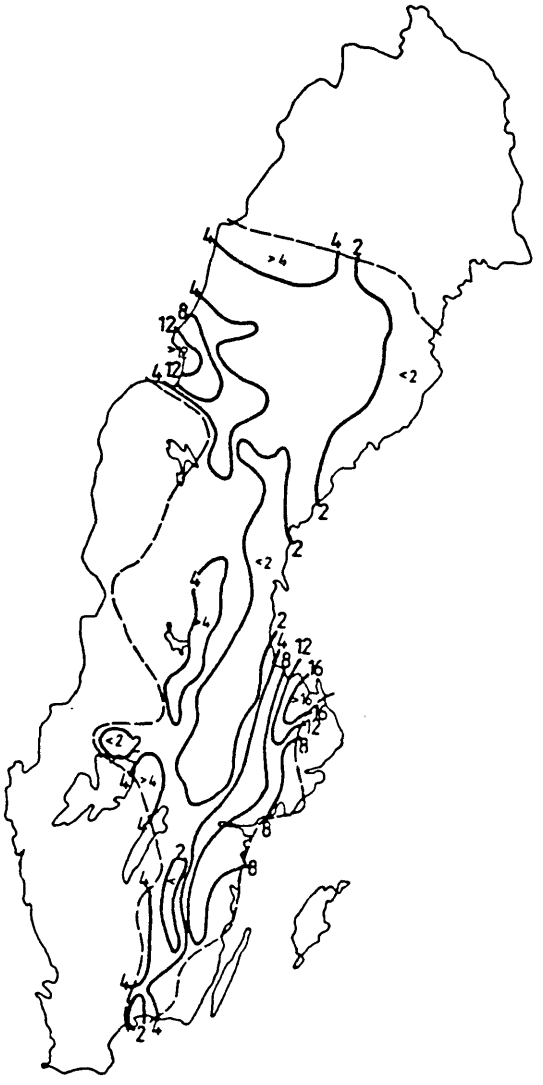


Figure 6.17 Concentration of ^{137}Cs in precipitation (kBq/l) during the period April 28-30 (from Persson et al, 1987)

6.4 Convective precipitation

6.4.1 Discussion : observation and modelling

Convective precipitation was discussed in section(5.5) and long lived convective storms were modelled in two dimensions. In this section calculations of consequences resulting from radioactivity processing through convective storms are made in the same manner as for line convection. Four convective storms studied by Ludlam(1980) moved with velocities between 8 and 18 m/s and the same three system velocities are used as in the previous section, 5, 10 and 15 m/s, to represent this range.

In the days following the accident at Chernobyl, satellite pictures showed many areas where there was likely to have been convective precipitation.They are easy to spot since convective clouds show up clearly as white circular blobs. Short lived convective showers were modelled in chapters 3 and 4 and in section(5.5.2) a calculation was made of the possible concentration factors operative in such systems. This calculation and the results from 2D convective storm modelling are used to estimate the possible depositions that may have been experienced following Chernobyl in localised hot spots of contamination.

6.4.2 Results

6.4.2.1 Serious PWR accidents

The same emergency reference levels and accidents are considered here as in section(6.3). Six cloud model runs are used and their parameters are given in table(5.6). Runs 1 and 2 are for a 9km updraught height and 10 m/s maximum updraught speed and runs 3 to 6 are for a 10km updraught height and 18 m/s maximum updraught speed. Peak precipitation rates are 30 and 110 mm/hr respectively. Results are shown in tables (6.16) to (6.21). Particulate material feeds into the updraught flow in runs 1,3,5 and

6 and into the downdraught flow in the other two runs; hence the distances out to which emergency reference levels are exceeded are generally larger for the former runs than for the latter. Overall, distances are considerably higher than for line convection. This is not surprising since precipitation rates are much higher and larger volumes of air are being processed by convective storm systems. Results for 5mSv milk erl for UK1 and UK8 are shown in tables (6.16),(6,17),(6,19) and (6.20). The UK1 results for the updraught flow runs are roughly the same as for the orographic cases but the UK8 results are much larger. Whereas all the release is assumed to affect deposition in orographic precipitation, only the fraction that is able to process through the storm system and affect a stationery point on the ground is considered here. Since the UK1 accident has a three hour duration and the UK8 accident lasts only half an hour, a larger fraction of the latter release may be processed than the former. For material feeding into the updraught flow, dynamics is seen to be more important than microphysics. With the larger updraught and inflow velocities and higher precipitation quantities of runs 3,5 and 6, distances for UK1 go up to 3000km compared to 2400 for run 1. Variation of microphysical parameters yields a variation in the distance of only 100km.

As with orographic precipitation there are immense increases in the distances from a UK1 accident at which the 500mSv ERL is exceeded when the release is affected by precipitation. Distances are as high as 4000km compared to 23km for dry deposition only. As discussed earlier this is due to the low dry deposition velocity of Cs and the correspondingly slow depletion of the plume. Although a Gaussian plume has little applicability out to such long distances, such a calculation does demonstrate how dramatically precipitation may increase the severity of consequences of Cs deposition for such a major accident as UK1. The same ERL may be exceeded up to 5km from a UK8 accident.

Table 6.16 UK1 - distances out to which 5 mSv milk ERL exceeded (100 % iodine in particulate form) (km) - dry depn. only 1300 km

Run no.	5 m/s	10 m/s	15 m/s
1	2392	2151	2012
2	2037	1802	1667
3	2955	2707	2564
4	2209	1971	1834
5	2971	2723	2580
6	2867	2621	2477

Table 6.17 UK1 - distances out to which 5 mSv milk ERL exceeded (25 % iodine in particulate form) (km)

Run no.	5 m/s	10 m/s	15 m/s
1	1904	1671	1538
2	1562	1338	1210
3	2452	2211	2071
4	1727	1498	1368
5	2468	2226	2087
6	2366	2126	1987

Table 6.18 UK1 - distances out to which 500 mSv ground gamma ERL exceeded (km) - dry depn. only 23 km

Run no.	5 m/s	10 m/s	15 m/s
1	1658	918	626
2	673	336	226
3	4547	3095	2379
4	1070	557	370
5	4651	3182	2454
6	4002	2649	1997

Table 6.19 UK8 - distances out to which 5 mSv milk ERL exceeded (100 % iodine in particulate form) (km) - dry depn. only 260 km

Run no.	5 m/s	10 m/s	15 m/s
1	1552	1361	1232
2	1223	1042	921
3	2087	1886	1749
4	1381	1195	1071
5	2102	1902	1765
6	2003	1803	1667

Table 6.20 UK8 - distances out to which 5 mSv milk ERL exceeded (25 % iodine in particulate form) (km)

Run no.	5 m/s	10 m/s	15 m/s
1	1110	934	817
2	808	648	545
3	1618	1426	1296
4	953	783	673
5	1633	1441	1311
6	1538	1347	1219

Table 6.21 UK8 - distances out to which 500 mSv ground gamma ERL exceeded (km) - dry depn. only 0.0 km

Run no.	5 m/s	10 m/s	15 m/s
1	1.82	1.28	1.00
2	0.98	0.68	0.51
3	4.76	3.33	2.61
4	1.33	0.93	0.72
5	4.89	3.42	2.68
6	4.09	2.87	2.25

6.4.2.2 Magnox and PWR design basis accidents

Distances out to which the 5mSv milk ERL and the 5mSv ground gamma ERL are exceeded for the two accidents are shown in tables(6.22) to (6.27). They are considerably higher than for the cold frontal circulation. The PWR accident has maxima of 16km for the milk ERL and 12km for the ground gamma ERL and the Magnox accident has maxima of 99km for the milk and 44km for the ground gamma ERLs.

6.4.2.3 Chernobyl

One story that was reported in the first few days following the initial release from Chernobyl was of the evacuation of children from Gomel, 140 km away following a convective storm there. Calculations are made to show how the concentration of radionuclides in a storm's core and their efficient deposition in precipitation might have led to such an action being necessary.

A Gaussian plume calculation indicates that the ground level concentration at 100km from a unit release rate is $5.7.10^{-9}$ Bq/m^3. The release of ^{137}Cs from Chernobyl over the first 2 days is taken to be 5.10^{16}Bq which gives a release rate of $2.9.10^{+11}$ Bq/s. Therefore the ground level concentration at 100 km is 1650 Bq/m^3. The total deposition at a stationery point on the ground from a convective storm as it moves overhead can be calculated from

$$D_t = 1650\, D_r\, T \qquad (6.5)$$

where D_r is the deposition rate beneath the storm for a unit concentration feeding into it and T is the total time the storm is overhead. This has been calculated for the six storm runs and three storm velocities used earlier

Table 6.22 Magnox - distances out to which 5 mSv milk ERL exceeded (100 % iodine in particulate form) (km) - dry depn. only 3.1 km

Run no.	5 m/s	10 m/s	15 m/s
1	35.7	23.0	17.8
2	18.7	12.1	9.5
3	99.1	63.5	48.9
4	25.6	16.5	12.9
5	99.4	65.4	50.3
6	85.2	54.1	41.7

Table 6.23 Magnox - distances out to which 5 mSv milk ERL exceeded (25 % iodine in particulate form) (km)

Run no.	5 m/s	10 m/s	15 m/s
1	14.9	9.7	7.6
2	8.0	5.3	4.2
3	40.6	26.1	20.2
4	10.8	7.1	5.6
5	41.8	26.9	20.8
6	34.7	22.4	17.4

Table 6.24 PWR design basis - distances out to which 5 mSv milk ERL exceeded (100% iodine in particulate form) (km) - dry depn. only 0.54 km

Run no.	5 m/s	10 m/s	15 m/s
1	5.90	3.92	3.09
2	3.23	2.16	1.71
3	15.49	10.11	7.91
4	4.33	2.89	2.28
5	15.93	10.39	8.13
6	13.30	8.71	6.82

Table 6.25 PWR design basis - distances out to which 5 mSv milk ERL exceeded (25 % iodine in particulate form) (km)

Run no.	5 m/s	10 m/s	15 m/s
1	2.6	1.8	1.4
2	1.4	1.0	0.8
3	6.7	4.4	3.5
4	1.9	1.3	1.0
5	6.8	4.5	3.6
6	5.8	3.8	3.0

Table 6.26 Magnox - distances out to which 5 mSv ground gamma ERL exceeded(km) - dry depn. only 0.0 km

Run no.	5 m/s	10 m/s	15 m/s
1	14.6	9.3	7.2
2	7.6	4.9	3.9
3	42.9	26.5	20.2
4	10.4	6.7	5.2
5	44.3	27.3	20.8
6	36.1	22.4	17.1

Table 6.27 PWR design basis - distances out to which 5 mSv ground gamma ERL exceeded (km) - dry depn. only 0.0 km

Run no.	5 m/s	10 m/s	15 m/s
1	4.6	3.0	2.4
2	2.5	1.6	1.3
3	12.3	7.9	6.2
4	3.3	2.2	1.7
5	12.7	8.2	6.3
6	10.5	6.8	5.3

Table 6.28 Predicted deposition and ground gamma dose beneath convective storm at 100km from Chernobyl

Run no.	5 m/s Depn. (Bq/m^2)	Dose (mSv)	10 m/s Depn. (Bq/m^2)	Dose (mSv)	15 m/s Depn. (Bq/m^2)	Dose (mSv)
1	$2.1x10^6$	21	$1.1x10^6$	11	$7.0x10^5$	7
2	$7.6x10^5$	8	$3.8x10^5$	4	$2.5x10^5$	3
3	$1.0x10^7$	100	$5.0x10^6$	50	$3.3x10^6$	33
4	$1.2x10^6$	12	$6.0x10^5$	6	$4.0x10^5$	4
5	$1.1x10^7$	110	$5.6x10^6$	56	$3.7x10^6$	37
6	$7.9x10^6$	79	$4.0x10^6$	40	$2.6x10^6$	26

and results are shown in table(6.28). Dose commitments which have been derived from the dose equivalent for ^{137}Cs due to inhalation of ground gamma radiation of 10^{-8} Sv/Bqm^{-2} are also given. Total dose commitments for runs where material is in the updraught flow vary from 7 to 110 mSv. 500mSv is the level at which ICRP recommends that evacuation should have begun and 1/5 of this is the level at which it should be considered. Therefore total dose commitments from depositions resulting from these storms would certainly cause concern and evacuation of the more vulnerable younger members of the community would seem justified.

In section(5.5.1) a calculation was made of the concentration factors operative in convective shower circulations. Deposition was calculated from (5.49),

$$D_s = Q\varepsilon / \pi l^2$$

where Q is the total quantity of material processed by the shower. This was compared with deposition due to washout spread out over the volume of boundary layer that would get sucked through the system. This value was

given by (5.55) from which

$$V = 2 L T v_k 1.208$$
$$= 1.2.10^{12} m^3.$$

The total activity in volume V is

$$Q = C V$$
$$= 1.98.10^{15} Bq.$$

However in time T = 2000s only $5.8.10^{14}$ Bq of ^{137}Cs are released and therefore only this quantity is allowed to process through the storm. Then

$$D_s = 5.8.10^{14}\ 0.4\ /\ (\ \pi\ (5.10^3)^2\ )$$
$$= 3.0.10^6\ Bq/m^2$$

which is equivalent to a dose of 30 mSv. On the other hand the same ammount of precipitation smeared out over the whole area of boundary layer would (from (5.51)) give a deposition of

$$D_w = \frac{5.8.10^{14}}{1.2.10^9}\ (\ 1 - e^{-5.10^{-5}\ 2\ 2000}\ )$$
$$= 8.8.10^4\ Bq/m^2,$$

about 30 times lower. If a precipitation rate of 25 mm/hr fell through the boundary layer washing out pollutant material, the deposition would be

$$D_w = \frac{5.8.10^{14}}{1.2.10^9}\ (\ 1 - e^{-5.10^{-5}\ 25\ 2000}\ )$$
$$= 4.4.10^5\ Bq/m^2$$

equivalent to 4m/sv. On average, depositions from the shower are about ten times higher and only with these concentration factors can dose levels be reached that might trigger evacuation procedures. The dry deposition received during the up to 2000 seconds a convective storm or shower might be passing overhead ammounts to

$$2.0.10^{11}\ 2000\ 5.7.10^{-12} = 3.3.10^{3}\ Bq/m^2$$

which would give a ground gamma dose of 0.03mSv. Over two days the total dose is $2.9.10^{5}$ Bq/m^2 or 3mSv but this is still of minor significance compared to a single convective storm.

6.5 Summary and conclusions

The subject of this chapter has been the influence of wet deposition in storm systems on accident consequence analysis. Four hypothetical accidents have been chosen to represent the range of possible release patterns. They are two severe PWR accidents, UK1 and UK8 and two smaller releases, a PWR design basis accident and a Magnox single channel melt and depressurisation accident. The Chernobyl accident has also been studied to see whether some of the observed hot spots of deposition could be accounted for by the storm processes discussed in this thesis. Dispersion of released radionuclides has ben modelled by a Gaussian plume and doses recieved by affected populations have been calculated using the dosimetric models discussed in chapter 2.

The effects of hypothetical accidents have been characterized by calculating the distances out to which emergency reference levels are exceeded when dispersed material is drawn into cloud systems. The severity of the larger of the PWR UK1-8 releases was noted in chapter 2 and this is even more striking when the effects of precipitation are taken into consideration. For instance, orographic precipitation may cause the 5mSv milk emergency reference level to be exceeded up to 3000km from the source. The distances

out to which ground gamma ERLs are exceeded may be increased enormously in certain circumstances. Not only are there large enhancements in deposition due to rainout processes and concentration mechanisms, but air concentrations of Cs with its low dry deposition velocity are depleted very slowly. Therefore if the material travels long distances without encountering precipitation and then becomes involved in a storm system, the consequences could be far more serious than might be expected at those distances. These effects mean that emergency reference levels that are not exceeded at all in the event of design basis accidents (e.g. the 5mSv ground gamma erl) may be exceeded several kilometers from the power station.

Following the Chernobyl accident, localised hot spots of contamination attracted great attention and concern. Three particular problems that arose in various types of precipitation have been investigated. In Northern England and Wales high levels of Cs deposition on hilly terrain can be explained by the seeder-feeder mechanism. This produces orographically enhanced precipitation and an even greater enhancement to wet deposition of hygroscopic particles. Frontal precipitation that fell in a couple of days over much of Sweden produced levels of Cs deposition that were consistent with washout of material dispersed from Chernobyl. However in a small region of Eastern Sweden concentrations in rain water were considerably higher. The cold frontal model has been used to show how rainout processes would lead to such increases in contamination. The models of convective precipitation developed in this thesis have been used to show how evacuation might have been justified up to 100km away from Chernobyl in the days immediately following the accident. This accords with reports of a storm at Gomel which resulted in children being evacuated from the city.

Three types of precipitation have been studied in this chapter. Orographic precipitation has a fairly low intensity of only a few mm/hr. However, hill clouds may persist over one area for many hours and thus large quantities of pollutant may process through the system and be liable to deposition on one patch of ground. Frontal systems move across country at several m/s and therefore the pattern of wet deposition beneath them will be smeared out. Line convection was modelled in chapter 5 as it is two dimensional in nature but there may be as much material deposited in the gently sloping conveyor belt of air behind the surface cold front as there is in the heavy band of precipitation at the front itself. Convective storms draw in much larger fluxes of boundary layer air than the frontal systems modelled. Pollutant material is concentrated within the storm updraught to be deposited on relatively small areas. Of the three types of precipitation modelled, convective storms are capable of producing the most severe effects.

The modelling as it has been applied in this chapter has a number of limitations. The Gaussian plume model is most successful up to 100km from a release although the recommendations of the Atmospheric Dispersion Working Group(Jones,1981) have been employed to simulate dispersion beyond that distance. For longer travel distances, a puff based model such as MESOS(ApSimon et al,1987) is more suitable. Here the motivation has been towards estimating the possible enhancements to wet deposition in storm systems following a nuclear accident, rather than in attempting to predict the deposition at a particular place following a specified release. In the latter case, the limitations of the Gaussian plume,especially beyond 100km from the source, would become most apparent. There are uncertainties also in the dosimetric models and these are discussed in the relevant publications (Charles et al,1982 and Linsley et al,1982). The limitations of the cloud models are discussed in the

concluding chapter, where recommendations for further improvements and enhancements are also made.

7 Summary and recommendations for future work

This thesis has investigated the role that precipitation plays in producing enhanced levels of contamination follwing an accidental release of radioactivity from a nuclear power station accident. Wet deposition of radionuclides is often described by the washout model which was discussed in chapter 2. It was used in conjunction with a Gaussian plume dispersion model to analyse the consequences of hypothetical accidents. The model simulations showed that deposition could be patchy, with hot spots of contamination produced where precipitation had fallen. Areas exceeding emergency reference levels, which are levels of dose commitment above which action such as evacuation or restriction of milk are required, were often considerably increased in the presence of precipitation. Indeed, thresholds for certain emergency responses were only exceeded where contaminated rain fell to ground. Alternatively, in certain circumstances, affected areas were reduced when precipitation depleted the plume of released material early on in its travel which allowed less to travel to greater distances.

The washout model simulates wet deposition by assuming that initially clean raindrops fall through regions of polluted air, scavenging pollutants as they go. In fact, precipitation is the end result of a complex series of microphysical and dynamic processes that operate in cloud systems. The microphysical processes in warm cloud ($> 0^{o}$ C) were modelled within the framework of a one-dimensional updraught in chapter 3. Scavenging of aerosol pollutants was incorporated and the principle mechansisms of impaction and nucleation were parametrised. The most important model parameter was shown to be updraught velocity. For small updraught velocities very little rain was produced and hence small quantities of aerosol were rained out, whereas for very large velocities most aerosols

were exported to higher layers of the atmosphere before they could be deposited in rain. The cloud was most efficient at scavenging aerosols for intermediate updraught velocities.

Iodine may be released in both gaseous and particulate form and the chemistry of gaseous scavenging was discussed in chapter 4. Model results showed that iodine was not deposited readily in rain unless it oxidised quickly once in solution. Data collected following the Chernobyl release indicated that gaseous iodine may have been scavenged as efficiently as caesium. More quantitative information on the oxidation mechanisms of gaseous iodine in solution is required for this to be investigated further.

Since one-dimensional models are dynamically very limited, two-dimensional modelling was carried out and this was described in chapter 5. Analytically specified streamlines were used to schematically represent orographic, frontal and convective precipitation systems. In orographic precipitation, wet deposition of aerosol particles was enhanced by an order of magnitude above the enhancement to precipitation rate due to the seeder-feeder mechanism. By modelling line convection at a rearward sloping cold front, comparison was made between the scavenging of aerosol pollutants drawn into the updraught and downdraught flows; pollution in the updraught flow was scavenged much more efficiently. Although the circulation in a long-lived convective storm is three-dimensional in nature, an attempt was made to model it in two dimensions using an untwisted and flattened schematic picture of the flows. Such storms were shown to be capable of producing very high levels of deposition, not only because of their high precipitation rates but also because they draw in large volumes of boundary layer air to feed their strong updraughts.

The storm models developed in the preceeding chapters were applied to cconsequence assessment in chapter 6. Here the importance of the dynamics of precipitation systems was demonstrated. The large concentration factors operative in convective storms ensured that they had the largest impact on accident consequences. Deposition from orographic rain was also shown to be potentially serious. Unlike the other systems modelled, orographic systems were assumed to be stationery allowing pollution processing through them to be deposited on one patch of ground rather than being smeared out over the area of land traversed by a moving system. Wet deposition of the Chernobyl release from the two-dimensional precipitation systems modelled in chapter 5 was calculated, so as to compare with observations. Orographic rain was shown to lead to the sort of enhanced levels of deposition on locally affected hillsides that were observed in Cumbria and North Wales on 3rd and 4th May, 1986. In Sweden, concentrations of ^{137}Cs in rain were observed to vary greatly over small distances. One explanation for this was shown to be the differences in efficiencies of scavenging in frontal precipitation depending on whether rainout or washout processes were dominant. It was also demonstrated how a convective storm up to 100km from Chernobyl may have produced levels of deposition sufficiently high to justify evacuation, such as occurred in Gomel following a storm there.

The two most important limitations to the cloud models developed in this thesis are firstly microphyiscal and secondly dynamic in nature. Only microphysical processes appropriate to warm cloud have been modelled. In the Northerly latitudes that Britain inhabits, the freezing level is reached in many clouds for large parts of the year. Therefore, inclusion of the ice-phase in the microphysical scheme is an enhancement that is certainly justified. The models that have been developed also have dynamic limitations. Although they have been extended to two spatial dimensions,

the anlytically specified streamlines employed are both schematic and very simplified. A better representation of the dynamics would be a most important future develpment. This could either be acheived by providing a more representative windfield for the model, such as is produced by WAFT (Kitson, 1988), or by making the model fully dynamic in nature. This would involve solving all the conservation equations(3.1) to (3.5), from which the air velocities would arise as solutions. Of the two possibilities, this would be much the more demanding of computational resources and would be even more so were the ice phase also included.

Appendix A Numerical Considerations

The conservation equations, expressed in their general form by equations(3.29) to (3.33), in their 1D form by (3.35) to (3.39) and in their 2D form by (5.1) to (5.5) are solved by a finite difference scheme suggested by Lax(1954). The method of solution is discussed in the context of the 1D equations in section A.1 and for the 2D equations in A.2. In section A.1.1 the characteristic equations are discussed and the classification of the equations made. In section A.1.2 the Lax finite difference scheme is shown to be conditionally stable.

A1 1D form

A1.1 Characteristic equations

The method of characteristics is discussed in connection with the 1D cloud water equations. The application to the pollutant equations and to the 2D form follows fairly straightforwardly. Equations (3.29) and (3.30) can be written as

$$q_{c\,t} + w\,q_{c\,z} = f_1(q_c, q_r) \tag{A.1}$$

$$q_{r\,t} + (V+w)\,q_{r\,z} = f_2(q_c, q_r) \tag{A.2}$$

where $q_{c\,t} = \partial q_c / \partial t$ and the functions f_1 and f_2 replace the source and sink terms. They can be classified by finding the characteristic equation(Ames,1977). In matrix form they become

$$\begin{bmatrix} 1 & w & 0 & 0 \\ 0 & 0 & 1 & V+w \\ dt & dz & 0 & 0 \\ 0 & 0 & dt & dz \end{bmatrix} \begin{bmatrix} q_{c\,t} \\ q_{c\,z} \\ q_{r\,t} \\ q_{r\,z} \end{bmatrix} = \begin{bmatrix} f_1 \\ f_2 \\ dq_c \\ dq_r \end{bmatrix}. \tag{A.3}$$

The characteristic equation is found by equating the matrix determinant to zero;

$$dz^2 - (V + 2w)\,dt\,dz + w(V + W)\,dt^2 = 0. \qquad (A.4)$$

Classification is achieved by evaluating the discriminant given by

$$((V+w) + w)^2 - 4.1.w(V+w) = V^2 > 0.$$

The discriminant is positive and therefore the equations are hyperbolic.

The 2 quasilinear hyperbolic equations(A.1) and (A.2) can be written as

$$A\phi_z + B\phi_t + d = 0 \qquad (A.5)$$

where

$$\phi = \begin{bmatrix} q_c \\ q_r \end{bmatrix} \qquad (A.6)$$

and in full

$$\begin{bmatrix} w & 0 \\ 0 & V+w \end{bmatrix} \begin{bmatrix} q_{c\,z} \\ q_{r\,z} \end{bmatrix} + \begin{bmatrix} 1 & 0 \\ 0 & 1 \end{bmatrix} \begin{bmatrix} q_{c\,t} \\ q_{r\,t} \end{bmatrix} - \begin{bmatrix} f_1 \\ f_2 \end{bmatrix} = \begin{bmatrix} 0 \\ 0 \end{bmatrix}. \qquad (A.7)$$

The characteristics are found by a linear transformation of (A.5) to give

$$TA\phi_z + TB\phi_t + Td = 0 \qquad (A.8)$$

and by finding a diagonal matrix

$$E = \begin{bmatrix} e_1 & \cdots & 0 \\ 0 & e_2 & \cdots & 0 \\ & & & \\ 0 & \cdots & & e_n \end{bmatrix} \qquad (A.9)$$

such that

$$TA = ETB. \qquad (A.10)$$

For a non-trivial E,

$$\det(A - e_j B) = 0. \qquad (A.11)$$

$$\mathrm{Det}(A-\lambda B) = \mathrm{Det}\begin{bmatrix} w-\lambda & 0 \\ 0 & (V+w)-\lambda \end{bmatrix}. \qquad (A.12)$$

Therefore solutions are

$$\lambda = w,\ V+w \qquad (A.13)$$

and the characteristics are

$$\frac{dz}{dt}\Big|_1 = w \qquad \text{and} \qquad \frac{dz}{dt}\Big|_2 = V + w\,. \qquad (A.14)$$

The characteristics are the natural coordinates of the system and in principle it is possible to solve the original system of hyperbolic equations by replacing them by a system whose coordinates are the characteristics. However there are problems in doing this, most notably in relating the grid of characteristics to a Cartesian grid. Providing the limitations imposed by the characteristics are considered in the development, it is possible to use a finite difference scheme instead. One must be careful not to try to provide a solution by finite difference methods in a region not reached by the continuous solution. The regions on which solutions are given are defined by the characteristics(see Ames,1977). The finite difference scheme employed and its region of applicabilty are discussed in the next section.

A.1.2 Stability

The Lax finite difference scheme approximates

$$\phi_t + w\,\phi_z = 0$$

by

$$\frac{\phi_j^{\tau+1} - \frac{1}{2}(\phi_{j+1}^{\tau} + \phi_{j-1}^{\tau})}{\Delta t} + \frac{w(\phi_{j+1}^{\tau} - \phi_{j-1}^{\tau})}{2\Delta z} = 0 \qquad (A.15)$$

where $\phi_j^{\tau} = \phi(j\Delta z, \tau\Delta t)$. It is not obvious why the simple forward in time, centred in space scheme

$$\frac{\phi_j^{\tau+1} - \phi_j^{\tau}}{\Delta t} + \frac{w(\phi_{j+1}^{\tau} - \phi_{j-1}^{\tau})}{2\Delta z} \qquad (A.16)$$

is not suitable, but Pielke(1984) demonstrates that this scheme is linearly unstable. The same techniques are used here to show that the Lax scheme is conditionally stable.

Represent $\phi(z,t)$ in terms of complex variables $\hat{\phi}$, k, ω;

$$\phi(z, t) = \hat{\phi}(k, \omega)\, e^{i(kz + \omega t)}. \qquad (A.17)$$

Then (A.15) becomes

$$\hat{\phi}(k, \omega)\, e^{i(k j\Delta z + \omega \tau\Delta t)} (e^{i\omega\Delta t} - 1/2 (e^{ik\Delta x} + e^{-ik\Delta x}))$$
$$= - w \Delta t / (2\Delta z) (e^{ik\Delta z} - e^{-ik\Delta z}) \hat{\phi}(k,\omega)\, e^{i(k j\Delta z + \omega \tau\Delta t)}. \qquad (A.18)$$

Following Pielke, set

$$\psi^1 = e^{i\omega\Delta t}, \ \psi_1 = e^{ik\Delta z}, \ \psi_{-1} = e^{-ik\Delta z}, \qquad (A.19)$$

$C = w \Delta t / \Delta z$ is the Courant number. Then (A.18) becomes

$$\psi^1 - 1/2(\psi_1 + \psi_{-1}) = -C/2 (\psi_1 - \psi_{-1}). \qquad (A.20)$$

Now

$$\psi_1 - \psi_{-1} = e^{ik\Delta z} - e^{-ik\Delta z} = \cos k\Delta z + i \sin k\Delta z - (\cos k\Delta z - i \sin k\Delta z)$$
$$= 2i \sin k\Delta z. \qquad (A.21)$$

Similarly, $\psi_1 + \psi_{-1} = 2 \cos k\Delta z.$ (A.22)

Thus from (A.20),

$$\psi^1 = \cos k\Delta z - C i \sin k\Delta z. \qquad (A.23)$$

Now write ω in terms of its real and imaginary parts : $\omega = \omega_r + i\, \omega_i$ and ψ^1 becomes

$$\psi^1 = e^{i\omega\Delta t} = e^{i(\omega r + i\omega i)\Delta t} = e^{-\omega i\Delta t} e^{i\omega r\Delta t} = \lambda e^{i\omega r\Delta t} \qquad (A.24)$$

where $\lambda = e^{-\omega_i\Delta t}$ is called the amplitude change of the solution per time step. Equating real and imaginary parts of (A.23) and (A.24)

$$\lambda \cos\omega_r\Delta t = \cos k\Delta z \qquad (A.25)$$

$$\lambda \sin\omega_r\Delta t = -C \sin k\Delta z. \qquad (A.26)$$

Squaring and adding,

$$\lambda^2 = \cos^2 k\Delta z + C^2 \sin^2 k\Delta z = 1 - (1-C^2)\sin^2 k\Delta z. \qquad (A.27)$$

If the amplitude change $|\lambda| > 1$ for any possible wavelength, the solution is linearly unstable. For this scheme it is stable provided $|\lambda| \leq 1$. This is conditional on

$$|C| \leq 1$$

or

$$\left| \frac{w\,\Delta t}{\Delta z} \right| \leq 1 . \qquad (A.28)$$

This is known as the Courant condition and can be stated as the requirement that the distance travelled in one time step due to advection must not be greater than the grid separation.

A.2 2D form

In 2D the general finite difference form of the equations

$$\frac{\partial \phi}{\partial t} + \frac{\partial}{\partial x}(u\phi) + \frac{\partial}{\partial z}(w\phi) = S , \qquad (A.29)$$

where S represents the source/sink terms is written

$$\phi_{i,j}^{\tau+1} = \frac{1}{4}\left(\phi_{i+1,j+1}^{\tau} + \phi_{i+1,j-1}^{\tau} + \phi_{i-1,j+1}^{\tau} + \phi_{i-1,j-1}^{\tau}\right) + k\left[\left[\frac{u_{i-1,j}^{\tau}\,\phi_{i-1,j}^{\tau} - u_{i+1,j}^{\tau}\,\phi_{i+1,j}^{\tau}}{2\Delta x}\right] + \left[\frac{w_{i,j-1}^{\tau}\,\phi_{i,j-1}^{\tau} - w_{i,j+1}^{\tau}\,\phi_{i,j+1}^{\tau}}{2\Delta z}\right] + 1/4\left(S_{i+1,j+1}^{\tau} + S_{i+1,j-1}^{\tau} + S_{i-1,j+1}^{\tau} + S_{i-1,j-1}^{\tau}\right)\right] . \qquad (A.30)$$

The averaging of ϕ and S over 4 values is the obvious extension to 2D of averaging over 2 neighbouring values for the 1D version. It was found that

this was more stable then the alternative version

$$1/4\,(\phi_{i,j+1}^{\tau} + \phi_{i+1,j}^{\tau} + \phi_{i-1,j}^{\tau} + \phi_{i,j-1}^{\tau}) \qquad \text{(A.31)}$$

and so the former was used. Of the two averaging procedures the first seems intuitively more stable then the second and it seems reasonable in this instance to be guided by experience and intuition rather than rigorous mathematical proofs.

At model domain boundaries, as in 1D, boundary conditions must be specified. The simple condition is for a constant value of the quantity. In this case $\phi = \phi_k$ where ϕ_k is a constant and no finite difference formula is required. For a flow through boundary condition either the x or z derivative is replaced by a form similar to the 1D model. For instance for the top boundary (j = N) the z derivative is replaced by

$$\frac{w_{i,N-1}^{\tau}\,\phi_{i,N-1}^{\tau} - w_{i,N}^{\tau}\,\phi_{i,N}^{\tau}}{\Delta z} \qquad \text{(A.32)}$$

and at the left hand boundary (i = 0) the x derivative is replaced by

$$\frac{u_{0,j}^{\tau}\,\phi_{0,j}^{\tau} - u_{1,j}^{\tau}\,\phi_{1,j}^{\tau}}{\Delta x}. \qquad \text{(A.33)}$$

There is no averaging at the boundaries. At the top boundary for instance the finite difference formula is

$$\phi_{i,N}^{\tau+1} = \phi_{i,N}^{\tau} + k\left[\frac{u_{i-1,N}^{\tau}\,\phi_{i-1,N}^{\tau} - u_{i+1,N}^{\tau}\,\phi_{i+1,N}^{\tau}}{2\Delta x} + \frac{w_{i,N-1}^{\tau}\,\phi_{i,N-1}^{\tau} - w_{i,N}^{\tau}\,\phi_{i,N}^{\tau}}{\Delta z} + S_{i,N}\right]. \qquad \text{(A.34)}$$

At a corner, such as the top left hand corner, it is even simpler;

$$\phi_{0,N}^{\tau+1} = \phi_{0,N}^{\tau} + k\left[\frac{u_{0,N}^{\tau}\phi_{0,N}^{\tau} - u_{1,N}^{\tau}\phi_{1,N}^{\tau}}{\Delta x} + \frac{w_{0,N-1}^{\tau}\phi_{0,N-1}^{\tau} - w_{0,N}^{\tau}\phi_{0,N}^{\tau}}{\Delta z} + S_{0,N}\right].$$

(A.35)

In addition, in the case where there are two separate regions within the model domain, an internal boundary is defined. This is to prevent small quantities of material leaking from one circulation to another due to the averaging terms. This would be from the updraught to the downdraught in the case of the rearward sloping cold front or from the updraught into the hill in the orographic situation.

Appendix B Calculation of reference level deposition rates

B.1 5mSv emergency reference level due to ingestion of milk for UK1

^{131}I is the most significant radionuclide for this pathway for UK1.

Effective dose equivalent for ^{131}I integrated to one year

$= 1.4.10^{-8}$ Sv / Bq (Table 31, DOSE-MARC, Charles et al, 1982)

^{131}I integrated activity in ingested milk after seven days and after initial deposition of 1 Bq / m^2

$= 3.01.10^{-3}$ Bq y / kg (Table A6, FOOD-MARC,Linsley et al, 1982)

An individual consumes

300 kg / yr (Table 11, Kelly and Clarke,1982)

In 7 days he ingests

$3.01.10^{-3} \times 300 = 0.903$ Bq ^{131}I

Effective dose equivalent for ^{131}I in milk after deposition of 1 Bq / m^2

$= 0.903 \times 1.4.10^{-8}$

$= 1.26.10^{-8}$ Sv / Bq m^{-2}

Restrict milk at a dose of 5.10^{-3} Sv which corresponds to a deposition rate

$= 5.10^{-3} / 1.26.10^{-8}$

$= 3.97.10^{5}$ Bq / m^2

UK1 releases

$2.37.10^{18}$ Bq of ^{131}I

Therefore reference level deposition rate for a unit release UK1 accident

$= 3.97.10^{5} / 2.37.10^{18}$

$= 1.67.10^{-13}$ Bq / m^2 .

B.2 5 mSv emergency reference level due to inhalation of ground gamma radiation for Magnox single channel melt and depressurisation accident

The most significant radionuclides for this pathway and the quantities released are

^{103}Ru	$6.01.10^{12}$ Bq
^{106}Ru	$1.63.10^{12}$ Bq
^{137}Cs	$3.37.10^{12}$ Bq
^{140}Ba	$7.10.10^{11}$ Bq

The effective dose equivalents to one year after initial deposit of 1 Bq/m^2 (Table 3, DOSE-MARC, Charles et al, 1982) are

^{103}Ru	$1.5.10^{-9}$ Sv
^{106}Ru	$2.8.10^{-9}$ Sv
^{137}Cs	$1.0.10^{-8}$ Sv
^{140}Ba	$5.2.10^{-9}$ Sv.

Therefore reference level deposition rate for unit release corresponding to 5 mSv

$$= 5.10^{-3} / [(6.01.10^{12} \times 1.5.10^{-9}) + (1.63.10^{12} \times 2.8.10^{-9}) + (3.37.10^{12} \times 1.10^{-8}) + (7.10.10^{11} \times 5.2.10^{-9})]$$

$$= 9.81.10^{-8} \text{ Bq} / \text{m}^2 .$$

References

Ames,W.F., 1977. Numerical methods for partial differential equations, 2nd Edn., New York, Academic Press.

ApSimon, H. M., Goddard, A. J. H. and Wrigley, J., 1985. Long-range atmospheric dispersion of radioisotopes - 1. The Mesos model, Atmos. Environ., 19, 99-111.

ApSimon, H. M. and Simms, K. L., 1986. Estimating the effects of rain and snow on potential reactor accident consequences, Nucl. Energy, 25, 235-242.

ApSimon, H. M., Simms, K. L. and Collier, C. G., 1988. The use of weather radar in assessing deposition of radioactivity from Chernobyl across England and Wales, to be published in Atmos. Environ.

ApSimon, H. M. and Wilson, J. J. N., 1987a. Modelling atmospheric dispersal of the Chernobyl release across Europe, Boundary-Layer Meteorology, 41, 123-133.

ApSimon, H. M. and Wilson, J. J. N., 1987b. A review of the pattern of radioactive releases from Chernobyl based on long range contamination patterns, CEC contract report No 86729.

ApSimon, H. M., Wilson, J. J. N., Guirguis, S. and Stott, P. A., 1987. Assessment of the Chernobyl release in the immediate aftermath of the accident, Nucl. Energy, 26, 295-301.

Atkinson, B. W., 1981. Meso-scale atmospheric circulations, Academic Press, 495pp.

Beard, K. V. and Grover, S. N., 1974. Numerical collision efficiencies for small raindrops colliding with micron sized particles, J. Atmos. Sci., 31, 543-550.

Beard, K. V. and Pruppacher,H. R., 1971. A wind tunnel investigation of collection kernels of small water drops in air, Quart. J. R. Meteor. Soc., 97, 242-248.

Berry, E. X. and Reinhardt, R. L., 1974. An analysis of cloud drop growth by collection, J. of Atmos. Sci., 31, 2118-2126.

Briggs,G. A., 1972. Chimney plumes in neutral and stable surroundings, Atmos. Environ., 6, 507.

Browning, K. A., 1964. Airflow and precipitation trajectories within severe local storms which travel to the right of the winds, J. Atmos. Sci., 21, 634-639.

Browning, K. A., 1983. Mesoscale structure and mechanisms of frontal precipitation systems, Met. Office Radar Research Laboratory, Research Report, No. 34.

Browning, K. A., 1985. Conceptual models of precipitation systems, Met. Mag., 114, 293-319.

Browning, K. A., Fankhauser, J. C., Chalon, J.-P., Eccles, P. J., Strauch, R. G., Merrem, F. H., Musil, D. J., May, E. L. and Sand, W. R., 1976. Structure of an evolving hailstorm. V. Synthesis and implications for hail growth and hail suppresion, Mon. Wea. Rev., 104, 603-610.

Browning, K. A. and Harold, T. W., 1970. Air motion and precipitation growth at a cold front, Quart. J. R. Met. Soc., 96, 369-389.

Browning, K. A. and Ludlam, F. H., 1962. Airflow in convective storms, Q. Jl. R. Met. Soc., 88, 117-135.

Carruthers, D. J. and Choularton, T. W., 1986. The microstructure of hill cap clouds, Quart. J. R. Met. Soc., 112, 113-129.

Charles, D., Crick, M.J., Fell, T. P. , Greenhalgh, J. R.,1982. DOSE-MARC : The dosimetric module in the methodology for assessing the radiological consequences of accidental releases, Chilton NRPB (London HMSO).

Chaumerliac, N., Nickerson, E. and Rosset, R., 1983. A three-dimensional mesoscale numerical simulation of atmospheric cleansing during the 1982 Boulder Upslope Cloud Observation Experiment (BUCOE), IN Precipitation scavenging, dry deposition, and resupsension (Pruppacher

et al. editors), Elsevier.

Chaumerliac, N. and Rosset, R., 1987. Pollutant scavenging in a mesoscale meteorological model with quasi-spectral microphysics, IN Proc. International conference on energy transformations and interaction with small and mesoscale atmospheric processes, Lausanne.

Chisholm, A. J. and Renick, J. H., 1972. The kinematics of multicell and supercell Alberta hailstorms, Alberta Hail Studies, Research Council of Alberta Hail Studies, Report 72-2, 24-31.

Clarke, R. H., 1979, The first report of a working group on atmospheric dispersion : A model for short and medium range dispersion of radionuclides released to the atmosphere, Chilton NRPB (London HMSO).

Easter, R.C. and Hales, J. M., 1984. PLUVIUS : a generalized one-dimensional model of reactive pollutant behaviour, including dry deposition, precipitation formation, and wet removal, Pacific Northwest Laboratory report PNL-4046 ED2.

Eggleton, A. E. J., 1967. A theoretical examination of iodine-water partition coefficients, AERA-R4887, United Kingdom Atomic Authority.

Fisher, B. E. A., 1982. The transport and removal of sulphur dioxide in a rain system, Atmos. Environ., 16, 775-783.

Fisher, B. E. A., 1987. Personal communication.

Fisher, B. E. A., and Clark, P. A., 1986. Removal of sulphur dioxide in a two-dimensional rain system based on a scale analysis of the conservation equations, Atmos. Environ., 20, 2219-2229.

Flossmann, A. L., Hall, W. D. and Pruppacher, H. R., 1985. A theoretical study of the wet removal of atmospheric pollutants. Part 1 : the redistribution of aerosol particles captured through nucleation and impaction scavenging by growing cloud drops, J. Atmos. Sci., 42, 583-606.

Gifford, F. A., 1968, Diffusion in the lower layers of the atmosphere, IN

Meteorology and Atomic Energy (D. Slade ed), US Atomic Energy Commision, TID-24190, p65.

Gittus, J. H. et al, 1982. PWR degraded core analysis, ND-R-610(S), United Kingdom Atomic Energy Authority.

Gunn, R. and Kinzer, G. D., 1949, The terminal velocity of fall for water droplets in stagnant air, J. Meteor., 6, 243-248.

Hales, J. M., 1972. Fundamentals of the theory of gas scavenging by rain, Atmos. Environ., 6, 635-659.

Hales, J. M., 1978. Wet removal of sulphur compounds from the atmosphere, Atmos. Environ., 12, 389-399.

Hales, J. M., 1982. Mechanistic analysis of precipitation scavenging using a one-dimensional, time variant model, Atmos. Environ., 16, 1775-1783.

Hong, M. and Carmichael, G. R., 1986. An investigation of sulfate production in an orographic storm using a detailed transport/chemistry model coupled with a detailed cloud scavenging model, Atmos. Environ., 20, 1989-1997.

Hosker, R. P., 1974. Estimates of dry deposition and plume depletion over forests and grasslands, IN Proc. Symposium on Physical Behaviour of Radioactive Contaminants in the Atmosphere, Vienna, IAEA,p291.

Jenkin, M., 1987. Personal communication.

Jones, J. A., 1981a. The second report of a working group on atmospheric dispersion : A procedure to include deposition in the model for short and medium range atmospheric dispersion of radionuclides, Chilton NRPB(London HMSO).

Jones, J. A., 1981b. The fourth report of a working group on atmospheric dispersion : A model for long range atmospheric dispersion of radionuclides released over a short period, ChiltonNRPB(London HMSO).

Jones, J. A., 1983. The fifth report of a working group on atmospheric

dispersion : Models to allow for the effects of coastal sites, plume rise and buildings on dispersion of radionuclides and guidance on the value of deposition velocity and washout coefficients, Chilton NRPB(London HMSO).

Jones, J. A., 1985. The sixth report of a working group on atmospheric dispersion : Modelling wet deposition from a short release, Chilton NRPB(London HMSO).

Kelly, G. N. and Clarke, R. H., 1982. An assessment of the radiological consequences of releases from degraded core accidents for the Sizewell PWR, Chilton NRPB(London HMSO).

Kessler, E., 1969. On the distribution and continuity of water substance in atmospheric circulations, Met. Monograph, 10, No 32, American Meteorological Society.

Kinzer,G. D. and Cobb, W. E., 1958. Laboratory measurements and analysis on the growth and collection efficiency of cloud drops, J. Meteor., 15, 138-148.

Kitson, N. K., 1988. Mass-consistent windfields for simulating radionuclide dispersion over complex terrain, PhD thesis.

Lax, P. D., 1954. Weak solutions of nonlinear hyperbolic equations and their numerical computation, Commun. Pure. Appl. Math., 7, 159-193.

Lin, C. C., 1975. Behaviour of radioiodine studies : iodine partition between aqueous solution and gas phases, NEDO-12583.

Linsley, G. S., Simmonds, J. R. and Haywood, S. M., 1982. FOOD-MARC : The foodchain transfer module in the methodology for assessing the radiological consequences of accidental releases, Chilton NRPB(London HMSO).

Ludlam, F. H., 1980, Clouds and Storms : The behavior and effect of water in the atmosphere, Penn. Univ. Press, 405pp.

Marshall, J. S. and Palmer, W. McK., 1948. The distribution of raindrops with size, J. Meteor., 5, 165-166.

Mason, B. J., 1971. The physics of clouds, Oxford University Press, 671 pp.

Monk and Jonas, 1986. Rainfall related deposition of radioactivity over the United Kingdom 3-4 May 1986, Presented at Meteorological Office, 10 December, 1986.

Moore, D. J., 1976. Calculation of ground level concentration for different sampling periods and source locations, IN Atmospheric Pollution, Amsterdam, Elsevier, p5160.

Pasquill, F., 1961. The estimation of the dispersion of windborne material, Met. Mag., 90, 33-49.

Pelletier, C. A. and Hemphill, R. T., 1979. Nuclear power plant related iodine partition coefficiants, EPRI-NP-1271, The Electric Power Research Institute, Palo Alto, California.

Persson, C., Rodhe, H. and De Geer, L., 1987. The Chernobyl Accident - a meteorological analysis of how radionuclides reached and were deposited in Sweden, Ambio, 16, 20-31.

Pielke, R. A., 1984. Mesoscale meteorological modeling, Academic Press, 612pp.

Postma, A. K., 1970. Effects of solubilities of gases on their scavenging by raindrops, IN Precipitation Scavenging : proceedings of a symposium held at Ridland, Washington, June, 1970 published by USAEC Division of Technical Information.

Pruppacher, H. R., 1987. New developments in the field of scavenging of air pollutants, IN Proc. International conference on energy transformations and interaction with small and mesoscale atmospheric processes, Lausanne, March 1987.

Rogers, R. R., 1979. A short course in cloud physics, 2nd edition, Pergamon Press, 235 pp.

Seigneur, C. and Saxena, P., 1988. A theoretical investigation of sulfate formation in clouds, Atmos. Environ., 22, 101-115.

Simms, K. L., 1988. The effects of precipitation on accidental releases of radioactivity, PhD thesis.

Smith, F. B., 1981. Probability prediction of the wet deposition of airborne pollution, IN Air pollution modelling and its application I, NATO challenges of modern society, Vol 1, (edited by C. De Wisplelaere), Plenum Press.

Smithsonian Meteorological Tables, 1958, The Smithsonian Institute, Washington D. C. (sixth revised edition), 527pp.

Taylor, F. E., 1986, Personal communication.

Ten Brink, H. M., Schwartz, S. E. and Daum, P. H., 1987. Efficient scavenging of aerosol sulfate by liquid-water clouds, Atmos. Environ., 21, 2035-2052.

Tremblay, A., 1987. Cumulus cloud transport, scavenging and chemistry : observations and simulations, Atmos. Environ., 21, 2345-2364.

Tremblay, A. and Leighton, H., 1984. The influence of cloud dynamics upon the redistribution and transformation of atmospheric SO_2 - a numerical simulation, Atmos. Environ., 18, 1885-1894.

Underwood, B. Y., 1983a. Dry deposition, IN Review of specific effects in atmospheric dispersion calculations, United Kingdom Atomic Energy Authority, XII/917/83-EN.

Underwood, B. Y., 1983b. Wet deposition, IN Review of specific effects in atmospheric dispersion calculations, United Kingdom Atomic Energy Authority, XII/917/83-EN.

Waldwogel, A., 1974, The N_0 jump of raindrop spectra, J. Atmos. Sci, 31, 1067-1078.

Wallace,J.M. and Hobbs,P.V., 1977. Atmospheric Science : an introductory survey, Academic Press, 467pp.

Working document for Chernobyl post accident review meeting, 1986, USSR.